

**SURFACE MODIFIED ELECTRODES AS A NOVEL TECHNIQUE  
FOR CHARACTERIZING *Adansonia digitata* FRUIT**

**By**

**ONDACHI PAULINE WANJIKU**

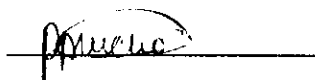
**B.Sc. Chem. (Hons) NAIROBI**

A thesis submitted in partial fulfillment of the degree of Master of Science of the  
University of Nairobi

**2000**

## DECLARATION

This thesis is my original work and has not been submitted for examination for a degree in any other University.



Date 12<sup>th</sup> July 2001

**ONDACHI PAULINE**

This work has been submitted for examination with our approval as the supervisors.



Date 13<sup>th</sup> July 2001

**Supervisor**

**Prof. D.O. Orata**

**Department of Chemistry**

**University of Nairobi**



Date 16<sup>th</sup> July 2001

**Co-supervisor**

**Dr. B. N. Chikamai**

**Kenya Forestry Research Institute**

**(KEFRI)**

## DEDICATION

*Dedicated to my very loving husband PIUS ONDACHI*

## ACKNOWLEDGEMENTS

I give GLORY, HONOUR, and THANKS first to the ALMIGHTY GOD for giving me the opportunity to do this course and the favour He has shown throughout this period.

I wish to express my sincere gratitude to my supervisors Prof. D. O. Orata and Dr. B. N. Chikamai for their supervision and assistance in doing this work. I am particularly thankful to my first supervisor Prof. Orata, for his inspiration and stepwise guidance throughout the course of investigation and compilation of the work.

My sincere and deep gratitude also goes to the African Academy of Sciences for the provision of a scholarship that enabled me to do the M. Sc. I thank my employers at Kenya Forestry Research Institute (KEFRI) for granting me study leave and for the assistance they accorded me. I am also thankful to Mr. Norman Wachira of KEFRI for all the help he so willingly rendered to me during this period. I thank Mr. Evans Miriti of geology department, UoN and Lucy Wanjiru of ICS for their assistance in scanning some of the diagrams and Mr. Martin Muyanga for availing his laptop for my use.

Very special thanks go to my husband Pius Ondachi, for his great support, encouragement and for the many sacrifices he made for my sake during this period. I am also deeply thankful to my parents, brothers and sister for their moral support and the many prayers they offered for me.

I thank all the friends, relatives and any other person who contributed in any way to the success of this work.

## TABLE OF CONTENTS

DECLARATION.....	II
DEDICATION.....	III
ACKNOWLEDGEMENTS.....	IV
LIST OF TABLES.....	IX
LIST OF FIGURES .....	XI
ABSTRACT .....	XVIII

### CHAPTER ONE

INTRODUCTION .....	1
1.0 <i>ADANSONIA DIGITATA</i> L. ....	1
1.1.0 Background Information.....	1
1.2.0 Ecology and Distribution in Kenya .....	2
1.3.0 Botanical Characteristics .....	4
1.4.0 Economic Uses .....	6
1.5.0 Chemical composition of the Tree Parts.....	13

### CHAPTER TWO

2.0 ELECTROCHEMISTRY .....	18
2.1.0 General Introduction on Utilization/application of Electrochemistry .....	18
2.1.1 Origin and Overview of Electrode Processes .....	19
2.2.0 SURFACE MODIFIED ELECTRODES .....	28
2.2.1 MODIFICATION METHODS.....	29
2.2.1.1 Chemisorption .....	29
2.2.1.2 Covalent bonding.....	30
2.2.1.3 Derivatization by Film Formation .....	34

2.2.2	ION EXCHANGE POLYMERS .....	37
2.2.3	REDOX POLYMERS .....	45
2.2.4	CONDUCTING POLYMERS .....	46
2.2.4.1	Mechanism of conduction in Conductive Polymers.....	49
2.2.4.2	Use of Conducting Polymer in Electrode Modification .....	52
2.3.0	ELECTROCHEMISTRY OF BIOLOGICAL AND NATURAL COMPOUNDS .....	54
2.3.1	Application of Modified Electrodes in Biological and Natural Products Redox Systems .....	59
2.4.0	OBJECTIVES OF THE RESEARCH PROJECT .....	60

### CHAPTER THREE

EXPERIMENTAL SECTION.....	62
3.0. METHODS OF ANALYSIS .....	62
3.1.0 BOMB CALORIMETER .....	62
3.1.1 Experimental Procedure .....	63
3.1.2 Calculations .....	64
3.2.0 CYCLIC VOLTAMMETRY .....	66
3.2.1 Principles of Cyclic Voltammetry .....	67
3.2.2 Instrumentation for Cyclic Voltammetry.....	72
3.2.2.1 Operation of a Potentiostat .....	72
3.2.2.2 Universal Programmer and X-Y Recorder .....	79
3.3.0 INFRARED SPECTROSCOPY .....	80
3.3.0.1 Near Infrared Region .....	81
3.3.0.2 Mid Infrared Region .....	82

3.3.0.3 Far Infrared .....	83
3.3.1 Instruments for Infrared Spectroscopy .....	83
3.3.1.1 Fourier Transformations .....	84
3.3.2 Principle of Fourier Transform Spectrophotometer .....	86
3.3.3 Advantages of FTIR Spectroscopy .....	92
3.3.4 Sample Handling .....	92
3.4.0 X-RAY FLUORESCENCE SPECTROMETRY .....	92
3.4.1 Instrumentation for the X-RF Spectrometry .....	93
3.5.0 ELECTRODES .....	94
3.5.1 Reference Electrode .....	95
3.5.2 Preparation of the Working Electrode .....	97
3.6.0 CHEMICALS AND REAGENTS .....	98
3.7.0 FRUIT SAMPLES .....	100

## CHAPTER FOUR

4.0. RESULTS AND DISCUSSIONS .....	101
4.1.0 PHYSICAL MEASUREMENTS .....	101
4.1.1 Density .....	101
4.1.2 Moisture Content .....	102
4.1.3 Solubility Measurements .....	103
4.1.4 Calorific Values .....	105
4.2.0 ELECTROCHEMICAL DISCUSSIONS OF <i>Adansonia digitata</i> FRUIT .....	108
4.2.1 The Spongy/ Hairy greenish Exterior, Ad <sub>1</sub> .....	108
4.2.1.1 Analysis using bare carbon graphite working electrode .....	108
4.2.1.2 Identification of Ad <sub>1</sub> .....	118

4.2.1.3	Electrochemical Activity of Ad <sub>1</sub> in Acetonitrile/water mixture .....	121
4.2.1.4	SURFACE MODIFIED ELECTRODES .....	122
4.2.2	THE BROWN WOODY COVERING, Ad <sub>2</sub> .....	128
4.2.2.1	Analysis using Bare Carbon working electrode .....	128
4.2.2.2	Identification of Ad <sub>2</sub> .....	134
4.2.2.3	Analysis of Ad <sub>2</sub> in Acetonitrile/water mixture .....	136
4.2.2.4	Analysis using modified Electrodes .....	137
4.2.3	THE WHITE-PINK PULP (Ad <sub>3</sub> ).....	146
4.2.3.1	Analysis on bare carbon working electrode .....	146
4.2.3.2	Identification of Ad <sub>3</sub> .....	153
4.2.3.3	Analyses using Acetonitrile /water mixture .....	160
4.2.3.4	SURFACE MODIFIED ELECTRODES .....	161
4.2.4	<i>Adansonia digitata</i> SEED, Ad <sub>4</sub> .....	175
4.2.4.1	Analyses using bare carbon .....	176
4.2.4.2	Identification of Ad <sub>4</sub> from FTIR spectrum .....	179
4.2.4.3	Effect of solvent on Ad <sub>4</sub> Redox Chemistry .....	180
4.2.4.4	Analysis of Ad <sub>4</sub> on Modified Electrodes.....	183
4.3.0	Use of Electrochemical Signal to Confirm the Presence of Flavonoids and Terpenes in parts of <i>A. digitata</i> Fruit.....	199
	CONCLUSION .....	203
	REFERENCES .....	205



## LIST OF TABLES

Table 1.1: Chemical Composition of <i>A. digitata</i> fruit as reported in Senegal, Malawi and Nigeria. -----	15
Table 2.1: Oxides in kriegers, Parminsters and Athi River bentonites -----	43
Table 3. 1: Composition of bentonite obtained from spectrum analysis. -----	100
Table 4.1: Densities of the whole fruit, and individual parts of <i>Adansonia digitata</i> ----	102
Table 4.2: Moisture contents of Ad <sub>1</sub> , Ad <sub>2</sub> and Ad <sub>3</sub> components of <i>A digitata</i> fruit. -----	103
Table 4.3: Percentage solubility of different components of <i>A. digitata</i> fruit in different solvent media. -----	104
Table 4.4: Diffusion coefficient of hypothetical bulk concentration of electroactive species in Ad <sub>1</sub> -----	116
Table 4.5: Concentration of electroactive sites, $\Gamma$ , as a function of time for Ad <sub>1</sub> in 1M HCl. -----	117
Table 4.6: Wavenumbers and associated functional groups in the FTIR spectrum of Ad <sub>1</sub> -----	120
Table 4.7: Rates of electrodeposition and redox efficiencies of Ad <sub>2</sub> in 1MHCl as functions of positive potential limit. -----	132
Table 4.8: Diffusion coefficient values for hypothetical bulk concentrations of electroactive species in Ad <sub>2</sub> -----	133
Table 4.9: Surface coverage, $\Gamma$ , (mol/cm <sup>2</sup> ) of electroactive species in Ad <sub>2</sub> as a function of time-----	133
Table 4.10: Wavenumbers and functional groups identified in the FITR spectrum of Ad <sub>2</sub> -----	135
Table 4.11: Diffusion coefficients for theoretical concentration of the bulk, Ad <sub>3</sub> in 1MHCl. -----	151
Table 4.12: Surface coverage, $\Gamma$ , (mol/cm <sup>2</sup> ) of Ad <sub>3</sub> electroactive species as a function of time. -----	151
Table 4.13: Responses of riboflavin, thiamine and ascorbic acid on CME subjected to electrochemistry from the beginning (Case 1) -----	167
Table 4.14: Response of Riboflavin, thiamine and ascorbic acid on CME initially dipped into the electrolyte before being subjected to potential cycling (Case 2). -----	167

Table 4.15: Variation of oxd/red potential, electrodeposition rate and redox efficiency of Ad <sub>3</sub> in different concentrations adsorbed onto bentonite (HCl media). -----	172
Table 4.16: Variation of oxd/red potential, Electrodeposition rate and redox efficiency of Ad <sub>3</sub> in varying concentrations adsorbed onto bentonite (H <sub>2</sub> SO <sub>4</sub> media). -----	172
Table 4.17: Mixtures of Ad <sub>4</sub> /HCl that were adsorbed onto the bentonite used in electrode modification and their corresponding oxidation/reduction potentials, electrodeposition rates and redox efficiencies. -----	194
Table 4.18: Comparison of oxidation potentials, electrodeposition rates and redox efficiency for various electrode systems used on Ad <sub>4</sub> with HCl as the supporting electrolyte.-----	196
Table 4.19: Oxidation potentials, electrodeposition rates and redox efficiencies for different Ad <sub>4</sub> /H <sub>2</sub> SO <sub>4</sub> mixtures that were adsorbed onto bentonite for modification of the working electrode surface. -----	198
Table 4.20: Summary of the oxidation/ reduction potentials of the four components of <i>A. digitata</i> fruit and the standards in the bare carbon working electrode system.-----	202

## LIST OF SCHEMES

Scheme I (a): Polyacetylene; Propagation of polaron through a conjugated polymer chain by shifting of double bonds. -----	50
Scheme I (b): Polaron and bipolaron formation on reduction of a polyparaphenylene--	50
Scheme I (c): Propagation of a polaron in a polymer. -----	51
Scheme I (d): Formation of solitons in polyacetylene. -----	52
Scheme II: Oxidation of products of polyaniline. -----	53
Scheme III: Illustration of reduction process in a pyrimidine compound. -----	57
Scheme IV: Illustration of a reduction process in a purine compound. -----	57
Scheme V: Reduction process in an isoalloxazine ring present in flavin compounds. ---	58

## LIST OF FIGURES

Fig. 2.1: The conduction bands of two dissimilar metals (a) when not in contact (b) at the instant of contact and (c) at equilibrium. -----	19
Fig. 2.2: Representation of (a) reduction and (b) oxidation of a species A in solution.---	23
Fig. 2.3: The general electrode reaction.-----	27
Fig. 2.4: Schematic illustration of chemical functionalities at the edge plane of pyrolytic graphite. -----	31
Fig. 2.5: A unit cell of the crystal of sodalite -----	39
Fig. 2.6: The general structure of montmorillonite clays-----	42
Fig. 3.1: The schematic illustration of a bomb calorimeter -----	62
Fig. 3.2: Illustration of a plot of temperature recorded in a bomb calorimeter as a function of time and of the heat of transfer $V$ as a function of temperature difference. -----	65
Fig. 3.3: Cyclic voltammogram of a reversible one-electron transfer reaction -----	68
Fig. 3.4: Schematic diagrams for operational amplifiers -----	73
Fig. 3.5 (a): A voltage amplifier -----	74
Fig. 3.5(b): A current follower -----	75
Fig. 3.5(c): Adder type operation amplifier potentiostat -----	76
Fig. 3.6: Vibrations and characteristic frequencies of acetaldehyde-----	80
Fig. 3.7: Fourier transform pairs (a) cosine functions and (b) square-wave function ----	85
Fig. 3.8: Fourier representation of data (a) individual $f(t)$ 's, (b) resultant $f(t)$ and (c) Fourier transforms to $F(v)$ . -----	86
Fig 3.9(a): Michelson Interferometer-----	87
Fig. 3.9(b): Optical path diagram for FTIR spectrometer -----	87
Fig. 3.10: Interference of light waves -----	89
Fig. 3.11: Saturated calomel electrode. -----	96
Fig. 4.1: Plot of temperature Vs time showing change in recorded temperature for each part of the fruit with time in the bomb calorimeter. -----	106

Fig. 4.2(a): Cyclic voltammetric response on a bare carbon working electrode cycled from -0.4V to 1.25V at 50mV/sec in a solution containing 0.1g of Ad <sub>1</sub> in 100mls of 0.5M H <sub>2</sub> SO <sub>4</sub> - initial scan. -----	108
Fig. 4.2(b): CV response on a bare carbon working electrode cycled from -0.4V to 1.25V at 50mV/sec in a solution containing 0.1g of Ad <sub>1</sub> in 100mls of 0.5M H <sub>2</sub> SO <sub>4</sub> on continued cycling.-----	109
Fig. 4.3: Plot of anodic peak current versus time for Ad <sub>1</sub> in different concentrations of H <sub>2</sub> SO <sub>4</sub> on a bare carbon working electrode.-----	110
Fig. 4.4: Plot of anodic peak current versus square root of scan rate for the two oxidative peaks obtained when bare carbon is cycled in a solution containing Ad <sub>1</sub> in 1.0M H <sub>2</sub> SO <sub>4</sub> from -0.4V to 1.4V. -----	112
Fig. 4.5: Plot of anodic peak current versus time for Ad <sub>1</sub> in 2M H <sub>2</sub> SO <sub>4</sub> when bare carbon working electrode was cycled from -0.4V to 1.4V. -----	113
Fig. 4.6: CV response when bare carbon working electrode is cycled in a solution containing Ad <sub>1</sub> in 1.0M HCl. Potential range -0.4V to 0.96V Scan rate 20mV/sec. -----	114
Fig. 4.7: Plot of anodic peak current versus time when bare carbon is cycled in a solution containing Ad <sub>1</sub> in 1.0M HCl from -0.2V to varying positive potentials Scan rate 20mV/sec. -----	115
Fig. 4.8: Plot of anodic peak current Vs square root of scan rate when bare carbon is cycled in solution containing Ad <sub>1</sub> in 1.0MHCl. Potential range -0.2V to 0.96V. -	116
Fig. 4.9: Plot of surface coverage, $\Gamma \times 10^{-9}$ , versus time for bare carbon in a solution of Ad <sub>1</sub> in 1M HCl. Potential range -0.2V to 0.96V. -----	118
Fig. 4.10: Cyclic voltammetric response for heat pillared chlorophyll-modified electrode in a 1M HCl solution. Potential range -0.2V to 0.98V. Scan rate 20mV/sec.-----	119
Fig. 4.11: FTIR spectrum for Ad <sub>1</sub> -----	120
Fig. 4.12: CV response of bare carbon working electrode cycled from -0.4V to 0.7V at a scan rate of 20mV/sec in a solution containing Ad <sub>1</sub> dissolved in 25mls of CH <sub>3</sub> CN/H <sub>2</sub> O mixture in the ratio of 1:1 and TEAB as the supporting electrolyte. 122	122
Fig. 4.13: Polyaniline electrodeposited on a bare carbon electrode cycled within the potential range -0.2V to 0.75V at a scan rate of 20mV/sec in a solution containing 0.1M aniline and 1MH <sub>2</sub> SO <sub>4</sub> .-----	123
Fig. 4.14: CV response for a bentonite modified electrode when cycled from -0.2V to 1.0V in a solution containing 0.1g of Ad <sub>1</sub> in 2M H <sub>2</sub> SO <sub>4</sub> . Scan rate 20mV/sec-----	124

Fig. 4.15: CV response obtained when an electrode modified with bentonite, on which Ad <sub>1</sub> in 4MHCl had initially been adsorbed, was cycled from -0.2V to 0.98V in a blank 1.0MHCl solution at a scan rate of 20mV/sec. -----	126
Fig. 4.16: CV response obtained when an electrode modified with Ad <sub>1</sub> in 4M H <sub>2</sub> SO <sub>4</sub> adsorbed onto bentonite was cycled from -0.4V to 1.2V in a blank 1MH <sub>2</sub> SO <sub>4</sub> solution. Scan rate 20mV/sec. -----	127
Fig. 4.17: Cyclic voltammetric response for bare carbon working electrode when cycled from -0.4V to 1.4V at a scan rate of 50mV/sec in a solution containing 0.1g of Ad <sub>2</sub> in 2M H <sub>2</sub> SO <sub>4</sub> . -----	129
Fig. 4.18: Plot of anodic peak current versus square root of scan rates when bare carbon electrode was cycled from -0.4V to 0.14V. -----	130
Fig. 4.19: Plot of anodic peak current versus time for Ad <sub>2</sub> in 2M H <sub>2</sub> SO <sub>4</sub> -----	130
Fig. 4.20: CV response for a bare carbon in a solution containing 0.1g of Ad <sub>2</sub> in 1M HCl. Potential range -0.4V to 0.94V. Scan rate 20mV/sec. -----	131
Fig. 4.21: pH dependence studies - A plot of anodic peak potential Vs pH for Ad <sub>2</sub> in 1MHCl electrodeposited on bare carbon in solutions containing 0.125M, 0.25M, 0.5M, 1M and 2M HCl. -----	132
Fig. 4.22: Plot of surface coverage, $\Gamma \times 10^{-9}$ , versus time of electroactive species in a solution of Ad <sub>2</sub> in 1M HCl -----	134
Fig. 4.23: FTIR spectrum for Ad <sub>2</sub> -----	135
Fig. 4.24: Cyclic voltammetric response of bare carbon in a solution containing 0.1g of Ad <sub>2</sub> dissolved in a 1:1 mixture of CH <sub>3</sub> CN/H <sub>2</sub> O and TEAB as the supporting electrolyte. Potential range -0.4V to 0.68V. Scan rate 20mV/sec. -----	136
Fig. 4.25: Cyclic voltammetric response of a polyaniline modified electrode when the potential was cycled from -0.2V to 0.65V in a solution containing Ad <sub>2</sub> in 2M H <sub>2</sub> SO <sub>4</sub> . Scan rate 20mV/ sec. -----	137
Fig. 4.26: Plot of anodic peak current versus time for two separate peaks (a) associated plant material and (b) associated with PAN- when a PAN modified electrode was allowed to cycle in a solution containing Ad <sub>2</sub> in 2MH <sub>2</sub> SO <sub>4</sub> . Potential range -0.2V to 0.65V. Scan rate of 20mV/sec -----	138
Fig. 4.27: Cyclic voltammetric response when a PAN modified electrode, generated using 1MHCl in place of 1MH <sub>2</sub> SO <sub>4</sub> , was cycled in a solution containing 0.1g of Ad <sub>2</sub> in 2MHCl. Potential range - 0.2 to 0.65V. Scan rate 20mV/sec. -----	140
Fig. 4.28: Plot of anodic peak current versus time for bentonite modified electrode cycled in the potential range -0.2V to 1.0 V at 20mV/sec in a solution containing 0.1g of Ad <sub>2</sub> in 2M H <sub>2</sub> SO <sub>4</sub> . -----	141

- Fig. 4.29: Plot of  $i_{pa}$  versus (a) scan rate and (b) square root of scan rate for a bentonite modified electrode cycled from -0.2V to 1.0V in a solution containing  $Ad_2$  in 2M  $H_2SO_4$ . ----- 141
- Fig. 4.30: Cyclic voltammetric response for bentonite modified electrode cycled from -0.2V to 1.0 V at scan rate of 20mV/sec in a solution containing  $Ad_2$  in 2M  $H_2SO_4$ . ----- 142
- Fig. 4.31: Plot of anodic peak current versus scan rate for  $Ad_2$  in 2M HCl adsorbed onto the electrode surface. ----- 145
- Fig. 4.32: Cyclic voltammetric response when an electrode modified with bentonite onto which  $Ad_2$  in 1.3M  $H_2SO_4$  had been initially adsorbed is cycled from -0.2V to 1.2V in a 1M  $H_2SO_4$  solution. Scan rate, 20mV/sec. ----- 146
- Fig. 4.33: CV response for bare carbon electrode cycled in a solution containing 0.1036 g of  $Ad_3$  in 2M  $H_2SO_4$ . Potential range -0.4 to 1.35V. Scan rate 50mV/sec. ----- 147
- Fig. 4.34: Plot of anodic peak current versus time for  $Ad_3$  in 2M  $H_2SO_4$  studied on a bare carbon. Potential range -0.4V to 1.35. Scan rate 20mV/sec. ----- 147
- Fig. 4.35: Scan rate dependence studies for a bare carbon-working electrode in a solution containing  $Ad_3$  in 2M  $H_2SO_4$ . Response (a), (b), (c) and (d) correspond to scan rates of 10, 20, 50, and 100mV/sec respectively. Potential range -0.4V to 1.35V. ----- 148
- Fig. 4.36: Plot of anodic peak current versus square root of scan rate for  $Ad_3$  in 2M  $H_2SO_4$ . ----- 148
- Fig. 4.37: pH dependence studies for  $Ad_3$  in 2M  $H_2SO_4$  studied on bare carbon working electrode in solution containing 0.125M, 0.25M, 0.5M, 1.0M and 2.0M  $H_2SO_4$ . Potential range -0.4V to 1.35V. Scan rate, 20mV/sec ----- 149
- Fig. 4.38: CV response when bare carbon working electrode is cycled from -0.4V to 0.98V in a solution containing  $Ad_3$  in 1M HCl. Scan rate, 20mV/sec. ----- 150
- Fig. 4.39: Plot of anodic peak current versus time for  $Ad_3$  in 1M HCl when studied on bare carbon within potential range -0.4V to 0.98V. ----- 150
- Fig. 4.40: Plot of surface coverage,  $\Gamma$ , versus time for electroactive species for  $Ad_3$  in 1M HCl. ----- 152
- Fig. 4.41: Plot of anodic peak current versus square root of scan rate for  $Ad_3$  in 1M HCl studied on bare carbon. ----- 152
- Fig. 4.42: CV responses for bare carbon working electrode cycled from -0.2V to 1.35V in solutions containing 0.01M (a) ascorbic acid (b) riboflavin and (c) thiamine in 1M  $H_2SO_4$  electrolyte media. ----- 154

- Fig. 4.43: CV responses for bare carbon in solutions of chemical standards 0.01M (a) ascorbic acid (b) riboflavin and (c) thiamine in 1M HCl. ----- 155
- Fig. 4.44: CV response when a carbon electrode on which  $\text{Ad}_3$  had been initially deposited, is cycled from -0.4V to 1.4V in separate solutions of 1M HCl and 1M NaCl. Scan rate, 20mV/sec. ----- 156
- Fig. 4.45: FTIR spectra for (a)  $\text{Ad}_3$  (b) ascorbic acid (c) riboflavin and (d) thiamine.-- 158
- Fig. 4.46: CV responses obtained when bare carbon working electrode was cycled within the potential -0.4V to 0.7V in a solution containing  $\text{Ad}_3$  in  $\text{CH}_3\text{CN}/\text{H}_2\text{O}$  at a scan rate of 20mV/sec.----- 160
- Fig. 4.47: CV response when a PAN-modified electrode was cycled from -0.2V to 0.65V in a solution containing  $\text{Ad}_3$  in  $2\text{M H}_2\text{SO}_4$ . Scan rate 20mV/sec. ----- 162
- Fig. 4.48: CV response obtained when PAN modified electrodes of three different thickness' (a)  $i_{pa} = 0.95\text{mA}$  (b)  $i_{pa} = 1.55\text{mA}$  and (c)  $i_{pa} = 3.85\text{mA}$  were cycled in a solution containing 0.1g of  $\text{Ad}_3$  in  $2\text{M H}_2\text{SO}_4$ . Scan rate 20mV/sec. ----- 162
- Fig. 4.49: CV response when bentonite modified electrode is cycled in a solution containing 0.1g of  $\text{Ad}_3$  in  $2\text{M H}_2\text{SO}_4$  within the potential range -0.2V to 1.0V. Scan rate 20mV/sec.----- 163
- Fig. 4.50: Plot of anodic peak current versus time for  $\text{Ad}_3$  in  $2\text{M H}_2\text{SO}_4$  on a bentonite modified electrode. Potential range -0.2V to 1.0V. ----- 164
- Fig. 4.51: Plot of anodic peak current versus cathodic peak current for  $\text{Ad}_3$  in  $2\text{M H}_2\text{SO}_4$  electrodeposited on a bentonite modified electrode. ----- 164
- Fig. 4.52: Scan rate dependence studies; Plot of  $i_{pa}$  versus square root of scan rate for  $\text{Ad}_3$  in  $2\text{M H}_2\text{SO}_4$ . ----- 165
- Fig. 4.53: pH dependence studies; Plot of  $E_{pa}$  versus pH for  $\text{Ad}_3$  in  $2\text{M H}_2\text{SO}_4$  on bentonite modified electrode. ----- 165
- Fig. 4.54: Plot of anodic peak current versus scan rate for ascorbic acid adsorbed onto bentonite-modified electrode. ----- 168
- Fig. 4.55: CV response for a bentonite modified electrode cycled from -0.2V to 1.0V in solution containing 0.1M ascorbic acid in  $1\text{M H}_2\text{SO}_4$  (Case 1). ----- 169
- Fig. 4.56: CV response when a bentonite modified electrode allowed to sit for two hours (no potential cycling) in a solution of 0.01M ascorbic acid in  $1\text{M H}_2\text{SO}_4$  before being cycled in within the potential -0.2V to 1.0V in the same solution at a scan rate of 20mV/sec (Case 2).----- 169
- Fig. 4.57: CV response when bentonite modified electrode is cycled from -0.2V to 0.98V in a solution containing  $\text{Ad}_3$  in  $2\text{M HCl}$ . Scan rate 20mV/sec.----- 170

- Fig. 4.58: Scan rate dependence studies; Plot of anodic peak current versus scan rate for  $\text{Ad}_3$  (in 4M HCl)- adsorbed onto bentonite electrode cycled in 1M HCl. ----- 173
- Fig. 4.59: Plot of anodic peak current versus scan rate for  $\text{Ad}_3$  in 2M  $\text{H}_2\text{SO}_4$  when studied on ordinary bentonite. ----- 173
- Fig. 4.60: CV response when heat pillared clay-modified electrode is cycled from -0.4V to 1.4V in a solution containing  $\text{Ad}_3$  in 2M  $\text{H}_2\text{SO}_4$ . Scan rate 20mV/sec. ----- 174
- Fig. 4.61: Plot of anodic peak current versus time for  $\text{Ad}_3$  on pillared clay modified electrode. ----- 175
- Fig. 4.62: Plot of anodic peak current versus scan rate  $\text{Ad}_3$  on pillared clay modified electrode. ----- 175
- Fig. 4.63: CV response when bare carbon working electrode is cycled from -0.4V to 1.4V in a solution containing (a) uncrushed seed and (b) crushed seed in 2M  $\text{H}_2\text{SO}_4$  at a scan rate of 20mV /sec.----- 176
- Fig. 4.64: Plot of anodic peak current versus square root of scan rate for crushed  $\text{Ad}_4$  in 2M  $\text{H}_2\text{SO}_4$ . ----- 178
- Fig. 4.65: Cyclic voltammetric response when bare carbon working electrode was cycled within the potential range -0.4V to 0.98V in a solution containing crushed  $\text{Ad}_4$  in 1M HCl. Scan rate 20mV/sec.----- 178
- Fig. 4.66: Plot of anodic peak current versus (a) time and (b) cathodic peak current for crushed seed in 1M HCl studied using bare carbon----- 179
- Fig. 4.67: FTIR spectrum for  $\text{Ad}_4$  ----- 180
- Fig. 4.68: CV response of the bare carbon-working electrode cycled from -0.4V to 0.7V in a solution containing  $\text{Ad}_4$  in  $\text{CH}_3\text{CN}/\text{H}_2\text{O}$  mixture. Scan rate, 20mV/sec. ----- 181
- Fig. 4.69: Plot of  $E_{pa}$  versus pH for  $\text{Ad}_4$  in  $\text{CH}_3\text{CN}/\text{H}_2\text{O}$  mixture ----- 182
- Fig. 4.70: CV response when a polyaniline (thin film) modified electrode was cycled from -0.2V to 0.65V in a solution containing  $\text{Ad}_4$  in 2M  $\text{H}_2\text{SO}_4$ . Scan rate, 20mV/sec. ----- 183
- Fig. 4.71: CV response for polyaniline (thick film) modified electrode was cycled from -0.2V to 0.65V in a solution containing  $\text{Ad}_4$  in 2M  $\text{H}_2\text{SO}_4$ . Scan rate, 20mV/sec.- 184
- Fig. 4.72: Scan rate dependence studies; Plots of  $i_{pa}$  versus scan rates (5 - 20 mV/sec and 10 - 100 mV/sec) for PAN modified electrode in a solution containing  $\text{Ad}_4$  in 2M  $\text{H}_2\text{SO}_4$ . ----- 185
- Fig. 4.73: CV response for a bentonite modified electrode cycled from -0.2V to 1.0V in a solution containing crushed  $\text{Ad}_4$  in 2M  $\text{H}_2\text{SO}_4$ . Scan rate, 20mV/sec. ----- 187



Fig. 4.74: Plot of anodic peak current versus time for crushed Ad <sub>4</sub> in 2M H <sub>2</sub> SO <sub>4</sub> studied on a bentonite modified electrode.-----	187
Fig. 4.75: Plot of $i_{pa}$ versus square root of scan rate for Ad <sub>4</sub> in 2M H <sub>2</sub> SO <sub>4</sub> studied on a bentonite modified electrode. -----	188
Fig. 4.76: CV response for bentonite modified electrode initially dipped into the solution of Ad <sub>4</sub> in 2M H <sub>2</sub> SO <sub>4</sub> for sometime (with no potential cycling), air-dried and then cycled within the potential -0.2V to 1.0V at 20mV/sec in the same solution.-----	189
Fig. 4.77: Plot of $i_{pa}$ versus $i_{pc}$ for bentonite modified electrode initially dipped into a solution of crushed Ad <sub>4</sub> before subjecting it to potential cycling. -----	191
Fig. 4.78: Plot of $i_{pa}$ versus time for the solution and adsorbed peaks in crushed Ad <sub>4</sub> --	191
Fig. 4.79: CV response when a bentonite modified electrode was cycled from -0.2V to 0.98V in a solution containing Ad <sub>4</sub> in 2M HCl. Scan rate 20mV/sec. -----	192
Fig. 4.80: Scan rate dependence studies; Plot of $i_{pa}$ versus square root of scan rate for crushed Ad <sub>4</sub> in 2M HCl. -----	193
Fig. 4.81: CV response when the potential of the Ad <sub>4</sub> -adsorbed bentonite modified electrode was cycled in a 1M HCl solution within the potential range -0.2V to 1.0V. Scan rate 20mV/sec. -----	194
Fig. 4.82: Plot of anodic peak current versus scan rate for Ad <sub>4</sub> -adsorbed bentonite modified electrode. -----	195
Fig. 4.84: Scan rate dependence studies; Plot of $i_{pa}$ versus scan rate for Ad <sub>4</sub> /H <sub>2</sub> SO <sub>4</sub> adsorbed bentonite modified electrode.-----	198
Fig. 4.85: CV response of bare carbon working electrode when cycled within the potential range -0.4V to 1.35V in a solution containing 0.05g of alkaloid extract in 2M H <sub>2</sub> SO <sub>4</sub> at a scan rate of 20mV/ sec.-----	199
Fig. 4.86: CV response of bare carbon working electrode when cycled within the potential range -0.4V to 1.4V in a solution containing 0.05g of Flavonoid extract in 2M H <sub>2</sub> SO <sub>4</sub> at a scan rate of 50mV/ sec.-----	200
Fig. 4.87: CV response of bare carbon working electrode when cycled within the potential range -0.4V to 1.4V in a solution containing 0.05g of diterpene extract in 2M H <sub>2</sub> SO <sub>4</sub> at a scan rate of 50mV/ sec.-----	200

## ABSTRACT

The results presented in this thesis show that electrochemical analysis have been successfully carried out on raw plant material of *Adansonia digitata* fruit. All the four components of the *A. digitata* fruit, i.e. the greenish hairy outer covering, the woody covering, the inner white pulp and the seed have redox active moieties and gave clearly defined cyclic voltammetric responses when studied using bare carbon working electrode. They all displayed oxidation/reduction peaks at various potentials.

The results show that both hydrochloric and sulphuric acid electrolyte media are suitable for the analysis of *A. digitata* fruit components. High electrodeposition rates and redox efficiencies revealed the significant role of the proton to the redox process. This was also confirmed by the poor response obtained in the non-aqueous media containing  $\text{CH}_3\text{CN}/\text{H}_2\text{O}$ .

Scan rate dependence studies showed that the processes were diffusion controlled on bare carbon working electrode but in the case of modified electrodes, there were cases of surface attached species. The processes in the white inner pulp and the seed were shown to be one proton, one electron, processes from the pH dependence studies.

Modification of the working electrode with a conducting polymer, polyaniline, and clay montmorillonite gave cyclic voltammetric responses with very well defined peaks. The modified electrodes yielded enhanced peaks with potentials shifted negatively suggesting there was electrocatalysis. The largest shifts were observed in the inner pulp and the seed parts of the fruit. The response from the clay-modified electrodes on the other hand, for all the fruit components showed larger shifts as compared to those of polyaniline modified electrodes.

Electrochemical signals of chemical standards of ascorbic acid, thiamine, riboflavin and chlorophyll, i.e. compounds known from other researchers to be present in parts of *A. digitata* fruit show that, the CV responses obtained from the standards closely match those in the actual plant materials. FTIR analysis confirmed the presence of the expected functional groups. The electrochemical signals on bare carbon confirmed the presence of flavonoids and terpenes in the woody part of the fruit.

The electrochemical results in the modified electrodes also confirm the presence of ascorbic acid in the seed of *Adansonia digitata*. The results show that the ascorbic acid redox peak is greatly enhanced and the oxidation/reduction peaks coincide with those of the corresponding chemical standards. It is also shown that ascorbic acid is adsorbed on the clay modified electrodes.

Physical parameters with respect to the various components show that the density of the whole fruit is  $0.3\text{g/cm}^3$  while for the individual parts the seed was found to have the highest density. The pulp had the highest moisture content, 12.5%, and it was the only part that was highly soluble in both organic and aqueous solvents. The other components were mainly soluble in organic solvents.

Calorimetric measurements revealed that the seed has the highest internal energy and the internal energy of the edible parts gave values that are comparable to what has been obtained by other researchers in Senegal and Malawi.

***Adansonia digitata* Tree (Baobab)**

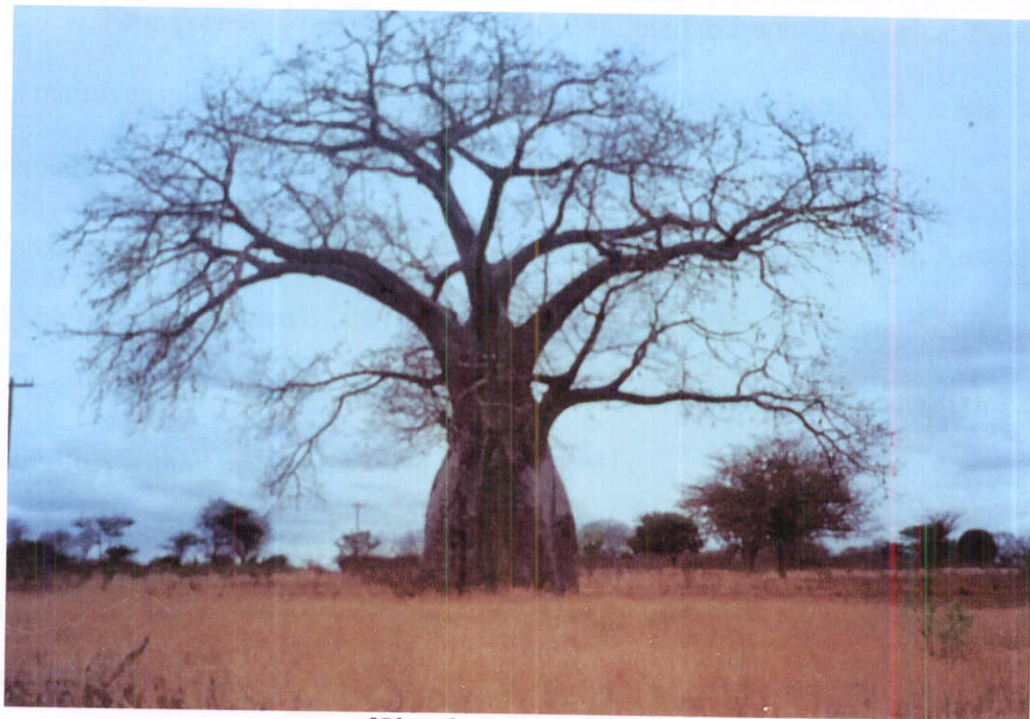


[Photo by F. Gachathi]

## CHAPTER ONE

### INTRODUCTION

#### 1.0 *Adansonia digitata* L.

##### 1.1.0 Background Information

The baobab tree, *Adansonia digitata* Linn, is ranked among the most fantastic and intriguing vegetable productions of the Earth. It belongs to a small family mainly found in the tropics, Bombacaceae otherwise known as the COTTON TREE family. It is made up of trees with enormous girth. There are twenty-nine genera with about 225 species recognized worldwide [1]. These are divided into six tribes, four of these are restricted to tropical America, one to Australasia (7 genera and 50 species) and remaining tribe, *Adansonieae*, is pantropical.

Four genera of the *Adansonieae* are restricted to tropical America; *Bombacopsis* is mainly tropical American but with 1 or more species in tropical Africa and *Bombax* extends from India to New Guinea. Finally *Adansonia* with 9 rather similar species occurs in tropical Africa (*A. digitata*), western Madagascar and western Australia (*A. gregorii*). This pattern of species distribution is in itself most unusual; plants of western Australia have a great deal in common with those of Cape Province of South Africa, but not often with plants from tropical Africa [2].

Of the nine species in the genus *Adansonia*, only *A. digitata* is known to occur in tropical Africa, the rest e.g. *A. gregorii* and *A. grandidieri* are found in Australia, Madagascar and parts of Asia. *Adansonia digitata* commonly known African baobab, cream-of-tartar tree or monkey bread occurs in most of the countries of Africa, south of the Sahara, except for Liberia, Burundi, Uganda and Djibouti [3]. It is considered indigenous to 23 countries and introduced to 33 more.

It is classified botanically as follows, [4, 5];

Phylum,	-	Agiospermae
Sub-phylum	-	Dicotyledons
Division	-	Lignosa
Order	-	Tiliales
Family	-	Bombacaceae
Genus	-	Adansonia

*A. digitata* has attracted a lot of attention from many botanists and conservation workers during the last few decades. A French naturalist, Michel Adanson first introduced it into Europe in the middle of the 18th century, and Linnaeus dedicated the genus and species to him [3]. The tree is famous for four things; (a) It's geological antiquity and the great age to which its specimens may live. The baobab is one of the largest and longest-lived trees, its known to have lived for up to 3000 years. (b) It's monstrous trunk or boles; it may have a trunk as thick as 100 feet in circumference. (c) It's markedly disjunctive distribution and (d) the usefulness of many of its parts to man and wild animals.

In Kenya only two genera of the Bombacaceae family grow i.e. *Adansonia* and *Bombax*. However *Adansonia* is the more prominent with the *Adansonia digitata* being the only species [6].

### 1.2.0 Ecology and Distribution in Kenya

The baobab tree, usually growing up to 20 m high, is typically found in the thorny woodlands of African savannas characterized by low attitudes (up to 1250 m). The northern limit of the baobab is Southern Mauritania (Lat. 16½ °N) and from whence it extends eastwards through the Sahel to the western Sudan [7]. Its southern limit, which

extends from southern Angola on the East Coast (15 °S) to the tropic of Capricorn in the Transvaal includes the northern areas of the Kalahari desert and Kruger national parks.

In Kenya it is found below the 1000m contour chiefly in *Acacia – Commiphora* bushland and scrub and the semi-arid grasslands of northern Kenya. It is widely distributed in parts of Machakos, Kitui, Taita-taveta, Garrissa, Meru, Isiolo and Kajiado districts. It is also found in the humid coastal region of Kenya especially in Kwale and Lamu districts. Some planted baobab trees are found in Baringo, East Pokot and Turkana districts. It is one of the 150 species of indigenous fruit trees in Kenya and in a survey carried out by scientists from Kenya Forestry Research Institute (KEFRI) and International Centre of Research in Agroforestry (ICRAF) in 1998 [8] in Kitui district, farmers ranked it fourth most preferred indigenous fruit tree.

It generally grows in areas with annual rainfall of between 200 mm and 1500 mm and extended dry periods. It shows preference for well-drained soils that are acidic (pH<6.5) preferably with sandy top soils overlaying loamy substrates. It is found in areas prone to seasonal water logging. It is not found in areas of deep sands presumably because it is unable to obtain sufficient anchorage and moisture [9].

The baobab is a home for many birds, which frequently roost or nest in it. It also produces shelter for the bush baby and various venomous snakes including the boomslang. Bees and many insects also live in it. It has numerous and interesting relationship with its environment, the most useful being its ability to withstand drought and fire, two major natural hazards to plant life in the drier Savannah region of Africa. They also exhibit peculiar habits at the end of their life, such as hallowing and enormous bulging of the bloated trunks and a greater bending down of the branches which makes

them quite unlike other trees especially as they are bare of leaves for the greater part of the year.

### **1.3.0 Botanical Characteristics**

#### **(i) Canopy of the Baobab**

This is usually spreading with the branches either well distributed along the trunk or confined to the top. In the young trees the branches tend to be more erect but they droop with age. The young branches are often hairy and ashy at least from the last node of the apex. The old branches are stout but generally taper toward their ends. During periods of drought the branches reduce in size, weaken and may often snap.

#### **(ii) Bark**

The bark is soft, smooth, fibrous and reddish brown, grayish brown or purplish gray in colour. It contains tannins, bark crude protein (30-45%); ash, (8.4-13.5%), Ca (2.2 – 4.5%) and crude fibre (42-57%). The bark of the leaf-bearing branches is normally ashy on the last node. Below the outer waxy layer of the bark is a green layer, which most likely assists with photosynthesis during periods when the tree has shed its leaves.

#### **(iii) Trunk**

The trunk is enormous as mentioned earlier and may grow to more than 10 metres in diameter. It bears stout, stiff tapering branches. The obesity of this tree is manifested in its early life where the young seedlings develop bulb like stem.

#### **(iv) Wood**

The wood is fibrous, soft and spongy that a rifle bullet will pass right through the trunk and whistle away beyond it, yet is not easy to cut. The spongy tissue causes the axe to bounce off rather than cut and if driven into the trunk, the axe is extricated with



difficulty. The wood is unsuitable for cutting into planks and makes poor firewood and charcoal. It is unfit for use unless thoroughly dried.

#### **(v) Roots**

The seedlings have a thick turnip-like root while the mature tree has a thick strong prominent tap, which at six months is three times the length of the seedling. The root grows fast but never penetrates far beyond a depth of 2 metres. The mature thick and extensive lateral roots end in clusters of potato-like tubers. These are the ones that anchor the baobab onto the ground.

#### **(vi) Leaves**

The leaves on young plants are simple but on older trees they are compound and arranged like digits with 5 or 7 leaflets which are spear-shaped and sometimes have rounded tops. The leaflets, which are usually up to 17 cm long and 7 cm broad, are borne alternately at the end of the branches or on short spurs on the trunk. The leaves fall off during dry season and the old tree begins each rainy season by producing simple leaves.

#### **(vii) Flowers**

The baobab has large, waxy or glossy white blossoms up to 20 cm in diameter, borne singly on long stalks up to 40 cm long. They are produced after the dry season during the onset of rainy season. Pollination is mostly by fruit bats and at the coast the bush babies also play a major role. The flowers normally open at night and the process from ball-like bud to an exquisite flower takes only an hour or so. Their beauty only lasts for the night and by morning the petals become limp. While on the trees the flowers give off a sweet fragrance but when plucked they emit a very unpleasant smell. They begin to open from late afternoon to soon after sunset. The whole process, from when it opens to when it falls off the tree, never lasts more than 24 hours.

### **(viii) Fruit**

The fruit is a large hard-shelled, yellow-brown capsule. It comes in various sizes and shapes ranging from rounded to ovoid and many times oblong, from 15 to 45 cm long. It is woody when ripe and covered with greenish-yellow or yellowish-grey fuzz/velvety hairs. It is indehiscent (meaning that it releases its seeds, propagates, by decay rather than splitting open). When the fruit falls off the tree and cracks, ants are able to enter and feed on the pulp in which the seeds are embedded. In this way soil is introduced into the fruit and in the rainy season they can germinate.

Inside the shell, are many seeds embedded within a white-pink dry edible pulp. There are more than 100 seeds embedded within the dry fruit mass, each with an approximate size and weight of 5 x 10 mm and 0.46 gm respectively. The seeds have a tough husk and a soft oil kernel devoid of starch. The husk makes up to 24 % of the seed weight and the kernel 76% [10]. The fruits mature within the long dry season i.e. between June and October. The relative proportions of the different elements of the fruit are as follows;

- Outer shell     - 45%
- Pulp             - 15%
- Seeds            - 40%

### **1.4.0 Economic Uses**

The baobab has got many uses and plays a useful role in the economy of the inhabitants of the area where it occurs because practically all parts of the tree are useful. It provides food for man and livestock, clothing, medicine as well as sundry necessities for hunting, fishing and entertainment. On occasions, the hollow trunks have served as

houses, prisons, storage barns and even places of refuge from mauling animals. These various uses are discussed below.

**(a) Fodder**

Young leaves provide valuable fodder especially in dry areas and stocks and wildlife browse them. Fruit pods and seeds are also fed to stocks. Cattle and goats browse on fallen dry leaves and flowers. Livestock and game often destroy the young trees and during droughts, donkeys and game animals chew both the bark and fibrous wood for sap. Baobab seedlings of up to three years old are hard to find as elephants and goats find the whole plant palatable.

The elephants seem to be the only agent capable of destroying this tree. Under conditions of enough forage, elephants will not necessarily feed on the baobabs but during draught, the trees suffer badly from elephant damage. They may even be essentially eliminated over large areas, as was the case in Tsavo East National Park in the late 70s.

**(b) On Farm forestry**

Often left standing when land is cleared for cultivation, the baobabs are useful for provision of fruits. A medium sized baobab tree can produce up to 200 kg of fruit and since the fruits play an important role in the local diets, the baobab is sometimes considered as a crop. The trees are also favoured for hanging beehives and their gigantic size makes them useful in honey production.

**(c) Water Storage**

In dry regions the baobab plays a vital role in water storage. The top of the trunk is usually hollowed for rainwater and dew to collect and this may be the only water available for miles around. This is by far the most common use for the intact tree and has

a long history of usage. In northern Kenya and Sudan, hollow trees filled with water were used by travellers in order to successfully cross the otherwise waterless country. The trunk has a high water content and manageable blocks of trunks can be cut out and water squeezed out for drinking. A medium tree can contain up to 1800 litres of water [9].

#### **(d) Fibre**

The tree is a major source of fibre. The inner bark yields a fibre that is particularly strong and durable. The bark is often completely stripped from the lower trunk yet the tree is able to survive and regenerate a new bark. The baobab fibre is made by pounding the bark and is normally made into different kinds of ropes with strength and reliability. When dampened the rope is much stronger and unlikely to break when used for lifting high objects. The fibre is used in honey harvesting for raising beehives high into trees, cordage ropes, harnessing straps, mats, nets, snares and fishing lines. Its also used in fibre cloth, musical instruments strings and even water proof hats amongst other things. The fibre is best for making the famous '*kiondo*' baskets.

#### **(e) Food**

The baobab is a source of staple diet for many communities in Africa, sometimes used only during famines but in some places, as a regular item of diet. The fruit is the principal item of food, though the leaves too are eaten as vegetable. The white powdery pulp found in the fruit is very rich in vitamin C. It is edible though mealy and slightly bitter or sour. The pulpy mass is about 50% soluble in water yielding a mucilaginous liquid and an insoluble residue of cellular tissue. The liquid has many additional uses, for example, it is used as a sauce for food, and mixed with milk and seasoned to make yoghurt. Sometimes it is poured in boiling water and stirred to flavour fermented porridge

by the Kamba community in Kenya. The fruit pulp makes refreshing drink, when boiled in water, it makes sweet beverage that is taken cold. In West Africa, the pulp is also used in hot and cold drinks in rural areas. It has recently become a popular ingredient in iced products in urban areas in Mali [11]. The palatable drink obtained when its soaked in water can be used to treat vitamin C deficiency complaints and as an appetizer. It is also used as a substitute for cream of tartar in baking, to curdle milk, smoke fish and coagulate rubber.

The pulp, though dry at first has a pleasant wine-gum flavour once moistened in the mouth, this is much appreciated by children. Lumps of dry pulp with seeds embedded within are commonly sold as children's sweets in towns here in Kenya. They are dyed bright colours and referred to as *Mabuyu* [9-10]. In Kenya the fruits are also sold in towns in areas where the trees grow especially Mombasa, while in Zambia it's a useful source of income when almost nothing else is available [12].

The seeds are acidic and edible when fresh, dry or cooked. They are widely used as food, prepared by boiling, roasting, soaking or fermenting and they taste like almonds. They are roasted and used as a coffee substitute [9]. The seed pulp is used as a fermenting agent by the Kambas in some local beer. Oil can be extracted from the seed kernel but this is not common. Traditionally, baobab seeds and pulp especially in West Africa are roasted, sun-dried or fermented to extend shelflife and enhance nutritive value [13].

The young tender leaves of baobab are used as green or dried vegetables, rich in vitamin A and calcium. They have also been reported to be rich in vitamin C [2,13]. In West Africa the leaves are used in the daily sauce that accompanies cereal or tuber porridge. They are pounded in a mortar with other condiments and stewed in a pot. They thicken the stew, giving a glutinous consistency and a pleasant taste. During the rainy

season when the leaves are tender people harvest them fresh and in the last month of the rainy season they are harvested in great abundance and dried for domestic use and for marketing during the dry season. The leaves are typically sun-dried and either stored as whole leaves or pounded and sieved into fine powder. In markets, the powder is the most common form. Baobab leaf consumption of dried leaf in Segou area of central Mali is estimated at about 2.5kg/person/year i.e. almost 7g/person/ day. Other reports indicate that 40 to 50g of baobab leaf powder is commonly provided in the daily sauce that accompanies the main meal [10].

The small stems and roots of the seedlings, are also eaten as vegetable and in times of famine the mature thick root ends, which is composed of clusters of potatoes-like tubers are eaten.

#### **(f) Medicine**

The fruit pulp is used for curing fever and dysentery and was at one time exported to Europe for this purpose [9]. It is also used in the treatment of small pox and measles as an eye instillation. The leaves, and to a lesser extent, the bark are used for curing fevers and inflammations. The leaves have also been shown to have hyposensitive and antihistamine properties, being used to treat kidney and bladder diseases, asthma, general fatigue, diarrhea, insect bites, guinea worm, etc. They are also used medicinally as a diaphoretic, an expectorant, to check excessive perspiration and as an astringent.

Leaf and flower infusions are valued for respiratory, digestive disorders and for eye inflammations. The seed paste is used for curing teeth and gum diseases. The fruit, pulp, seed and bark are reputedly used as an antidote to *Strophantus* poisoning. Gum from the bark is used for cleansing sore and as an expectorant and a diaphoretic.

The bark is used in steam baths for calming shivering and high fever. A decoction from the roots is taken as a remedy for impotence and kwashiorkor. The bark infusion is used to cure gastric, kidney and joint diseases. The bark has been used against malaria in several countries, for example it's used as a substitute for quinine in Tanzania and Guinea. Dried bark is used for sickle cell anemia in Nigeria [14 -15]. In Kenya, decoction of the roots is taken as remedy for lassitude while the bark is used for bathing infants if they are weak.

**(g) Wood**

The wood is long fibred and is not suitable for fibreboards but it produces a paper that is remarkably strong, tough and tear resistant. It is also used for making canoes, wooden platters and trays, boxes, floats for fishing nets, etc.

**(h) Soap**

Ash from fruit shell, barks and seeds are rich in potash and therefore widely used in soap making. The fruit outer shell ash contains 47% potash, while from the burned seeds contain 31% potash and 34.2% phosphates. This makes them useful as fertilizer as well as in soap making. The soap can be prepared by boiling the bark and fruit in oil. The wood ash has been used as salt substitute.

**(i) Shell**

The baobab fruit shells can be hollowed out and used as scoops or dishes for food or liquid snuff box and they also make excellent rattraps. A British Company imports them as musical shakers [10]. The shell and seeds are used as fuel, which is used by potters to smoothen earthenware necklaces before firing. The powdered shell may be smoked as tobacco substitute or added to snuff to increase the pungency.

#### **(j) Seed Oil**

Oil has been extracted from the seed and the standard laboratory method used in extracting the oil uses petroleum ether. Crushed seeds are mixed with ether and heated. The vapour is condensed and the resultant liquid is heated again and the ether evaporated off. Oil may also be distilled directly from the seeds without the use of ether by straight-forward heat and distillation. This is the case in Senegal. An export company in Arusha, Tanzania heats seeds in a water bath and then presses them whole. The resulting oil is filtered. The company markets the product as a "clear yellow oil" with slightly nutty odour and taste and supplies it for export [10].

#### **(k) Feed Cakes**

In Madagascar, baobab seeds were being processed whole as livestock feed cakes in the 1950s and 1960s. Six hundred tonnes of baobab cakes were fabricated in 1961 alone. Oil was a by-product [10].

The seeds embedded in fruit pulp were first mechanically crushed in rollers to produce a mixture comprising of 45% shell and 55% kernel. This seed mixture was passed through a hot press at  $105^{\circ} - 110^{\circ}\text{C}$  and the oil squeezed out. Left behind in the press were dark brown slabs marketable as animal feed. They were said to have a pleasant smell that would not change over time. Baobab feed cakes contains quite a high proportion of cellulose (19%) strongly lignified and hence not easily digested by animal. For this reason, and also because of the relatively low protein level in some baobab varieties, it was considered necessary in Madagascar to mix the feed cakes with other ingredients before feeding to livestock.



While the feed cakes are relatively low in protein and high in cellulose, they have high levels of Calcium and vitamins B<sub>1</sub> and C. They are easy to store and do not easily decay which makes them an attractive supplement to other vegetable feeds for animals.

#### **(I) Others**

The roots produce useful red dye. The flower pollen mixed with water has been used to make glue. The fruit pulp burns with an acid irritating smoke and has been used as a cattlefly repellent. The pulp extract has been used as a hair-wash. The bark is used for tanning and is also boiled for days to extract a substance poisonous to ants.

Apart from the economic importance the tree has also got a lot of cultural importance among many African communities.

#### **1.5.0 Chemical composition of the Tree Parts**

The fruit pulp is very nutritious and as indicated earlier, about 50% is soluble in water yielding a mucilaginous liquid and an insoluble residue of cellular tissue. Half of this amount comprises of reducing sugars acids, proteins and the remainder is chiefly made of pectin substances [16].

The pulp has particularly high values for carbohydrates, energy, calcium, potassium and vitamin C. It also contains appreciable quantities of tartaric and potassium bitartrate [13, 17-20]. Vitamin C (ascorbic acid) content is especially impressive, for example in Mali, levels ranging from 170-500mg / 100g and averaging 303mg/100g have been reported [10]. This is much higher than that of oranges (57mg/100g), grape juice (38mg/100g) and strawberries (59mg/100g). Just 20-26g of pulp from an average baobab fruit could supply the human daily requirements of 60-80mg. There is great stability in the levels of vitamin C in fruits of individual *A. digitata* trees from year to year. This is

especially interesting for trees producing fruits with high vitamin C content, as they could be expected to maintain these high levels over many seasons.

*Adansonia digitata* leaf on the other hand is rich in vitamin A and calcium. It is reported to be an excellent source of calcium, iron, potassium, magnesium, manganese, molybdenum, phosphorous and zinc and has an amino acid composition that compares favourably with that of an 'ideal' protein [11,13,22]. The dried leaves are rich in  $\beta$ -carotene and contain an important amount of mucilage while young tender leaves, used as green or dried vegetables, are rich in vitamin A. In a study carried out in Mali, the average vitamin A values of dried leaf material ranged from 9.3 - 27.2mg/g retinol equivalent [13]. Vitamin A essential for normal growth, vision and general good health, is usually estimated in human diets in terms of 'retinol equivalent' (1mg retinol equivalent = 6mg  $\beta$ -carotene or 12mg  $\alpha$ -carotene).

In Malawi proximate analysis of the seed kernel at 92.12% dry matter indicated that it was 29.6% fat, 28.7% crude protein and 7.3% crude fibre while K and Ca were found to be 1186 and 456mg per 100g respectively. They were also found to contain phosphorous, sodium and iron in smaller quantities i.e. 5.8mg, 75.2mg and 0.5mg per 100g respectively [21]. They are also reported to contain appreciable quantities of tartaric acid and potassium bitartrate. *Adansonia digitata* seeds have been reported to contain high levels of vitamin B<sub>1</sub> (1.5mg/100g) and Vitamin C and low levels of thiamine, riboflavin and niacin [10].

From other work done in Nigeria, Senegal and Malawi the composition of the *A. digitata* fruit is as shown in table 1.1 below.

Table 1.1: Chemical Composition of *A. digitata* fruit as reported in Kenya, Senegal, Malawi and Nigeria.

Content of 100g edible portion	Kenya [22]	Malawi [20,21]	Senegal [18]	Nigeria [19]
Dry matter (%)	84	86.8	85.5	-
Ash (%)	4.3	5.0	-	-
Energy (KJ)	1214	1480	846	-
Carbohydrates (g)	76.7	79.4	81.3	-
Crude protein (g)	2.2	3.1	2.5	-
Fat (g)	0.8	4.3	0.8	-
Cellulose/fibre (g)	6.8	8.3	11.4	-
Phosphorous (mg)	118	45	1330	5
Calcium (mg)	284	115.6	530	60
Potassium (mg)	-	2,836.4	-	-
Magnesium (mg)	-	209	-	208.8
Fe (mg)	7.4	5.8	2.52	4.4
Na (mg)	-	18.8	-	-
Manganese (mg)	-	-	-	0.6
Zinc (mg)	-	-	-	2.4
Copper (mg)	-	-	-	0.6
Vitamin C (mg)	270	179	360	337
Thiamine (Vit B <sub>1</sub> ) (mg)	0.37	-	0.04	-
Riboflavin (Vit B <sub>2</sub> ) (mg)	0.06	-	0.07	-
Nacin (Vit. PP )(mg)	2.1	-	2.16	-

The baobab seed kernel also contains oil and its proportional by weight has been estimated by various researchers to be as follows.

- 12.5% (Senegal)
- 15.18% (Madagascar, 1963)
- 16% (India, 1948)

- 18% (Senegal)
- 23% (Nigeria 1996)
- 32% (Tanzania 1991).
- 30.7% (Senegal)

The average of these estimates is 12% equivalent to 714 mg of oil per seed. This equates to 16% of the whole seed mass [9 and the references therein].

Baobab oil is described as semi-fluid, golden yellow and gently scented. Various chemical indicators show its strongly non-siccative (non-drying). Another advantage it exhibits over other oils is its limited tendency to deteriorate in storage. From work done in Malawi [21], fatty acid composition is reported to be;

Palmitic acid	30.8%
Stearic Acid	5.5%
Oleic Acid	31.7%
Linoleic acid	25.2%

Other physico-chemical properties reported include;

Refractive index ( $n_d^{40}$ )	1456
Saponification value (mgKOH/g)	172.9
Iodine value	155.5
Unsaponified matter (g/kg)	40.5
Free fatty acid (g/kg)	6.8

The oil from the baobab seed is similar to that of groundnut since the major acids present in both oils are palmitic, oleic and linoleic. However, *A. digitata* has twice as much palmitic acid, while the reverse is true for oleic acid. However unlike groundnut oil, *A. digitata* oil contains malvalic acid, a toxic cyclopropanoid fatty acid. This would limit its use for human consumption but the malvalic acid can be eliminated by hydrogenation.

The baobab seed husk is hard and adheres strongly to the kernel, this makes its removal very difficult and is the biggest obstacle to industrial processing. In northern Togo, however, this has been achieved by boiling the seed in water and manually dehulling it. This labour-intensive system appears to be the only method thus far developed for separation of the two elements. There is no evidence found in the research of automated dehulling systems, which may be attributed to the small size of the seed and the strong bond between the husk and the kernel. Most processing is therefore based on the whole seed.

Other phytochemical compounds that have been reported in different parts of the plant include triterpene, flavonoid steroids and lipids in the roots; triterpenes, coumarins and steroids in leaves and triterpenes in the bark [23-24].

The main objective of this work was to study the fruit of *Adansonia digitata* using electrochemistry in particular cyclic voltammetry and derivatized electrodes.

## CHAPTER TWO

### 2.0 ELECTROCHEMISTRY

#### 2.1.0 General Introduction on Utilization/application of Electrochemistry

An increasing number of chemists use electrochemistry as a characterization technique in a fashion analogous to their use of infrared, UV-visible, NMR, and ESR spectroscopy. Analytical techniques based on electrochemical principles make up one of the three major divisions of instrumental analytical chemistry, the other two being spectroscopic techniques and chromatographic techniques.

Some of the applications of electrochemistry have occurred in the areas of organic and inorganic chemistry as well as biochemistry. The applications have ranged from mechanistic studies to the synthesis of unstable or difficult to obtain species. The control of an oxidation or reduction process through electrochemistry is much more precise than is possible with chemical reactions. In the area of inorganic chemistry, electrochemistry has been very useful in determination of formulae of coordination complexes and electron transfer stoichiometry of new organometallic chemistry.

Numerous exciting extensions of electrochemistry to the field of analytical chemistry have also occurred. A series of selective-ion potentiometric electrodes have been developed such that most of the common ionic species can be quantitatively monitored in aqueous solution. A highly effective electrolytic moisture analyzer has become the method for quantitative moisture analyses of gases. In practical analysis, electrochemistry is used in the pesticide analyzer, which uses a coulometric electrochemical system as a gas chromatographic detector. Another practical development is the polarographic oxygen membrane electrode, which responds to the partial pressure of oxygen either in gas or the solution phase [25].

### 2.1.1 Origin and Overview of Electrode Processes

When a piece of metal is immersed in an electrolyte solution, an electric potential difference is developed between the metal and the solution. This phenomenon is not unique to a metal and electrolyte; in general whenever two dissimilar conducting phases are brought into contact, an electric potential is developed across the interface. Considering a case of two dissimilar metals in contact; when two atoms condense to form a solid, the various atomic orbital energy levels broaden and merge generally forming two bands of allowed energy levels. The band of levels that correspond to the bonding molecular orbital in a small molecule is known as the valence band and is usually completely filled. The band of levels corresponding to non-bonding molecular orbital is the conduction band. This band is partially filled in a metal and is responsible for the electrical conductivity. Electrons fill the conduction band up to an energy level called the Fermi level as shown in fig 2.1.

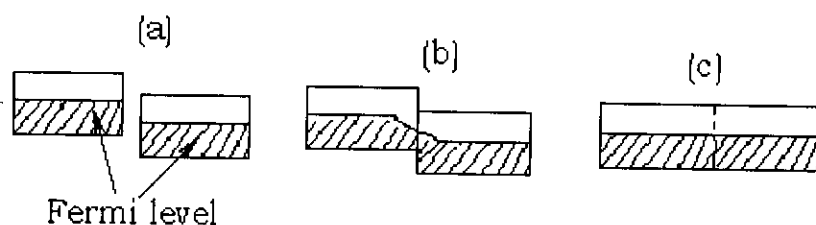


Fig. 2.1: The conduction bands of two dissimilar metals (a) when not in contact (b) at the instant of contact and (c) at equilibrium.

The energy of the Fermi level, relative to the zero defined by ionization, depends on the atomic orbital energies of the metal and on the number of electrons occupying the band and therefore it varies from one metal to another. When two dissimilar metals with Fermi levels at different energies are brought into contact, electrons flow from the metal with the higher Fermi level into the metal with the lower Fermi level. This electron transfer results in a separation of charge and an electric potential difference across the phase

boundary. The effect of the electric potential difference is to raise the energy of the conduction band of the second metal and lower the energy of conduction of the first band until the two Fermi levels are equal in energy. After this no further electron transfer takes place. This means that the intrinsically lower energy of the second-metal conduction band is exactly compensated by the electrical work required to move an electron from the first metal to the second against the electric potential difference.

The background of this is the band theory, which explains very well the electrical properties of materials based on their electronic structures. Solids consist of a large number of atoms brought together in a regular way. Each of these atoms contains atomic orbital, which overlap with each other in all directions producing molecular orbital. These many orbitals spread out according to their energies forming energy bands. The number of electrons in these bands depends on the number in the original atomic orbitals.

In semi-conductors and insulators, there are only enough electrons to completely fill only a number of energy bands leaving the rest of the energy bands empty. The highest filled band is called valence band while the next higher band, which is empty is called conduction band. The two bands are separated by an energy gap or band gap. In order to increase the energy of the electrons, they need to be raised from the valence band to the conduction band across the gap. But the electric fields normally encountered are not enough to accomplish this, so high temperatures are required depending on the magnitude of the energy gap for a number of electrons to gain enough thermal energy to be raised to the conduction band. We therefore have electrons in the unfilled conduction band which participate in conduction. A corresponding number of vacancies or holes are also created in the electron population of the valence band and these have the effect of carriers of positive charge. In this way, the valence band, makes a contribution to the



conduction process. Therefore, the electrons in the almost empty conduction bands and holes in the almost filled valence bands make electronic conduction possible in semiconductors. A very wide energy (or band) gap results in insignificant thermal excitation and hence the solid is an insulator.

In metals, the highest energy band that is occupied by the electrons is only partially filled. The high conductivity in metals is a result of partially occupied bands (i.e. partially filled conduction bands; a partially empty valence band or a zero band gap). A very similar process occurs when a metal is placed in a solution containing its ions e.g. copper metal in a copper solution. The copper ions may deposit on the metal, accepting electrons from the metal conducting band and leaving the metal with a small positive charge and the solution with a small negative charge. When a more active metal is used, the reverse happens i.e. few atoms leave the metal surface as ions, giving the metal a small negative charge and the solution a small positive charge. The direction of the charge transfer is dependent on the metal, but in general charge separation occurs and an electric potential difference is developed between the metal and the solution.

When two dissimilar electrolytes are brought into contact there is generally a charge separation at the phase boundary due to the different rates of diffusion of the various ions. The resulting electric potential difference is referred to as a liquid junction potential. In general whenever two conducting phases are brought into contact, an interphase electric potential difference will develop [26,27].

Electrochemical cells, generally defined as two electrodes separated by at least one electrolyte phase, have a measurable potential difference between the two electrodes whether, the cell is passing a current or not. Potentials are usually measured and quoted with respect to a reference electrode. Any changes in the cell therefore are ascribed to

the working electrode and its potential is said to be observed or controlled with respect to the reference. That is equivalent to observing or controlling the energy of the electrons within the working electrode. By driving the electrode to more negative potentials the energy of the electrons is raised, and they will eventually reach a level high enough to occupy vacant states on species in the electrolyte. In this case, a flow of electrons from electrode to the solution occurs (reduction current). Similarly imposing more positive potential can lower the energy of the electrons and at some point electrons on solutes in the electrolyte will find more favourable energy on the electrode and transfer there. The flow of electrons from the solution to electrode is an oxidation current (see fig. 2.2). The critical potentials at which these processes occur are related to the standard potentials,  $E^\circ$ , for the specific chemical substances in the system.

In general when the potential of an electrode is moved from its equilibrium value (i.e. its zero-current), towards more negative potentials, the substance that would be reduced first (assuming that all possible electrode electrons are rapid) is the oxidant in the couple with the least negative  $E^\circ$  (i.e. most positive). On the other hand, when the potential of the electrode is moved from its zero-current value towards more positive potentials, the substance to be oxidized first is the reductant in the couple of the least positive  $E^\circ$  (i.e. most negative).

Two types of processes occur at electrodes. One kind, known as the *faradaic* processes, comprises of those discussed in the above paragraph in which charges (e.g. electrons) are transferred across the metal-solution interface. This electron transfer causes oxidation or reduction to occur and they are governed by Faradays law (i.e. the amount of chemical reaction caused by the flow of current is proportional to the amount

of electricity passed). Electrodes where faradaic processes occur are sometimes referred to as charge transfer electrodes.

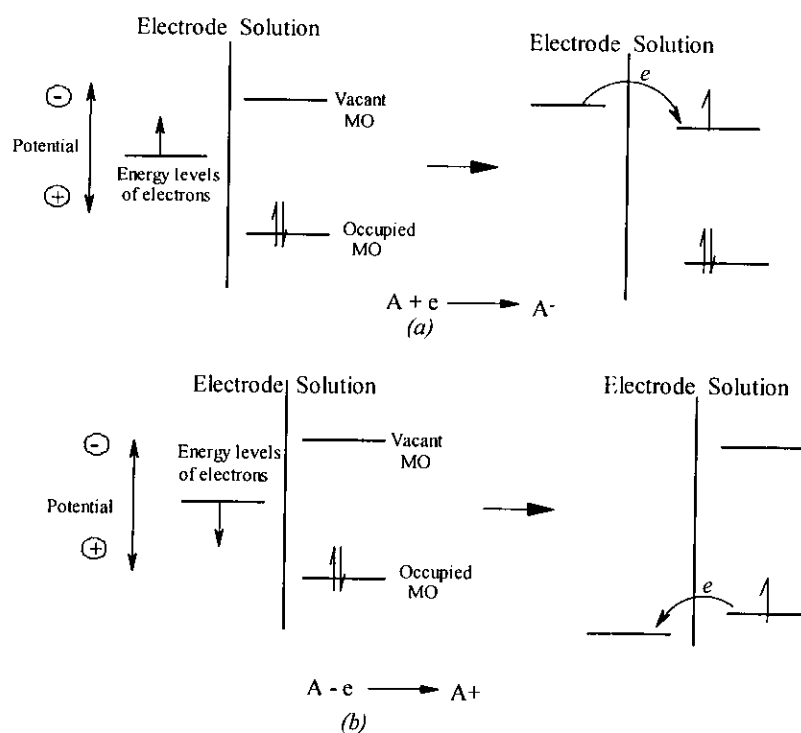


Fig. 2.2: Representation of (a) reduction and (b) oxidation of a species A in solution. The molecular orbitals (M.O) of a species A shown are the highest occupied (M. O) and the lowest vacant M. O. These correspond in an approximate way to the  $E^\circ$ 's of  $A/A^-$  and  $A^+/A$  couples.

Under certain conditions a given electrode-solution interface will show a range of potentials where no charge transfer reactions occur because such reactions are thermodynamically or kinetically unfavourable. However processes such as adsorption or desorption occur and the structure of the electrode-solution interface can change with changing solution composition. Such processes are called *nonfaradaic* processes. Although charge does not cross the interface under these conditions, external currents can flow (at least transiently) when the potential, electrode area or solution composition changes.

Both faradaic and nonfaradaic processes occur when electrode reactions take place but the former are usually of primary interest in the investigation of an electrode reaction (except in the studies of the nature of electrode-solution interface). However, even here the effects of nonfaradaic processes must be taken into account using the electrochemical data to obtain information about charge transfer and associated reaction.

When a direct current develops in an electrochemical cell, the measured cell potential usually departs from that derived by from thermodynamic calculations. The departure can be traced to three phenomena namely ohmic potential, concentration polarization and kinetic polarization [90]. To develop a current in either galvanic or an electrolytic cell, a potential is required to overcome the resistance of the ions to movement towards the anode and the cathode. This follows ohms law (i.e.  $E = IR$  where  $E$  is the potential,  $I$  is the current and  $R$  is the resistance) and is referred to as the ohmic potential or  $IR$  drop. The net effect of the  $IR$  drop is to increase the potential required to operate an electrolytic cell and to decrease the measured potential of a galvanic cell. Therefore, the  $IR$  drop is always subtracted from the theoretical cell potential i.e.

$$E_{cell} = E_{cathode} - E_{anode} - IR \quad (\text{A-1})$$

Where  $E_{cathode}$  and  $E_{anode}$  are electrode potentials computed with the Nernst Equation.

$$E = E^{\circ} - \frac{RT}{nF} \ln \frac{a_{red}}{a_{ox}} = E^{\circ} - \frac{2.303}{nF} RT \log \frac{a_{red}}{a_{ox}}$$

$E^{\circ}$  is the standard potential,  $R$  is the molar gas constant,  $T$  is the absolute temperature;  $n$  is the number of electrons in the redox process,  $F$  is the Faradays constant ( $96,500 \text{ mol}^{-1}$ ) and  $a_{ox}/a_{red}$  are the activities of oxidized and reduced species.

The equation (A-1) can be rearranged to give

$$I = -\frac{1}{R} E_{cell} + \frac{1}{R} (E_{cathode} - E_{anode})$$

For small currents and brief periods of time  $E_{cathode}$  and  $E_{anode}$  remain relatively constant during electrolysis. The cell behaviour can then be approximated by the relationship

$$I = -\frac{1}{R} E_{cell} + K \quad (\text{A-2})$$

Where K is a constant.

According to Eq. (A-2), a plot of current in an electrolytic cell as a function of applied potential should be a straight line with a slope equal to the negative reciprocal of the resistance. However, it is observed that the plot is only linear with small currents. As the applied voltage increases, the current deviates significantly from linearity. This is true for both electrolytic cells and galvanic cells. Cells that exhibit nonlinear behaviour are said to be polarized and the degree of polarization is given by an overvoltage or overpotential symbolised by  $\Pi$ . This is the potential difference between the theoretical and the actual cell potential at a given level of current. Thus for a cell affected by overvoltage equation (A-1) becomes

$$E_{cell} = E_{cathode} - E_{anode} - IR - \Pi \quad (\text{A-3})$$

Polarization is an electrode phenomenon that may affect either or both of the electrodes in a cell. The degree of polarization of an electrode varies widely and this phenomenon can be divided into 2 categories, concentration polarization and kinetic polarization.

Electron transfer between a reactive species in a solution and an electrode can take place only from a thin film of solution located immediately adjacent to the electrode surface. This film is only a few angstroms ( $\text{\AA}$ ) thick and contains a limited number of

reactive ions or molecules. This film must be continuously replenished with the reactant from the bulk of the solution for there to be a steady current in a cell. When the reaction at the electrode surface is rapid and displays thermodynamic reversibility the concentration of the reacting species in the layer of solution adjacent to the electrode is always as would be predicted from Nernst equation.

. Concentration polarization occurs when reactant species do not arrive at the cathode surface or product species do not leave the anode fast enough to maintain the desired current. When this happens, the current is limited to values less than those predicted in equation (A-2).

Reactants are transported to an electrode surface by three mechanisms (i) diffusion; caused by concentration difference between two regions of a solution such that ions or molecules move to the region that is more dilute, (ii) migration; in which the ions move under the influence of an electric field and (3) convection; whereby the reactants are transferred to or from the electrode surface by mechanical means e.g. stirring or agitation. Concentration polarization therefore sets in when the effects of diffusion, migration and convection are insufficient to transport a reactant to or from an electrode surface at a rate that produces a current of the magnitude given by equation. (A-2). It requires applied potentials that are larger than theoretical to maintain a given current in an electrolytic cell.

In kinetic polarization, the magnitude of the current is limited by the rate of one or both electrode reactions i.e. the rate of electron transfer between reactants and electrodes. It can be traced to activation energy barrier for the electrode reaction. To offset kinetic polarization an additional potential or overvoltage is required to overcome the energy barrier to the half-reaction. However, it is most pronounced for electrode

processes that yield gaseous products and often negligible for reactions that involve deposition by solution of a metal. Kinetic polarization tends to decrease with increasing temperature.

If we consider an overall electrode reaction,  $O + n e^- \rightleftharpoons R$  composed of a series of steps that cause conversion of the dissolved oxidized species  $O$ , to a reduced form  $R$  also in solution (see fig. 2.3).

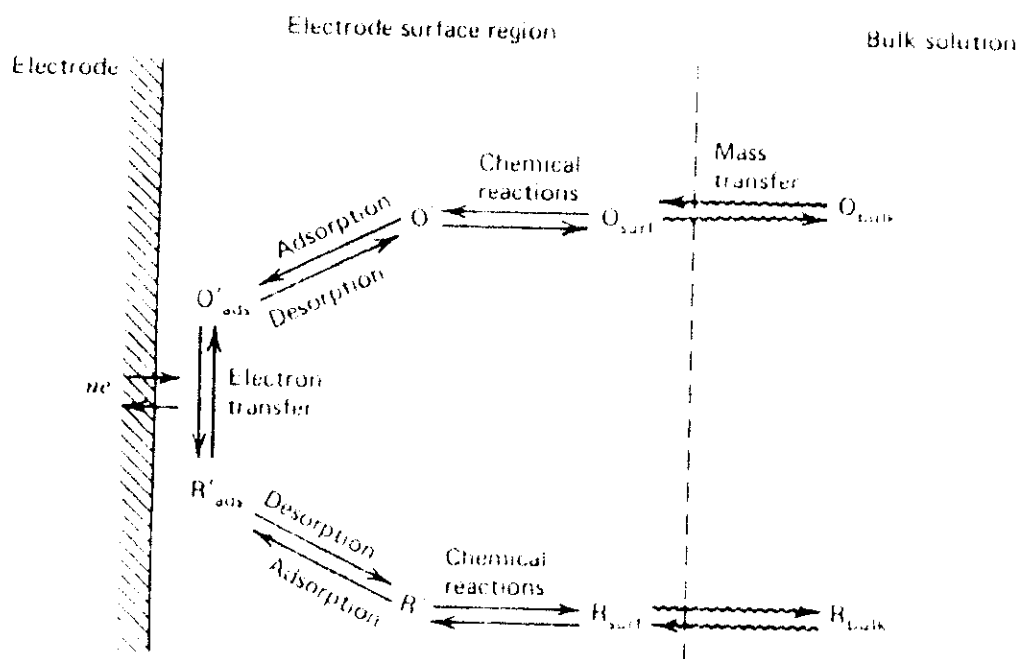


Fig. 2.3: The general electrode reaction.

In general the current (or electrode reaction rate) is governed by the rates of processes such as; (1) Mass transfer e.g., of  $O$  from the bulk solution to the electrode surface; (2) Electron transfer at the electrode surface; (3) Chemical reaction preceding or following the electron transfer. These might be homogeneous processes such as protonations or dimerization, or heterogeneous ones, such as catalytic decompositions on the electrode

surface and (4) Other surface reactions such as adsorption, desorption or crystallization (electrodeposition).

The simplest reactions involve only mass transfer of a reactant to the electrode, heterogeneous electron transfer involving non adsorbed species and mass transfer of the bulk solution [27].

### **2.2.0 SURFACE MODIFIED ELECTRODES**

The term "surface modified electrode" has been used by researchers to describe electrodes which have foreign molecules deliberately immobilized on the surface so that the electrode displays chemical and electrochemical characteristics of the attached species. The alteration of an electrode's chemical, physical, optical and electrochemical characteristic by immobilizing foreign material has been referred to by several names i.e. chemical modification, derivatization, functionalization, electrostatic trapping or polymer coating [28]. The materials to be immobilized are selected on the basis of their known or desired properties. For example, fast outer-sphere electron transfer agents, chiral centers, electron transfer mediator catalysts for a valuable substrate reaction, functionalities which scavenge trace molecules or ions from solutions for analysis in preconcentrated form, corrosion inhibitors, etc.

The electrochemical reactions of the immobilized material are also special since these species are confined to the electrode surface, they provide an opportunity to study the basis of electrochemical reactions. The most studied immobilized chemicals are those which are electrochemically reactive.



## 2.2.1 MODIFICATION METHODS

There are three main methods used to immobilize these materials i.e. chemisorption, covalent bonding and film deposition.

### 2.2.1.1 Chemisorption

This refers to strong irreversible adsorption of electroactive substances on the electrode surface. It is not as widely used as the covalent bonding approach. Irreversible adsorption of compounds on electrode surfaces can be induced by an electrode potential (electrosorption) or by soaking of an electrode in a solution containing the species of interest. Some type of bond formation is thought to occur in the adsorption process. Hubbard and Lane [29,30] pioneered this kind of work when they took advantage of the strong adsorption of the olefinic compounds on platinum, hence formed such coated electrodes by soaking the Pt in a dilute solution of the organic compounds. By using olefinic molecules with different groups they obtained a variety of surface functional groups and from the surface coverage measurements concluded that loss of  $\pi$ -bonds and formation of Pt-C  $\sigma$ -bonds had taken place. The strength of adsorption is dependent on the type of compound considered for example, stronger adsorption is observed for the increasing number of aromatic rings.

Chemisorption and electrochemical reactions of electroactive substances on carbon electrodes have been more diverse than those of Pt and the former have largely focussed on the interaction of molecules having extended  $\pi$ -electron systems with the basal plane in pyrolytic graphite. The  $\pi$ -system-graphite chemisorptions tend to be impermanent when the immobilization reagent is soluble in the electrolyte media [31-33].

### 2.2.1.2 Covalent bonding

Covalent immobilization of an optically active molecule on carbon electrode was one of the earliest publications involving covalent bonding. Watkins *et. al.* [34] heated graphite in air and optically bound active amino acids to these sites via amine bonds thereby providing a stable chiral surface interface region for electrochemical reactions. Murray and co-workers [35] also covalently immobilized a hydrolysis sensitive trichlorosilane to a tin (IV) oxide ( $\text{SnO}_2$ ) electrode by reaction with surface hydroxyl groups. X-ray photoelectron spectroscopy (XPS) provided evidence of the formation of Si-O-Sn bonds and confirmed the presence of surface immobilized compounds. This method is otherwise known as salinization. Covalent immobilization can be effected on both metal oxide and carbon electrodes.

#### (i) Metal Oxide Surfaces

A number of metal oxide surfaces are useful as electrodes;  $\text{SnO}_2$ ,  $\text{RuO}_2$ ,  $\text{TiO}_2$ , Pt/PtO, Au/AuO, Ge/GeO and Si/SiO [36-40]. These have been modified with a variety of chloro- and alkoxysilanes for example, ensilane, [or  $(\text{CH}_3\text{O})_3\text{Si}(\text{CH}_2)_3\text{NH}(\text{CH}_2)_2\text{NH}$ ],  $\text{PrNH}_2$  silane [ or  $(\text{CH}_3\text{CH}_2\text{O})_3\text{Si}(\text{CH}_2)_3\text{NH}_2$ ], etc.

In salinization procedure, hydroxyl - groups are formed by action of atmospheric moisture or concentrated sodium hydroxide to form one to three bonds with the electrode. From studies done, it has been shown that on average two surface bonds are formed [34,41]. Silane monolayers are usually formed under anhydrous conditions because presence of small amounts water in the reaction may result in the formation of multilayers, presumably due to polymerization of the surface silanes. The multilayers have been observed to give rise to more linearly ideal cyclic voltammetric behaviour than monolayer [42], which may be attributed to the more flexible two-dimensional structure

for the silane layer. Modification of electrode surface with specific electroactive groups have been achieved by attachment of silane containing terminal functional groups like  $\text{-NH}_2$ ,  $\text{-CN}$ , and  $\text{-SH}$ . These surfaces can be coupled variously as amides and sulfoamides, quarternized and coordinated to metal [36,37,43,44]. Salinization is therefore a versatile covalent immobilization strategy.

## (ii) Derivatization on Carbon Electrodes

Covalent bonds are also utilized in carbon modification. Carbon surface reactions have been achieved through two schemes i.e. oxidized sites on the carbon surface and oxide free surface. However, before giving further elaboration on this, it is important to discuss the structure of carbon. Graphitic carbon consists of giant sheets of fused aromatic rings, stacked co-planarly (see fig. 2.4).

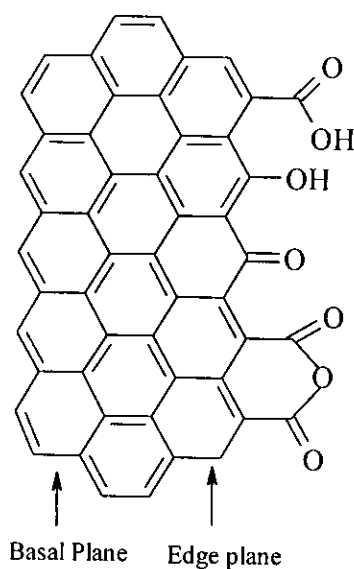


Fig. 2.4: Schematic illustration of chemical functionalities at the edge plane of pyrolytic graphite.

An uninterrupted basal plane surface is non-ionic, of low polarity, hydrophobic and rich in  $\pi$ -electron density. The population of chemical functionalities is low and probably

concentrated along surface imperfections exposing edge plane. Without alterations the carbon basal is somewhat barren to synthetic coupling reactions. On the other hand, the high  $\pi$ -electron density is conducive to strong chemisorption interactions especially with unsaturated compounds including aromatic types. This adsorption property is what is utilized on the basal plane pyrolytic graphite surface for chemisorptive electrode modifications.

The perimeter of the basal plane structure is terminated as a graphite edge on which chemical functionalities abound. Any cleavage process, chemical or mechanical, generates reactive edge plane dangling valencies, which normally react with oxygen and water resulting in oxygenated functionalities. For "acidic carbon oxides", i.e. those generated by oxidative (thermal or chemical) treatments, the edge planes are thought to have chemical groups, which include phenolic, quinone, carboxylic, lactone and other kinetic functions. These groups are the ones thought to be involved in chemical coupling and modification procedure [28]. Edge planes are also polar thus fairly hydrophilic and contain ionic sites which cause double layer capacitance of the edge plane to be larger than that of the basal surface.

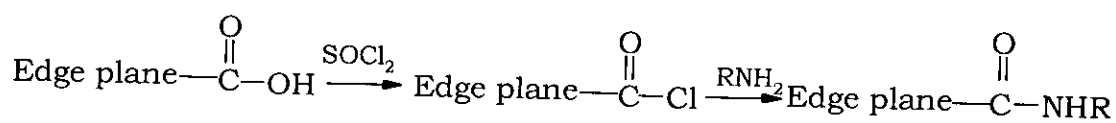
Carbon is obtainable in a wide variety of physical and chemical forms e.g. graphite single crystals, pyrolytic graphite, glassy carbon, powder, fibres etc. each of these being available in different shapes and grades. Most electrode modification experiments have used pyrolytic graphite and glassy carbon. Pyrolytic graphite is a highly imperfect approximation to single crystal graphite with basal edge plane surface. Glassy carbon can be described as a random tangle of graphitic strips such that any given exposed surface exhibits a mixture of basal and plane characteristics. For both of these carbon materials, the portion of edge and plane characteristics exposed on a surface

depends on the pretreatment steps used. For example, mechanical polishing of the basal plane of pyrolytic graphite will expose edge plane sites. Similarly, polished edge plane surfaces will display some basal plane areas if structure folding of the graphitic sheets occurs during polishing.

Several chemical pretreatment procedures have been proposed for enhancing synthetically useful carboxylic and hydroxyl groups on the edge planes. For example, carboxylic coverage on pyrolytic graphite and glassy carbon can be enhanced by heating in air at 400 -500°C [45]. On the other hand, to enhance the hydroxylic group on (initially basal plane) pyrolytic graphite, Lin *et al* [46] first thoroughly oxidized the surface with an O<sub>2</sub> radiofrequency (RF) plasma and then reduced with LiAlH<sub>4</sub>. The actual knowledge of the absolute and relative population and chemical reactivities of carboxylic, hydroxylic and other groupings on carbon surface is still limited. However, the two schemes used in modifying these surface are;

**a) Oxidized sites on carbon surface;** The carboxylic functions on edge planes

generated by thermal or O<sub>2</sub> plasma oxidation can be coupled with amines or alcohols after activation with thionyl or acetyl chloride [34,47].



The reaction above has been used to prepare chiral electrode surface and to immobilize tetra(amino phenyl)porphyrins [*m*-(NH<sub>2</sub>)<sub>4</sub>TPP and *p*-(NH<sub>2</sub>)<sub>4</sub>TPP] and a pyridine ligand [45,48]. The immobilized porphyrin can be metallated with Co, Mn, Zn, or Fe [48,49]. Carbon surface hydroxyls can be activated for coupling reactions with cyanuric [28,46]. Carbon surface quinone reacts with nitrophenyl hydrazine to form phenylhydrazone [50].

**b) Oxide-free Carbon Surface:** This involves reaction with surface carbon atoms. It was first demonstrated by Mazur [51], who reasoning that vacuum pyrolysis of carbon surface oxides should create usefully reactive surfaces, coupled olefins to "oxide-free" carbon. He used the  $\pi$ -bonds of acrylyl chloride. Improved coupling yields of reagents with "oxide-free" carbon were subsequently demonstrated by Oyama and co-workers [52] who exposed carbon electrode first to Argon plasma (to make it oxide free) then to amine gases. They later extended the amine chemistry on the argon plasma treated edge plane pyrolytic graphite to coupling reactions with the dangling carboxylic acid group of  $\text{Ru(EDTA) (OH}_2\text{)}^{3+}$ .

A third approach to producing oxide free carbon electrode surface is mechanical abrasion or fracture in the absence of oxygen [28]. This was demonstrated by abrasion of glassy carbon electrode in an inert atmosphere enclosure. The abrasion was conducted in a puddle of concentrated vinyl ferrocene solution so that the oxide free surface was immediately exposed to the vinyl ferrocene reagent. The abrasion experiment is also effective for binding vinylpyridine and subsequently coordinated to ruthenium. The true chemical nature of "oxide free" carbon surface coupling products, however, remain adequately limited

#### **2.2.1.3 Derivatization by Film Formation**

Modification of electrode surface with organic polymer or some inorganic equivalent is done by electrodeposition of a conducting polymer on the electrode. The film is held on the electrode by some combination of chemisorption effects and low solubility in the electrolyte media. This has proved to be the more superior method and is currently the most widely used method for the purpose of electrode modification [28,53,54].

The main advantage of this method is that films with a thickness ranging from 1 to 20,000 monolayers are obtainable while the modification methods relying only on covalent bond formation or chemisorptive properties, hardly exceed a monolayer. Monolayer refers to approx.  $1.5 \times 10^{-10}$  mol /cm<sup>2</sup> of the surface coverage depending on the size of molecules used for modification. The low solubility combined with chemisorption covalent bonding and adsorption of films allows the formation of very thick polymer films.

Polymer coatings have been appealing for several reasons. First immobilization experiments are technically less demanding than working with monolayers. Secondly, electrochemical responses are larger (since multiple layers of redox sites react). Thirdly, it has been supposed that improved stability results from incorporating reagents into polymer. A polymer framework may however be highly stable while an electrochemically reactive moiety attached to it is no more stable than when immobilized as a nonpolymer monolayer.

Polymers have been coated on electrodes by several methods. These include;

(i) Dip coating - involves exposing the electrode to a dilute solution of polymer for a period of time during which an adsorbed film forms on the surface. The film is then allowed to dry [53]. It may already contain a redox moiety or this may be bound subsequently to the film as by amide or metal complex formation [48,55,56].

(ii) Droplet evaporation - involves spreading and evaporation a few microlitres of a dilute solution of either polymer or a hydrolytically unstable organosilane copolymer. Films prepared in this manner can be topologically rough unless evaporation is very slow. However, film uniformity can be improved by spinning the solution off or removing it after only partial evaporation.

(iii) Oxidative and Reductive Deposition - The idea that polymer solubility depends on its ionic state which can be changed by oxidation or reduction, has been used to deposit polyvinylferrocene films from  $\text{CH}_2\text{Cl}_2$  solution, oxidizing the polymer to its less soluble (more absorbable) ferricenium form either electrochemically or photochemically [57,58].

(iv) Spin coating - has been used for several preformed redox polymer (one which is directly applied to the electrode). Spin coating usually requires a large number of monolayers to be applied for pinhole - free films [28].

(v) Electrochemical Polymerization - A solution of monomer is oxidized (as with phenols, aniline, and pyrrole) or reduced (as with activated olefins under dry conditions) to intermediates which polymerize sufficiently rapidly to form a polymer film directly on the electrode. To electrodeposit films of significant thickness, the polymer film must itself be redox active and capable of electrocatalytically oxidizing or reducing fresh monomer. Alternatively, the polymer film must be rather permeable to fresh monomer otherwise electrode passivation soon occurs and polymerization is halted. This is the most widely used procedure [59-61].

Polymers have also been coated by organosilane bonding, electrochemical precipitation and plasma discharge polymerization [31,42,57]. The polymers on electrodes can be classified as conducting polymers, redox polymers and ion exchange polymers. Redox and conducting polymers contain an electroactive centre as part of the polymer chain backbone or the electroactive centre may be coupled to a functionalized polymer either before, or after the polymer is applied to the electrode surface. Ion exchange polymer films, on the other hand, depend on drawing ionic redox substances



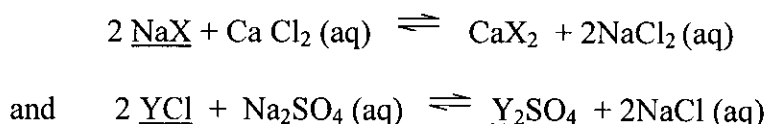
from their solutions into the film as counter ions having favourable ion exchange partition coefficient. This process is called "electrostatic binding".

## 2.2.2 ION EXCHANGE POLYMERS

### (i) Theory of ion exchangers

By definition, ion exchangers are insoluble solid materials that carry exchangeable ions. The ions may be exchanged for a stoichiometrically equivalent amounts of other ions of the same charge sign when the exchanger is in contact with an electrolyte solution. Carriers of exchangeable cations are called cation exchangers while those that carry exchangeable anions are called anion exchangers [62].

For the cationic or anionic exchangers  $\underline{\text{NaX}}$  and  $\underline{\text{YCl}}$ , when in contact with the electrolyte solutions  $\text{CaCl}_2$  and  $\text{Na}_2\text{SO}_4$  respectively, the following reactions take place.



X and Y represent structural unit of the exchanger; solid phases are underlined and (aq) indicates the electrolyte is in aqueous media. The  $\text{Na}^+$  and  $\text{Cl}^-$  ions act as the exchangeable cation and anion and they are changed for  $\text{Ca}^{2+}$  and  $\text{SO}_4^{2-}$  respectively.

Ion exchange is a reversible process except for very few cases. The exchangers owe their characteristic properties to a peculiar feature in their structure. They consist of a framework which is held together by chemical bonds or lattice energy. This framework carries a positive or negative electric surplus charge, which is compensated by ions of opposite sign (counter ions). The counter ions move freely within the framework and can be replaced by other ions of the same sign. The ion exchange capacity of an ion

exchange is equal to the counter ion content. This is a constant given solely by the magnitude of the framework and is independent of the nature of the counter ion.

The pores in an exchanger are occupied not only by the counter ion but also by the solvent and solute which can enter the pores when the ion exchanger is in contact with a solution. The process is called sorption and has a significant role in the exchange process for example, sorption of the solvent results in swelling of the framework (increasing the size of the channels) and as such large cations become more exchangeable. The exchange properties of an exchanger are basically determined by structure of the framework.

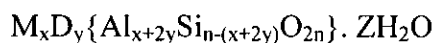
There are many types of exchangers some occurring naturally while others are synthetic. These include synthetic inorganic exchangers, ion-exchanger resins, coal and mineral exchangers. The general structural principle of framework with an electric surplus charge and mobile counter ions, however, is common to all these ion exchangers. For now, only the mineral ion exchangers especially clay montmorillonite shall be discussed.

#### **(ii) Mineral Ion Exchangers**

Most naturally occurring aluminosilicates such as zeolites and clays have cationic ion exchange properties. Clays, glauconites, zeolites and humic acid are the materials responsible for ion exchange in soils. They all have a crystalline structure with channels and inter-connecting cavities within the lattice. Counter ions reside within these cavities and may be replaced by other cations, which for one reason or another may be preferred by the framework and are able to permeate through the cavities [63,64].

Zeolites are formed from silica by substitution of some silicon atoms with aluminum atoms. The replacement leads to an excess negative charge since aluminium is

trivalent while silicon is tetravalent. This excess negative charge is neutralized by alkali or alkali earth metal counter ions. Compositionally, zeolites are represented as



M is usually Na or K, and D is Mg, Ca or Fe and more rarely Li, Sr or Ba may substitute M or D. Although M cations are exchangeable, location within the zeolite structure will determine their ease of exchange. Z is the number of moles of water of hydration, which is highly variable. Examples include chabazite  $[Ca_6Al_{12}Si_{24}O_{72} \cdot 40H_2O]$ , Natrolite  $[(Na_2Ca)_4 Al_8 Si_{16}O_{48} \cdot 24H_2O; Na_2 Si_3 Al_2O_{10} \cdot 2H_2O]$  and hormotone  $[(K, Ba) Si_5 Al_2O_{14} \cdot 5H_2O]$ [62].

The lattice structure of a typical zeolite (see fig. 2.5) consists of  $SiO_4$  and  $AlO_4$  tetrahedrals that share their oxygen atoms.

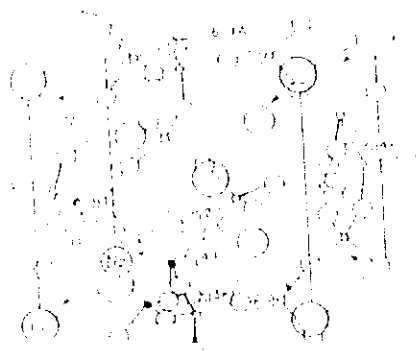


Fig. 2.5: A unit cell of the crystal of sodalite,  $Na_4(Si_3Al_3ClO_{12})$ . The arrows indicate channels, which connect the cavities in the aluminosilicates framework [62].

Presence of counter ions within the cavities makes zeolites useful as ion exchangers. However, the size of the cavities, usually ranging from 4 to 10 Å (angstrong), changes insignificantly on sorption of solvents. This implies that zeolites do not absorb all those molecules or ions that are too big to enter the cavities. Since the pores are uniform, the zeolites absorb only weakly, the small ions or molecules that can enter and leave easily.

This "sieving action" at a molecular level makes them very useful in laboratories and industries as molecular sieves [62,65,66].

Glaucanites on the other hand, are ferrous aluminosilicates that contain exchangeable potassium. They possess a rather rigid and dense crystal lattice, which can only undergo cation exchange at the surfaces. They have nevertheless been shown to possess a considerable capacity in the colloidal form [63, 64].

Unlike zeolites and glaucanites, montmorillonite clays have a loose structure. The term clay is used both as a particle term (not bigger than 2  $\mu\text{m}$  in size) and as a rock term. As a rock term, it's used to describe natural earthy fine-grained material that swells on adsorption of water [67]. It is composed largely of a limited group of crystalline clay mineral groups of sodium, calcium, magnesium, iron, lithium, aluminum silicates which include minerals sodium montmorillonite, calcium montmorillonite, nontronite, saponite and hectorite. The rock in which these smectite minerals are usually dominant is called bentonite.

Sodium montmorillonite is a smectite in which sodium and water molecules are the interlayer materials. Calcium montmorillonite is a smectite in which calcium and water molecules are the interlayer material. Saponite is a smectite in which zinc has replaced some of the aluminum and hectorite results when magnesium replaces aluminum and lithium is the ion between the layer.

### **(iii) Bentonite**

Bentonite is a montmorillonite clay with principal intercalated cations being alkaline earth ions and alkali ions and a fixed amount of other components like Al, Fe and  $\text{SiO}_2$  [68]. It varies in colour from white to gray, yellow, green, blue, black but it is most often yellow or yellowish green [69].

Bentonite in which sodium montmorillonite is the major mineral constituent have a high swelling capacity and the largest and highest quality deposits in the world are located in South Dakota, Wyoming and Montana. On the other hand, bentonites in which calcium montmorillonite is the major mineral constituent have a low swelling capacity. Most of the bentonite in world contains calcium montmorillonite including the one found in Kenya.

The properties of individual bentonites vary because each of these minerals has unique properties and likewise their uses. The exchangeable cations present between the silica and alumina sheets have a strong influence on the uses and properties of the bentonites but the major uses are in drilling mud, foundry, sand bond and iron-ore pelletizing.

With regard to the exchangeable cations, most bentonites carry their counter ions within the layers and swell in one dimension by increasing the interlayer distance. Their lattice layer structure being expandable has ions and large molecules penetrating between the sheets, which results in increased basal spacing. They therefore have high exchange capacity especially for large cations and large organic molecules that penetrate and orient themselves along the plane of the silica sheet. The approximate composition can be represented by  $\text{Al}_2\{\text{SiO}_4\text{O}_{10}(\text{OH})_2\} \cdot n \text{H}_2\text{O}$  and the general structure represented as in fig. 2.6 [64,70,71].

They possess a layered structure in which two-dimensional oxyanions are separated by a layer of hydrated cation. The oxyanion layer consisting of two silicate inverted sheets sharing their apical oxygen with an octahedral sheets, have a 2:1 relationship between the tetrahedral and octahedral sheets within a layer which allows the clays to be classified as 2:1 phyllosilicates [72]. There is a positive charge deficiency in

oxyanion layer of montmorillonites ranging from -0.4 to 1.2 electrons per  $\text{Si}_8\text{O}_{20}$  and layers of hydrated cations of intercalated cations, either  $\text{Na}^+$  or  $\text{Ca}^{2+}$  balance this.

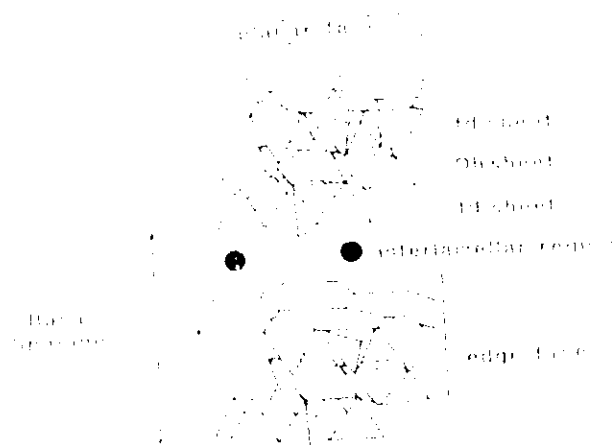


Fig. 2.6: The general structure of montmorillonite clays

In Kenya, bentonite clays occur in three areas, Amboseli, Athi River and Nanyuki. The clay in Amboseli has been reported to contain sepotite with a swelling index of 32, which is much lower than that of Wyoming bentonites (USA) with a swelling index of 150. The Athi River clay found in shallow beds as a matrix to gypsum modules in areas owned by East Africa Portland Cement Limited, is a Ca-montmorillonite. It is usually converted into Na-montmorillonite by addition of soda ash [73].

In Nanyuki the greenish gray and purplish clay occurs in several places. Two of these deposits are called Parminters and Kriegers. Technical tests carried out on these samples indicated that the best of these three deposits is Parminters while Athi River bentonite is of the lowest quality. The oxides in Kriegers, Parminters and Athi River bentonites as obtained from mineralogical and x-ray diffraction are shown in Table 2:1.

Table 2.1: Oxides in kriegers, Parminters and Athi River bentonites as recorded by Pulfrey [73].

Oxide	1	2	3	4
SiO <sub>2</sub>	51.66	46.24	43.93	52.99
Al <sub>2</sub> O <sub>3</sub>	14.97	17.00	14.77	14.27
Fe <sub>2</sub> O <sub>3</sub>	-	12.08	13.80	9.81
FeO	7.49	0.28	0.25	0.43
MgO	2.01	2.11	2.65	3.69
MnO	0.04	0.04	0.03	0.04
CaO	11.58	1.58	2.48	0.95
Na <sub>2</sub> O	1.81	0.99	0.78	0.52
K <sub>2</sub> O	1.98	1.31	1.77	4.28
TiO <sub>2</sub>	0.64	2.19	2.31	0.45
CO <sub>2</sub>	0.4	-	0.51	-
H <sub>2</sub> O <sup>+</sup>	5.71	0.05	7.72	6.51
H <sub>2</sub> O <sup>-</sup>	11.88	7.75	0.47	5.50
P <sub>2</sub> O <sub>5</sub>	0.06	0.27	0.57	0.03
<b>Total</b>	<b>97.23</b>	<b>99.94</b>	<b>100.02</b>	<b>99.95</b>

Sample 1&2 -Kriegers, sample 3 - Parminter and sample 4 - Athi River

There are only few aluminosilicates that have been known to act as anion exchanges. Exchange of OH<sup>-</sup> for Cl<sup>-</sup>, SO<sub>4</sub><sup>2-</sup> and PO<sub>4</sub><sup>3-</sup> has been observed in montmorillonite, kaolonites and feldspar. However only two have been used for practical purposes as anion exchanger i.e. apatite [Ca<sub>5</sub> (PO<sub>4</sub>)<sub>3</sub>]F and hydroxylapatite [Ca<sub>5</sub> (PO<sub>4</sub>)<sub>3</sub>]OH.

#### (iv) Use of Ion Exchangers in Electrode Modification

Ion exchangers have been used extensively as electrode modification materials. They are applied from colloidal solution by simple dip and spin coating [74]. In their

electroactive state they have been shown not to affect the electrochemistry of a reasonable electron transfer rate even when their films are quite thick.

Clay modified electrode (CME) are of interest because clay minerals are cheap, widely available naturally occurring materials. Bentonite clay minerals (Na-montmorillonite) have proved to be the most important and widely used material in electrode modification due to their excellent ion exchange and adsorption capacity. Their well-defined layer structure, flexible adsorption properties and potential as catalyst and /or catalyst supports make them attractive for modifying electrode surface. They also have higher thermal and chemical stability than many other materials that have been used for such modifications. It has been shown that only a small fraction of the total species contained in a clay layer is electroactive. Studies suggest that species intercalated into the interlamellar spaces are not electroactive [75,76].

Clay modified electrodes are prepared by the deposition of clay films on a conductive substrate. For example, montmorillonite and hectorite clays have been used to prepare colloidal suspension, which are then cast on the electrode surface. The aim is to take advantage of the adsorption and /or catalytic properties to improve the selectivity or sensitivity of the electrode toward solution species. Its selectivity has been shown to segregate  $\text{Ru}(\text{bpy})_3^{2+}$  (where bpy = 2,2 bipyridine) from  $\text{Na}^+$  [76]. Thicker films (approx. 3  $\mu\text{m}$ ) can be made more stable by addition of polyvinyl alcohol, which also enhances the swelling of the clay.

Ion exchangers have also been shown to exchange their counter ions with others that are redox active thus making the film electroactive. This exchange may be done by electrochemistry or by initial soaking of the exchange in a solution containing the ions of interest to form what is referred to as redox ion exchanger modified electrode [62,74].



#### **(v) Application of Ion Exchanger modified Electrodes**

The electrodes have been found to be very important as pre-concentrators. Their ability to accumulate redox species from a dilute solution enables the voltammetric detection of trace elements and organic molecules [74]. Incorporation of minute amounts of certain ion into the exchange films has been observed to enhance the electrochemical sensitivity of an electrode. For example, a thicker electrode modified with  $[\text{FeNi}(\text{CN})_6]^{3+}$  has been shown to detect  $\text{Na}^+$  and  $\text{Cs}^+$  at  $10^{-8}\text{M}$  level.

They have potential of being used as ion selective electrodes. This is because they act as a substrate selective diffusion layer which will only allow ions of a given charge and a size smaller than their pore size to diffuse through to the electrode surface. This ability may allow their use in analyzing specific ions or molecules among other interfering ones.

They are valuable in electrocatalysis because of their ability to adsorb organic compounds and restrict them to the electrode surface. The oxidation/reduction of a substrate with slow electron transfer kinetics at the electrode can be mediated (catalysed) by a redox system that is able to exchange electrons rapidly with both the electrode and the substrate. These are just but a few of the numerous areas where these electrodes find use.

#### **2.2.3 REDOX POLYMERS**

Redox polymers contain redox species in their backbone and find use in areas such as macromolecular electronics, electrocatalysis, sensor electrodes, biological and medicinal chemistry [28,30,34,35]. They have the advantage that their behaviour in electrolyte solutions may be monitored and characterized by electroanalytical methods

*insitu*. Due to the changing properties of molecules with change in potential (redox states), an electrode surface coated with a redox film may have its properties adjusted to suit specific needs [74].

There are three classes of redox polymers which are used i.e. (i) metal complexes e.g. ruthenium bipyridyl; (ii) polymers of the ferrocene origin and (iii) those of organic origin for example quinone, dopamine, azobenzene, thionine and porphyrins [28,74]. Most of these are applied to the electrode surface as preformed polymeric material by dip, spin or droplet coating or by *insitu* polymerization.

Examples of redox polymer films and application are given in details in references 28 and 74. The most important application include electrocatalysis whereby the redox polymer used to modify the electrode is chosen in such a way that its  $E^0_{\text{surf}}$  is approximately equal to the formal potential.

One group of compounds in this class that has attracted a lot of interest lately is the conducting polymers. They have attracted many researchers due to the wide range of possible areas in which they can be applied. The conductivity mechanism of conducting polymers is by delocalized band structure, rather than site to site hopping as is the case in other redox polymers.

#### 2.2.4 CONDUCTING POLYMERS

In the past, polymers have been associated with plastics and textile fabrics. They are distinguished from metals by their inability to carry electricity, which has made them useful as insulators.

Recently a new class of organic polymers with a remarkable ability to conduct electrical current has been devised. Conductive polymer study is a branch of a large and

old field of organic electrical conductors, otherwise known as "synthetic metals". A key discovery in the evolution of conductive polymers in the early 1970s was the high conductivity of polysulfurnitride  $-(SN)_x-$ , superconducting at 0.26k. This was the first polymeric material that was shown to have metallic properties and it led to researchers directing their interest to organic conductive polymer in the late 1970s.

A common feature in all conductive polymers is that they were all found to have an extended  $\pi$ -conjugated system i.e. single and double bonds alternating along the polymer chain. The very first conductive polymer to be identified was polyacetylene  $(CH)_x$  [77]. It is the simplest conjugate polymer consisting of weakly coupled chains of CH units forming a pseudo one-dimensional lattice. This was found to be of low conductivity but a major breakthrough came when MacDiarmid and co-workers discovered that partial oxidation with iodine or other reagents increased polyacetylenes film conductance by more than  $10^9$  folds compared to what it was originally.

The process by which a polymer is transformed to its conductive form through chemical oxidation or reduction is called doping. Polyacetylene conductive form is thus called "dope". Studies show that after synthesis,  $(CH)_x$  films can be doped chemically or electrochemically at room temperature with a variety of donor or acceptors to form n- or p- type semi-conductors. The conductivity of the doped polyacetylene can be varied in a controlled manner over twelve orders of magnitude, values greater than  $3 \times 10^3 \Omega \text{ cm}^{-1}$  have been achieved which is much higher than any known polymer.

Although polyacetylene had the highest conductivity its instability in air and moisture was a major draw back and therefore it was not the first conductive polymer to reach commercialization. This however, encouraged further research and other organic

polymers were soon discovered. These include polypyrrole, polyanthracene, polythiophene, polyaniline etc. Conductive polymers have found use in;

**(i) Rechargeable batteries** - the ability of some conducting polymers to exhibit redox characteristics where they can be switched between their conducting and insulating states through a redox process has made it possible for them to be used in rechargeable batteries. The batteries utilize conducting polymers as the cathode and lithium or its alloy (e.g. Li-Al) at the anode. The polymers usually used are polypyrrole, polythiophene or polyaniline or their derivatives. These type of batteries were found to have a longer life, a 3 Volt usable voltage and an energy density several times that of currently available nickel/cadmium and lead/acid batteries.

**(ii) Electrochromic devices** - Most conductive polymers display a whole variety of colours in their conducting and insulating states. These polymers display different colours depending on their electrochemical state, a property referred to as, electrochromism. For example, polythiophene, polypyrrole and polyaniline display red, yellow-green and yellow colours respectively in their undoped form, while they display blue, blue-black and green-blue colour respectively in their doped form. Therefore, conducting polymers have found use in production of electrochromic devices like "smart windows". These change colours in response to sunlight or temperature by application of electrical potential to cause doping and undoping of its conductive polymer consequently inducing controlled colour changes.

Other uses include electrolytic capacitors where polypyrrole has been used, and in gas separation e.g. separating oxygen from nitrogen or carbon dioxide from methane, polyaniline is used. Studies revealed that if conductive polymer is doped and undoped repeatedly it becomes porous and acts as a gas separation membrane.

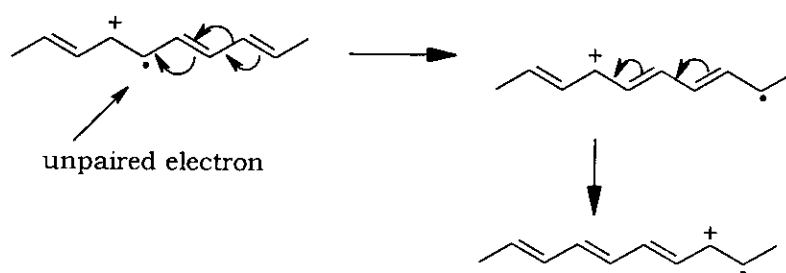
#### 2.2.4.1 Mechanism of conduction in Conductive Polymers

Although band theory sufficiently explains conductivity in metals and semi-conductors, both of which utilize partially empty or partially filled bands, it fails to explain electrical conductivity in polymers. Polymers conduct electricity without having partially empty or partially filled bands. The mode of conduction of current in the polymers has been explained in terms of solitons, polarons and bipolarons, which are terms borrowed from Physics [74].

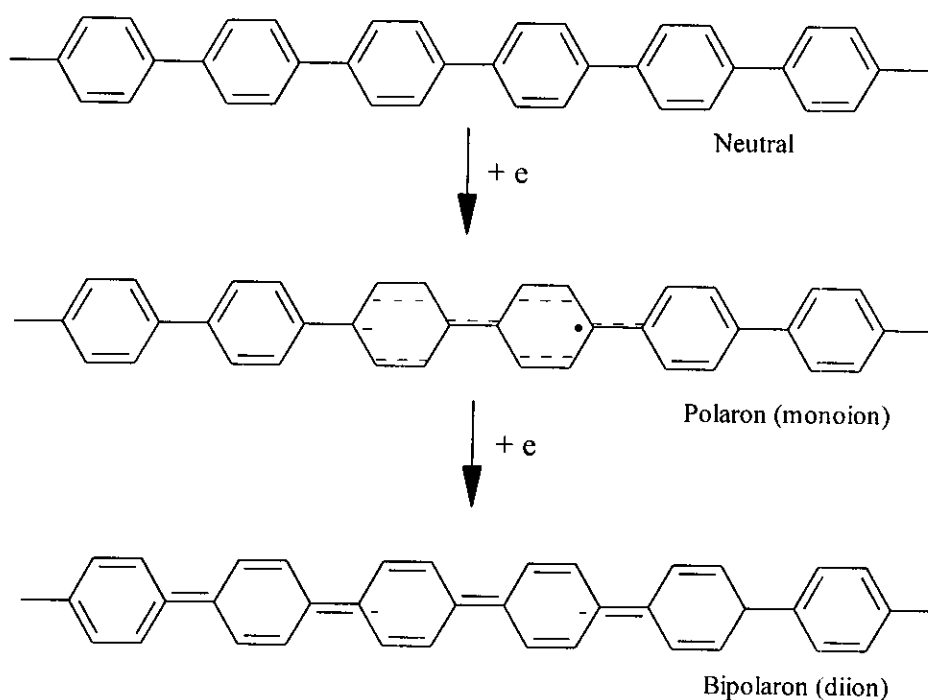
All conducting polymers contain extended  $\pi$ -conjugated system. Removal of an electron from the valence band of such a conjugated polymer creates a vacancy (hole or radical cation) which delocalizes partially along several units (this is unlike band theory where complete delocalization occurs). This results in a local modification in geometry of the chain or in structural deformation. Therefore, there is a hole or radical cation, which is partially delocalized over a polymer segment and thus is referred to as a polaron. It stabilizes itself by polarizing the region around it hence its name. A polaron, which is actually a radical cation, has a spin of  $\frac{1}{2}$ .

Since one electron has now been removed from the polymer it is already oxidized. If another electron is removed from an oxidized polymer that already has a polaron, two things may result. (i) This second electron could come from a different segment of the polymer chain thus creating another independent polaron or (ii) It could come from the first polaron level creating a special dication, which is referred to as Bipolaron. Polarons result from low doping levels whereas bipolarons result from high doping levels. There is a structural deformation associated with Bipolarons since the two positive charges are not independent but act as pair.

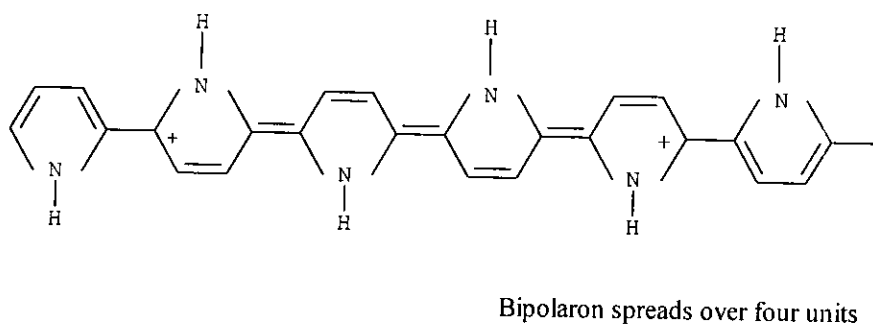
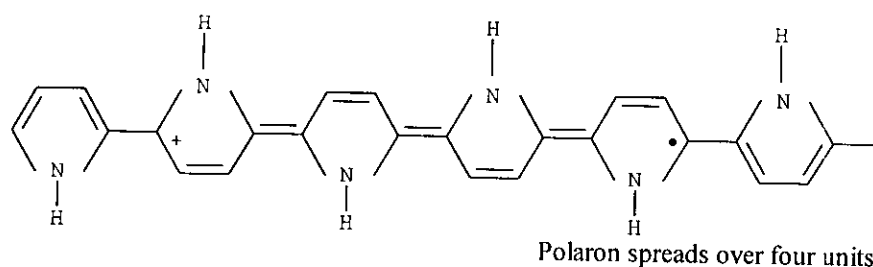
Both Polarons and bipolarons are mobile and can move along the polymer chain by the arrangement of double and single bonds in the conjugated system that occurs in an electric field. If, as a result of high doping, too many bipolarons are formed their energies can start overlapping at the edges creating narrow bipolaron bands in the energy gap. Examples of some conduction polymer forming polarons and Bipolarons are shown in Schemes I (a)-(c).



Scheme I (a): Polyacetylene; Propagation of a polaron through a conjugated polymer chain by shifting of double bonds.



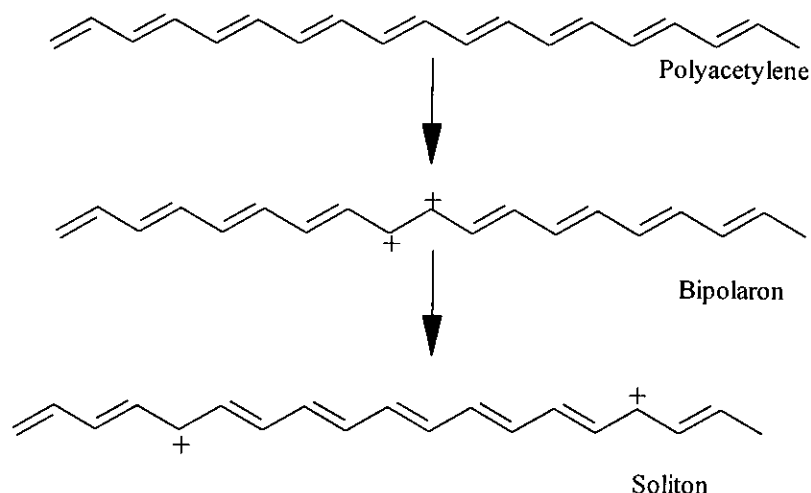
Scheme I(b): Polaron and bipolaron formation on reduction of polyparaphenylenes



Scheme I(c): Propagation of a polaron in polymer

Conduction by polarons and bipolarons is thought to be the predominant mechanism of charge transport in polymers non-degenerate states. The concept also explains the optical adsorption changes seen in these polymers with doping. Conductivity of polyacetylene rises with temperatures just like that of typical semiconductors, which is unlike metal conductors whose conductivity, decrease with temperature.

In polymers with degenerate ground state, e.g. polyacetylene (2 equivalent resonance forms, cis and trans), bipolarons may split to form solitons as shown in Scheme I(d) below. A soliton may be neutral, negative or positive and conduction involves movement of electrons intermolecularly via positive or negative solitons.



Scheme I(d): Formation of Solitons in polyacetylene

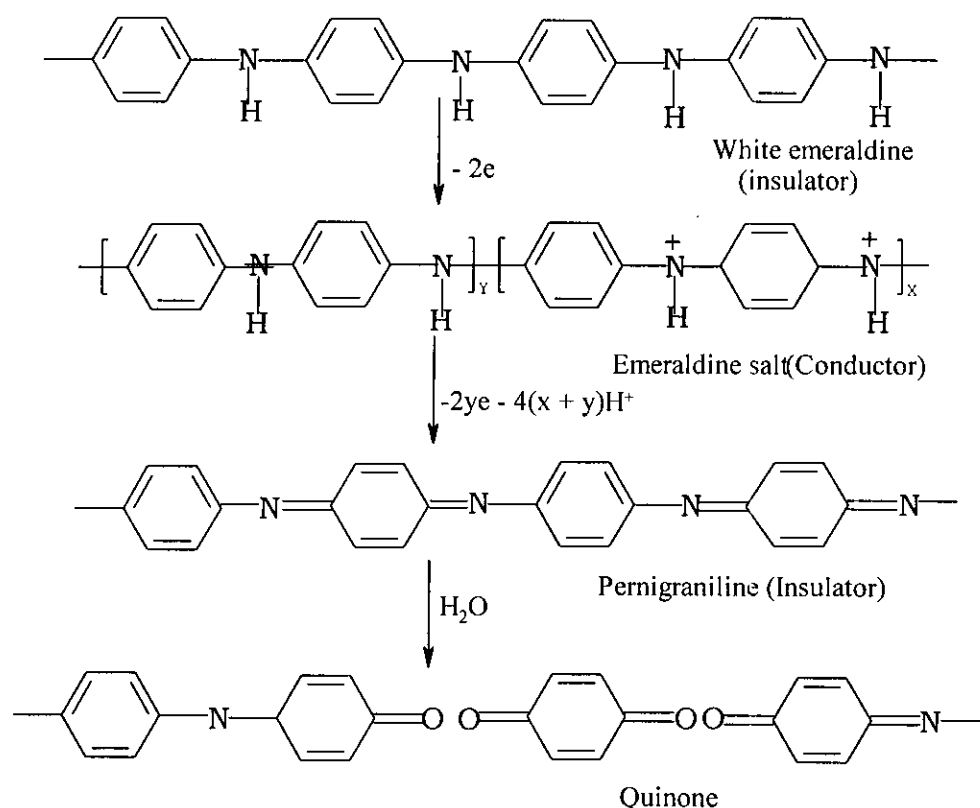
#### 2.2.4.2 Use of Conducting Polymer in Electrode Modification

Films of conducting polymer are applied on electrode surface by electropolymerization of the respective monomers from an aqueous or non-aqueous media. Oxidation or reduction of the monomer produces precursors, typically cation radicals and these polymerize rapidly on the electrode surface. Since the conductive polymer films are redox active they electrocatalyze the oxidation/reduction of fresh monomers enabling the formation of films with sufficient thickness [28,61,74].

Though polypyrrole, polyacetylene and polythiophene have attracted substantial attention in the past, polyaniline is currently the most pursued of these polymers. Polyaniline (PAN) is a particularly attractive substance because it has a high conductivity, is easily synthesized, has well behaved electrochemistry and is stable under ambient conditions [54,60,61]. This is in contrast to most other conducting polymers, which are often adversely affected by oxygen or impurities.



The structure of polyaniline consists up to 1000 or more repeating units. The polymer and its derivatives are formed via a head to tail coupling yielding different and electrical property. There are four oxidation states in which PAN exists as shown in scheme II.



Scheme II: Oxidation products of polyaniline

PAN displays a sharp oxidation peak at around 0.2V Vs SCE in a process that has been proposed to involve the loss of two electrons to form its conductive form called Emeraldine salt. On reduction it is switched back to the insulating state the white emeraldine. The reduction media peak occurs at approximately 0.04V Vs SCE in aqueous media. A large charging current is observed at the positive end of the redox process while a small charging current is observed at the negative end. This behaviour is consistent with the transition from a conductor to an insulator.

A major handicap in the use of polyaniline is that it undergoes irreversible electrochemical degradation at potentials above 0.75V Vs SCE to the pernigraniline form which due to its instability towards hydrolysis is oxidized to quinone-imine as shown in scheme II. These products are soluble leading to deterioration of polyaniline electrochemical features. Attempts have been made to extend the useful range of polyaniline, these include co-polymerization with p-aminophenol [59], use of salt solution [78] and formation of composites between various non-conducting materials [79,80]. These attempts have allowed extension of the potential window in PAN to 0.85V without significant degradation of the polymer.

The other problem experienced with polymers is that when electrodeposited beyond a certain thickness on a bare electrode they tend to crystallize. This has limited their applicability as they find much use only when in the film form. Electrodeposition of PAN on an insulating host matrix like nafion or on clays to form composites allows the polymer thickness to be increased substantially without crystallization.

### **2.3.0 ELECTROCHEMISTRY OF BIOLOGICAL AND NATURAL COMPOUNDS**

Several studies which are distinctly electroanalytical involving compounds possessing important biological function have been done. Chemists of all disciplines are moving into this field which organic chemists have long been interested in such areas as the structure, synthesis and biogenesis of natural products.

Nature has many important redox systems and the value of electrochemical studies has long been apparent. Early workers, Michaelis *et al*, [81], undertook potentiometric

measurements on redox couples that behaved reversibly, and extended these to certain irreversible or electrochemically sluggish systems by means of mediators. Several attempts have been made to study some of the compounds and three classes are discussed in brief below.

(i) Nicotiamide adenine dinucleotide (NAD) otherwise known as coenzyme I. It is a derivative of pyridine and exists in oxidized and reduced forms represented as  $\text{NAD}^+$  and  $\text{NADH}$  respectively. In nature,  $\text{NAD}^+$  is the enzyme required oxidant while  $\text{NADH}$  is the reductant in a host of biological redox reactions. The  $\text{NAD}^+$ - $\text{NADH}$  system was found to be electromotively sluggish with regard to potentiometric measurements. The standard potential was originally estimated from equilibrium constant of enzymic reactions with other systems of known potential. The best data available are those of Rodkey [81], who determined potentiometry at several temperatures and pH values using enzyme *xanthine oxidase* to accelerate equilibrium with electromotively active mediators benzyl viologen.

The potential obtained at 25 °C and pH=7 for the reaction was indicated as shown below



The slope of  $E^0$  versus pH plot was found to be  $-0.0301\text{V}$  per pH unit in the pH range 6.5 to 10.5. A one-electron intermediate in the NAD system is not prominent although it has been considered occasionally. Some of the studies done have reported that  $\text{NADH}$  was oxidized to  $\text{NAD}^+$  rapidly only by reagents that function as one electron acceptors and the sequence proposed [81] is as indicated below.

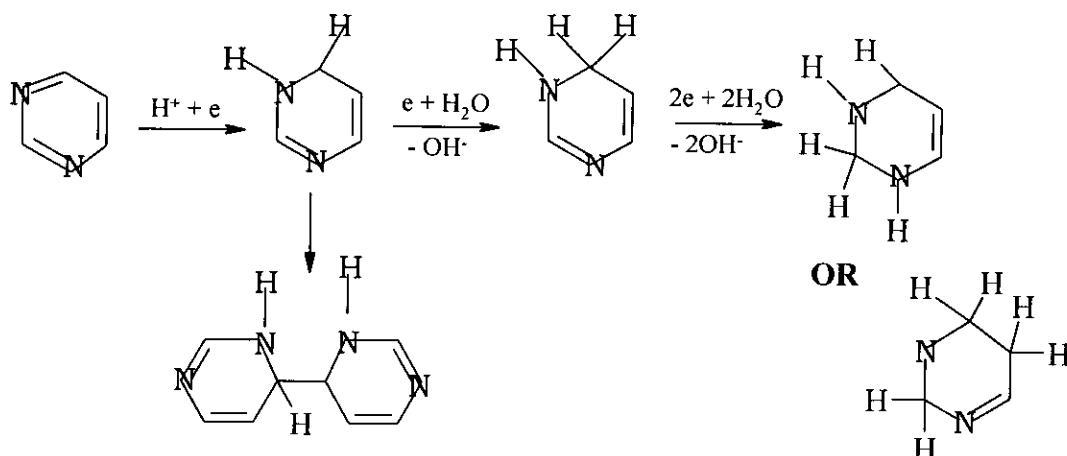


A study employing cyclic voltammetric technique on methyl-, ethyl-, n-propyl- and benzylnicotinamides revealed that these compounds exhibit a cathodic peak in the vicinity of  $-1\text{V}$  vs SCE at pH above 7 and at low sweep rate, a single anodic peak occurs at about  $-0.35\text{V}$ .

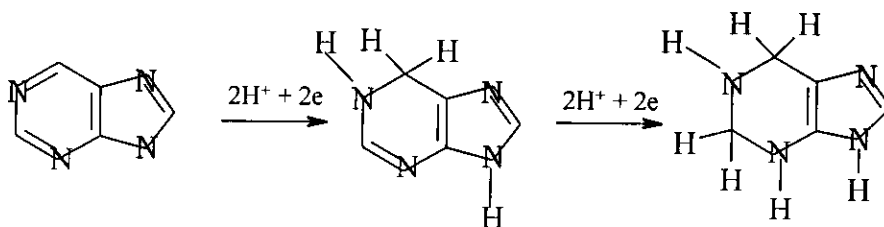
(ii) Derivatives of purine and pyrimidine are another class biological compound. The most common pyrimidine compounds being adenine, thymine, guanine, cytosine and uracil. They are found in cells either as nucleosides or nucleotides e.g. ATP (adenine triphosphate). The nucleosides possess  $\beta$ -glycosidic linkages between the base and either D-ribofuranose or D- (2-deoxy) ribofuranose, while the nucleotides are phosphate esters of the nucleosides. Electrochemical data available for the nucleosides and nucleotides indicate that the patterns of reduction are essentially the same as for the free bases. Smith and Elving [82] using polarography and controlled potential coulometry revealed that pyrimidine has a pH dependent two-electron reduction process between pH values of 5 and 7. Above pH 7 or so, a second pH-independent two-electron process is seen in addition to the first, the product is a tetrahydropyrimidine, but the position of the double bond is uncertain. The two waves merge near pH 9 to form one pH-independent four-electron wave. Below pH 5 the first two-electron process splits into two one-electron steps; below pH 3 only the first step of these steps is seen before hydrogen evolution. Smith and Elvin summarized these processes as shown in scheme III.

The two scientists also studied purine and two two-electron waves were seen in acidic solution but, in contrast with pyrimidine, in this compound none was found (in their study) in neutral or alkaline media [81]. The reduction process is shown in Scheme IV. They showed that in the first process, the product is apparently, 1,6-

dihydropurine, while at a potential on the second wave 1,2,3,6-tetrahydropurine probably results.



Scheme III: Illustration of reduction process in a pyrimidine compound [81]

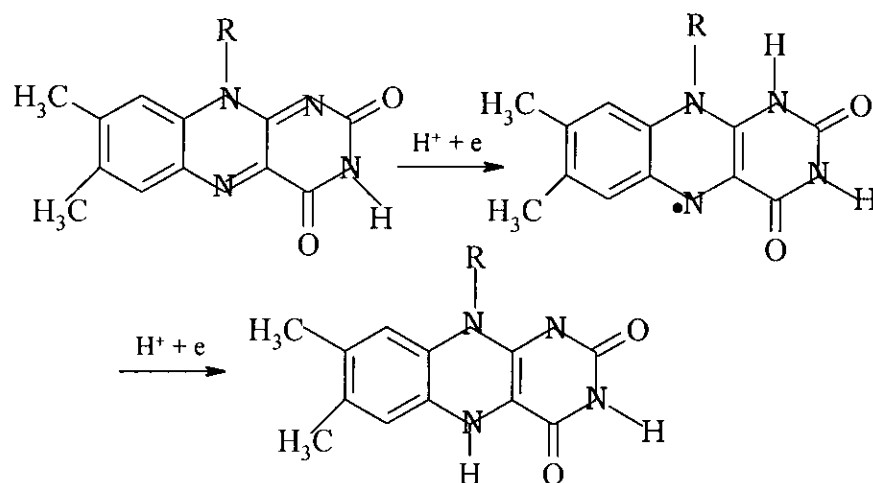


Scheme IV: Illustration of reduction process in a purine compound [81]

(iii) Flavin compound: The isoalloxazine moiety, present in all flavin compounds has been reported to undergo reduction in two one-electron steps as shown in scheme V.

Each step is reversible and the system is often referred to as "quinoid", "semiquinone" and "Hydroquinone" respectively. The potentiometric and polarographic behaviour of riboflavin and flavin nucleotides has been widely studied and reports show that though flavins are reduced in two one-electron steps these steps overlap to the extent that only one wave is evident. Polarographic half-wave potentials for the flavin systems have been found to correspond to potentiometrically determined formal potentials.  $E_{1/2}$

values vary linearly with pH. In addition to the main reduction wave, flavin compounds have also been reported to exhibit an adsorption wave whose potential varies with pH [81].



Scheme V: Reduction process in an isoalloxazine ring present in flavin compounds e.g. Riboflavin [81].

Other biological and natural compounds that have been studied using cyclic voltammetry are quinone system in thyroxine oxidation, (thyroxine is the principal hormone secreted by thyroid glands and is necessary for normal growth and development, and it also exerts a stimulating effect upon metabolism). Epinephrine (also known as adrenaline) and norepinephrine have also been studied at carbon paste electrode using cyclic voltammetry. Attempts have also been made to study porphyrins (i.e. hemoglobin, chlorophyll and cytochromes) and oxidations corresponded to one-electron reversible reactions in most cases [81- 83].

### 2.3.1 Application of Modified Electrodes in Biological and Natural Products

#### Redox Systems

Modified electrodes have found application in analysis and measurements with biological redox systems and natural compounds. As indicated above biologically active redox system give sluggish electrochemical responses due to inaccessibility of redox site and/or unfavourable adsorption. Studies of such systems and their electroanalytical application involve some added reversible electron transfer couples to mediate the biological couple's reaction or electrochemical detection of a product of the reaction between the biological component (e.g. an enzyme) and an analyte-substrate.

Modified surface-mediated reduction, oxidation or oxidation and reduction of an otherwise electrochemically sluggish biological redox system can in principle be accomplished by attaching to the electrode a redox mediator-catalyst which has  $E^0_{\text{surf}}$  more negative, more positive and approximately equal to, respectively, the formal potential of the biological couple. These three circumstances were illustrated for cytochrome C solutions by coating Pt electrodes with polymers of different hydrolytically unstable organosilines [28]. Mediator schemes like these have been extended to a number of previously intractable biological reactions, both for their analysis and for studies of the biological couples.

Other recent work done using modified electrodes in this field showed that clay modified electrode enhances the iodine redox process and electrosynthesis of thyroxine. In this work Orata and Segor [84] proposed that electrosynthesis of thyroxine occurred via formation of radical cations in the tyrosin which can then be attacked by the iodine ion forming the iodotyrosin derivative ie thyroxine.

The same workers reported that polyaniline modified electrode [85] greatly improved the oxidation characteristic of ascorbic acid. In PAN modified electrode the oxidation peak was found to be much sharper and very well defined as compared to the bare carbon case. They could not attribute this observation to improved electron transfer dynamics since plot of oxidation peak current versus square root of scan rate did not yield linear plots and so they suggested adsorption as the factor in the electrochemical behaviour of ascorbic acid

There is a not much that has been done in natural compounds and this work is an attempt to venture into application of modified electrode in characterization of a plant material.

#### **2.4.0 OBJECTIVES OF THE RESEARCH PROJECT**

The broad objectives was to adopt derivatized electrodes (DE) in electrochemical characterization of *Adansonia digitata* fruit. The specific objectives were;

- (i) Characterize fundamental physical properties of the different components of the fruit, which included moisture content, density, total internal energy and solubility, tests. FTIR analyses were carried out to identify functional groups present in the various components of the fruit.
- (ii) Identify appropriate media for electrochemical analysis i.e. aqueous or non-aqueous and effect of different supporting electrolyte.
- (iii) Obtain electrochemical standards based on existing information on composition of the fruit.



- (iv) Electrochemical characterization of the fruit components using bare carbon-working electrode.
- (v) Use conducting polymer modified electrodes in an attempt to enhance the electrochemical signal via electrocatalysis.
- (vi) Use montmorillonite modified electrodes to improve electrochemical signals via electrocatalysis and preconcentration.

## CHAPTER THREE

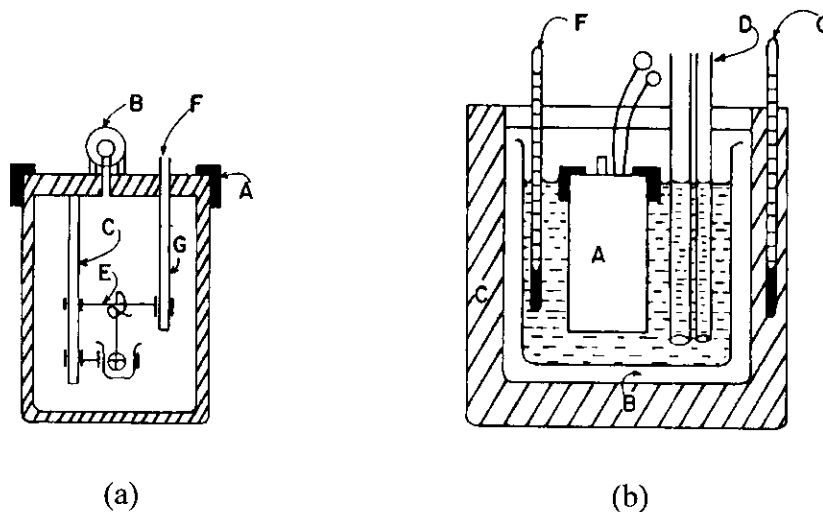
### EXPERIMENTAL SECTION

#### 3.0. METHODS OF ANALYSIS

In these experiments three methods of analysis were employed i.e. electrochemical measurements using cyclic voltammetry, spectroanalysis using Fourier transform Infrared (FTIR) and X-rays Fluorescence spectrometry was utilized for quantitative determination of elemental composition of bentonite (clay). Along side these three, the calorific values were obtained using a bomb calorimeter. The principles involved in these methods and their instrumentation are discussed below.

#### 3.1.0 BOMB CALORIMETER

In the bomb calorimeter the reaction takes place between a compound, usually an organic compound and oxygen gas at high pressure and the reaction is supposed to give well-defined products i.e.  $\text{CO}_2$  (g) and  $\text{H}_2\text{O}$  (l) [86, 87]. It is made up of two parts i.e. the bomb and the calorimeter. The bomb (fig. 3.1(a)) consists of a stainless steel pressure vessel.



(a) (b)  
Fig. 3.1: The schematic illustration of a bomb calorimeter

The lid is held in place by a strong locking-nut A, and rendered gaslight by a seal. Oxygen is introduced into the bomb through the valve B, which automatically closes when pressure for inlet of gas is reduced. A rod, C, supports a crucible of silica that contains the sample to be burnt. Combustion is initiated by means of a fine platinum wire, E, which is heated to redness by passage of an insulated terminal, F and the rod C.

The calorimeter, as shown in fig 3.1(b) comprises of the bomb, A, placed in water in a stainless steel container, B, which is surrounded by a double-walled water-jacket, C whose temperature is fairly constant. The stirrer, D, is driven by a small electric motor and stirs the water in the vessel B. The stirrer is partly made of material of low thermal conductivity to minimize heat loss from the inner vessel, B. The top of the apparatus is covered by an ebonite lid. Temperature changes inside the vessel B are measured with thermometer, F, of high accuracy and the temperature of the outer jacket is measured with a thermometer, G. In this work a Bird & Tatlock bomb calorimeter was used.

### 3.1.1 Experimental Procedure

About 0.5g of the substance to be burnt is first pressed into a pellet, which is then weighed accurately. A platinum wire of about 5cm is connected to the terminals C and G in fig. 3.1 (a), and 6cm No.60 sewing cotton thread is tied to the platinum wire. The ends of the cotton are placed under the pellet. The lid is then placed on the bomb and locking-nut A, screwed on. For safety measures the bomb has to be properly sealed. A high-pressure line, having a manometer, to an oxygen cylinder connects the valve, B in fig. 3.1 (a). The valve of the oxygen cylinder is carefully opened and the bomb filled slowly with oxygen until the pressure reaches 25atm, then the oxygen cylinder valve is closed. The

high-pressure line is then automatically released of the pressure and the valve B can be opened. The bomb is placed in the proper position in the container B, as shown in fig. 3.1 (b), which is filled with 1700mls of tap water accurately measured.

To minimize heat exchange between the calorimeter vessel B and the water-jacket the temperature of the water in B is such that it is below the temperature of the water jacket before burning the sample, and above after burning it. Since the temperature rise is about  $3^{\circ}\text{C}$  the temperature of the water in B is kept at about  $2^{\circ}\text{C}$  below that of the water-jacket before the sample is burnt. Connections are then made from the bomb terminals to the firing unit, the lid of the calorimeters is put in place thermometers and stirrer are inserted and the stirring motor is started.

Readings of the temperature of the thermometer F is started after about 5 minutes and its taken after 30 seconds for about 10 minutes or until a steady state is reached. The thermometer G is read about once every 5 minutes. The bomb is then fired and time for firing noted. Temperatures is recorded continuously every half a minute until the temperature change is again very uniform (about 30 minutes after firing). The bomb is then removed from the calorimeter, and the pressure released by a screw attached to valve B (fig. 3.1 (a)) until its down to 1 atm and the bomb can then be opened.

### 3.1.2 Calculations

The recorded temperature of the calorimeter vessel as function of time gives a curve as shown in fig. 3.2(a). Time period A represents the slow heat absorption of the vessel before firing. Period B is time after firing and before the heat of reaction is transferred completely to the calorimeter. An assumption is made that the thermometer

records the temperature of the water without any time lag. Period C is where heat is given off from the calorimeter in a regular way.

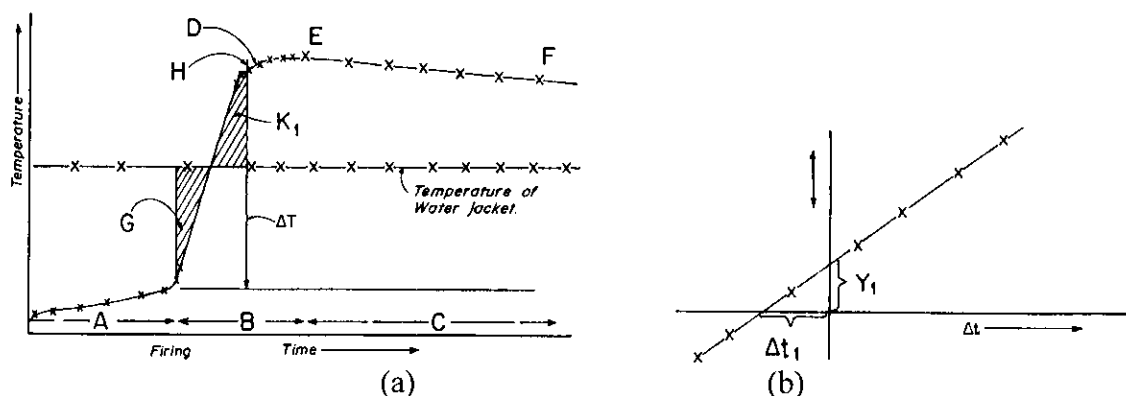


Fig. 3.2: Illustration of (a) plot of temperature recorded in a bomb calorimeter as a function of time and (b) plot of the heat of transfer  $V$  as a function of temperature difference  $\Delta t$  between the vessel B and the water jacket.

The increase in temperature,  $T$ , which is of interest, is the one due to the heat of reaction only and not to heat lost or gained from surrounding. From experiments it has been found that the rate of heat gained and heat lost is proportional to the temperature differences between the calorimeter vessel and water jacket. (The small joule-heat due to stirring is not taken into account specifically here. This can be done by plotting the rate of heat transfer  $V$ , as a function of temperature differences  $\Delta t$  between the vessel B and water jacket as shown in fig. 3.2 (b). Here  $V_1$  is due to joule-heat).

Based on the above mentioned conditions for this experiment, it can be derived that  $\Delta T$  can be found by drawing a horizontal line from the point D, extrapolating the line EF to the left and drawing a vertical line in the region B in such a way that the sum of the areas G and H are approximately equal to the area K as shown in figure 3.2(a). Knowing  $\Delta T$  and the heat capacity  $W$  of the calorimeter, the heat of the reaction be calculated.

$$-q = W \cdot \Delta T$$

W consists of the heat capacity of the water of the calorimeter (1700ml), which is taken as 1700 cal/degree, plus the heat capacity of the container B (fig 2.1(b)), the bomb, etc,  $W_b$ . To find the heat capacity of all these parts, a combustion experiments was previously carried out with a compound of known heat of combustion ie benzoic acid (heat of combustion 6318 cal/g) and  $\Delta T$  was measured. The W in equation above could then be obtained since  $-q$  and  $\Delta T$  were known. This experiment gave  $w = 2335\text{cal/deg}$  for the bomb calorimeter used in this experiment. This partly compensates for the heat of combustion of the cotton thread and the different sources of error. Since  $W=1700+W_b$  then  $W_b$  is calculated to be 635 cal/deg.

### 3.2.0 CYCLIC VOLTAMMETRY

A sophisticated collection of analytical techniques is based on voltammetry. These methods are based on observing the relationship between voltage and current during an electrochemical process. The major subdivision of voltammetry is polarography (a highly sensitive electroanalytical technique that is especially useful for trace analysis) and amperometry [88]. In polarography the current flowing through the cell is measured as function of potential of the working electrode.

There are many variations on the classical direct current polarography that have been developed and cyclic voltammetry is one of them. Cyclic voltammetry is a form of polarography that is used principally to characterize the redox properties of compounds and to study the measurements of redox reactions. It is a chronoamprometric technique i.e. involves the controlled variations of voltage while the changing current is monitored. This is achieved by use of a potentiostat.

### 3.2.1 Principles of Cyclic Voltammetry

Cyclic voltammetry (CV) involves cycling the potential of a stationary electrode, (surface area  $< 1\text{cm}^2$ ), immersed in an unstirred solution containing a suitable solvent and supporting electrolyte. The potential is scanned linearly from an initial potential,  $E_i$  to a set switching potential,  $E_f$ , after which the potential scan direction is immediately reversed and the potential scanned in the reverse direction from  $E_f$  to  $E_i$ .

The excitation signal, i.e. the potential scan, has a triangular waveform. This triangular potential excitation signal sweeps the potential of the working electrode back and forth between the switching potentials.

Current measurements are done throughout the experiments and the resulting current-potential envelope is referred to as cyclic voltammogram, with anodic (oxidation) and cathodic (reduction) one above the other. An X-Y recorder displays the results. The current at the stationary working electrode is measured under diffusion-controlled, mass-transfer conditions [89].

The principal variables for any particular chemical system are the potential range,  $E_i - E_f$  and the potential scan rate (typically the scan rate is from 20V/sec to 100V/sec although in some cases it can be higher or lower). The scan rate is used to vary time scale on which the chemistry of the reactive species is observed. Although the potential scan is frequently terminated at the end of the first scan, it can be continued for any number of cycles. However it is important to distinguish between the initial scan and the continuing cycle since most of the qualitative data is based on the first scan. Continued cycling only alters the concentration profiles at the immediate vicinity of the electrode surface unless there are coupled chemical reactions. The position of the peaks at the potential axis relates to the formal potential of the redox process and both the peak shape and height

give information about the reaction concentration and number of electrons in the half-reaction.

For a thermodynamically reversible system oxidation and reduction peaks occur at the same potential, although small separation is normally observed e.g. in the case of quasi-reversible systems [83]. For a very slow charge-transfer one sees the complete separation of anodic and cathodic processes. Consider a case where a stationary electrode is dipped in a solution with only O as the oxidizable species. Assume the reaction is the simplest i.e. involving a single electron transferred in a fast process to give a stable products R, i.e. reducible species. The electrode redox process yields a cyclic voltammogram as shown fig. 3.3, which may be interpreted as follows.

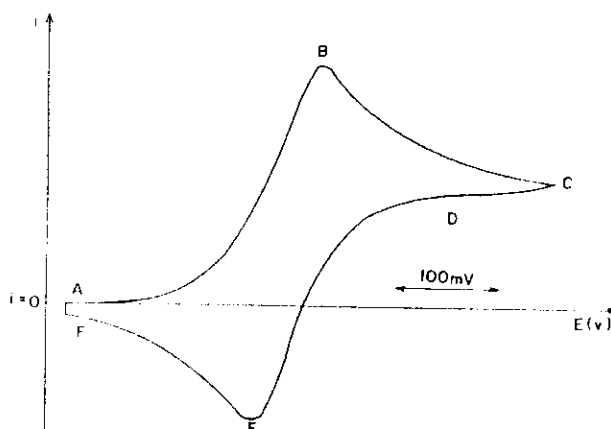


Fig. 3.3: Cyclic voltammogram of a reversible one-electron transfer reaction

The portion AB corresponds to the potential region where the ratio of the surface concentration of R to the surface concentration of O is increasing rapidly and hence the current is increasing rapidly. Non faradaic currents flow for a while if the scan began at a potential well positive than the reduction potential  $E^0$ .



When the electrode potential reaches the vicinity of  $E^0$ , reduction begins and a current is flowing. At point B the surface concentration of O is tending to zero implying the electrode is purely diffusion controlled.

The reduction in current (delay) over the part BCD reflects the decrease in the rate of diffusion of O to the surface as its flux falls off with time towards a steady value. DE is the potential region where the ratio of R to O at the surface again changes favouring O. The point E represents the potential where the flux of R to the surface and hence the current for the reverse process are at maximum. Beyond this peak both decrease towards zero, where there is again no electron-transfer taking place.

There are two related roles of the electrode in voltammetric experiments.

- (a) By controlling the current or electrode potential a known amount of oxidation or reduction is caused to occur in a small volume of solution within 0.1 mm of surface.
- (b) The current-potential data obtained during or after the above step gives information about the intermediates and products formed at the electrode surface. Information related to both the standard (formal) potentials and rates of reaction of intermediates and products can also be obtained.

Electrode reactions may be classified according to the degree of interaction between reactants, intermediates and products with the electrode surface. If the interaction is strong then the species are bonded to the surface, while in the case of electrodeposition of metal they may be a part of the surface such as lattice defect. Weaker interactions like chemisorption or physical adsorption are important in many electrode reactions since they provide new chemical information about participants in the electrode reactions when its electrochemical data is used. In non-aqueous solvent, many organic species are not adsorbed at the electrode hence their reactions fit the weaker interaction closely, which

contrast with aqueous media where adsorption occurs. For the very weak interactions the reactants, intermediates and products are unaffected by the electrode. The chemical nature of the reactants, intermediates and the electrode determine the kind of interaction between the four materials [27].

Therefore in the case of chemisorption, the free diffusion of reactants, intermediates and/or products from the electrode surface yields a nernstain (reversible) voltammogram while strong interactions where species get adsorbed or bonded to the electrode surface result in quasi-reversible or totally irreversible systems. The parameters of interest include  $i_{pa}$ ,  $i_{pc}$ ,  $E_{pa}$ ,  $E_{pc}$  and the general shape of the peak. For a reversible process at 25°C the peak current is given by the equations below regardless of the scan rate [25,27].

$$i_p = 2.67 \times 10^5 n^{3/2} AD^{1/2} Cv^{1/2} \quad (C-1)$$

While the peak separation

$$\Delta E = E_{pa} - E_{pc} = \frac{59}{n} \text{ mV} \quad \text{and} \quad \frac{i_{pa}}{i_{pc}} = 1$$

Where  $i_p$  is peak current (A)

$n$  is the number of electrons involved in the redox process

$A$  is the surface area of the electrode ( $\text{cm}^2$ )

$D$  is the diffusion coefficient ( $\text{cm}^2/\text{sec}$ )

$C$  is the concentration of electroactive species ( $\text{mol}/\text{cm}^2$ )

$v$  is the scan rate ( $\text{V}/\text{sec}$ )

In this case  $\Delta E$  is independent of scan rate and only varies slightly with  $E_f$ . When either oxidized or reduced species get adsorbed on the electrode surface the peak is given by;

$$i_p = n^2 F^2 x A \frac{Fv}{4RT} \quad (\text{C-2})$$

While the peak potential is given by

$$E_p = E^\theta - \frac{RT}{nF} \ln \frac{b_o}{b_R}$$

Where  $b = \alpha n_a \frac{Fv}{RT}$  and  $\alpha$  is the transfer coefficient

When the two equations (C-1) and (C-2) are compared, it is found that in a case of diffusion controlled processes,  $i_p$  is proportional to  $v^{1/2}$  (i.e. squareroot of scan rate) while in a case where either the reactant or product are adsorbed on the electrode surface,  $i_p$  is proportional to  $v$ . The latter is similar to what is observed for a purely capacitive current and the area under the peak corrected for residual current, represents the charge associated with reduction/oxidation of adsorbed layer i.e.  $nFA\Gamma$  (where  $\Gamma$  is the surface coverage in  $\text{mol}/\text{cm}^2$ ) [27].

Peak currents and separation may be used for quantitative and qualitative analysis, determination of the reversibility of a redox process and the diffusion coefficient of an electroactive species. The second major role of cyclic voltammetry is to provide information on any side processes e.g. pre- and post-chemical reactions leading to information of side products or intermediates. This is of great importance in finding out the mechanism of electrochemical reaction. High scan rates associated with cyclic voltammetry may also be used to determining the lifetime of unstable intermediates.

### **3.2.2 Instrumentation for Cyclic Voltammetry**

The electrochemical instrumentation used for generating the cyclic redox potential scans comprised of Princeton Applied Research (PAR) model 173 potentiostat/galvanostat, a logarithmic current converter model 376 that controlled the current. This was used in conjunction with PAR model 175 Universal Programmer that generated triangular waves. The output signal was fed into PAR RE0089 X-Y recorder.

The potentiostat/galvanostat is a dual function electrochemical instrument. When operated as a potentiostat it holds the potential between two electrodes of an electrochemical cell constant i.e. it changes the voltage between two electrodes in a controlled manner despite large changes in the current demanded by the system. When operated as a galvanostat it holds the current though in a controlled manner despite the large changes in the applied potential required to maintain current control. Throughout these analysis the model 173 equipment was used as a potentiostat.

#### **3.2.2.1 Operation of a Potentiostat**

A potentiostat maintains the potential between the working electrode and the reference electrode equal to some signal-generator potential (excitation signal). The signal generator potential may either be a constant voltage or a time varying signal. In its fundamental operation the controller reacts to the difference between these two potentials through a negative feedback circuit containing the counter electrode in such a way as to reduce the difference to zero. This operation must be performed without drawing significant current through the reference electrode. In other words, a potentiostat has control of the voltage across the working electrode-counter electrode pair and it adjusts

this voltage to maintain the potential difference between the working electrode and reference electrode (which it senses through a high impedance feedback loop) in accordance with the program supplied by a function generator. One can therefore view the potentiostat as an active element whose job is force through the working electrode whatever current is required to achieve the desired potential at any time and its response (the current) actually is the experimental observable [25, 27, 91].

The potentiostat utilizes operational amplifiers which although complex electronically, can be regarded as a three terminal black box with several connections. Usually, the amplifiers have two power supplies, one at +15V and the other at -15V, relative to a common circuit point defined at the power supplies called ground. Many measurements are made relative to this point which may or may not be related to the earth ground (see fig. 3.4).

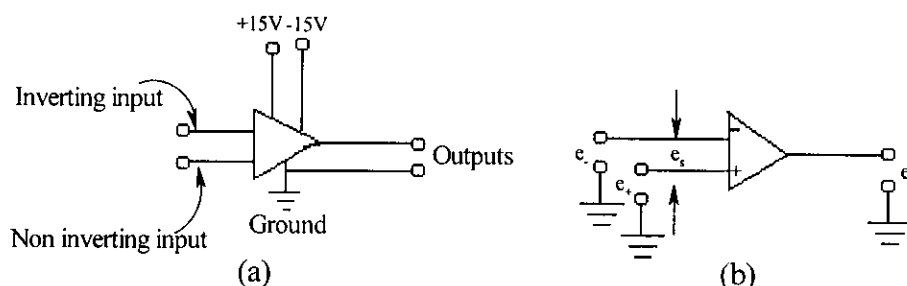


Fig. 3.4: Schematic diagrams for operational amplifiers (a) shows the power connections (b) shows the way the amplifiers are usually depicted.

There are also input and output connections and one side of the output is ground. In most cases neither of the input is ground hence they are both floating away from the ground.

In general the amplifiers have 4 useful properties:

(a) Two terminals are inputs and are referred to as the inverting (-) and non-inverting inputs (+). They have infinite input impedance, meaning they can accept an input voltage without drawing current into the device through the voltage source.

- (b) The third terminal is the output,  $e_o$  or  $E_{out}$ , which has zero impedance so that the output voltage remains constant irrespective of the current drawn by the load.
- (c) The amplifier is essentially an inverting differential amplifier with infinite gain,  $A$ , so that  $E_{out} = -A(E_- - E_+)$  and any voltage difference at inputs drives the output  $\pm \infty$ . The fundamental property of the amplifier is that the output,  $e_o$ , is the inverted amplified voltage difference,  $e_s$ , where  $e_s$  is the voltage of the inverting input with respect to the noninverting input, i.e.

$$e_o = Ae_s \quad (\text{P} - 1)$$

$A$  is the open loop gain and  $e_s$  is the sum of the inverted amplified signal  $e_-$  and the non inverted amplified signal  $e_+$  such that the above equation becomes

$$e_o = Ae_- + Ae_+ \quad (\text{P} - 2)$$

$$\text{since } e_s = e_- + e_+$$

- (d) The amplifier is able to follow changes with infinite speed.

However these are ideal properties and real devices have many limitations because of failure of the operation amplifiers to meet fully these properties. To use operational amplifiers as a control device it is necessary to introduce the principle of negative feed back where part of the output voltage is fed to the inverting input of the amplifier as shown in fig 3.5(a).

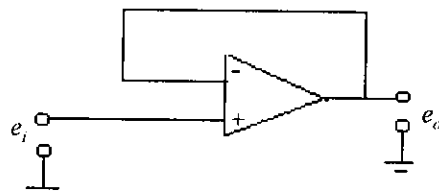


Fig. 3.5 (a): A voltage amplifier

In this configuration the amplifier operates to maintain the potential difference between the inputs at zero. Any error that appears across these inputs ( $+\delta V$ ) is amplified to give an output ( $-A\delta V$ ) that acts to reduce the error  $+\delta V$  back to zero. This simple configuration is extremely useful circuit known as the voltage follower because within the limits imposed by the sensitivity of the real device, the output voltage follows exactly the input voltage. The input impedance of the device is infinite and the output impedance is zero. This means that the circuit can measure potential at its input without drawing current from the voltage source and display the result on a measuring device, which draws current.

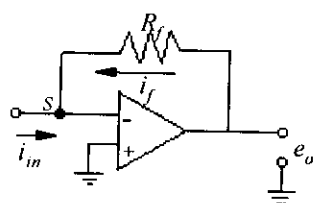


Fig. 3.5(b): A current follower

The current follower on the other hand, finds application in the measurement of the cell circuit. Considering the circuit shown in Fig. 3.5(b), the resistor,  $R_f$ , is the feedback element through which there is a feedback current,  $i_f$ . The input is a current,  $i_{in}$ , which might be from a working electrode or a photomultiplier tube. From the conservation of charge the sum of all the currents into the summing point S must be zero and since negligibly a small current passes between the inputs,

$$i_f = -i_{in} \quad (\text{P - 3})$$

$$\text{From Ohms law, } \frac{e_o - e_s}{R_f} = i_{in} \quad (\text{P - 4})$$

and by substitution from equation (P - 1)

**(P - 5)**

Since the value  $A$  is very high, the parenthesized quantity is virtually unit and

**(P - 6)**

Thus the output voltage is proportional to the input current by a scale factor determined by  $R$ . The circuit is called a current follower or a current-to-voltage ( $i/E$  or  $i/V$ ) converter. The voltage of the summing point  $e_s$  is  $-e_o/A$ , which for a typical device, lies between  $\pm 15V/10^5$  or  $\pm 150\mu V$  i.e.  $S$  is a virtual ground. Though it is not a true ground in that there is no direct connection it has virtually the same potential as ground, a very important feature because it allows currents to be converted to equivalent voltages while the current source is maintained at ground potential. This virtue is utilized in the building of a potentiostat.

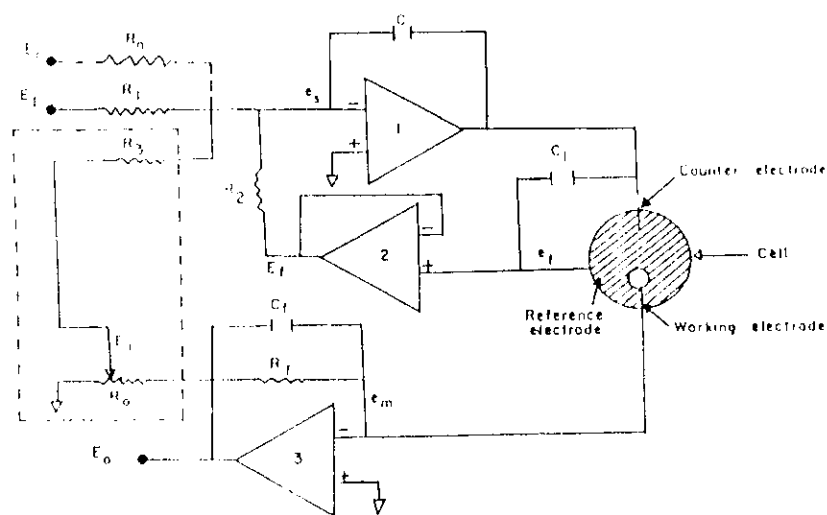


Fig. 3.5(c): Adder type operation amplifier potentiostat. Components in the dashed rectangle provide positive feedback  $iR$  compensation. Amplifiers 1, control amplifier; amplifier 2, voltage follower; amplifier 3, current follower;  $C$ ,  $C_1$ ,  $C_f$ , network stabilizing capacitors.



Figure 3.5(c) represents a potentiostat configuration that has been most widely used. It is sometimes referred to as the "adder" configuration. It has an advantage over other configurations because all of the control inputs can be referred to the ground as well as the output voltage of the current follower (amplifier 3) which is proportional to the current. However the internal impedance of the control inputs must be low. To understand the operation of this circuit, the capacitors  $C$ ,  $C_1$  and  $C_f$  (which are used to stabilize the frequency response) and the components enclosed by the dotted rectangle (used for positive feedback compensation) are ignored. The working electrode is maintained by amplifier 3 at virtual ground, which is a current follower configuration. The output of the amplifier 3 is given by

$$E_0 = -iR_f \quad (\text{AP - 1})$$

meaning that  $E_0$  is proportional to the current flowing through the working electrode.

Amplifier 2 is a voltage follower such that the output,  $E_f$  is equal to the input  $e_f$ . The potential  $e_f$  is the potential of the reference electrode measured with respect to the working electrode because this is the reverse of the conventional definition of  $E_{cell}$ ,

$$E_f = e_f = -E_{cell} = -(E_{working} - E_{reference}) \quad (\text{AP - 2})$$

This assumes that there is no uncompensated  $iR$  drop in the cell, which includes the solution, the leads to the working electrode and the working electrode itself. The voltage follower draws only minute current through the reference electrode, so that  $iR$  drops in the reference electrode are negligible. If  $iR$  drops are present in the solution or in the electrode

$$E_f = -E_{cell} + iR_u \quad (\text{AP - 3})$$

where  $R_u$  is the uncompensated resistance and  $i$  is the cell current (cathodic current taken as positive and anodic current as negative). The only electrically measurable quantity is the potential of the lead from the reference electrode measured with respect to the lead from the working electrode. At zero current this is equal to  $-E_{cell}$ .

The control inputs,  $E_l$  (upto  $E_n$ ) and the voltage follower output,  $E_f$ , are added or summed through separate input resistors connected to the summing points of amplifier 1, the control amplifier. Amplifier 1 maintains its summing point at ground ( $e_s = 0$ ) by virtue of the feedback loop that contains the counter electrode, reference electrode and follower. The summing point is a current node where the algebraic sum of all the input current is zero such that

$$\frac{E_n}{R_n} + \frac{E_l}{R_1} + \frac{E_f}{R_2} = 0 \quad (\text{AP} - 5)$$

If  $R_1=R_2=R_n$ , then  $-E_f=E_l+ E_n$  and in view of equation (AP-2),

$$E_{cell} = E_l + E_n \quad (\text{AP} - 6)$$

Simply stated the control amplifier forces current to flow through the counter and working electrodes to enforce the conditions described by equation (AP-6). For example, any tendency of the summing point to drift negative with respect to ground causes the control-amplifier output and counter-electrode voltage to become more positive,  $E_{cell}$  to become more negative and  $E_f$  to become more positive, all of which tend to cancel the negative drift at the summit point.

If the gain or frequency response of the amplifiers is inadequate there will be potential-control errors, particularly if the control inputs change rapidly with time. Likewise if the voltage and current output of amplifiers 1 and 3 are inadequate to meet

the demands, there will be an overload condition. Neon lights or meters usually are incorporated in the circuit to detect overloads.

The current is versatile and permits as many control inputs as desired to be connected to the input terminal of the control amplifier each with its own resistor. For example, a voltage ramp generator based on the integrator configuration can be connected to the input to provide a linearly changing voltage. The potential at which the voltage sweep starts can be varied by applying to a second input a variable voltage source to provide initial potential control, which is the basic configuration used in DC polarography and linear potential-sweep voltammetry. A triangular waveform applied at the input enables one to do cyclic voltammetry.

#### **3.2.2.2. Universal Programmer and X-Y Recorder**

The PAR model 175 universal programmer is a programmable waveform generator with very high precision. It has two operating modes SWEEP and PULSE. Precisely controlled single cycle or continuous cycle outputs can be obtained in both modes. Four sets of potential controls allow upto four inflection points to be set for a single output waveform. There is a provision for synchronizing, starting, stopping and reversing a programmed waveform. It has adjustable scan rates from 1mV to  $10^4$ V/sec.

In all the analysis carried in this work, the model 175 programmer was used in the SWEEP mode, with each of the potential set points independently adjusted over a range of  $\pm 10$ V.

The signal output from either the PAR model 175 programmer or model 175 potentiostat/galvanostat is fed into the model RE0089 X-Y recorder. The signal output

from the PAR model 175 programmer is that which is originally set or programmed in the equipment. When the recorder is connected normally, a positive potential will cause the X-axis to move in the upward direction. The recorder is pre-calibrated for several potential ranges. It has a 15inch X-axis and 10inch Y-axis. Single cycle or continuous voltammograms can be generated from the recorder depending on the programmed specifications.

### 3.3.0 INFRARED SPECTROSCOPY

The infrared region of electromagnetic spectrum extends from the red end of the visible spectrum to the microwave region. The region includes radiation at wavelengths between 0.7 and 500 $\mu\text{m}$  or in wavenumbers 14000 $\text{cm}^{-1}$  and 20 $\text{cm}^{-1}$ . The spectral range used most, is the mid-infrared region that covers frequencies from 200 to 4000  $\text{cm}^{-1}$  (50 to 2.5 $\mu\text{m}$ ). Infrared spectrophotometry involves examination of the twisting, bending, rotating and vibration motions of the atoms in a molecule. Atoms or atomic groups in molecules are in continuous motion with respect to one another. The possible vibrational nodes in a polyatomic molecule can be visualized from a mechanical model of the system as shown schematically in fig. 3.6.

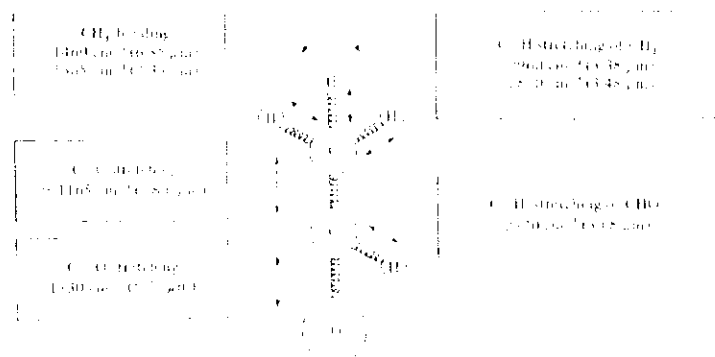


Fig. 3.6: Vibrations and characteristic frequencies of acetaldehyde

Atomic masses are represented by balls, their weights being proportional to the corresponding atomic weight, and arranged in accordance with the actual space geometry of the molecule. Mechanical springs with forces that are a proportional to the bonding forces of the chemical links, connect and keep the balls in the positions of balance. If the model is suspended in space and struck, the balls appear to undergo random chaotic motions. However if the vibrating model is observed with stroboscopic light of variable frequencies, certain light frequencies are found at which the balls seem to remain stationary. These present the specific vibrational frequencies for the motion.

The infrared spectrum of a compound is essentially the superposition of absorption bands of a specific functional groups, yet subtle interaction with the surrounding atoms of the molecule impose the stamp of individuality on the spectrum of each compound. The absorption or lack of absorption in specific frequency regions can be correlated with specific stretching and bending motions and in some cases, with the relationship of these groups to the rest of the molecule. The infrared region is divided into 3 parts.

#### **3.3.0.1 Near Infrared Region**

The near infrared region (NIR) meets the visible region at  $12,500\text{ cm}^{-1}$  ( $0.8\mu\text{m}$ ) and extends to about  $4000\text{ cm}^{-1}$  ( $2.5\mu\text{m}$ ). In this region there are many absorption bands that result from harmonics overtones of fundamental and combination bands often associated with hydrogen atoms e.g. overtones of the O-H and N-H stretching vibrations near  $7140\text{ cm}^{-1}$  and  $6667\text{ cm}^{-1}$  respectively. The absorptivity of NIR bands is from 10 to 1000 times less than that of mid infrared bands. Thicker sample layers compensate for these smaller molar absorptivities. Because the absorptivities are low, the NIR beam

penetrates deeper into the sample in the reflectance techniques giving a more representative analysis. NIR spectrometry is a valuable tool for analyzing mixture of aromatic amines. The NIR reflectance spectra find wide acceptance in the food industry for the determination of protein, fat, moisture, sugar oils, iodine numbers (unsaturation), etc. They have also been used for the determination of substances in wood, components of polymer and even geological exploration from aircraft. The intensities are weak but measurable and reproducible.

### **3.3.0.2 Mid Infrared Region**

Many useful correlations are found in this region, which is divided into the “group frequency” region  $4000 - 1300 \text{ cm}^{-1}$  ( $2.50 - 7.69 \mu\text{m}$ ) and the fingerprint region  $1300 - 650 \text{ cm}^{-1}$  ( $7.69 - 15.38 \mu\text{m}$ ). In the ‘group frequency’ region the principal absorption bands are assigned to vibration units consisting of only two atoms of molecule i.e. units that are more or less dependent on only the functional group that gives the absorption and not on the complete molecular structure. Structural influences do reveal themselves however, as significant shifts from one compound to another. In the derivation of information from an infrared spectrum prominent bands in this region are noted and assigned first. In the interval from  $4000$  to  $2500 \text{ cm}^{-1}$  ( $2.50 - 4.00 \mu\text{m}$ ), the absorption is characteristic of hydrogen stretching vibrations with elements of mass 19 or less. The C-H stretching frequencies are especially helpful in establishing the type of compound present e.g.  $\text{C}\equiv\text{C-H}$  occurs around  $3300 \text{ cm}^{-1}$ , aromatic and unsaturated compounds around  $3000 - 3100 \text{ cm}^{-1}$  and aliphatic compounds at  $3000 - 2800 \text{ cm}^{-1}$ . When coupled with heavier masses, the hydrogen, stretching frequencies overlap the triple – bond region.

The intermediate frequency range  $2500\text{-}1540\text{cm}^{-1}$  is referred to as the unsaturated region. Triple bonds are the ones that occur from  $2500$  to  $2000\text{cm}^{-1}$  while double bond frequencies fall in the region between  $2000$  to  $1540\text{ cm}^{-1}$ . By judicious application of accumulated empirical data, it is possible to distinguish among C=O, C=C, C=N, N=O and S=O bands.

The major factors in the spectrum between  $1300$  and  $650\text{ cm}^{-1}$  are single bonds stretching frequencies and bending vibrations (skeletal frequencies) of polyatomic systems that involve motions of bonds linking a substituent group to the remainder of the molecule. This is the fingerprint region. Multiplicity is too great for assured individual identification of the bands but collectively the absorption bands are in identifying the material.

### **3.3.0.3 Far Infrared**

The region  $667\text{-}10\text{cm}^{-1}$  contains the bending vibration of carbon, nitrogen, oxygen and fluorine with atoms heavier than 19 and additional bending motions in cyclic or unsaturated systems.

### **3.3.1 Instruments for Infrared Spectroscopy**

Three types of infrared instruments are found in modern laboratories, dispersive spectrometer (or spectrophotometers), Fourier-transform (FTIR) spectrometer and filter photometers. The infrared instrumentation can also be divided into two classes dispersive and non-dispersive: Fourier transforms and filter instruments are non-dispersive in the sense that neither employs a grating or a prism to disperse radiation into its component wavelength. The non-dispersive spectrometers may use interference filters, turnable laser

sources or an interferometer as in the case of FTIR. The standard dispersive infrared spectrometer is a filter-grating or prism instrument covering the range from 4000 to 650  $\text{cm}^{-1}$ . Grating instruments offers high resolution which permits the separation of closely spaced absorption bands, accurate measurement of band position and intensities and high scanning speeds for a given resolution and noise.

Fourier transform infrared spectrometer, on the other hand, offers advantages of unusually high sensitivity, resolution and speed of data acquisition (data of an entire spectrum can be obtained in 1 second or less). Offsetting these advantages is the complexity of the instrument and the high cost because a moderately sophisticated dedicated computer is needed to decode the output data.

#### **3.3.1.1 Fourier Transformations**

The mathematical operations known as fourier transformations (FT) provide a powerful method for S/N enhancement [89]. This technique is applied in instrumental analysis in two general categories:

(i) Use of FT to produce spectroscopic methods that are much faster than conventional frequency domain methods. In this technique data are rapidly collected in the time domain and converted by FT to the conventional frequency domain. Since the time required for a single scan is greatly reduced the time required for ensemble averaging is also decreased. Thus the efficiency of ensemble averaging is improved by FT spectroscopy.

(ii) Transformation of conventional signals may be multiplied by appropriate conditioning functions to achieve digital filtering and other signal modifications. A



second mathematical operation, i.e. an inverse Fourier transformation, is required to restore the conditioned signal to its original form.

There are two methods of data representation i.e. the frequency amplitude function  $F(\nu)$  and the less common time-amplitude function,  $f(t)$ . Both functions contain the same physical information expressed in different formats. The functions referred to as Fourier transform pairs are related by the following equations;

$$F(\nu) = \int_{-\infty}^{\infty} f(t) e^{-i(2\pi)\nu t} dt$$

$$f(t) = \int_{-\infty}^{\infty} F(\nu) e^{i(2\pi)\nu t} 2\pi d\nu$$

For example, if  $f(t) = A \cos 2\pi\nu_0 t$ , then  $F(\nu)$  is a single line at  $\nu_0$ , with amplitude  $A$  (see fig. 3.7 (a)). If  $f(t)$  is a square wave, the  $F(\nu)$  broadens into the form shown in fig. 3.7 (b).

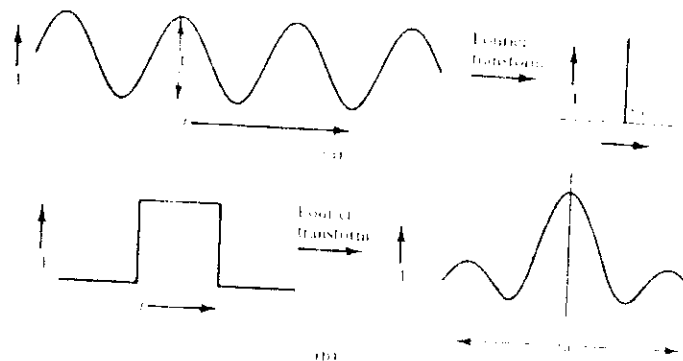


Fig. 3.7: Fourier transform pairs (a) cosine functions and (b) square-wave function

Addition of three component waveforms each occurring at a different frequency produces the  $f(t)$  pattern shown in fig 3.8. The corresponding Fourier transformation,  $F(\nu)$ , consists

of three lines located at the frequencies of the original waveforms. In this example,  $f(t)$  represents the data produced by an optical interferometer or pulsed nuclear magnetic resonance (NMR) signal source and  $F(\nu)$  is the conventional frequency spectrum. In the Fourier transform spectroscopy the data are rapidly generated in the time domain  $[f(t)]$  form by either an interferometer in the case of optical spectroscopy or a pulsed nuclear magnetic resonance signal.

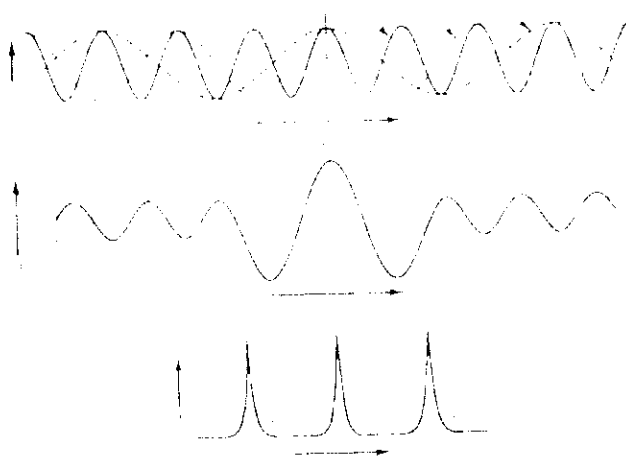


Fig. 3.8: Fourier representation of data (a) individual  $f(t)$ 's, (b) resultant  $f(t)$  and (c) Fourier transforms to  $F(\nu)$ .

### 3.3.2 Principle of Fourier Transform Spectrophotometer

In this work the Shimadzu Fourier transform infrared spectrophotometer model 8101 was used. This is equipped with a Michelson interferometer beam splitter of germanium coated on KBr plate with a black coated heated wire as the source and a high sensitivity pyroelectric detection ( $\text{LiTaO}_3$ ). The wavenumber range is  $4600\text{cm}^{-1}$  to  $400\text{cm}^{-1}$  and He-Ne laser was used for data sampling [92]. The interferogram is Fourier transformed by a 16-bit microcomputer MC 68000 to be turned to a power spectrum.

## Operation

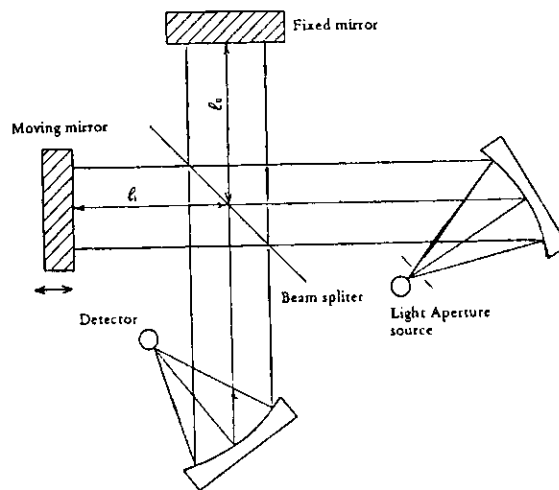


Fig 3.9(a): Michelson Interferometer

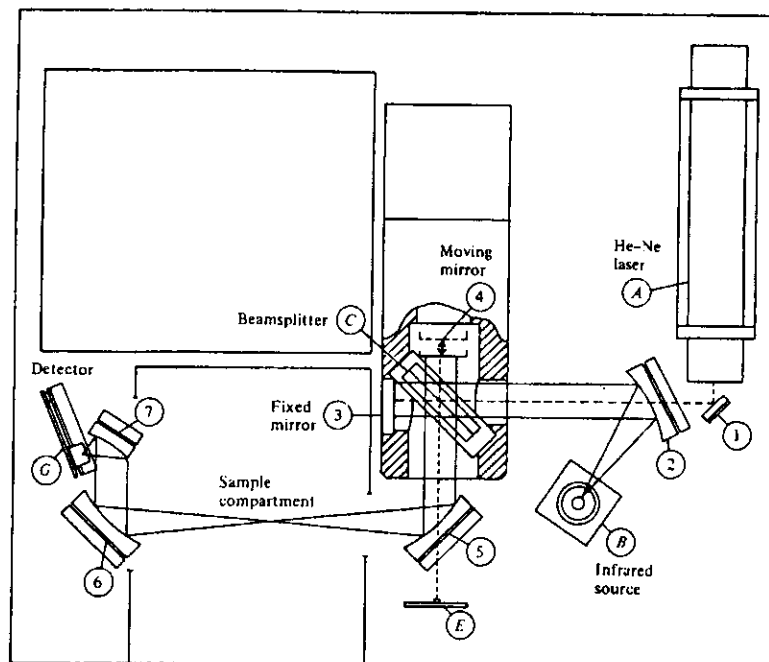


Fig. 3.9(b): Optical path diagram for FTIR spectrometer

Figure 3.9 (a) is a concept diagram of the Michelson interferometer which consists of a moving mirror (4), in fig. 3.9(b), a fixed mirror (3) and a beam splitter (C).

Radiation from the infrared source (B) is collimated by a mirror (2), and the resultant beam is divided at the beam splitter; half the beam passes to a fixed mirror (3) and half is reflected to the moving mirror. After reflection, the two beams recombine at the beam splitter and, for any particular wavelength, constructively or destructively interfere, depending on the difference in optical paths between the two arms of the interferometer. With a constant mirror velocity, the intensity of the emerging radiation at any particular wavelength modulates in a regular sinusoidal manner. In the case of a broadband source the emerging beam is a complex mixture of modulation frequencies that, after passing through the sample compartment is focussed onto the detector (G). This detector signal is sampled at very precise intervals during the mirror scan. Both the sampling rate and the mirror velocity are controlled by a reference signal incident upon a detector (E), which is produced by modulation of the beam from the helium-neon laser (A). The resulting signal from detector G, known as an interferogram, is stored in the memory and it contains all the information required to reconstruct the spectrum via Fourier transformation.

Assume that monochromatic light of wavelength  $\lambda$  (cm) is emitted from the light source. When the distance ( $l_o$ ) between the fixed mirror and the beam splitter is equal, to that of ( $l_l$ ) between the moving mirror and the beam splitter (fig. 3.9 (a)), i.e. when the optical path difference between two beams,  $x = 2 (l_l - l_o)$  is equal to zero, the two beams are in phase and so interfere constructively with each other (see fig. 3.10 (A) (B)).

As the moving mirror is displaced by  $\lambda/4$  from the position of zero retardation, the optical path difference becomes  $\lambda/2$  and the two beams interfere destructively as shown in fig.

3.10 (A) (C). Therefore the two beams interfere constructively when  $x = n\lambda$  ( $n$  is an integer) and destructively when  $x = (n + \frac{1}{2}) \lambda$ .

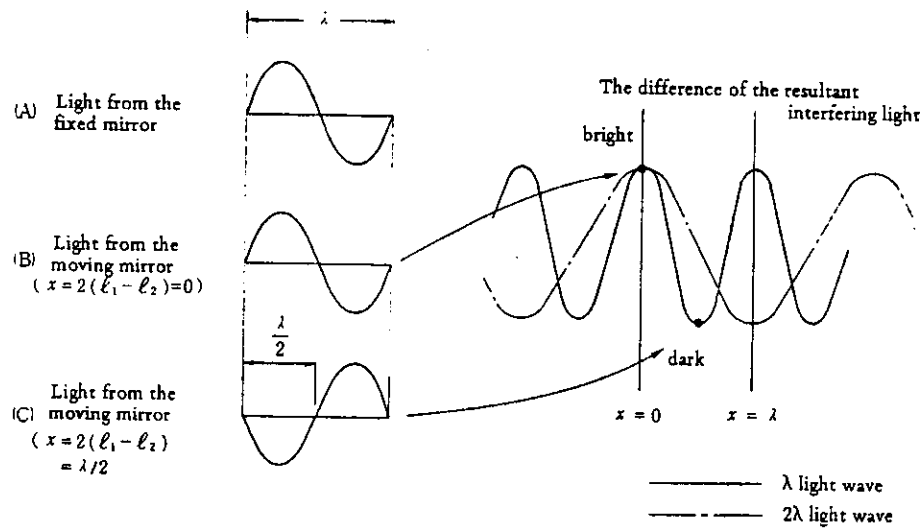


Fig. 3.10: Interference of light waves

On the basis of these facts, the intensity  $I^*(x)$  of light (wavelength  $\lambda$ ) incident to the detector is represented by the following formula.

$$I^*(x) = 4RTS(\lambda) \left[ \frac{1}{2} + \frac{1}{2} \cos 2\pi \frac{x}{\lambda} \right] \quad (\text{IR} - 1)$$

Where R: energy reflectance of the beam splitter

T: energy transmittance of the beam splitter.

$S(\lambda)$ : radiation energy distribution of the light source.

Since the intensity of the light observed by the detector is the AC component of the equation (IR - 1), the latter is denoted with  $I(x)$  and the wavelength  $\lambda$  is replaced by the wave number  $\sigma$  ( $\text{cm}^{-1}$ ), then

$$I(x) = 4RTS(\lambda) \cdot \frac{1}{2} \cos 2\pi \sigma x$$

$$= B(\sigma) \cos 2\pi\sigma x \quad (\text{IR} - 2)$$

where  $B(\sigma) = 4RT.S(\lambda). \frac{1}{2}$

The signal  $I(x)$  observed by the detector is the interferogram and  $4RT$  is termed as beam splitter efficiency. If the light emits a polychromatic light,  $I(x)$  is given by integration of (IR - 2) with respect to wavenumber.

$$I(x) = \int_0^{\infty} B(\sigma) \cos 2\pi\sigma x . d\sigma \quad (\text{IR} - 3)$$

This equation indicates that  $I(x)$  is a Fourier cosine transform of spectrum  $B(\sigma)$  and that means that inverse Fourier cosine transform of  $I(x)$  recovers the original spectrum  $B(\sigma)$ .

That is;

$$B(\sigma) = \int_{-\infty}^{\infty} I(x) \cos 2\pi\sigma x dx \quad (\text{IR} - 4)$$

While the conventional dispersive spectrometer determines directly the intensity  $B(\sigma)$  at a certain wavenumber  $\sigma$ , in the Fourier transform spectrophotometer the detector observes the interferogram  $I(x)$ , which must be subjected to Fourier transform to obtain the spectrum. While according to the equation (IR - 4) the interferogram should be recorded from  $-\infty$  to  $\infty$  of the optical path difference, this is not practically possible and so the integration is cut to a finite optical difference  $L$ , which is determined by the range of the moving mirror. It follows then that the spectrum actually obtained  $B^1(\sigma)$  is different from the true spectrum  $B(\sigma)$ .

$$B^l(\sigma) = \int_{-L}^L I(x) \cos 2\pi\sigma x dx = \int_{-\infty}^{+\infty} A(x) I(x) \cos 2\pi\sigma x dx \quad (\text{IR} - 5)$$

$$\text{where } A(x) = \begin{cases} 1 & \text{if } (x) \leq L \\ 0 & \text{if } (x) > L \end{cases} \quad (\text{IR} - 6)$$

According to the convolution theorem

$$B^l(\sigma) = B(\sigma) * F(\sigma) \quad (\text{IR} - 7)$$

Where  $F(\sigma)$  is a fourier transform of the function  $A(x)$  in the equation (IR -6)

$$\begin{aligned} F(\sigma) &= 2L \sin(2\pi\sigma L) / (2\pi\sigma L) \\ &= 2L \operatorname{sinc}(2\sigma L) \end{aligned} \quad (\text{IR} - 8)$$

This means that the obtained spectrum  $B^l(\sigma)$  is a convolution of true spectrum  $B(\sigma)$  with  $F(\sigma)$ , which is the fourier transform of  $a(x)$ , called instrument function or instrumental lines slope (ILS) [92].

Functions  $A(x)$  and  $F(\sigma)$ , represented by (IR - 6) and (IR - 8) respectively are given in fig 3.8 (b). The function  $F(\sigma)$  defined by the equation (IR - 6) first becomes zero at  $\sigma = \pm (1/2L)$  and the half value width is  $0.605/L$ . The greater the optical path difference is, the smaller the half value width is i.e. when the moving mirror is driven further resolution is improved. Resolution of a Fourier transform spectrometer is given by:

$$R = \frac{1}{\Delta_{\max}} \text{ cm}^{-1}$$

Where  $R$  is the maximum attainable resolution in wavenumbers and  $\Delta_{\max}$  is the maximum retardation i.e. twice the distance of the mirror movement in cm [89].

### **3.3.3 Advantages of FTIR Spectroscopy**

This technique has several advantages over the conventional dispersive techniques. There is only one moving part involved i.e. mirror 4, mounted on a frictionless air bearing. Dispersion or filtering is not required so that energy wasting slits are not needed. The use of helium–neon laser as a reference results in near absolute frequency accuracy, better than  $0.01 \text{ cm}^{-1}$  over the range  $4800 \text{ cm}^{-1}$  to  $400 \text{ cm}^{-1}$ .

Because all wavelengths are simultaneously detected throughout the scan, the scanning interferometer achieves the same spectral signal-to-noise ratio as a dispersive spectrometer in a fraction of the time.

### **3.3.4 Sample Handling**

The pellet technique was used in handling the solid plant samples. Plant material was finely ground and 0.1 mg of this mixed with 100 mg of KBr (transparent to IR radiation) and this pressed using an evacuable die at sufficient pressure (60,000 – 100,000 psi) to yield a transparent pellet.

## **3.4.0 X-RAY FLUORESCENCE SPECTROMETRY**

The x-ray spectrometry is a method of analyses for chemical elements. The characteristic x-ray lines of an element arise from transition of electrons within the atoms of the element. Every atom has a structure consisting of a dense central nucleus surrounded by orbitals that have elections. The election orbitals are grouped in shells



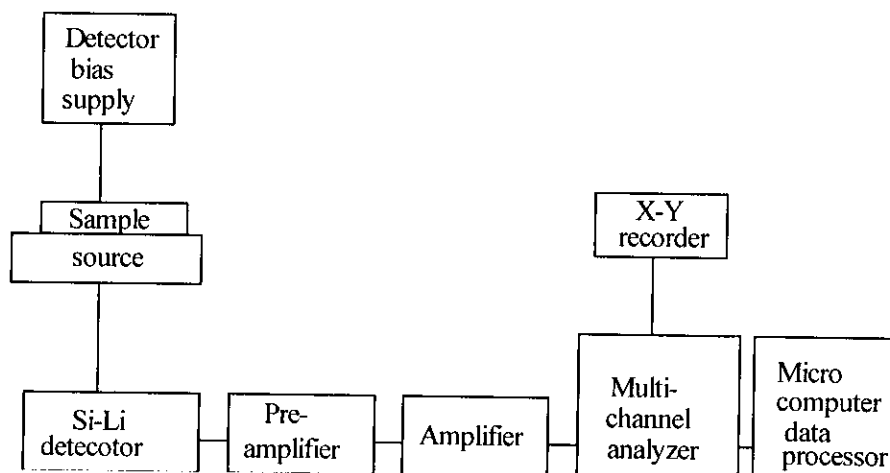
namely K, L, M, N with K shell being the closest to the nucleus and N the farthest. The closer a shell is to the nucleus the more tightly its electrons, which are negatively charged, are bound in the atom.

When an element is exposed to energy that expels electrons from the inner orbitals (K, L, M) of its atoms as the electrons from the outer orbitals fall into the vacancies created in these inner orbitals x-ray line spectrum results. Each such transition constitutes an energy loss, which appears as the x-ray photon. For example, if a K-shell vacancy is created in a heavy atom, a series of spontaneous electron transitions follow, each fills a vacancy in a level further lower which results in emission of an x-ray photon but also creates a vacancy in a level further out. The result of processes in many atoms is the simultaneous emission of the K, L and M series of x-ray spectra of that element. X-ray spectral lines are therefore grouped in series K, L, M and N. All the lines in a given series result from electron transition from various high orbitals to the indicated shell. In x-ray fluorescence spectrometry, the elements to be excited is irradiated by sufficiently energetic x-ray photons. Sources used for these excitation x-rays may be x-ray tubes, secondary radiators or radioisotope sources.

The least energy that the x-rays require to knock out orbital electrons is known as x-ray absorption edge wavelength. This is the longest x-ray wavelength that can expel an electron from a specific orbital in an atom of a specific element.

#### **3.4.1 Instrumentation for the X-RF Spectrometry**

In x-ray fluorescence spectrometry the most commonly used instrument is energy dispersive x-ray spectrometer. The schematic diagram of such a spectrometer that was used for determination of the elemental composition of bentonite is shown below.



The sample (clay) was closed in an oven at 107° C for 48 hours and then crushed into small particles. These were then pulverized into smaller particles with a grinder and further pulverization was done using agate mortar. The resulting finer clay was sieved with a 400 mesh that reduced the particle size to less than 50 microns. Sample pellets were then prepared by pressing the powder between 2 stainless steel/tungsten carbide dies at a pressure of 3-5 kpa. The pellet was then placed on the source. The spectrometer consists of Cd<sup>109</sup> radioisotope x-ray source, a solid state Si-Li detector that is inside a cryostat with a high voltage power supply, a preamplifier, a pulse-shaping amplifier and a multi-channel analyzer (MCA). The spectral data analysis was done on an IBM personal computer with relevant interface and software. These include and Axil program for the spectrum analysis and QAES for quantitative analysis using algorithm based on fundamental parameter techniques [93-94].

### 3.5.0 ELECTRODES

A three-electrode assembly in an undivided cell was used throughout this work. These consisted of a saturated calomel electrode (SCE) as the reference electrode,

platinum wire as the auxiliary or counter electrode and a carbon graphite, with a surface area of  $0.38 \text{ cm}^2$  as the working electrode.

### 3.5.1 Reference Electrode

A reference electrode is one whose half-cell potential is known at a particular temperature and is completely inert to the composition of the solution under study. It is normally used in conjunction with a working electrode, whose response depends upon the analyte concentration. Ideally it should have the following characteristics;

- (a) Exhibit a potential that is constant with time.
- (b) Return to the original potential after being subjected to small currents.
- (c) Be reversible and obey Nernst equation.
- (d) Behave as an ideal non-polarizable electrode.

A reference electrode consists of three principle parts (i) an internal element; (ii) some filling solution which constitutes the salt bridge and (iii) an area in the top of the electrode which permits a slow controlled flow of filling solution to escape the electrode (i.e. a fluid junction) into a sample under a head of a few inches and where an electrical connection is made with other components of the electrochemical cell. Reference electrodes are in three categories namely:

- (a) The first kind which have a half cell involving a metallic or soluble phase in equilibrium with its ion e.g.  $\text{H}^+/\text{H}_2$  (Pt),  $\text{Ag}^+/\text{Ag}$ .
- (b) Reference electrode of the second kind, involve a metallic phase in equilibrium with its sparingly soluble salt e.g.  $\text{Ag}/\text{AgCl}$ ,  $\text{Hg}_2\text{Cl}_2/\text{Hg}$ ,  $\text{Hg}_2\text{SO}_4/\text{Hg}$ .

- (c) Reference electrode of the third kind which include all miscellaneous electrodes e.g. glass electrode, ion- specific electrode etc.

The most commonly used of these electrodes in electrochemical analysis is the calomel electrode which comprises of non-attackable metal, platinum, in contact with mercury, mercury (I) chloride and potassium chloride moistened with the filling solution of KCl of known concentration (usually 0.1 M, 1.0M or saturated i.e. 4.2M). The saturated calomel electrode is the one often used because of the ease in preparation and maintenance. The half-cell reaction is represented by;

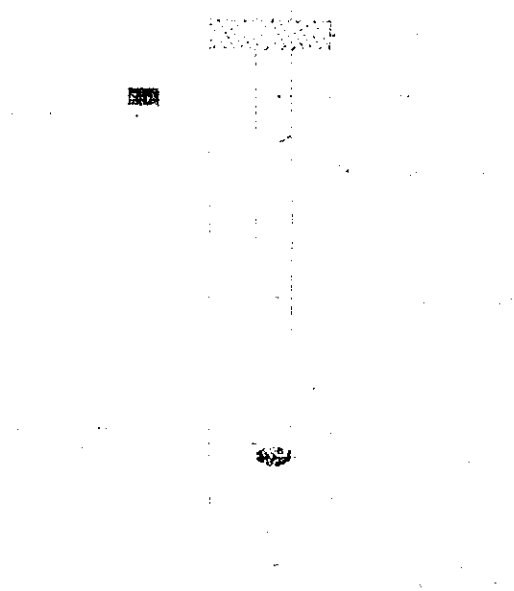
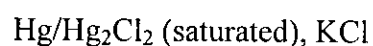
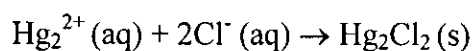
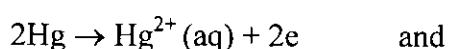
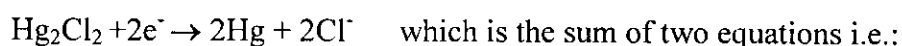


Fig. 3.11: Saturated calomel electrode.

The mercury, mercury (I) chloride (calomel) and potassium chloride paste is contained in the inner tube which is connected to the potassium chloride solution in the outer tube by means of glass wool plugged in at the end of the inner tube. The whole electrode then interacts with the analyte present in the cell via a platinum fibre at the end

of the outer tube. This type of junction has a relatively high resistance ranging from 2000 to 3000  $\Omega$  and a limited current carrying capacity before exhibition of severe polarization [90]. It however makes it difficult for the ions to move in and out of the reference electrodes, which helps prevent contamination. The half reaction for the calomel is given by;



A commercial calomel electrode consists of a tube 5 to 15 cm in length and 0.5 to 1.0 cm in diameter. The one used in these experiments was 12 cm in length and 1.5 cm diameter.

The counter electrode on the other hand can be any electrode since its electrochemical properties do not affect the behaviour of the working electrode. Usually its chosen to be an electrode that produces no substance by electrolysis that will reach working electrode surface and cause interfering reactions.

### 3.5.2 Preparation of the Working Electrode

As stated earlier, carbon graphite electrode was used throughout, as the working electrode. Bare carbon and modified electrodes were used in the analysis. The bare carbon was prepared by polishing material, till a smooth surface was obtained. This was then rinsed thoroughly with distilled water and allowed to dry at room temperature. The

electrode was then ready for analysis. This procedure was followed whenever bare carbon was used as the working electrode.

The clay used to modify the working electrode throughout the analysis was bentonite (mineral clay), which was kept at room temperature. In preparing bentonite modified electrode for use as the working electrodes, a small amount of bentonite was placed on a clean tile. Adhesive (Henkel), which is electron-inactive, was then mixed with the clay thoroughly until a thick slurry was obtained. The slurry was then smeared uniformly on a smooth surface of a freshly prepared carbon electrode. The electrode was left to dry at room temperature for 24 hours resulting in dry bentonite on the surface of the electrode.

Polyaniline modified electrodes were prepared by electrodepositing polyaniline on a freshly polished bare carbon electrode by cycling the potential from  $-0.2\text{V}$  to  $0.75\text{V}$  in a solution containing  $0.1\text{M}$  aniline and  $1\text{M}$   $\text{H}_2\text{SO}_4$ . This is normally the optimum electrolyte composition for electrodepositing aniline [54]. The scan rate was set at  $20\text{ mV/sec}$  while the current was at  $10\text{mA/V}$ . The sensitivity of the recorder was set at  $50\text{ mV/cm}$ .

### **3.6.0 CHEMICALS AND REAGENTS**

All the chemicals and reagents were used as received without further purification except for aniline and tetraethyl ammonium bromide (TEAB). Aniline (Aldrich) was triply distilled until a colourless liquid was obtained. Storing under nitrogen stabilized the

aniline. The tetra ethylammonium bromide (BDH) was purified by recrystallization [25].

All solutions were prepared using triply distilled water.

The list of chemicals and reagents used is given below:

Concentrated sulphuric acid	(Rhone – phoulenc).
Concentrated hydrochloric acid	(Gower)
Acetonitrile	(Merck)
Ascorbic acid (Vit. C)	(Howse & Mc George)
Riboflavin (Vit. B <sub>2</sub> )	(BDH)
Thiamine (Vit. B <sub>1</sub> )	(BDH)
Bentonite	(Athi River Mining Company)
Heat pillared clay and chlorophyll	(from Mukoya, Cambridge University Laboratory)

The flavonoids and alkaloids (courtesy of Alouch, A. O. of Department of Chemistry University of Nairobi) were pure extracts from *Erythrina excelsa* and *Zanthoxylum chalybeum* respectively while the diterpenes (courtesy of Juma, B. F. of Department of Chemistry, University of Nairobi) were extracts from *Psiadia punctulata*.

Elemental composition of bentonite was determined using the x-ray spectrometer and the composition in gram of element per gram of bentonite was as shown in table 3.1. Fe with 0.0498g/1g of bentonite had the highest composition followed by Ca (0.0258g/1g bentonite) and K (0.0108g/1g of bentonite). The other elements were in much smaller quantities.

Table 3. 1: Composition of bentonite obtained from spectrum analysis.

Element	Concentration in g/g of bentonite
K	$1.08 \times 10^{-2}$
Ca	$2.58 \times 10^{-2}$
Ti	$5.06 \times 10^{-3}$
Cr	$3.10 \times 10^{-5}$
Mn	$2.92 \times 10^{-4}$
Fe	$4.98 \times 10^{-2}$
Cu	$5.25 \times 10^{-5}$
Zn	$8.82 \times 10^{-5}$
Ga	$1.97 \times 10^{-5}$
Pb	$1.93 \times 10^{-5}$
Rb	$7.07 \times 10^{-5}$
Sr	$2.08 \times 10^{-4}$
Y	$2.89 \times 10^{-5}$
Zr	$1.44 \times 10^{-4}$
Nb	$1.70 \times 10^{-5}$

### 3.7.0 FRUIT SAMPLES

The *Adansonia digitata* fruit was separated into 4 parts, which were used to carry out the analysis. They were abbreviated as Ad<sub>1</sub>, Ad<sub>2</sub>, Ad<sub>3</sub>, and Ad<sub>4</sub> as follows:

Ad<sub>1</sub> – The spongy/hairy greenish part, covering the fruit

Ad<sub>2</sub> – The woody outer covering of the fruit

Ad<sub>3</sub> – The inner edible white/pink pulp

Ad<sub>4</sub> – The seed





*Adansonia digitata*- Whole Fruit



Parts of *Adansonia digitata* Fruit used in the analysis



Whole Fruit with stalks

## CHAPTER FOUR

### 4.0. RESULTS AND DISCUSSIONS

#### 4.1.0 PHYSICAL MEASUREMENTS

Several physical measurements were carried out on parts of the *Adansonia digitata* fruit i.e. density, moisture content, solubility and internal energy determination.

##### 4.1.1 Density

We determined the density of the whole fruit and individual densities of the 4 different parts of the fruit. The densities for the whole fruit, woody covering ( $Ad_2$ ) and seed ( $Ad_4$ ) were determined by weighing the sample and then putting it in some volume of water in a measuring cylinder to find out the volume displaced. Density values were then computed from the volume of water displaced and the mass of each sample.

In the case of the white-pink pulp ( $Ad_3$ ) and the hairy greenish exterior ( $Ad_1$ ) the samples were weighed and then put in measuring cylinders to determine the volume. From the two parameters, the densities were calculated. For  $Ad_1$  and  $Ad_3$  densities were obtained for the compacted and uncompact samples. In all the cases several measurements were done and the values given are the averages. The results with a standard deviation of 0.001 are tabulated in Table 4.1.

From these results it can be seen that the seed has the highest density. This is not surprising due to its composition as discussed earlier, its rich in fats. The lowest density is given by the uncompact hairy greenish covering. This is expected considering its texture. As can be seen there is a big difference between the density of the compacted and uncompact  $Ad_1$ . The reason for this is that it has a flaffy/spongy texture, which unless compacted has a lot of air spaces. This is not the case with  $Ad_3$  where the densities of the

uncompacted and the compacted do not differ very much, which may also be attributed to its texture since its fine and homogeneous.

Table 4.1: Densities of the whole fruit, and individual parts of *Adansonia digitata*

Part of the fruit	Average density (g/cm <sup>3</sup> )		
		uncompacted	compacted
Whole fruit	0.284		
Ad <sub>2</sub>	0.326		
Ad <sub>4</sub>	1.004		
Ad <sub>1</sub>		0.133	0.299
Ad <sub>3</sub>		0.241	0.295

When we compare the densities of all parts of the fruit, it is observed that the seed has the highest density followed by the woody covering then the white pulp and finally the hairy outer covering. The differences in density are as a result of the physical properties but there could be a correlation in chemical composition. The whole fruit of *Adansonia digitata* was found to have a density of approximately 0.3g/cm<sup>3</sup>.

#### 4.1.2 Moisture Content

Moisture contents for Ad<sub>1</sub>, Ad<sub>2</sub> and Ad<sub>3</sub> were determined by weighing the samples and leaving them in Gallenkamp oven model OV-160 at about 80°C for about 18 hours. These were then reweighed and from the weight loss the moisture content was calculated. The experiments were done in quadruplets for each sample and the averages obtained are shown in Table 4.2.

Table 4.2: Moisture contents of Ad<sub>1</sub>, Ad<sub>2</sub> and Ad<sub>3</sub> components of *Adansonia digitata* fruit.

Sample	% Moisture content
Ad <sub>1</sub>	7.5
Ad <sub>2</sub>	11.7
Ad <sub>3</sub>	12.5

Though the results given are showing the averages, reproducibility for some of the samples was difficult, for example, Ad<sub>2</sub> had the lowest value at 5.5% and the highest at 19.9%. On average Ad<sub>3</sub> had the highest moisture content which may be attributed to the fact that it's inside the fruit and its powdery texture. Ad<sub>1</sub> on the other hand, had the lowest moisture content, which may also be attributed to its external locality in the fruit and the hairy texture.

The results obtained in our case for Ad<sub>3</sub> are very close to those obtained in work done elsewhere by other researchers. For example, in Senegal, Becker [18] reported moisture content of 14.5% while in Malawi, Msonthi *et. al.* [21], reported a value of 13.2%. The minor differences can be attributed to the differences in localities.

#### 4.1.3 Solubility Measurements

We undertook solubility measurements for three part of *A. digitata* fruit i.e. Ad<sub>1</sub>, Ad<sub>2</sub> and Ad<sub>3</sub> in 5 different media i.e. ethanol, ethylacetate, water, 0.1MHCl and 0.1M NaOH. Measurements were done by weighing a certain amount of sample (0.2g) and dissolving it in 20 mls of solvent. This was then stirred vigorously and left to stand for 2 hours. The solutions were then filtered into a pre-weighed filter paper and the residue allowed to dry in a Gallenkamp oven set at 70-80°C. Residues from the aqueous media

were left in the oven for at least 12 hours to allow complete drying while residues from the organic solvents were left for a much shorter time. The dried filter paper with residue was then reweighed and the percentage of the sample that has dissolved was calculated from the weight differences. The experiments were done in triplicates and table 4.3 shows the average results in four of the solvent media.

Table 4.3: Percentage solubility of different components of *A. digitata* fruit in different solvent media.

Sample	% Solubility			
	Ethanol	Ethylacetate	Water	0.1M HCl
Ad <sub>1</sub>	68.9	68.9	17.3	28.8
Ad <sub>2</sub>	78.7	66.2	27.9	32.0
Ad <sub>3</sub>	69.1	72.3	63.6	87.2

The solubility results in 0.1M NaOH were not reported because it was difficult to determine them. This is because final weight was found to exceed the original weight. The samples in NaOH also yielded highly coloured compounds, Ad<sub>1</sub> greenish colour, Ad<sub>2</sub>, reddish colour, and Ad<sub>3</sub> a brownish colour. It is possible that there could have been a reaction, probably hydrolysis, yielding different compounds. Ring cleavage and/or salt formation could probably account for the inconsistency in the solubility data in NaOH. The different colours most likely indicate that the reaction with NaOH in the three samples involved different types of chemical substances.

However, from the results in Table 4.3, we found that Ad<sub>1</sub>, Ad<sub>2</sub>, Ad<sub>3</sub> are more soluble in organic solvents than in aqueous media. Ad<sub>1</sub> was found to have a much lower solubility in water, which seems not surprising considering it had the lowest moisture

content. Its compositions could be consisting of compounds that are highly organic for example, there could be long hydrocarbon chains with minimal OH group e.g. cellulose.

Ad<sub>2</sub> results show a similar trend as Ad<sub>1</sub>, being more soluble in the organic solvents and less soluble in the aqueous ones. However, from our results it seems more soluble in the aqueous solvent than Ad<sub>1</sub>. Since Ad<sub>2</sub> is woody in nature, it must be composed of lignin and cellulose which explains the way its more soluble in the organic solvents.

Ad<sub>3</sub> had a high solubility in both organic and aqueous media but the highest solubility was observed in 0.1M HCl. This high solubility could be attributed to the composition of Ad<sub>3</sub> as reported by other researchers [10, 11, 12, 17, 18, 20, and 21]. The fruit pulp (Ad<sub>3</sub>) is known to be composed of carbohydrates (monosaccharides) in high percentages (approx. 80%) and high levels of water soluble vitamins i.e. ascorbic acid. These being very soluble in the solvents we used explains the high solubilities of Ad<sub>3</sub>. Since carbohydrates and ascorbic acids have many OH groups, the much higher solubility in 0.1MHCl could be as a result of condensation reaction.

#### **4.1.4 Calorific Values**

The calorific values for Ad<sub>1</sub>, Ad<sub>2</sub>, Ad<sub>3</sub> and Ad<sub>4</sub> were obtained using a Baird & Tatlock bomb calorimeter. The procedure followed is outlined in the experimental section 3.1. The change in temperature of the calorimeter was recorded for each sample, before and after firing. Figure 4.1 shows the plot of recorded temperatures as a function of time for all the 4 samples.

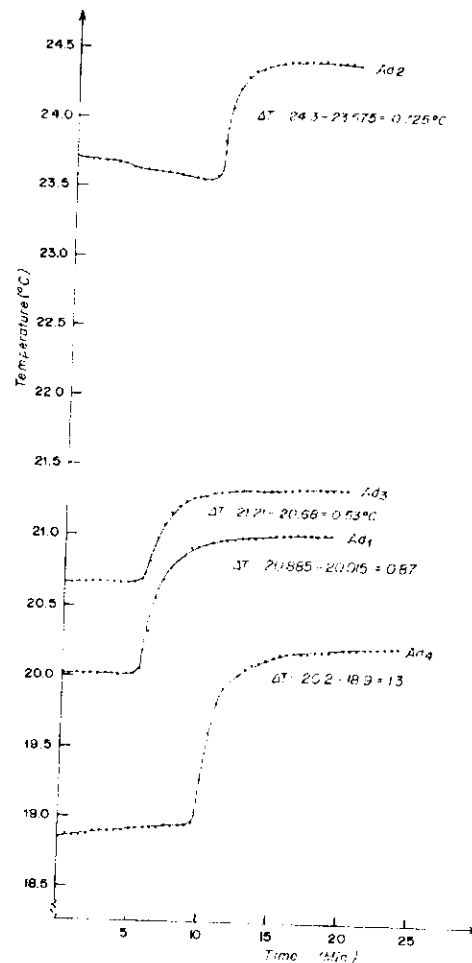


Fig. 4.1: Plot of temperature Vs time showing change in recorded temperature for each part of the fruit with time in the bomb calorimeter.

Using  $\Delta T$  the internal energies of the samples were computed. The experiments were done in duplicates and averages of these results obtained are as follows.

$Ad_1$  - 17,049.2 J/ g of sample

$Ad_2$  - 15,959.2 J/ g of sample

$Ad_3$  - 13,268.4 J/ g of sample

$Ad_4$  - 21,059.0 J/ g of sample

From these results it is apparent that  $Ad_4$  has the highest internal energy values. Comparing these with the other samples we find that between  $Ad_4$  and  $Ad_1$  there is a

difference of 12.9%, between Ad<sub>4</sub> and Ad<sub>2</sub> the difference is 18.4% and between Ad<sub>4</sub> and Ad<sub>3</sub> the difference is 32.2%.

The fact that the seed has the highest internal energy is not surprising since from literature references [10, 13, and 21], it has been reported to be rich in fats, carbohydrates and protein. In fact oil from Ad<sub>4</sub> has been found to compare well with that of groundnut. Ad<sub>4</sub> is visibly oily when crushed and smeared on a piece of paper.

Ad<sub>1</sub> was found to be second highest in internal energies values. Looking at the moisture content and solubility results reported in this thesis, the high internal energy could be attributed to the composition of Ad<sub>1</sub>, which most likely comprises of cellulose, a structural polysaccharide widely distributed in plants. Its made of at least 1500 glucose units with a molecular weight ranging from 250,000 to 1,000,000 or more [95] and its insoluble in water. Cellulose is the chief component of wood and plant fibers, for instance cotton is known to be nearly purely cellulose. Ad<sub>1</sub>, being green in colour, must also be containing chlorophyll, which is another big heterocyclic molecule. (See structure in the appendix).

Ad<sub>2</sub> has the third highest internal energy and from visual observation, it is made up of a woody material, which implies that it has lignin and cellulose in its composition. Lignin is the cementing material found between walls of woody tissue, reinforcing cellulose. It's a complex polymer formed by oxidative coupling of phenylpropane derivatives.

Ad<sub>3</sub> has the lowest internal energy which is not surprising because its composed of monosaccharides and vitamins. These are much more smaller molecules than cellulose and lignin found in Ad<sub>1</sub> and Ad<sub>2</sub> or the fats found in Ad<sub>4</sub> which would explain why it has the lowest internal energy.



The internal energy of the edible part, Ad<sub>3</sub>, obtained in these results is higher than what was reported in Senegal [18] and lower than that of Malawi [21], i.e. 8460 J/g and 14800 J/g of sample respectively. This could mean that internal energy value of the edible pulp differ in different localities. Since internal energy is an extensive property, which increased as the amount of substance increases, it may be found to vary depending on the quantity considered.

## 4.2.0 ELECTROCHEMICAL DISCUSSIONS OF *Adansonia digitata* FRUIT

### 4.2.1 The Spongy/ Hairy greenish Exterior, Ad<sub>1</sub>

#### 4.2.1.1 Analysis using bare carbon graphite working electrode

##### (a) Sulphuric Acid as the supporting electrolyte

The greenish exterior of *A. digitata* fruit was carefully scraped off the fruit plant and 0.1g weighed. This was added to 100mls of 0.5M H<sub>2</sub>SO<sub>4</sub> and studied on a bare carbon graphite working electrode by cycling the potential from -0.4V to 1.25V at a scan rate of 50mV/sec. Results of the voltammetric response are shown in fig 4.2 (a) and 4.2 (b).

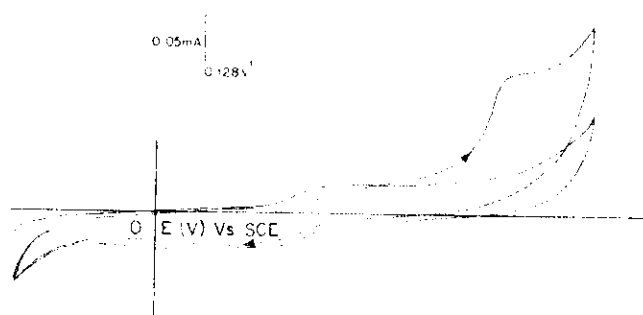


Fig. 4.2(a): Cyclic voltammetric response on a bare carbon working electrode cycled from -0.4V to 1.25V at 50mV/sec in a solution containing 0.1g of Ad<sub>1</sub> in 100mls of 0.5M H<sub>2</sub>SO<sub>4</sub> - initial scan.

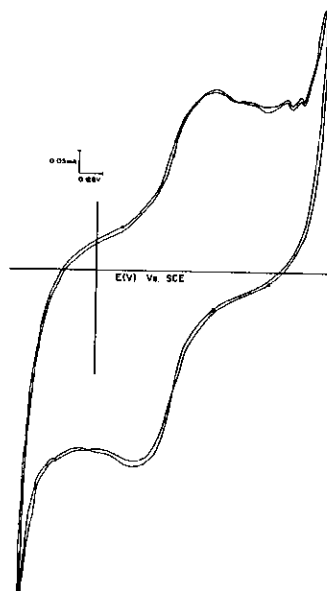
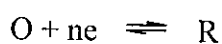


Fig. 4.2(b): CV response on a bare carbon working electrode cycled from -0.4V to 1.25V at 50mV/sec in a solution containing 0.1g of Ad<sub>1</sub> in 100mls of 0.5M H<sub>2</sub>SO<sub>4</sub> on continued cycling.

As can be seen from the CVs, during the first scan we obtained a broad oxidation peak at 0.977V and no reduction peak. On continued cyclic a quasi-reversible redox process is observed with oxidation/reduction peak potentials at 0.449V/0.359V. The resultant shift in the oxidation peak represents a negative shift of approximately 540mV. We propose the shift in oxidation peak could be attributed to;

- (i) The presence of oxidizable materials at the surface of the electrode after the first scan.
- (ii) The first material oxidized has formed a species that is oxidizable at a lower oxidation potential. This oxidizable substance could have undergone a chemical reaction forming the substance with an oxidation/reduction potential at 0.449V/0.359V. This is referred to as an EC type mechanism i.e;



In this case the product of the electrode process R reacts to produce a species that is not electroactive at potentials where the reduction of O occurred. We also observe an increase in the oxidative peak currents as we continue cycling the potentials. The rate of change of the anodic peak current as given by the initial slope of the plot of the anodic peak current versus time is  $3.3 \times 10^{-3}$  mA/min (see fig. 4.3).

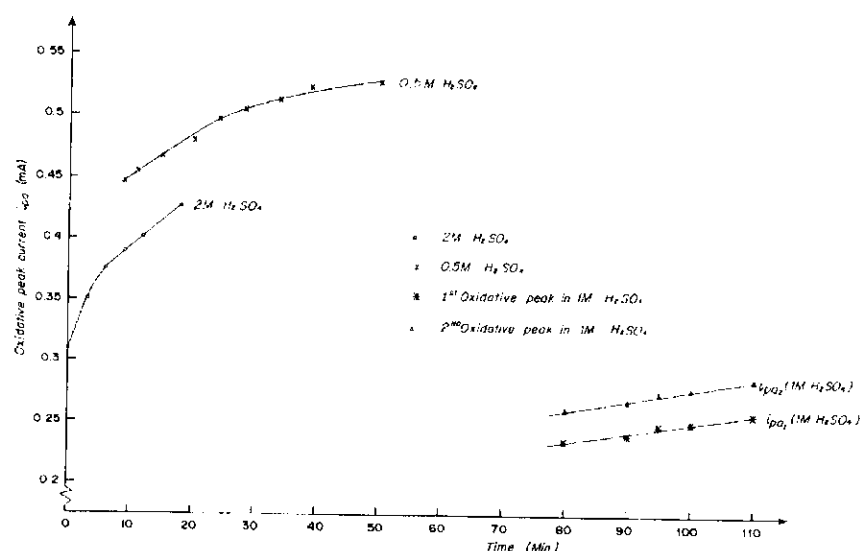


Fig. 4.3: Plot of anodic peak current versus time for  $Ad_1$  in different concentrations of  $H_2SO_4$  on a bare carbon working electrode.

The efficiency of the redox process was computed from the reciprocal of the slope of the plot of anodic peak current versus cathodic peak current and a value of 84.2% was obtained. The efficiency of the redox process is a measure of the correlation between the incremental increase in the anodic peak current versus corresponding change in the cathodic peak current.

When we increased the concentration of the acid from 0.5M to 1.0M i.e. dissolved a fresh amount of 0.1g of  $Ad_1$  in 1.0M  $H_2SO_4$  there was a change in the voltammogram. Two oxidation peaks were observed the first one at the potential 0.448V while the second

oxidation potential was at 0.563V. However, there was only one reductive peak at 0.358V.

It is obvious that the first oxidation peak potential appears to corresponds with oxidative peak recorded in 0.5M  $\text{H}_2\text{SO}_4$  the reduction peaks in both concentrations (i.e. 0.5M and 1.0M) occur at the same potential. The first and second peak persisted for well over an hour on continuous cycling of  $\text{Ad}_1$  in 1.0M  $\text{H}_2\text{SO}_4$ . But when the electrode is transferred to a solution containing 1.0M  $\text{H}_2\text{SO}_4$  (with no plant material), during the first scan, the second peak becomes well defined, though is appears 77mV more positive. This electrode was then subjected to pH analysis i.e. 0.602, 0.301, 0, -0301 and we observe that the peak is only appearing during the first scan only in the solution in which it is first analyzed regardless of the concentration, it is non-existent in subsequent cycles. We propose that this observation indicates that the plant material retained on the electrode surface on transfer to the acid solution (with no plant material) undergoes oxidation/reduction process forming soluble substances which dissipate from the electrode surface. This accounts for the lack of signal in subsequent cycles, which makes it a transient species.

Scan rate dependence analysis of the two oxidative peaks yield linear plots of peak current versus square root of scan rate suggesting a diffusion controlled process and the absence of attached species (see fig. 4.4).

Plots of oxidative peak current with time for the two oxidative peaks yielded linear plots as shown in fig. 4.3. The rates of change of peak current were computed to be  $8.33 \times 10^{-4}$  mA/min and  $7.5 \times 10^{-4}$  for first and second peak respectively. As can be seen the first oxidation peak has faster growth rate. The efficiency of the redox process of the first peak was found to be 85%.

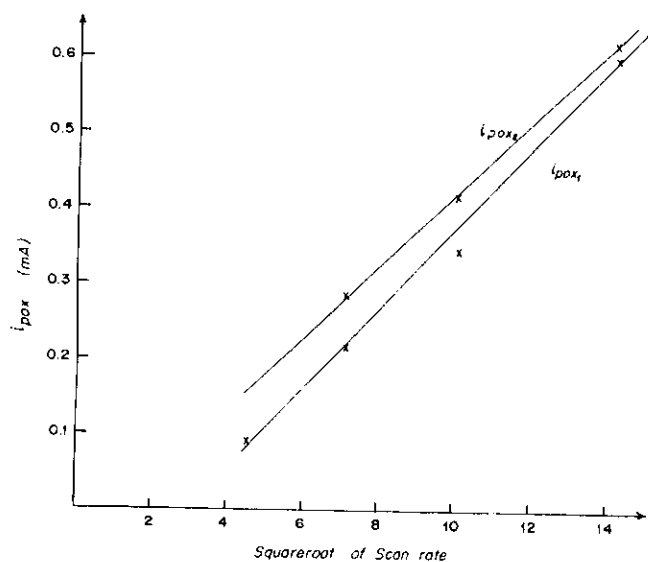


Fig. 4.4: Plot of anodic peak current versus square root of scan rate for the two oxidative peaks obtained when bare carbon is cycled in a solution containing  $Ad_1$  in 1.0M  $H_2SO_4$  from -0.4V to 1.4V.

The same experiment was repeated using a freshly polished electrode and the same amount of  $Ad_1$  but this time it was dissolved in 2.0M  $H_2SO_4$ . The resultant voltammetric response had an oxidative peak potential at 0.501V, but on continued cycling was shifting positively. This potential indicates a 52mV more positive shift as compared to the potential obtained in 0.5M and 1.0M  $H_2SO_4$  cases. It was also observed that the peak obtained in 2.0M  $H_2SO_4$  was much broader which could indicate a slow electron transfer process.

The oxidation peak potential range for the first 36 minutes was 0.501V-0.52V while the reduction peak potential at 0.353V was shifting negatively and the range was 0.353V-0.327V after 36 minutes of cycling. The redox efficiency of this process was found to be 74.1%. Comparing this with the efficiencies of 0.5M and 1M  $H_2SO_4$  we observe that;

- (i) The efficiency is higher in higher pH
- (ii) For 0.5M and 1.0M oxidative peak potentials coincide suggesting equivalent redox centres unlike the case of 2.0M  $\text{H}_2\text{SO}_4$ .

Non-equivalence of the redox centers for the latter, account for the differences in the oxidative/reductive potentials and the efficiencies. The growth rate i.e. rate of change of the anodic peak with time was computed and found to be  $4.25 \times 10^{-3}$  mA/min. This is higher than those of 0.5M and 1M (see fig. 4.5) but these differences do not reflect on the efficiencies. This is not surprising given that the rate of a process is not necessary linearly related to the efficiency e.g. thermodynamic reversibility. The slope of the plot of anodic peak potential versus pH yielded a figure of 66mV/pH indicating a one-proton one-electron process.

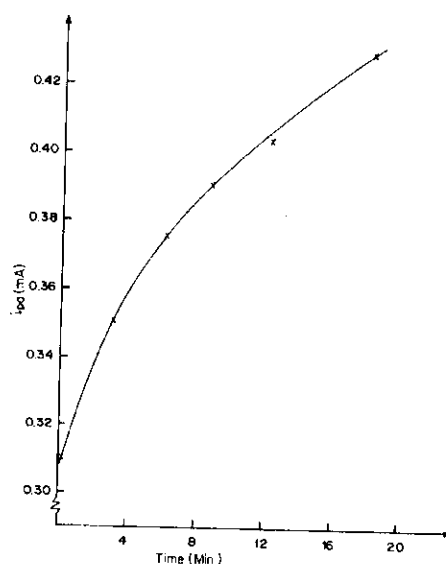


Fig. 4.5: Plot of anodic peak current versus time for  $\text{Ad}_1$  in 2M  $\text{H}_2\text{SO}_4$  when bare carbon working electrode was cycled from -0.4V to 1.4V.

#### (b) Hydrochloric Acid as supporting Electrolyte

0.106g of  $\text{Ad}_1$  was dissolved in 1.0M HCl solution and the potential of the working electrode cycled from -0.4V and 0.96V at a scan rate of 20mV/sec. The resultant cyclic

voltammetry was found to have an oxidation potential at 0.474V and a reduction peak potential 0.416V (see fig. 4.6).

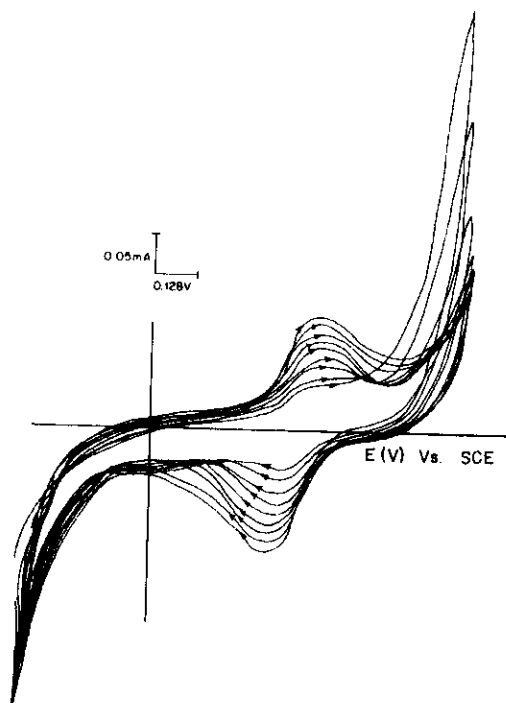


Fig. 4.6: CV response when bare carbon working electrode is cycled in a solution containing Ad in 1.0M HCl. Potential range  $-0.4\text{V}$  to  $0.96\text{V}$  Scan rate  $20\text{mV/sec}$ .

The rate of electrodeposition of the plant materials was monitored and a plot of anodic peak current versus time yielded an initial slope of  $2.35 \times 10^{-3} \text{ mA/min}$ . On continuous cycling however, there is a shift in the redox potential. The oxidation peak potential shifts from  $0.474\text{V}$  to  $0.506\text{V}$  and the reduction peak potential from  $0.416\text{V}$  to  $0.365\text{V}$ .

The sample solution was also cycled from  $-0.4\text{V}$  to various positive potentials, most of which showed redox potential shifting. In all cases irrespective of the positive potential limit it is observed that the plant material becomes difficult to oxidize as cycling progresses. A notable deviation from this is the one where the potential limit was  $1.0\text{V}$  (see fig. 4.7).

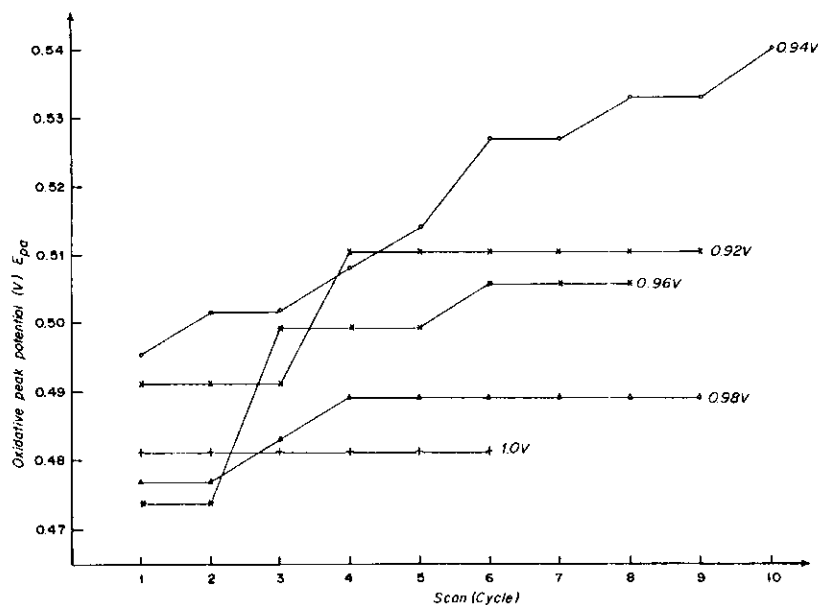


Fig. 4.7: Plot of anodic peak current versus time when bare carbon is cycled in a solution containing  $Ad_1$  in 1.0M HCl from -0.2V to varying positive potentials Scan rate 20mV/sec.

We propose that this increase in oxidation potential during the cycling can be attributed to surface phenomena whereby continued electrodeposition of plant material on the surface lowers the surface entropy. This in turn increases the Gibbs free energy since we know from thermodynamics that;

$$G = H - TS$$

In case of 1.0V as the upper limit we propose that it represents the equilibrium electrodeposition potential for the redox active plant material.

$Ad_1$  redox process was also found to be diffusion controlled which was verified by the linear plots obtained from plot of anodic peak current versus square root of scan rate (see fig 4.8). It is noteworthy that the shifts in the potentials are relatively haphazard because we are dealing with non-orderly surface phenomena resulting from electrodeposition as opposed to ordered lattice structures characterizing ionic crystals.



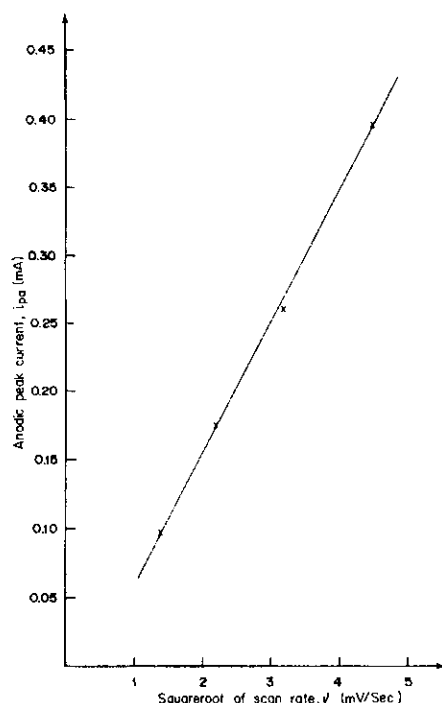


Fig. 4.8: Plot of anodic peak current Vs square root of scan rate when bare carbon is cycled in solution containing  $Ad_1$  in 1.0M HCl. Potential range  $-0.2V$  to  $0.96V$ .

Diffusion coefficient,  $D_o$ , values for electroactive species were computed over hypothetical concentration of the bulk ranging from  $10^{-6}M$  to  $10^{-2}M$  (- see Table 4.4). The diffusion coefficient is calculated using the equation;  $i_p = (2.69 \times 10^5)n^{3/2}AD_o^{1/2}v^{1/2}C_o$  where  $n$  is the number of electrons involved in the reaction and  $A$  is the surface area of the electrode.

Table 4.4: Diffusion coefficient of hypothetical bulk concentration of electroactive species in  $Ad_1$

Theoretical concentration, $C_o^*(M)$	Diffusion coefficient, $D_o$ (cm <sup>2</sup> /sec)
$10^{-6}$	$8.72 \times 10^{-5}$
$10^{-5}$	$8.72 \times 10^{-7}$
$10^{-4}$	$8.72 \times 10^{-9}$
$10^{-3}$	$8.72 \times 10^{-11}$
$10^{-2}$	$8.72 \times 10^{-13}$

The choice of the concentration range is based on the bulkiness of the molecules. The values as can be seen above varied from  $8.72 \times 10^{-5} \text{ cm}^2/\text{sec}$  to  $8.72 \times 10^{-13} \text{ cm}^2/\text{sec}$ .

The concentration of the electroactive sites,  $\Gamma$ , yielded a value of  $2.2 \times 10^{-8} \text{ mol/cm}^2$  after 60 minutes of continuous cycling indicating it is more than a monolayer ( $1 \times 10^{-10} \text{ mol/cm}^2$ ).  $\Gamma$  was calculated using the equation  $\frac{Q}{nFA}$  where Q is the charge (current x time) per square obtained by multiplying  $\frac{\text{current}}{\text{time}} \times \frac{V}{\text{cm}} \times \frac{1}{\text{scan rate (V/sec)}}$ . All these parameters were obtained from the potentiostat settings. A plot of  $\Gamma$  versus time, for several cycles starting from 0.65 to 60 minutes, yielded a curve whose initial slope gave the rate of change in coverage to be  $1.22 \times 10^{-9} \text{ mol/cm}^2/\text{min}^1$ . (See table 4.5 and fig 4.9 for the linear dynamic range from 0.64 min to 12 minutes.)

Table 4.5: Concentration of electroactive sites,  $\Gamma$ , as a function of time for  $\text{Ad}_1$  in 1M HCl.

Time (min)	Surface coverage, $\Gamma$ , ( $\text{Mol/cm}^2$ )
0.65	$3.14 \times 10^{-9}$
2.9	$6 \times 10^{-9}$
6.4	$10.9 \times 10^{-9}$
11.92	$12.14 \times 10^{-9}$
20.92	$15.13 \times 10^{-9}$
27.65	$18.54 \times 10^{-9}$

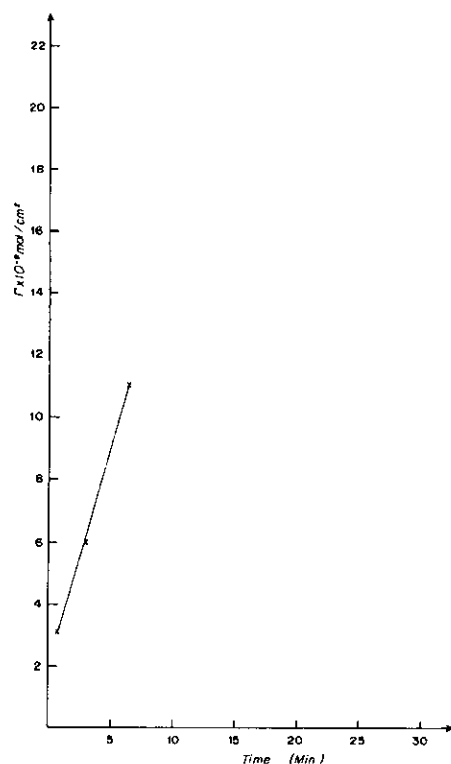


Fig. 4.9: Plot of surface coverage,  $\Gamma \times 10^{-9}$ , versus time for bare carbon in a solution of  $\text{Ad}_1$  in 1M HCl. Potential range  $-0.2\text{V}$  to  $0.96\text{V}$ .

#### 4.2.1.2 Identification of $\text{Ad}_1$

The next task was to identify  $\text{Ad}_1$  using spectroelectrochemical considerations. From a visual score of the sample, the green colouring pointed to the presence of chlorophyll. To verify this, the electrode surface was modified with heat pillared chlorophyll, courtesy of Mukaya and Jones (Cambridge university laboratories, UK) and the cyclic voltammetry obtained on scanning from  $-0.2\text{V}$  to  $0.98\text{V}$  at a scan rate of  $20\text{mV/sec}$ .

The resultant cyclic voltammetric response yielded a quasi-reversible redox peaks with oxidation and reduction peaks occurring between  $0.501\text{V}$ - $0.531\text{V}$  and  $0.419 - 0.382\text{V}$  respectively (see fig. 4.10). The redox potentials were found to be shifting just as had been the case of the raw plant material.

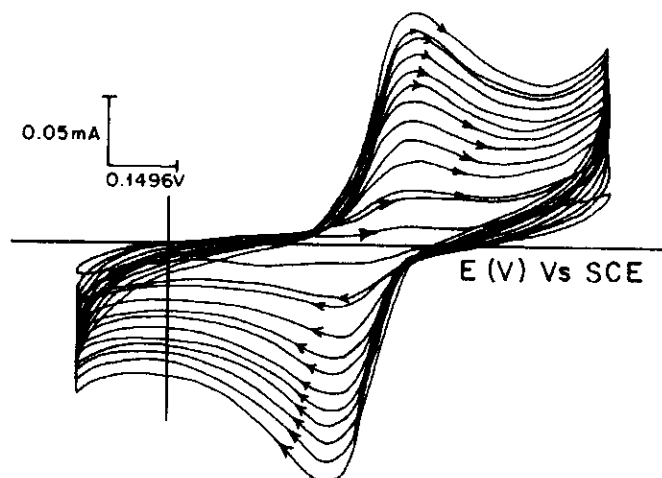
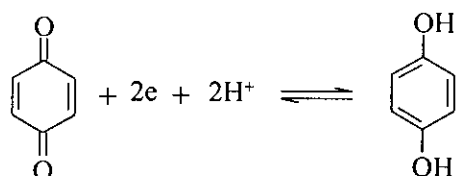
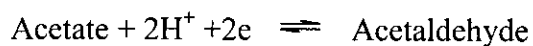


Fig. 4.10: Cyclic voltammetric response for heat pillared chlorophyll-modified electrode in a 1M HCl solution. Potential range  $-0.2\text{V}$  to  $0.98\text{V}$ . Scan rate  $20\text{mV/sec}$ .

The heat pillared chlorophyll redox potentials approximately corresponds to those of the plant material when the electrode was cycled to  $0.98\text{V}$  and  $0.94\text{V}$  positive potential limits. The latter had the oxidation peak in the range  $0.495\text{V} - 0.5398\text{V}$  and reduction peak in the range  $0.400\text{V} - 0.343\text{V}$ . In the case  $\text{H}_2\text{SO}_4$  as the supporting electrolyte the CV response was not very well defined which may be attributed to the effect of pillaring on the larger anions, but the oxidation/reduction peak appeared at  $0.494\text{V}/0.382\text{V}$ . The slight differences may be attributed to the fact that in the raw plant material there could be other electroactive centers other than those caused chlorophyll that may cause the slight variation in the potentials. A plot of oxidation peak current versus scan rates yielded a curve while oxidation peak current versus square root of scan rate yielded a linear plot implying a diffusion controlled process.

Chlorophyll has been reported in past to be redox active and it was postulated to have a one electron reversible process [83]. We are in agreement with this, given that

chlorophyll has both ester functional group (i.e. acetoacetate) and quinoid functional group. We propose that the following can represent the redox active reactions;



To further confirm the presence of chlorophyll the sample was subjected to FTIR analysis and absorption typical of the functional groups in chlorophyll were observed as shown in table 4.6 and fig. 4.11 below.

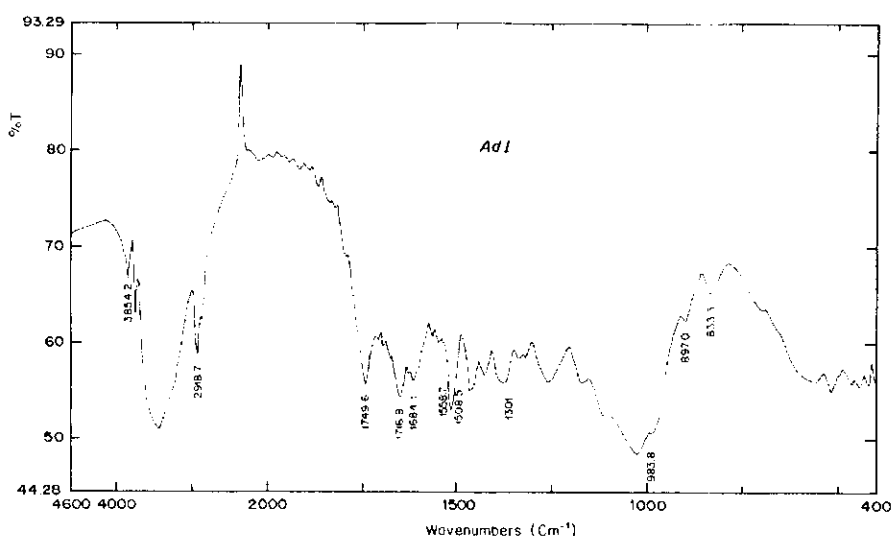


Fig. 4.11: FTIR spectrum for Ad<sub>1</sub>

Table 4.6: Wavenumbers and associated functional groups in the FTIR spectrum of Ad<sub>1</sub>

Wavenumber range (cm <sup>-1</sup> )	Functional group
2850-2980	C-H stretching bands
1470-1450	Characteristic of alkyl group.

3095-3080	Vinyl groups (CH = CH)
1645-1605	
1000-900	
1680-1560	C = C –conjugated
1765-1720	Ester group
1290-1180	
1870-1650	Carbonyl groups
1475-1450	CH <sub>2</sub> CH <sub>3</sub>
1370-1380	CH <sub>3</sub>

A broad band was observed between  $3000\text{cm}^{-1}$  and  $3700\text{ cm}^{-1}$ . This may be attributed to several functional groups some of which are present in chlorophyll e.g. alkenes and vinyl groups and others that are not in chlorophyll e.g. OH in cellulose expected to be present in Ad<sub>1</sub>.

#### 4.2.1.3 Electrochemical Activity of Ad<sub>1</sub> in Acetonitrile/water mixture.

0.125g of Ad<sub>1</sub> was weighed and dissolved in 25mls of a 1:1 ratio mixture of Acetonitrile and water. Tetraethylammonium bromide, TEAB, (0.1M) was added as the supporting electrolyte. This was then cycled from  $-0.4\text{V}$  to  $0.7\text{V}$  on bare carbon working electrode at a scan rate of  $20\text{mV/sec}$ . The resultant cyclic voltammetric response is quite different from that obtained in aqueous media with acid as the supporting electrolyte see fig. 4.12.

This is not surprising since we are dealing with semi-aqueous media where electron transport is sluggish. For example we obtained very broad oxidation and reduction peaks that made it difficult to assign the specific redox potentials. This in itself

highlights the importance of the solvent media used in electrochemical analysis when dealing with plant material.

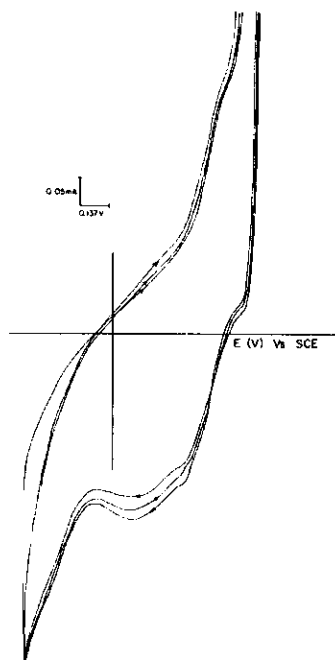


Fig. 4.12: Cyclic voltammetric response of bare carbon working electrode cycled from  $-0.4\text{V}$  to  $0.7\text{V}$  at a scan rate of  $20\text{mV/sec}$  in a solution containing  $\text{Ad}_1$  dissolved in  $25\text{mls}$  of  $\text{CH}_3\text{CN}/\text{H}_2\text{O}$  mixture in the ratio of  $1:1$  and TEAB as the supporting electrolyte.

#### 4.2.1.4 SURFACE MODIFIED ELECTRODES

##### (i) Conducting Polymer Modified Electrode

The working electrode surface was modified using a conducting polymer, polyaniline in an attempt to see whether polyaniline redox will catalyze the redox activity of  $\text{Ad}_1$ . This was achieved by electrodepositing polyaniline on a carbon graphite working electrode by cycling the potential on a carbon graphite working electrode in a solution containing  $0.1\text{M}$  aniline and  $1\text{M}$   $\text{H}_2\text{SO}_4$  in the range of  $-0.2\text{V}$  to  $0.75\text{V}$  at a scan rate  $20\text{mV/sec}$ .

Substantial amount of polyaniline was allowed to electrodeposit for varying time periods hence giving rise to films of different thickness'. The oxidation/reduction potential for polyaniline is observed at about 0.17V/0.052V respectively (see fig 4.13).

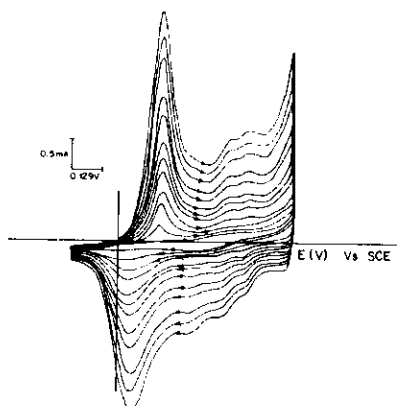


Fig. 4.13: Polyaniline electrodeposited on a bare carbon electrode cycled within the potential range  $-0.2\text{V}$  to  $0.75\text{V}$  at a scan rate of  $20\text{mV/sec}$  in a solution containing  $0.1\text{M}$  aniline and  $1\text{MH}_2\text{SO}_4$ .

The polyaniline-modified electrode was used in the study of  $\text{Ad}_1$  in  $2.0\text{M H}_2\text{SO}_4$ . This change in concentration from  $1\text{M}$  to  $2\text{MH}_2\text{SO}_4$  contrary to what was used to electrodeposit polyaniline was to deliberately shift the oxidation/reduction potentials ( $60\text{mV/pH}$ ) towards the positive end, a phenomena which has been observed by several researchers [54,59,83]. The cyclic voltammetric response obtained for both thin ( $\Gamma = 2.54 \times 10^{-8} \text{mol/cm}^2$ ) and thick films ( $\Gamma = 1.04 \times 10^{-7} \text{mol/cm}^2$ ) yielded well-defined redox peaks for  $\text{Ad}_1$ . The oxidation/reduction potentials for the thin and thick films occurred at  $0.494\text{V}/0.384\text{V}$  and  $0.52\text{V}/0.325\text{V}$  respectively. This contrasts with the values obtained in bare carbon case of  $\text{Ad}_1$  in  $2\text{MH}_2\text{SO}_4$  (i.e.  $0.501\text{V}/0.353\text{V}$ ).

The oxidation potential is reduced by  $7\text{mV}$  in the thin film case and the reduction potential by  $30.5\text{mV}$  while in the thick film case the oxidation potential increased by  $19\text{mV}$  and reduction potential by  $28\text{mV}$ . Clearly from the foregoing information it is



apparent that the thin polyaniline film electrocatalysis the redox activity of the electroactive component of  $Ad_1$ .

That electrocatalysis is not observed in the case of the thick film is not surprising based on consideration in the differences in the morphologies of the thick and thin film [59, 83]. The same electrocatalytic properties were observed in similar cases where HCl was used as the supporting electrolyte.

#### (ii) Clay montmorillonite (Bentonite) Modified Electrodes - CME

The carbon graphite working electrode was modified with bentonite and the electrode transferred into a solution containing 0.1g of  $Ad_1$  in  $2M H_2SO_4$ . The potential was then cycled from  $-0.2V$  to  $1.0V$  at a scan rate of  $20mV/sec$ . The resultant cyclic voltammogram obtained is shown in fig. 4.14. The oxidation/reduction potential occurred at  $0.456V/0.368V$ .

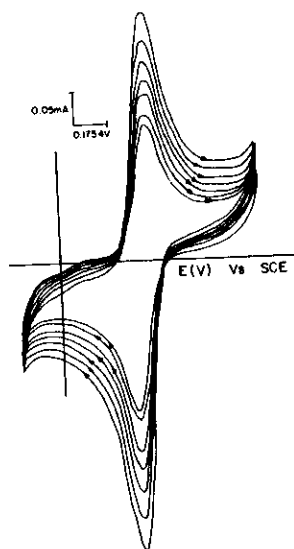


Fig. 4.14: CV response for a bentonite modified electrode when cycled from  $-0.2V$  to  $1.0V$  in a solution containing 0.1g of  $Ad_1$  in  $2M H_2SO_4$ . Scan rate  $20mV/sec$

Comparing this with the bare carbon potentials that occurred at 0.501V/0.353V and polyaniline modified electrode at 0.494V/0.384V, it is apparent that the oxidation potential is lower in the case of bentonite modified electrode.

When  $\text{Ad}_1$  is dissolved in 2M HCl as the electrolyte and the bentonite modified electrode scanned through the potential range  $-0.2\text{V}$  to  $0.98\text{V}$  at a scan rate of  $20\text{mV/sec}$ , oxidation/ reduction potentials are observed at  $0.457\text{V}/0.363\text{V}$ . From these results it is obvious that when the electrode is modified with bentonite, substantial drops in oxidation/reduction potential of the plant materials are observed when both HCl and  $\text{H}_2\text{SO}_4$  electrolyte media are used. The shifts in oxidation potentials, in both cases, are approximately  $50\text{mV}$ .

These differences are taken as a difference of the modified electrode potentials visaviz that of the highest oxidation potential in the range given for the bare carbon. The fact there is a reduction in the oxidation potentials is a pointer to the electrocatalytic properties of bentonite which is not surprising given that bentonite contains redox active centers (i.e.  $\text{Fe}^{3+}$ ,  $\text{Fe}^{2+}$  in the octahedral layer) which can interact with near/or equivalent centers in the plant material. The fact that the reduction in the oxidation potential is approximately the same for both HCl and  $\text{H}_2\text{SO}_4$  downplays the effect of the anion type in the electrolyte media, on the  $\text{Ad}_1$  redox potentials. However it was observed that in the HCl media  $\text{Ad}_1$  develops very fast as compared to the  $\text{H}_2\text{SO}_4$  media where it had to be in the solution for a much longer time before the well-defined peak could be obtained.

The redox efficiency is higher in the HCl than the  $\text{H}_2\text{SO}_4$  case i.e. 100% visaviz 80%. This probably can be explained from the fact that  $\text{Cl}^-$  ions, with the higher charge density as compared to  $\text{SO}_4^{2-}/\text{HSO}_4^-$  ions, will easily penetrate the bentonite matrix and have a higher hydration ratio. Solvent population is known to be an important aspect of

charge propagation in any matrix [54]. Scan rate dependence studies yielded linear plots for anodic peak current versus square root of scan rate for both media suggesting diffusion controlled processes.

Further manipulation of the use of bentonite in electrode modification entailed adsorption of the plant material on bentonite by allowing 5g of bentonite to stay for about 15 hours in a solution containing 0.1g of  $Ad_1$  in solutions of different concentrations ranging from 1M to 4M. The bentonite was then dried in an air oven at  $80^{\circ}\text{C}$  for about 15 hours and the dried powder crushed and used to modify the electrode surface.

Selecting the 4M case for comparison on the effect of adsorption in the HCl and  $\text{H}_2\text{SO}_4$ , it is apparent that the CV responses differ with the electrolyte media (see fig. 4.15 and 4.16). In the case of HCl the oxidation/reduction potential ranges from 0.472-0.575V/0.376-0.302V while for  $\text{H}_2\text{SO}_4$ , it ranges from 0.452-0.644V/0.326V (the oxidative peaks shift positively on continuous cycling).

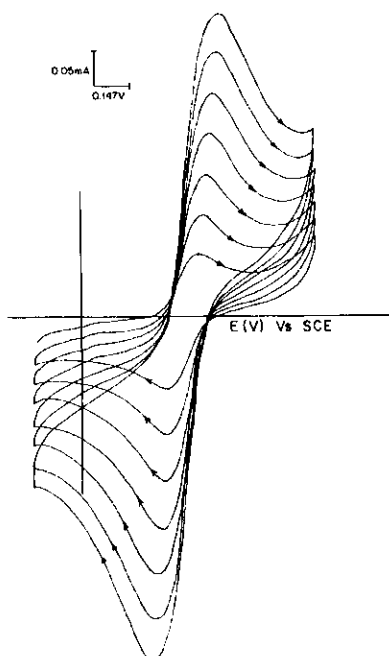


Fig. 4.15: CV response obtained when an electrode modified with bentonite, on which  $Ad_1$  in 4M HCl had initially been adsorbed, was cycled from -0.2V to 0.98V in a blank 1.0M HCl solution at a scan rate of 20mV/sec.

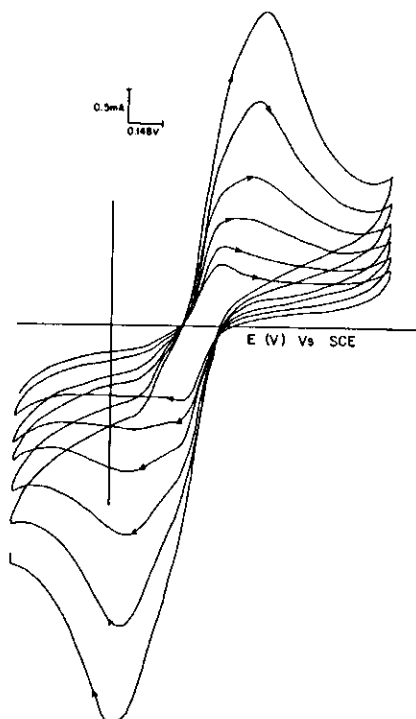


Fig. 4.16: CV response obtained when an electrode modified with  $Ad_1$  in 4M  $H_2SO_4$  adsorbed onto bentonite was cycled from -0.4V to 1.2V in a blank 1M  $H_2SO_4$  solution. Scan rate 20mV/sec.

It is apparent that in both cases we have substantial shifts in oxidation and reduction potentials. In general the cyclic voltammogram is the same except that in the case of sulphuric acid the oxidation/ reduction peaks appear to consist of several peaks/shoulders. We propose that the shoulders are probably an indicator of the adsorption phenomena in play (this will become more apparent in  $Ad_4$ ).

The same features were observed for other concentration of  $H_2SO_4$  and HCl that have not been discussed. While the general features of the oxidation/reduction potentials were following the same pattern, the redox efficiencies were different, with one of  $H_2SO_4$  being 91.4% and that of HCl 86.7%. Both redox processes were found to be diffusion limited from the plots of peak current versus square root of scan rate irrespective of the electrolyte media.

## 4.2.2 THE BROWN WOODY COVERING, Ad<sub>2</sub>

### 4.2.2.1 Analysis using Bare Carbon working electrode

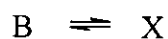
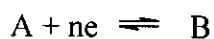
For the experiments done, 0.1g of this component of *Adansonia digitata* fruit was weighed and crushed into fine powder. The resultant solution was characterized by precipitation in both H<sub>2</sub>SO<sub>4</sub> and HCl and so the solution was decanted in each case and then subjected to electrochemical analysis.

#### (a) Sulphuric acid as supporting electrolyte

A solution of Ad<sub>2</sub> in 1M H<sub>2</sub>SO<sub>4</sub> was subjected to electrochemistry by cycling the potential of the working electrode from -0.4V to 1.4V at scan rate of 50mV/sec.

The cyclic voltammetric response obtained did not show any well-defined peak and so the experiment was repeated using a fresh sample of Ad<sub>2</sub> in 2MH<sub>2</sub>SO<sub>4</sub>. The resultant cyclic voltammetric response of the latter is shown in fig. 4.17.

Two oxidation peaks and reduction peaks were observed in the first few minutes of cycling after which one set of the redox peaks disappears. The oxidation peak disappears after about 30 minutes of cycling and occurs in the range 0.803V-0.835V while the reduction peaks disappeared after only 5 minutes (i.e. after two cycles) and it occurred at 0.084V. The disappearance of these peaks can probably be attributed to EC mechanism.



The oxidation peak that occurs at 0.449V but on continued cycling it shifts positively while the reduction peak occurs at 0.379V and shifts negatively on continued cycling

such that after 17 minutes of cycling oxidation and reduction peaks are in the range 0.449-0.482V and 0.379-0.366V respectively. The  $\Delta E$  ranges from 64mV for the first scan to 116mV after 17 minutes of cycling. This means that on continued cycling the redox moiety becomes more difficult to oxidize.

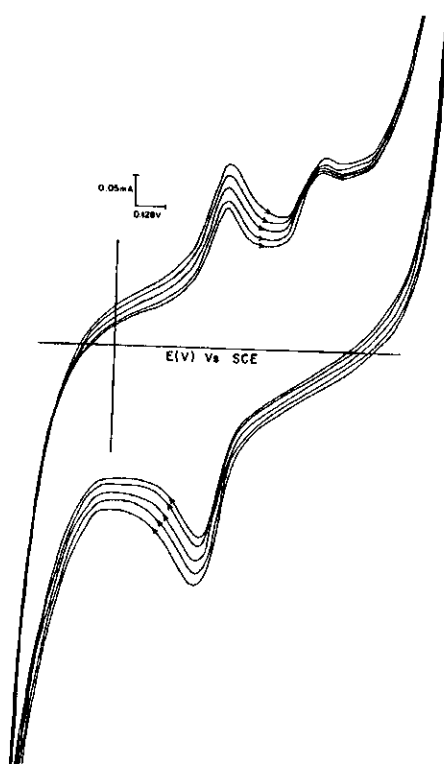


Fig. 4.17: Cyclic voltammetric response for bare carbon working electrode when cycled from  $-0.4\text{V}$  to  $1.4\text{V}$  at a scan rate of  $50\text{mV/sec}$  in a solution containing  $0.1\text{g}$  of  $\text{Ad}_2$  in  $2\text{M H}_2\text{SO}_4$ .

The scan rate dependence studies computed from the initial slope yielded a linear plot for the case of anodic peak current versus square root of scan rate indicating a diffusion controlled process (see fig. 4.18). The rate of electrodeposition was found to be  $1.28 \times 10^{-2} \text{ mA/min}$  (see fig. 4.19) while the redox efficiency for the process was 87.5%. The pH dependence studies indicate there are positive shifts in oxidation potential as pH is lowered. This could mean that the redox processes are dependent on protonation/deprotonation equilibrium. A shift of  $21\text{mV/pH}$  unit was computed.

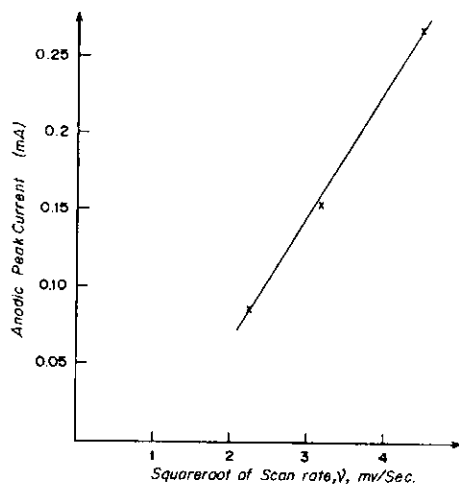


Fig. 4.18: Plot of anodic peak current versus square root of scan rates when bare carbon electrode was cycled from  $-0.4\text{V}$  to  $0.14\text{V}$ .

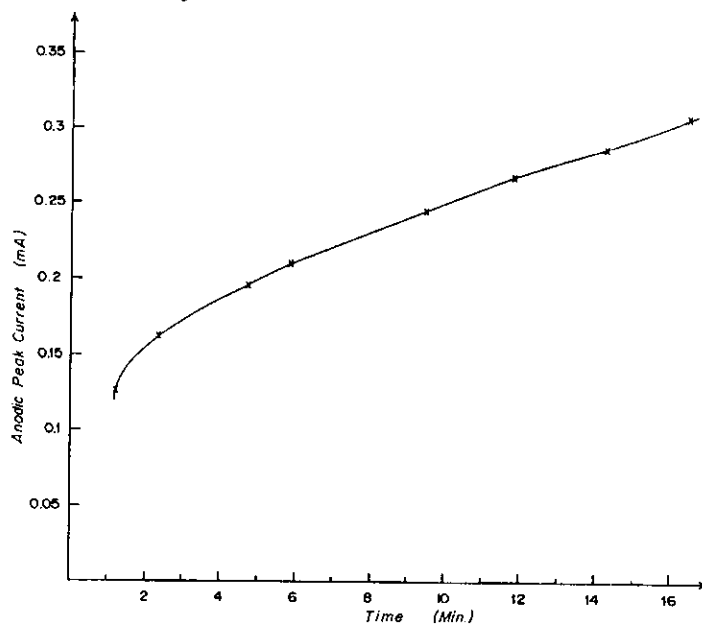


Fig. 4.19: Plot of anodic peak current versus time for  $\text{Ad}_2$  in  $2\text{M H}_2\text{SO}_4$

#### (b) Hydrochloric acid as the supporting Electrolyte

A fresh solution of  $0.1\text{g}$  of  $\text{Ad}_2$  in  $1\text{M HCl}$  was subjected to electrochemical analysis in which the working electrode was cycled from  $-0.4\text{V}$  (constant) to varying potential limits i.e.  $0.92\text{V}$  to  $1.0\text{V}$ . The scan rate was maintained at  $20\text{mV/sec}$ . The resultant cyclic voltammetric response yielded a well-defined redox peak with oxidation

potential varying from 0.473V-0.545V on continued cycling for the 0.94V positive potential limit case which was the most well defined (see fig. 4.20).

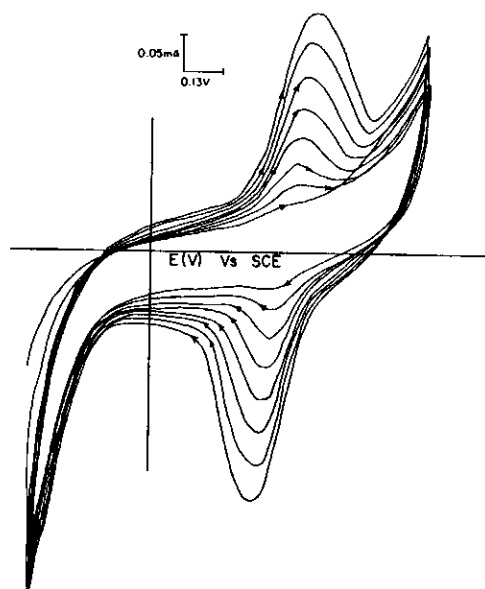


Fig. 4.20: CV response for a bare carbon in a solution containing 0.1g of  $\text{Ad}_2$  in 1M HCl. Potential range  $-0.4\text{V}$  to  $0.94\text{V}$ . Scan rate  $20\text{mV/sec}$ .

The scan rate dependence studies in HCl revealed that the slope of the anodic peak current with square root of scan rate was linear. This is a clear indication just as in the case of  $\text{Ad}_1$  that we are dealing with a diffusion-limited process. The pH dependence studies indicate that the redox process is dependent on protonation/deprotonation equilibrium. In this case the shift is  $87.5\text{mV/pH}$ , suggesting a 3-proton, 2 electron process [26]. See fig. 4.21.

From the potential windows studied it is apparent from the variation of anodic peak current that the rates of growth varied with the positive potential limit – see table 4.7. From the table the highest growth rate is seen to be in the  $0.94\text{V}$  limit case. It was observed that the redox efficiency of the process in most cases was corresponding with the growth except for with  $0.92\text{V}$ . On comparing with  $\text{H}_2\text{SO}_4$  electrolyte media these



redox efficiencies were much higher. This can be explained from the high charge density of  $\text{Cl}^-$  and high hydration ratio.

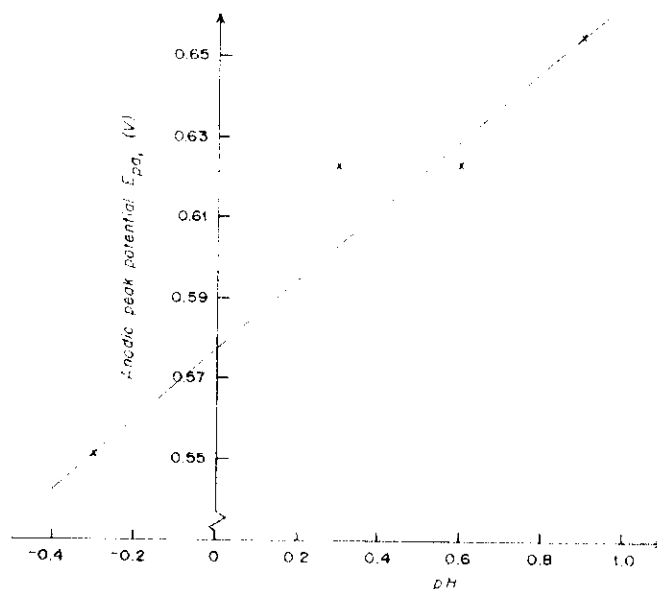


Fig. 4.21: pH dependence studies - A plot of anodic peak potential Vs pH for  $\text{Ad}_2$  in 1M HCl electrodeposited on bare carbon in solutions containing 0.125M, 0.25M, 0.5M, 1M and 2M HCl.

Table 4.7: Rates of electrodeposition and redox efficiencies of  $\text{Ad}_2$  in 1M HCl as functions of positive potential limit.

Positive potential limit, E (V)	Rate of electrodeposition, $di_{pa}/dt$ (mA/min)	Redox efficiency (%)
0.92	$9.7 \times 10^{-3}$	90
0.94	$1.45 \times 10^{-2}$	94.8
0.96	$6.96 \times 10^{-3}$	93.7
0.98	$2.17 \times 10^{-3}$	92.8

An estimation of the diffusion coefficient assuming concentrations of the bulk in the range of  $10^{-6}\text{M}$  to  $10^{-2}\text{M}$  yielded the following values as shown in table 4.8. On the

other hand,  $\Gamma$ , which quantifies the concentration of the electroactive sites, yielded a value of  $2.72 \times 10^{-8} \text{ mol/cm}^2$  after 16 minutes of cycling for the 0.94V case (see table 4.9).

Table 4.8: Diffusion coefficient values for hypothetical bulk concentrations of electroactive species in  $\text{Ad}_2$

Theoretical concentration $C^*_o \text{ (M)}$	Diffusion coefficient $D_o, \text{ cm}^2/\text{sec}$
$10^{-6}$	$2.04 \times 10^{-4}$
$10^{-5}$	$2.04 \times 10^{-5}$
$10^{-4}$	$2.04 \times 10^{-8}$
$10^{-3}$	$2.04 \times 10^{-10}$
$10^{-2}$	$2.04 \times 10^{-12}$

Table 4.9: Surface coverage,  $\Gamma$ , ( $\text{mol/cm}^2$ ) of electroactive species in  $\text{Ad}_2$  as a function of time.

Time (min)	$\Gamma, (\text{mol/cm}^2)$
2.5	$2.36 \times 10^{-9}$
4.8	$6.01 \times 10^{-9}$
7	$8.28 \times 10^{-9}$
9.3	$12.6 \times 10^{-9}$
11.5	$17.4 \times 10^{-9}$
13.7	$22.8 \times 10^{-9}$
15.9	$27.2 \times 10^{-9}$

The rate of change of the amounts of  $\text{Ad}_2$  deposited per unit time i.e.  $d\Gamma/dt$  differs between the first six minutes and between the 6<sup>th</sup> and 16<sup>th</sup> minute. The  $d\Gamma/dt$  for the first

six minutes was found to be  $1.2 \times 10^{-9}$  mol/cm<sup>2</sup>/min and  $2.7 \times 10^{-9}$  mol/cm<sup>2</sup>/min for the 6<sup>th</sup> and 16<sup>th</sup> minute. It is proposed that there two different rates is as a result of autocatalysis i.e. enhanced electrodeposition of the plant material as more is deposited on the electrode surface, see fig. 4.22.

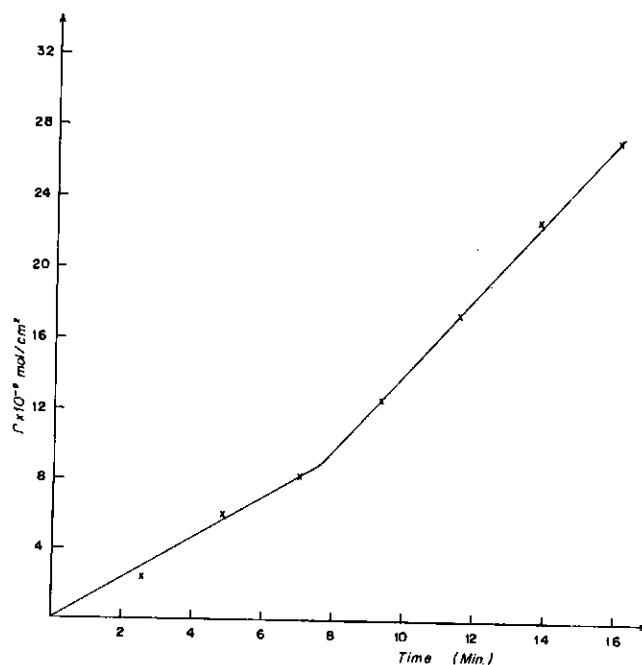


Fig. 4.22: Plot of surface coverage,  $\Gamma \times 10^{-9}$ , versus time of electroactive species in a solution of  $\text{Ad}_2$  in 1M HCl

The  $d\Gamma/dt$  in the case of  $\text{Ad}_1$  differs from that of  $\text{Ad}_2$  in the sense that, within the 16 minutes there is no indication of changes in the rate i.e. no autocatalysis. It is noteworthy that the rate of change of the amount of  $\text{Ad}_2$  in the first six minutes equals that of  $\text{Ad}_1$  in the same period.

#### 4.2.2.2 Identification of $\text{Ad}_2$

FTIR analyses were done on  $\text{Ad}_2$  to help identify the functional groups present. Figure 4.23 shows the FTIR spectrum for  $\text{Ad}_2$  while table 4.10 shows the wavenumbers that have been associated with certain functional groups. From what we know of  $\text{Ad}_2$ , it

should contain some lignin and cellulose. Lignin is known to contain methoxy groups and ester groups, which is what is most likely yielding electrochemical signal. From the FTIR results we are able to confirm the presence these groups.

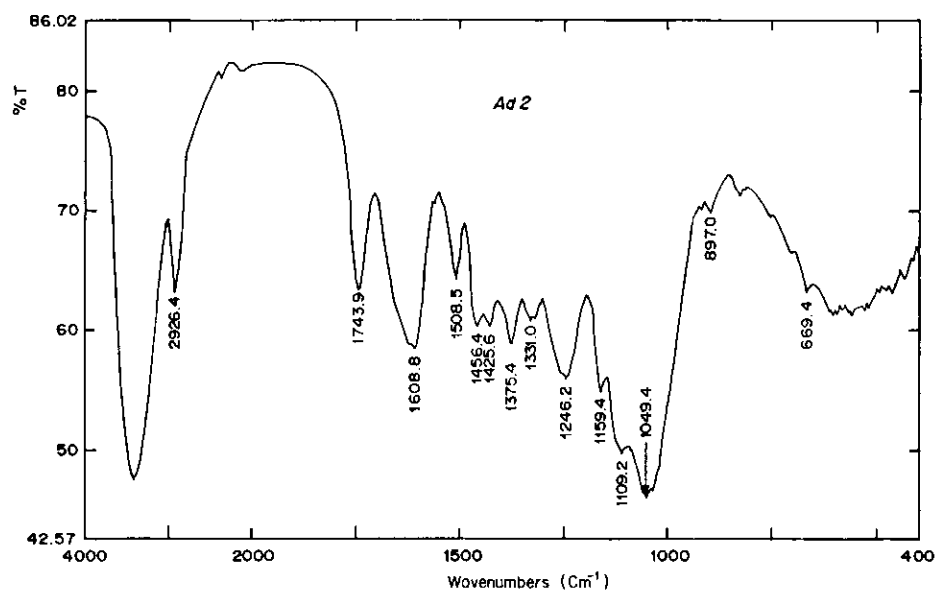


Fig. 4.23: FTIR spectrum for Ad<sub>2</sub>

Table 4.10: Wavenumbers and functional groups identified in the FITR spectrum of Ad<sub>2</sub>

Wavenumbers (cm <sup>-1</sup> )	Functional group
3500-3250	OH Polymers
2926.4	C-H, (C=C-H, CH <sub>3</sub> X, CH <sub>2</sub> X)
1743.9	Ester
1246.2	
1608.8	Vinyl groups

#### 4.2.2.3 Analysis of $\text{Ad}_2$ in Acetonitrile/water mixture

0.1g of  $\text{Ad}_2$  was once again dissolved in 1:1 acetonitrile/ water mixture in the presence of 0.2M tetraethylammomium bromide and the potential cycled from  $-0.4\text{V}$  to varying positive limits i.e.  $0.68\text{V}$  to  $0.74\text{V}$  at a scan rate of  $20\text{mV/sec}$ . In all the cases the cyclic voltammetric responses yielded a non-reversible redox peak with only the reduction peak being well defined at a potential of  $0.287\text{V}$ , see fig. 4.24.

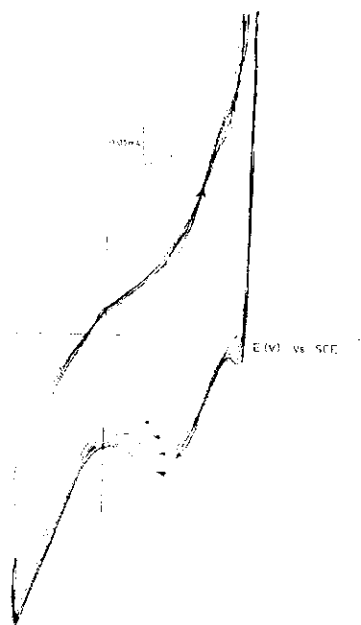


Fig. 4.24: Cyclic voltammetric response of bare carbon in a solution containing 0.1g of  $\text{Ad}_2$  dissolved in a 1:1 mixture of  $\text{CH}_3\text{CN}/\text{H}_2\text{O}$  and TEAB as the supporting electrolyte. Potential range  $-0.4\text{V}$  to  $0.68\text{V}$ . Scan rate  $20\text{mV/sec}$ .

The non-reversibility of the redox process whereby the oxidation peak is characterized by a shoulder at  $0.51\text{V}$  is a pointer to the fact that the solvent media definitely affects the redox mechanism since, in the case of aqueous acid media we had perfectly reversible redox processes. The latter observation points further to the significance of protons in the overall redox process of  $\text{Ad}_2$ .

#### 4.2.2.4 Analysis using modified Electrodes

##### (a) Polyaniline modified Electrode

As already discussed in the case of  $Ad_1$  the polyaniline-modified electrode was generated by cycling the potential of carbon graphite working electrode in 1M  $H_2SO_4$  and 0.1M aniline. The potential was cycled from  $-0.2V$  to  $0.75V$  at a scan rate of  $20mV/sec$ . The polyaniline modified electrode was then transferred to a solution containing  $0.1021g$  of  $Ad_2$  in 2M  $H_2SO_4$  and the potential of the electrode cycled from  $-0.2V$  to  $0.65V$  at a scan rate of  $10mV/sec$ . The resultant cyclic voltammetric response recorded is shown in fig. 4.25.

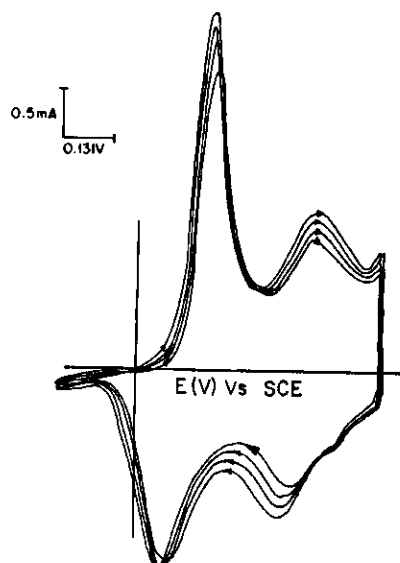


Fig. 4.25: Cyclic voltammetric response of a polyaniline modified electrode when the potential was cycled from  $-0.2V$  to  $0.65V$  in a solution containing  $Ad_2$  in 2M  $H_2SO_4$ . Scan rate  $20mV/sec$ .

The potential was cycled for a period of 22 minutes and the cyclic voltammogram was characterized by normal polyaniline redox peaks at oxidation/reduction potentials of  $0.18V/0.08V$  and another set of peaks at  $0.452V-0.459V/0.400V-0.38V$ . These latter

peaks are representatives of  $\text{Ad}_2$ . This is apparent in that in the absence of  $\text{Ad}_2$  when polyaniline was cycled in bare sulphuric acid solution these peaks are not observed.

Plot of anodic peak versus time for the two separate oxidation peaks in the electrolyte containing the plant material and sulphuric acid yielded a linear plot in the case of the peak associated with  $\text{Ad}_2$ , with a correlation coefficient of approximately 0.98. While the oxidation peak associated with polyaniline registered an increase during the first five minutes followed by a linear drop in the time interval of 5 to 22 minutes, see fig. 4.26 (a) and (b).

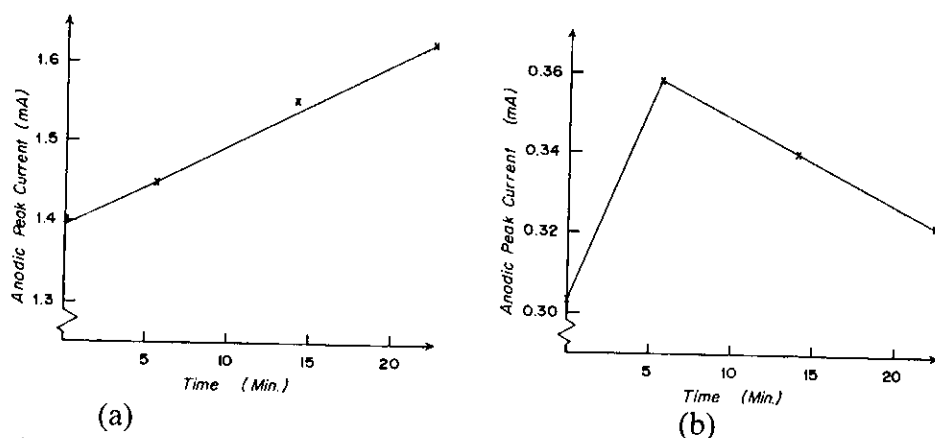


Fig. 4.26: Plot of anodic peak current versus time for two separate peaks (a) associated plant material and (b) associated with PAN- when a PAN modified electrode was allowed to cycle in a solution containing  $\text{Ad}_2$  in  $2\text{MH}_2\text{SO}_4$ . Potential range  $-0.2\text{V}$  to  $0.65\text{V}$ . Scan rate of  $20\text{mV/sec}$

On comparing this with the bare carbon response in which the oxidation potential of the plant material as mentioned earlier occurred at  $0.449\text{V}/0.385\text{V}$ . We find that the peak is  $3\text{mV}$  more positive in polyaniline which can be considered as an insignificant difference. However, the range of the oxidation peak in the bare carbon for the first 22 minutes was  $0.449\text{V}$ - $0.482\text{V}$  while in a polyaniline-modified electrode for the same duration the oxidation peak potential range is  $0.452\text{V}$ - $0.459\text{V}$ . This means that after 22 minutes the peak potential is  $23\text{mV}$  more negative than in the case of bare carbon. This suggests that

polyaniline may be playing an electrocatalytic role. In addition the redox peaks for the plant materials are much better defined in the case of a polyaniline-modified electrode which suggests a first electron transfer kinetic.

The redox efficiency for  $\text{Ad}_2$  on polyaniline modified electrode does not differ significantly with that of bare carbon and this is not of particular significance since there is no proven relationship between redox efficiency and electron transfer. When the same process was repeated on a thick polyaniline film the  $\text{Ad}_2$  oxidation/reduction potentials were observed at 0.517V/0.319V implying that the oxidation of  $\text{Ad}_2$  is much more difficult in the case of thick film. It is notable that there is significant capacitive tailing. This increased double layer charge in the thick film case [54] definitely affects the faradaic components of the total charge which in turn will affect  $\text{Ad}_2$  redox efficiency.

When fresh films of polyaniline was prepared in 1M HCl and the resultant polyaniline modified electrode transferred to a solution containing plant material dissolved in HCl, the redox peaks attributed to electrocatalysis in the case of  $\text{H}_2\text{SO}_4$  were diminutive. See fig. 4.27.

This type of response can only be associated with the type of dopant anion, in this case  $\text{Cl}^-$  ions as opposed to  $\text{SO}_4^{2-}$  or  $\text{HSO}_4^-$  in the case of  $\text{H}_2\text{SO}_4$  electrolyte. Since the oxidation potential of polyaniline film prepared in either  $\text{H}_2\text{SO}_4$  or HCl does not show any significant difference, the effect of the dopant anion on the redox centre of the plant material would be purely speculative as it can be attributed to hydration ratio and charge density of the anion. When similar experiments are repeated with a thick polyaniline film there was still substantial reduction in the oxidation and reduction peak currents of the electrocatalytic peak as compared to the case of  $\text{H}_2\text{SO}_4$ .



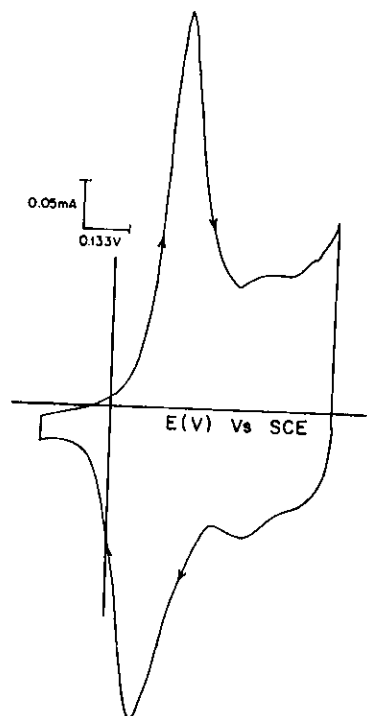


Fig. 4.27: Cyclic voltammetric response when a PAN modified electrode, generated using 1M HCl in place of 1M H<sub>2</sub>SO<sub>4</sub>, was cycled in a solution containing 0.1g of Ad<sub>2</sub> in 2M HCl. Potential range - 0.2 to 0.65V. Scan rate 20mV/sec.

#### (b) Bentonite modified Electrodes

Bentonite electrode were prepared as already discussed in Section 3.5.2 and transferred into a solution containing 0.1011g of Ad<sub>2</sub> in 2M H<sub>2</sub>SO<sub>4</sub>. The potential of the working electrode was then cycled from -0.2V to 1.0V at 20mV/sec for a total of 90 minutes. This was done by cycling the electrode over the given potential window first for 70 minutes and then it was left for 12 hours (overnight) out of the solution without any electrochemistry after which, it was cycled for another 20 minutes.

We obtained well-defined peaks with the oxidation/reduction peaks occurring at 0.446V/0.365V. The change in the anodic peak current versus time was plotted and a linear plot with a gradient of  $1.4 \times 10^{-2}$  mA/min was obtained (see fig. 4.28). The redox efficiency was found to be 100% and from the scan rate dependence studies, the anodic

peak varied linearly with the square root of scan rate suggesting its a diffusion controlled process.

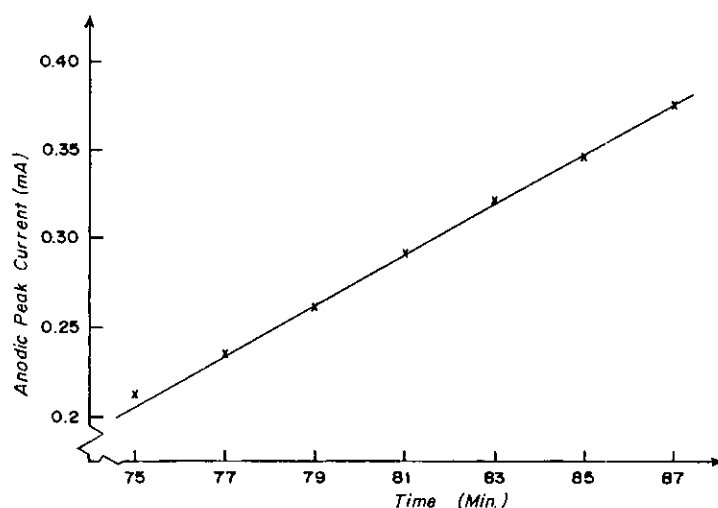


Fig. 4.28: Plot of anodic peak current versus time for bentonite modified electrode cycled in the potential range -0.2V to 1.0 V at 20mV/sec in a solution containing 0.1g of  $\text{Ad}_2$  in 2M  $\text{H}_2\text{SO}_4$ .

However, it was also noted that the anodic peak current versus scan rate also yielded a linear plot with a correlation coefficient of about 0.96 (see fig 3.29 (a) and (b)).

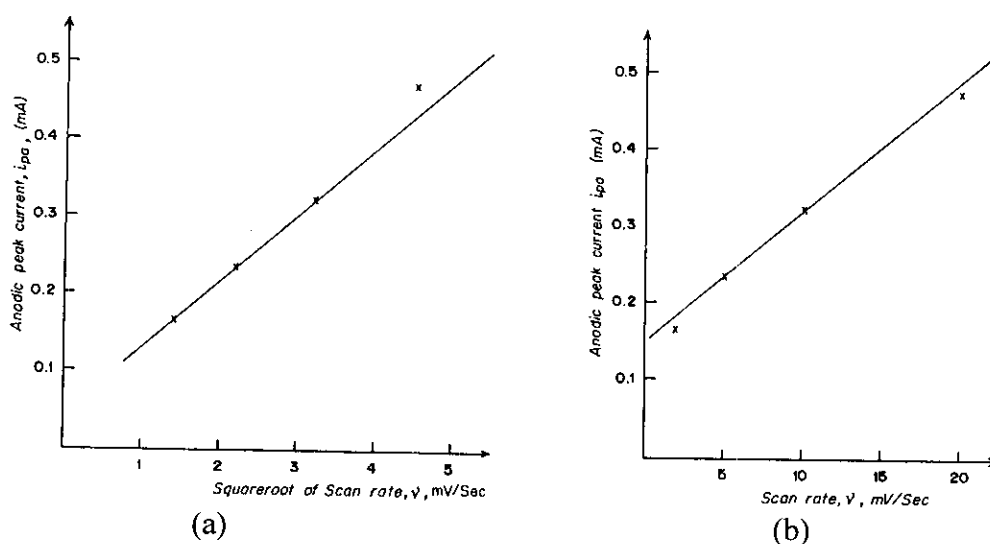


Fig. 4.29: Plot of  $i_{pa}$  versus (a) scan rate and (b) square root of scan rate for a bentonite modified electrode cycled from -0.2V to 1.0V in a solution containing  $\text{Ad}_2$  in 2M  $\text{H}_2\text{SO}_4$ .

That we are dealing with a surface attached species is not surprising given that from that cyclic voltammetric response the anodic potential is approximately equal to reduction potential as seen in fig 4.30. The duality of this process can only be explained as a case where we are dealing with a surface attached species resulting from a diffusion-limited process.

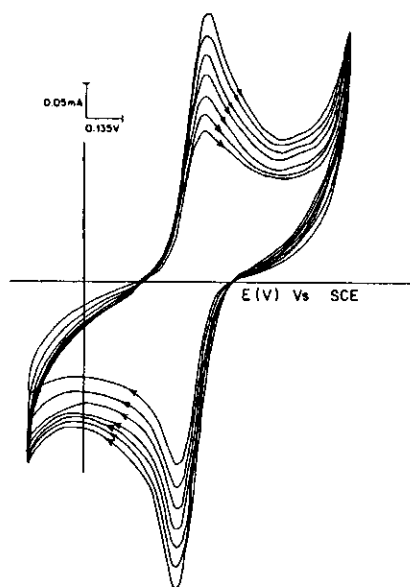


Fig. 4.30: Cyclic voltammetric response for bentonite modified electrode cycled from  $-0.2\text{V}$  to  $1.0\text{ V}$  at scan rate of  $20\text{mV/sec}$  in a solution containing  $\text{Ad}_2$  in  $2\text{MH}_2\text{SO}_4$ .

A freshly prepared electrode was allowed to stay in the electrolyte solution containing the plant material  $\text{Ad}_2$ , without any electrochemical activity for 70 minutes and then removed and left for 12 hours just as the previous case discussed above. On cycling the potential of this electrode in the electrolyte containing plant material, we obtained well defined redox peaks in the first 20 minutes occurring at  $0.453\text{V}/0.378\text{V}$ . These potentials are not substantially shifted far to the right and therefore the difference can be treated as insignificant.

The scan rate dependence studies yielded linear plots for peak current versus square root of scan rate while the change in the anodic peak current with time was computed to be  $1.5 \times 10^{-2}$  mA/min in the case of the initial slope. This is almost equal to the case discussed earlier. The efficiency of the redox process however, was found to be 86.7%, which is substantially, lower than the former case. The pH dependence studies revealed that the rate of change of oxidation potential as a function of internal solution pH yielded a value of 86.9mV/pH just as in the case of bare carbon working electrode and HCl as the supporting electrolyte. This corresponds to a 3 proton, 2 electron process.

It is interesting to note that in the case where the bentonite modified electrode was exposed to electrochemical cycling prior to being left overnight (without any electrochemical activity) then cycled again for short while, it yielded pH versus anodic peak potential plot with a slope of 60.8 mV/pH implying a one electron, one proton process.

This difference clearly points out that the modification of the electrode surface affects protonation/deprotonation equilibrium of the redox moieties in the plant material. When the experiments were repeated with freshly prepared electrode and HCl as the supporting electrolyte we obtained similar results with oxidation/reduction peak potential having no significant differences from the case of H<sub>2</sub>SO<sub>4</sub>. The oxidation/reduction potentials were found to occur at 0.446V/0.338V.

### **(c) Adsorption studies with bentonite modified electrode**

Prior to the bentonite being used to modify the electrode, it was allowed to stay in solutions containing 0.1g each of Ad<sub>2</sub> in various concentrations i.e. 1M, 1.3M, 2M and 4M of either HCl or H<sub>2</sub>SO<sub>4</sub>. 5 g of bentonite were added to each of the solutions and left

for 15 hours. This was then oven dried at approximately 80°C for another 15 hours in an air oven. The resultant materials were crushed to fine powder that was then used to prepare electrodes as already indicated in the experimental section.

The electrodes were then transferred to a solution containing 1M acid (with no plant material). The electrodes prepared using HCl were cycled in 1M HCl solution while those prepared using H<sub>2</sub>SO<sub>4</sub> were cycled in 1M H<sub>2</sub>SO<sub>4</sub> solution. On cycling the potential from -0.2V (constant) to either 1.0V or 1.2V for either HCl and H<sub>2</sub>SO<sub>4</sub> respectively at a scan rate of 20mV/sec we obtained very well defined redox peaks.

In the case of HCl the oxidation/reduction peaks occurred at 0.485V/0.38V for 1M, 0.478V/0.419V for 1.3M, 0.463V/0.39V for 2M and 0.463V/0.39V for 4M. It is important to note that the oxidation/reduction potentials shifted on continued cycling and the differences in the oxidation potential for different concentrations ranged from 15mV (in the case of 1M), 20mV (in the case of 1.3M) to 22mV (in the case of 4M and 2M).

From the results it is apparent that the oxidation potentials decrease, as the pH is decreased. It is interesting to note from pH studies on plain bentonite modified electrode subjected to an electrolyte with plant material, the oxidation potentials was observed to increased for HCl concentration range studied (i.e. 0.125 to 2M) as the concentration increases (i.e. pH lowered). Based on these observation one can infer that adsorption forces are a factor in the oxidation potentials from an entropic point.

The rate of change of the anodic peak current was found to be  $2.57 \times 10^{-2}$  mA/min in 1.3M case,  $1.7 \times 10^{-2}$  in the 2M case and  $2.83 \times 10^{-2}$  in the 4M case. In the 1M case the anodic peak current versus time was not linear thus the slope was not calculated. Redox efficiencies were found to be 90% (1M), 94.7% (1.3M) 88% (2M) and 93% (4M).

From this data on the rate of change of anodic peak current and redox efficiency, the 4M case seems to have the highest growth rate, followed closely by 1.3M case although the latter has slightly higher redox efficiency. From the deposition rates it is apparent that there is no linear correlation between the pH of the external solution in which adsorption is carried out and the rate of deposition. However, there is a relationship between the rate of deposition and the redox efficiency, since higher deposition rates registered higher efficiencies. These results are not surprising given that there is no established linear correlation between the pH of the matrix and the external pH. One would expect a linear correlation between the redox efficiency and deposition rates. The scan rate dependence studies in the 2M HCl case yielded a linear plot for anodic peak current versus scan rate. (See fig. 4.31). This confirms we are dealing with a surface attached species verifying the concept of adsorption.

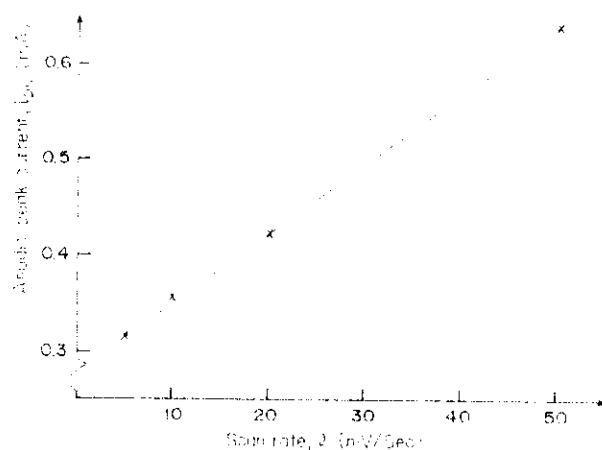


Fig. 4.31: Plot of anodic peak current versus scan rate for  $Ad_2$  in 2M HCl adsorbed onto the electrode surface.

In the case where the adsorption experiments were carried out using  $H_2SO_4$  as the electrolyte media, significantly different results were obtained. The cyclic voltammetric response in the 1.3M  $H_2SO_4$  yielded oxidation/reduction peak potentials at 0.783V/0.029V. On continued cycling, the oxidation peak shifts to the right while the

reduction peak shifts further to the left until the reduction potentials are negative values as observed in fig. 4.32.

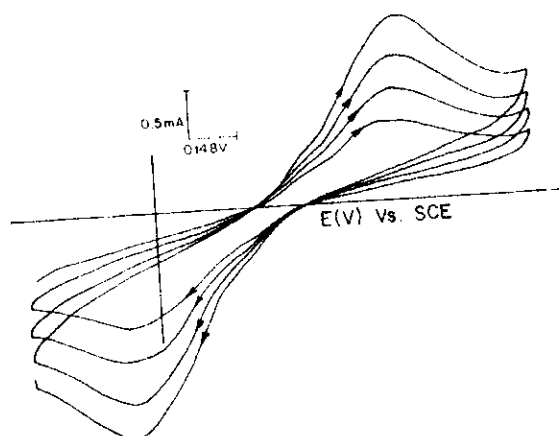


Fig. 4.32: Cyclic voltammetric response when an electrode modified with bentonite onto which  $\text{Ad}_2$  in  $1.3\text{M H}_2\text{SO}_4$  had been initially adsorbed is cycled from  $-0.2\text{V}$  to  $1.2\text{V}$  in a  $1\text{M H}_2\text{SO}_4$  solution. Scan rate,  $20\text{mV/sec}$ .

An apparent feature in this voltammogram is the very large  $\Delta E_p$  as compared to the  $\text{HCl}$  case and the very large changes in peak current versus time yielded segmented curve, which is probably an indication of the rapidly changing matrix conditions. Plots of anodic peak current versus cathodic peak current gave two lines, which could imply two segments where the rates of electrodeposition differ.

### 4.2.3 THE WHITE-PINK PULP ( $\text{Ad}_3$ )

#### 4.2.3.1 Analysis on bare carbon working electrode

$0.103\text{ g}$  of  $\text{Ad}_3$  was dissolved in  $2\text{M H}_2\text{SO}_4$  and the potential of the bare carbon-working electrode cycled from  $-0.4\text{V}$  to  $1.35\text{V}$  at scan rate of  $50\text{mV/sec}$ . The resultant cyclic voltammetric response is shown in fig 4.33. A quasi-reversible redox peak with oxidation/reduction potential occurring at  $0.546\text{V}/0.279\text{V}$  was obtained. On continued

cycling the oxidation potential shifted positively by approximately 38mV and the reduction potential negatively by 25mV.

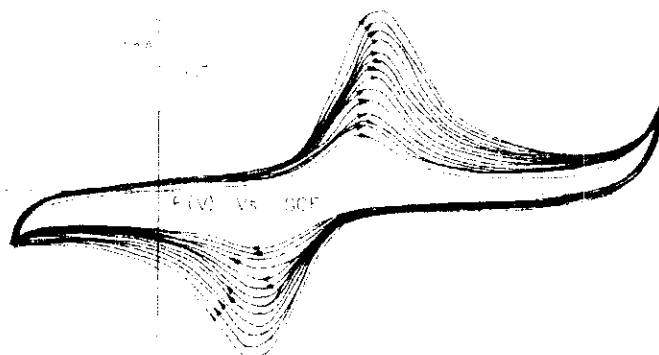


Fig. 4.33: CV response for bare carbon electrode cycled in a solution containing 0.1036 g of  $\text{Ad}_3$  in  $2\text{M H}_2\text{SO}_4$ . Potential range -0.4 to 1.35V. Scan rate 50mV/sec.

The rate of change of anodic peak current with time is shown in fig. 4.34 with the initial slope being  $1.5 \times 10^{-2} \text{ mA/min}$ . The redox efficiency of the process is 100% implying that for every incremental increase in the oxidative peak current we have a corresponding increase in reduction peak current.

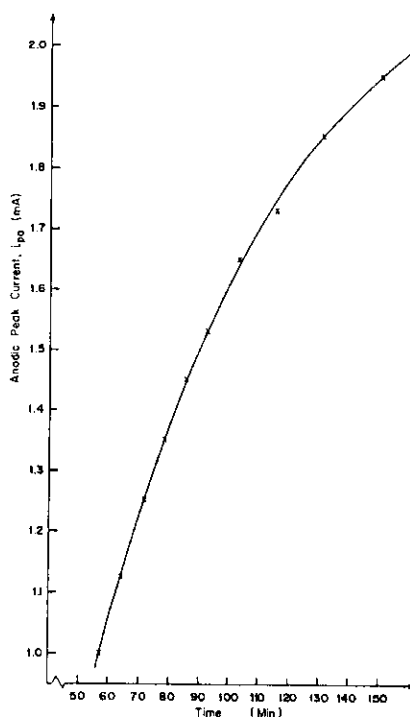


Fig. 4.34: Plot of anodic peak current versus time for  $\text{Ad}_3$  in  $2\text{M H}_2\text{SO}_4$  studied on a bare carbon. Potential range -0.4V to 1.35. Scan rate 20mV/sec.



From the scan rate dependence studies a plot of anodic peak current versus square root of scan rate yielded a linear plot, see fig. 4.35 and 4.36, suggesting that the process is diffusion controlled.

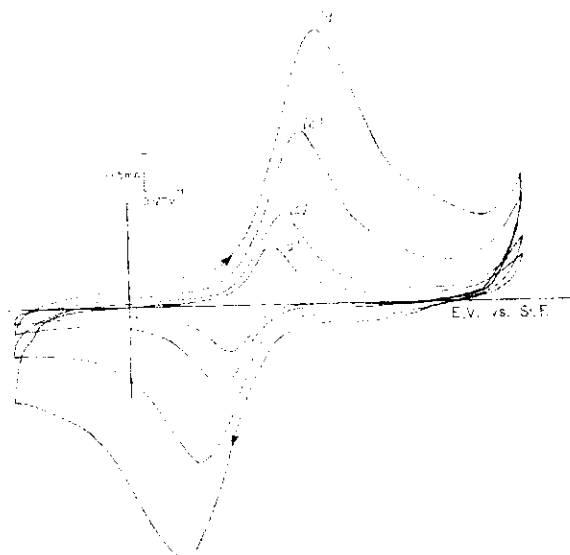


Fig. 4.35: Scan rate dependence studies for a bare carbon-working electrode in a solution containing  $\text{Ad}_3$  in  $2\text{M H}_2\text{SO}_4$ . Response (a), (b), (c) and (d) correspond to scan rates of 10, 20, 50, and  $100\text{mV/sec}$  respectively. Potential range  $-0.4\text{V}$  to  $1.35\text{V}$ .

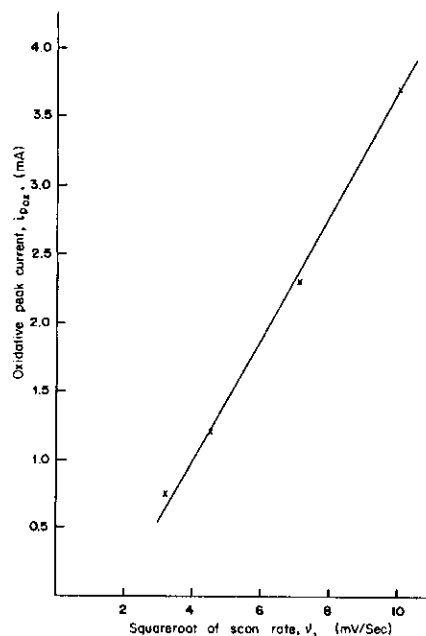


Fig. 4.36: Plot of anodic peak current versus square root of scan rate for  $\text{Ad}_3$  in  $2\text{M H}_2\text{SO}_4$ .

The effect of the external solution pH on the oxidative potential yielded a linear plot of approximately 60 mV/pH. This suggests a one proton, one electron process. The shifts in the redox peaks with pH are shown in fig. 4.37.

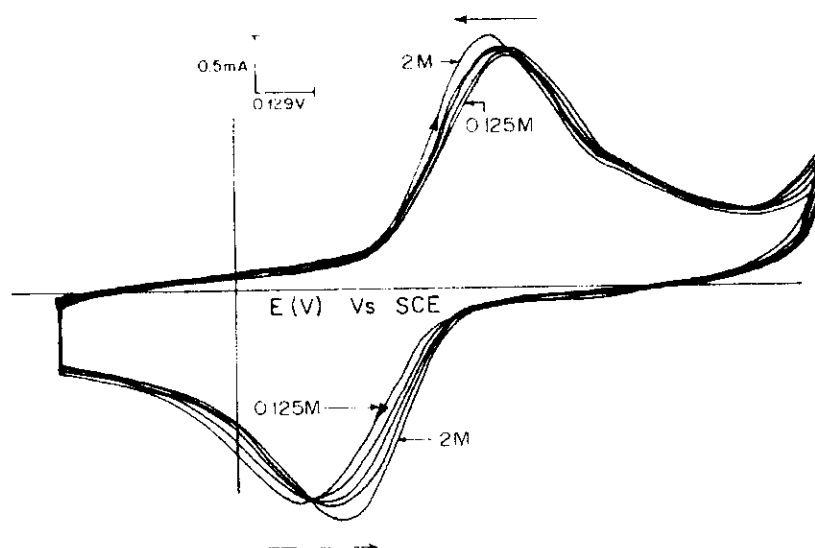


Fig. 4.37: pH dependence studies for  $\text{Ad}_3$  in 2M  $\text{H}_2\text{SO}_4$  studied on bare carbon working electrode in solution containing 0.125M, 0.25M, 0.5M, 1.0M and 2.0M  $\text{H}_2\text{SO}_4$ . Potential range -0.4V to 1.35V. Scan rate, 20mV/sec

The same experiments were repeated but with 1M HCl as the supporting electrolyte and the potential of working electrode cycled from -0.4V to varying positive potential limits, i.e. 0.92V to 1.0V at intervals of 200mV, while the scan rate was maintained at 20mV/sec. The resultant cyclic voltammetric response for the 0.98V limit yielded a quasi-reversible process with the oxidation/reduction potentials occurring at 0.477V/0.361V (see fig. 4.38). One interesting observation is that for the low potential limits the oxidation peaks broadened with the current approaching limiting value i.e. a plateau. The variation of anodic peak current versus time is shown in fig. 4.39 and initial slope approximately  $1.95 \times 10^{-2}$  mA/min, is higher than the value obtained in the case of  $\text{H}_2\text{SO}_4$ .

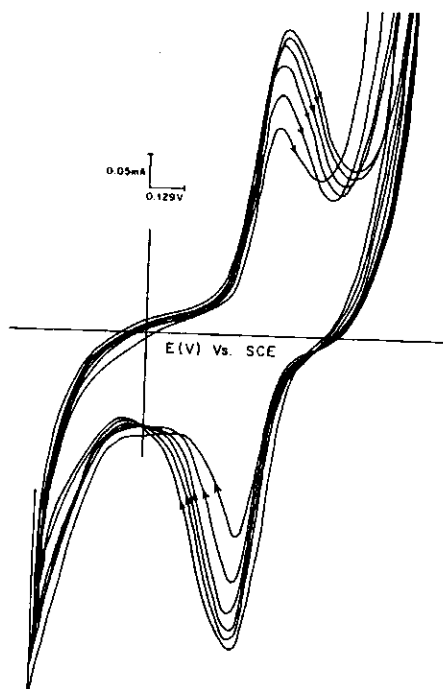


Fig. 4.38: CV response when bare carbon working electrode is cycled from -0.4V to 0.98V in a solution containing  $\text{Ad}_3$  in 1M HCl. Scan rate, 20mV/sec.

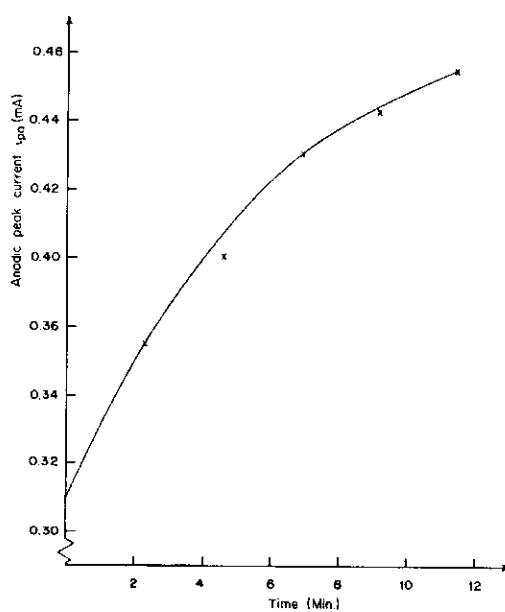


Fig. 4.39: Plot of anodic peak current versus time for  $\text{Ad}_3$  in 1M HCl when studied on bare carbon within potential range -0.4V to 0.98V.

The redox efficiency, computed to be 90%, is however lower than the case of  $\text{H}_2\text{SO}_4$ .

This trend differs from what was observed in the case of  $\text{Ad}_1$  and  $\text{Ad}_2$ .

Diffusion coefficients were calculated for theoretical concentration ranges  $10^{-6}$  to  $10^{-2}$ M and the results are displayed in table 4.11.

Table 4.11: Diffusion coefficients for theoretical concentration of the bulk,  $\text{Ad}_3$  in 1M HCl.

Theoretical Concentration, $C_o^*(\text{M})$	Diffusion Coefficient, $D_o (\text{mol})/\text{cm}^2$
$10^{-6}$	$9.9 \times 10^{-4}$
$10^{-5}$	$9.9 \times 10^{-6}$
$10^{-4}$	$9.9 \times 10^{-8}$
$10^{-3}$	$9.9 \times 10^{-10}$
$10^{-2}$	$9.9 \times 10^{-12}$

The values of  $D_o$  were averagely higher than the case of  $\text{Ad}_1$  and  $\text{Ad}_2$ , a fact which is corroborated by the excellent cyclic voltammetric features i.e. near complete reversibility of the redox process. This was further attested by the very high rate of change in the surface coverage (see fig. 4.40) which has a value of  $6.84 \times 10^{-8} \text{ mol}/\text{cm}^2/\text{min}$  for the initial slope suggesting we are depositing more than a monolayer as can be seen also in table 4.12.

Table 4.12: Surface coverage,  $\Gamma$ , ( $\text{mol}/\text{cm}^2$ ) of  $\text{Ad}_3$  electroactive species as a function of time.

Time (minutes)	Surface coverage , $\Gamma$ , ( $\text{mol}/\text{cm}^2$ )
0.6	$3.2 \times 10^{-7}$
2.9	$5.35 \times 10^{-7}$
5.2	$7.09 \times 10^{-7}$

7.4	$8.45 \times 10^{-7}$
9.7	$9.5 \times 10^{-7}$
12	$10.1 \times 10^{-7}$

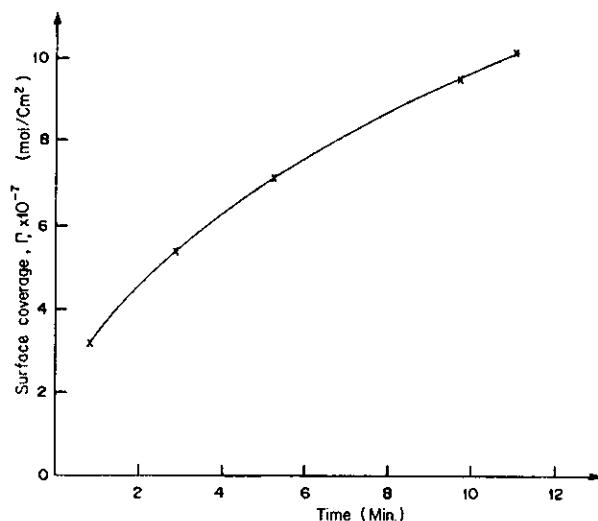


Fig. 4.40: Plot of surface coverage,  $\Gamma$ , versus time for electroactive species for  $\text{Ad}_3$  in 1M HCl.

The scan rate dependence studies for  $\text{Ad}_3$  in 1M HCl yields a linear plot for anodic peak current versus square root of scan rate confirming that this process is diffusion limited. This is similar to what was observed in  $\text{H}_2\text{SO}_4$  (see fig. 4.41).

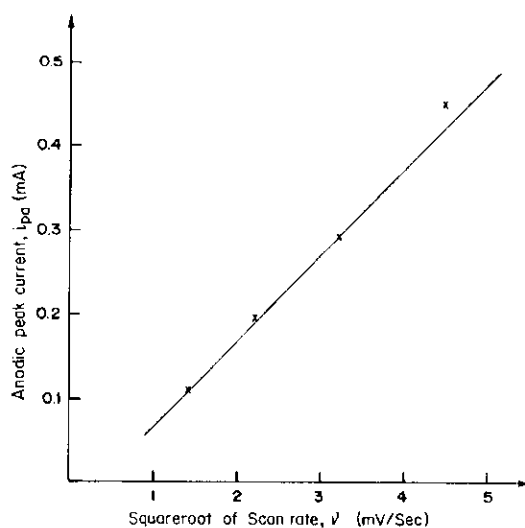


Fig. 4.41: Plot of anodic peak current versus square root of scan rate for  $\text{Ad}_3$  in 1M HCl studied on bare carbon.

The pH dependence studies in HCl yielded a value of about 53mV/pH which points to one proton one electron process.

#### 4.2.3.2 Identification of Ad<sub>3</sub>

The constituents of Ad<sub>3</sub> from electrochemical studies include ascorbic acid, riboflavin and thiamine. Other researchers using non-electrochemical techniques have identified these components in the edible part of the *A. digitata* fruit, (Ad<sub>3</sub>), [9, 10, 11, 13, 17,18, 19, 20 and 21]. This was verified based on the fact that when chemical standards for the said components were subjected to electrochemistry we obtained similar CVs. Figures 4.42 (a) to (c) show the CV responses in the H<sub>2</sub>SO<sub>4</sub> electrolyte media while 4.43 (a) to (c) show the responses in HCl supporting electrolyte.

The components are rich in redox active moieties like amine and carbonyl functional groups. The functional groups for example the amine, can be oxidized to form radical cation which in turn can couple to form dimers and polymers subject to steric considerations. The oxidation/reduction peak potentials in the H<sub>2</sub>SO<sub>4</sub> case appear at 0.52V-0.56V for ascorbic acid (no reduction peak). Riboflavin had three peaks appearing at -0.026V/-0.051V and 0.501V/0.34V while the third one, which had no reduction peak at 1.027V. Thiamine had a peak appearing at 0.488V/0.364V. In the HCl case the peaks potentials were at 0.55V for ascorbic, -0.013V/-0.05V and 0.490V/0.384V for riboflavin and 0.483V/0.381V for thiamine.

The oxidation peak potential for Ad<sub>3</sub> in H<sub>2</sub>SO<sub>4</sub>, 0.546V, falls within the range that ascorbic acid shows its oxidation peak in the same electrolyte. However, in the case of Ad<sub>3</sub> there is also a reduction peak unlike the case of ascorbic acid, which is not surprising considering that in the raw plant material there could other redox active moieties. The

results in the HCl media are not exactly matching which could be attributed to the fact that ascorbic acid may have been affected by moisture as will become more apparent in the case of Ad<sub>4</sub>.

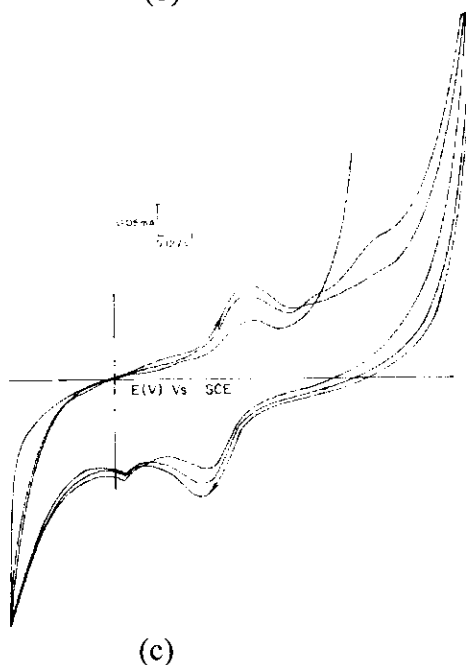
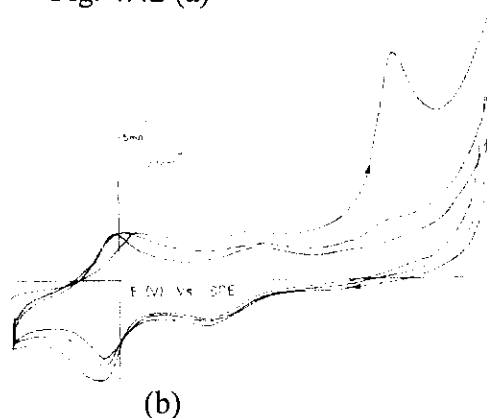
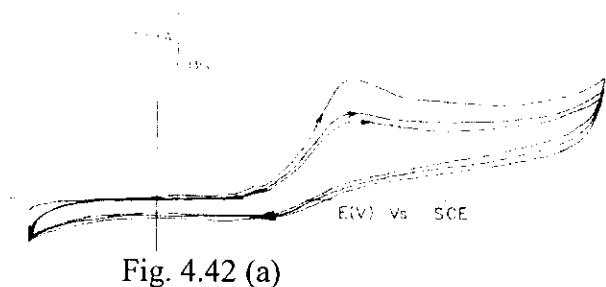


Fig. 4.42: CV responses for bare carbon working electrode cycled from -0.2V to 1.35V in solutions containing 0.01M (a) ascorbic acid (b) riboflavin and (c) thiamine in 1M H<sub>2</sub>SO<sub>4</sub> electrolyte media.

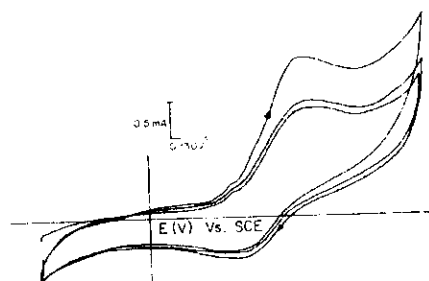
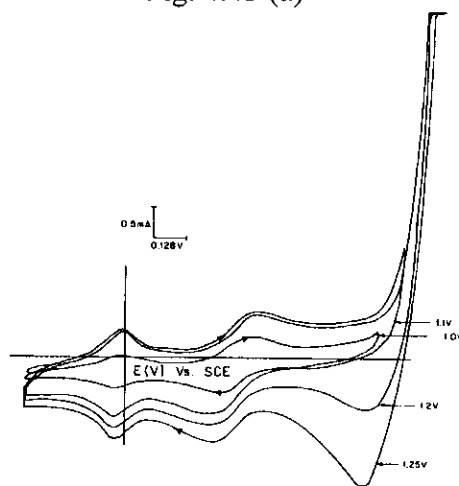
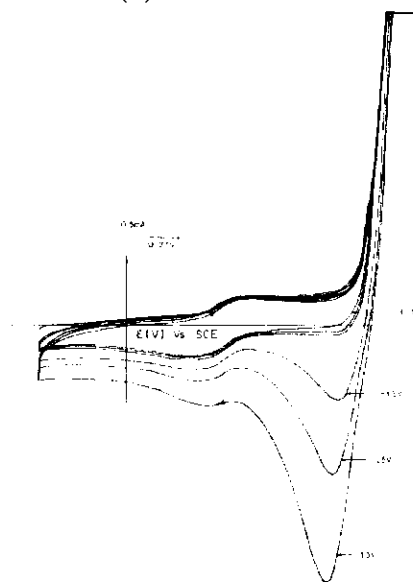


Fig. 4.43 (a)



(b)



(c)

Fig. 4.43: CV responses for bare carbon in solutions of chemical standards 0.01M (a) ascorbic acid (b) riboflavin and (c) thiamine in 1M HCl.

When  $\text{Ad}_3$  initially developed on the electrode surface was subjected to 1M NaCl and 1M HCl separately, a new oxidation peak was observed at -0.16V in the case of NaCl



electrolyte (see fig. 4.44). This was particularly interesting in that it was observed in the riboflavin standard - see 4.42(b) and 4.43(b). This observation suggests a deficiency/absence of  $\text{Na}^+$  in the  $\text{Ad}_3$  plant sample because if this were not the position this redox peak would not have appeared only after injection of sodium into the media. This is not surprising given that the nature and type of metal element present in a plant material is dependent on the environment in which it grows.

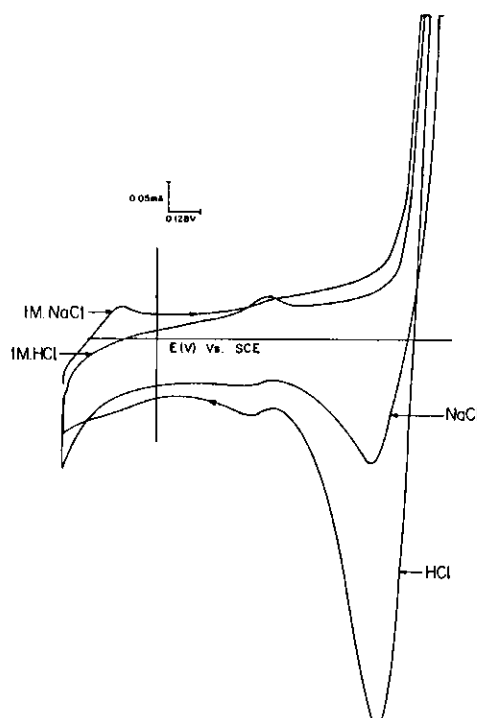


Fig. 4.44: CV response when a carbon electrode on which  $\text{Ad}_3$  had been initially deposited, is cycled from  $-0.4\text{V}$  to  $1.4\text{V}$  in separate solutions of  $1\text{M HCl}$  and  $1\text{M NaCl}$ . Scan rate,  $20\text{mV/sec}$ .

The fact that riboflavin is in small quantities in the fruit could also be another factor contributing to lack of its distinct peaks being observed in the  $\text{Ad}_3$  electrochemical signal. The signal for thiamin on the other hand, could be overlapping with that of ascorbic acid since its quantities are also much lower than the latter.

The presence of functional groups attributed to these components was further confirmed from FTIR analysis, see figures 4.45(a) to (d).

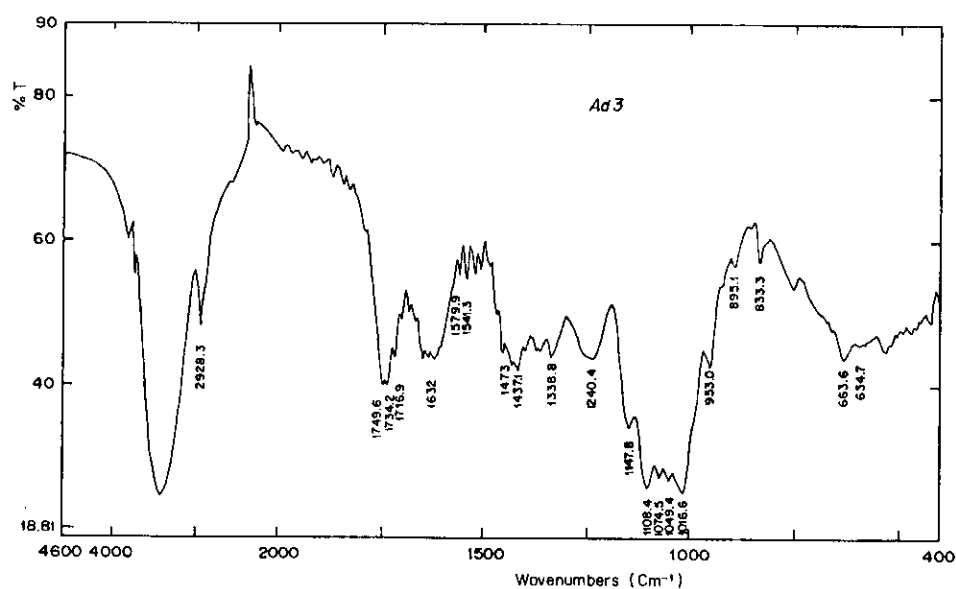
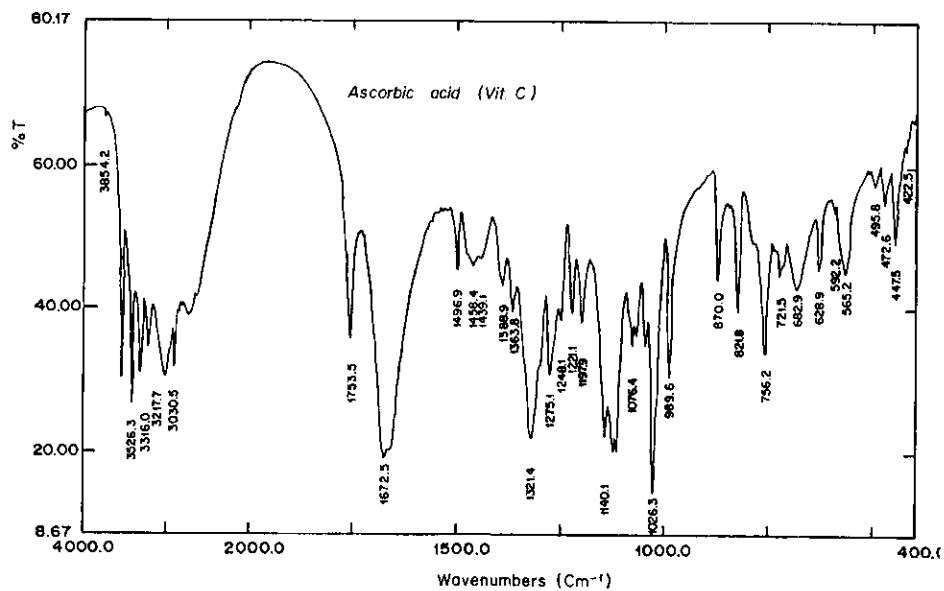
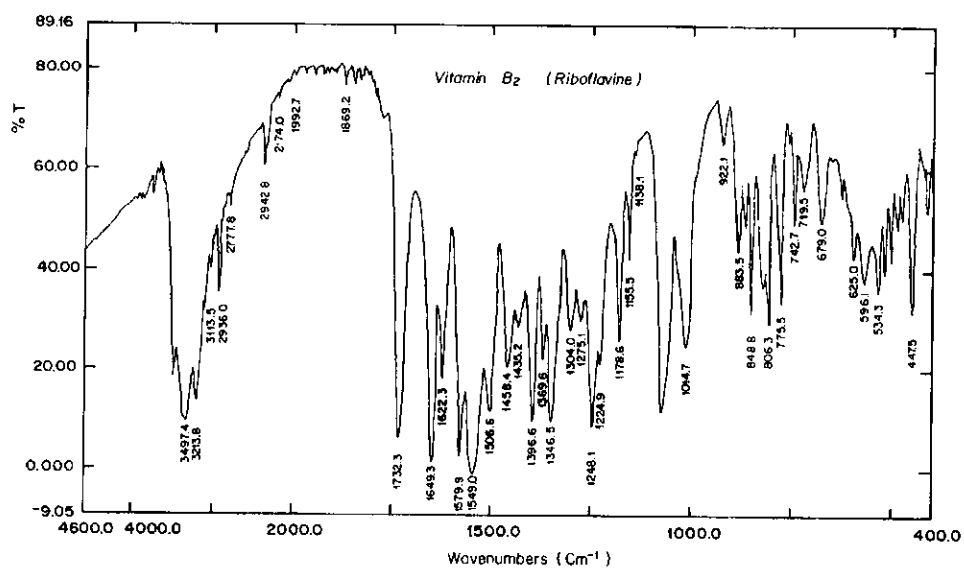


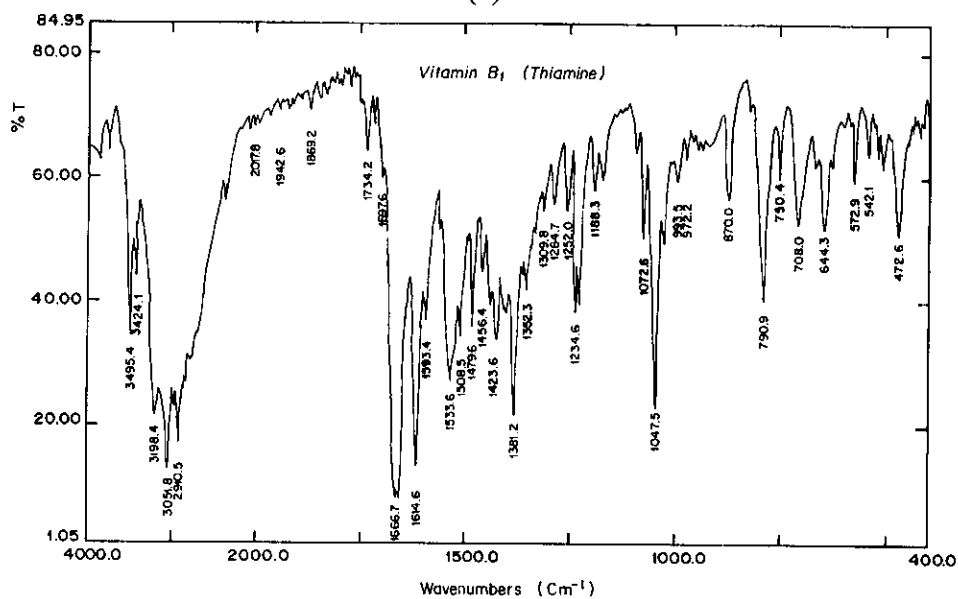
Fig. 4.45a)



(b)



(c)



(d)

Fig. 4.45: FTIR spectra for (a) Ad<sub>3</sub> (b) ascorbic acid (c) riboflavin and (d) thiamine.

The FTIR confirms the presence of amine and carbonyl groups as indicated below.

(i) In the case of thiamine

C-NH<sub>2</sub> 3495-3424 (cm<sup>-1</sup>)

2831 cm<sup>-1</sup>

1120-1030 cm<sup>-1</sup>

C-N (aromatic)	1280-1180 cm <sup>-1</sup>
----------------	----------------------------

(ii) In the case of Riboflavin

-CONHR	3440-3420 cm <sup>-1</sup>
	1680 – 1640 cm <sup>-1</sup>
	1560 – 1530 cm <sup>-1</sup>
	1310 –1290 cm <sup>-1</sup>
	710 – 690 cm <sup>-1</sup>

Secondary amine	1190 – 1130 cm <sup>-1</sup>
	740 – 700 cm <sup>-1</sup>

C = O	1750-1600 cm <sup>-1</sup>
-------	----------------------------

(iii) In the case of ascorbic acid

C = O	1750-1600 cm <sup>-1</sup>
-------	----------------------------

Ester	1753 cm <sup>-1</sup>
	1290 –1180 cm <sup>-1</sup>

In Ad<sub>3</sub> there are broad and sharp peaks in the regions where the above groups absorb i.e.

3700-3000cm<sup>-1</sup>

2928cm<sup>-1</sup>

1800 –1600 cm<sup>-1</sup>

1170 –1000 cm<sup>-1</sup>

It is noteworthy that the first oxidation peak in polymerization of aniline yields a shift of 60mV/pH suggesting that the culprit moiety in the foregoing components is the amine group, since we observe a shift of 60mv/pH implying one proton, one electron process. While oxidation potential does not exactly coincide with that of polyaniline this can be

attributed to the different chemical environments that the functional groups are associated with.

#### 4.2.3.3. Analyses using Acetonitrile /water mixture

An analysis of  $\text{Ad}_3$  was repeated in a 1:1 ratio mixture of acetonitrile and water. TEAB was added as the supporting electrolyte. The potential of the working electrode was cycled from  $-0.4\text{V}$  to  $0.7\text{V}$  at  $20\text{mV/sec}$  and the resultant cyclic voltammetric response was characterized by reduction peaks appearing at approximately  $-0.23\text{V}$  and  $0.6\text{V}$  (see fig. 4.46 (a)). The latter is attributed to the supporting electrolyte given that when a blank was run with the supporting electrolyte for the same potentials the peak was observed. This has also been observed by other researchers [25].

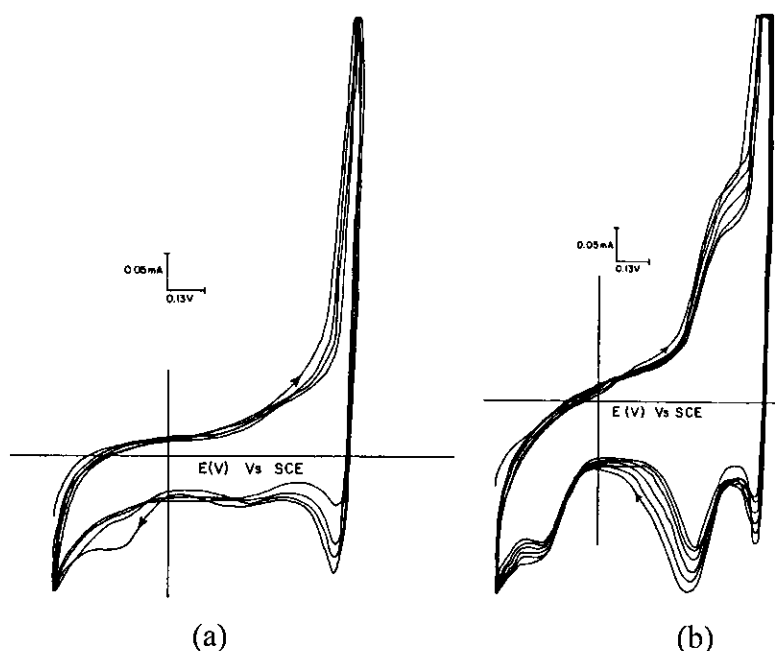


Fig. 4.46: CV responses obtained when bare carbon working electrode was cycled within the potential  $-0.4\text{V}$  to  $0.7\text{V}$  in a solution containing  $\text{Ad}_3$  in  $\text{CH}_3\text{CN}/\text{H}_2\text{O}$  at a scan rate of  $20\text{mV/sec}$ .

In further attempts to identify the redox moieties responsible for the peak at  $-0.23\text{V}$  little  $\text{HCl}$ /or  $\text{H}_2\text{SO}_4$  was added to the electrolyte. The cyclic voltammetric response improved

substantially with an oxidation shoulder appearing between 0.494V - 0.572V and a well-defined reduction peak at 0.392V as shown in fig. 4.46(b).

The potential of this particular peak kept shifting negatively on continued cycling. The other two peaks previously observed in the absence of the acid were also present. This observation is a clear pointer to the significance of protons in the redox chemistry of the electroactive components in the plant material. Due to the poor electrochemical response in the absence of the acid it was not important to pursue this line of investigations further.

#### **4.2.3.4 SURFACE MODIFIED ELECTRODES**

##### **(a) Polyaniline modified electrode**

The surface of the carbon graphite working electrode was modified using polyaniline prepared by cycling the potential of the working electrode from -0.2V to 0.75V in a solution containing 0.1M aniline and 1M H<sub>2</sub>SO<sub>4</sub> at a scan rate of 20mV/sec. The potential of the polyaniline-modified electrode was then cycled in a solution of Ad<sub>3</sub> in 2M H<sub>2</sub>SO<sub>4</sub> within the potential range -0.2V to 0.65V. The positive limit was reduced to avoid electrodegradation as normally happens in absence of aniline monomer. The resultant cyclic voltammetric response is shown in fig. 4.47.

Typical polyaniline oxidation/reduction peaks occurred at 0.18V/0.08V while the oxidation/reduction peaks for Ad<sub>3</sub> appeared at 0.481V/0.384V. It is apparent that the oxidation potential of Ad<sub>3</sub> has been reduced by approximately 65mV once again suggesting the electrocatalytic role of the polyaniline. This has been observed in other parts of plant components of the *Adansonia digitata* fruit as already discussed elsewhere.

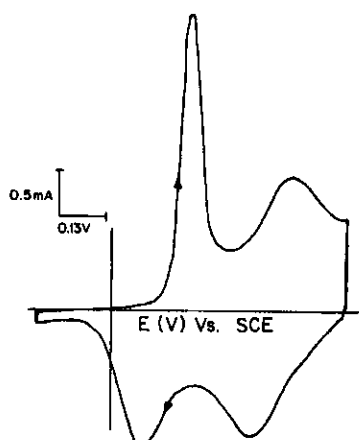


Fig. 4.47: CV response when a PAN-modified electrode was cycled from -0.2V to 0.65V in a solution containing  $\text{Ad}_3$  in  $2\text{M H}_2\text{SO}_4$ . Scan rate 20mV/sec.

Scan rate dependence studies on  $\text{Ad}_3$ , yielded a linear plot for anodic peak current versus square root of scan rate. Further experiments were carried out with fresh, films of polyaniline of different thickness to establish whether the quantity or thickness of polyaniline had a bearing on its electrocatalytic role. The films analyzed had the thickness'  $1.15 \times 10^{-2} \mu\text{m}$ ,  $2.18 \times 10^{-2} \mu\text{m}$  and  $5.6 \times 10^{-2} \mu\text{m}$  (Assumption made,  $33\text{mC/cm}^2$  represents  $0.1\mu\text{m}$  thickness [96]). The resultant cyclic voltammetric response is shown in fig 4.48. Well-defined redox peaks characterized the thicker films but they were shifted slightly to the right.

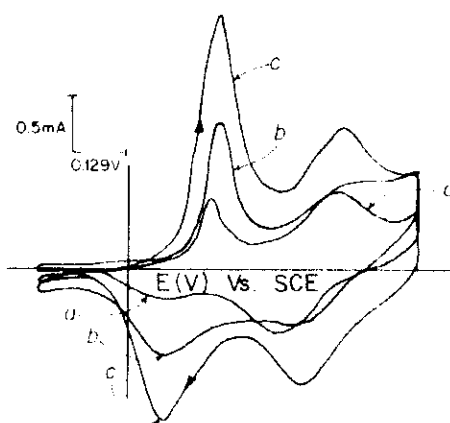


Fig. 4.48: CV response obtained when PAN modified electrodes of three different thickness' (a)  $i_{pa} = 0.95\text{mA}$  (b)  $i_{pa} = 1.55\text{mA}$  and (c)  $i_{pa} = 3.85\text{mA}$  were cycled in a solution containing 0.1g of  $\text{Ad}_3$  in  $2\text{M H}_2\text{SO}_4$ . Scan rate 20mV/sec.

### (b) Bentonite Modified Electrodes

The surface of the carbon graphite working electrode was derivatized using bentonite as the matrix (see chapter 3 for preparation procedure). The bentonite electrode was then cycled in a solution containing 0.1g of  $\text{Ad}_3$  in 2M  $\text{H}_2\text{SO}_4$  and cycled through the potential  $-0.2\text{V}$  to  $1.0\text{V}$  at a scan rate of  $20\text{mV/sec}$  (see fig. 4.49).

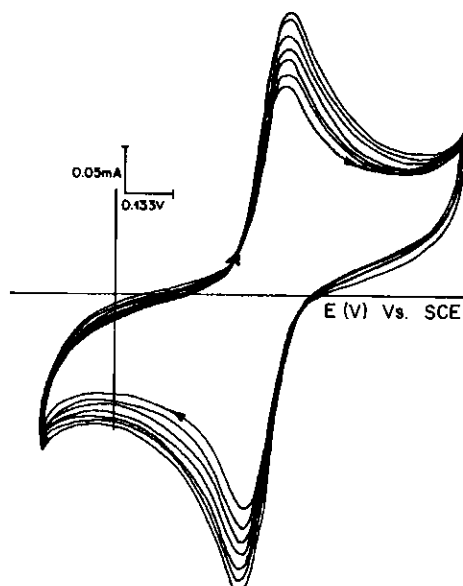


Fig. 4.49: CV response when bentonite modified electrode is cycled in a solution containing 0.1g of  $\text{Ad}_3$  in 2M  $\text{H}_2\text{SO}_4$  within the potential range  $-0.2\text{V}$  to  $1.0\text{V}$ . Scan rate  $20\text{mV/sec}$ .

The oxidation/reduction potential occurred at  $0.48\text{V}/0.373\text{V}$  while the change in the anodic peak current versus time was found to be  $3.26 \times 10^{-3} \text{ mA/min}$ . The redox efficiency of the process approaches 100% see fig. 4.50 and 4.51.



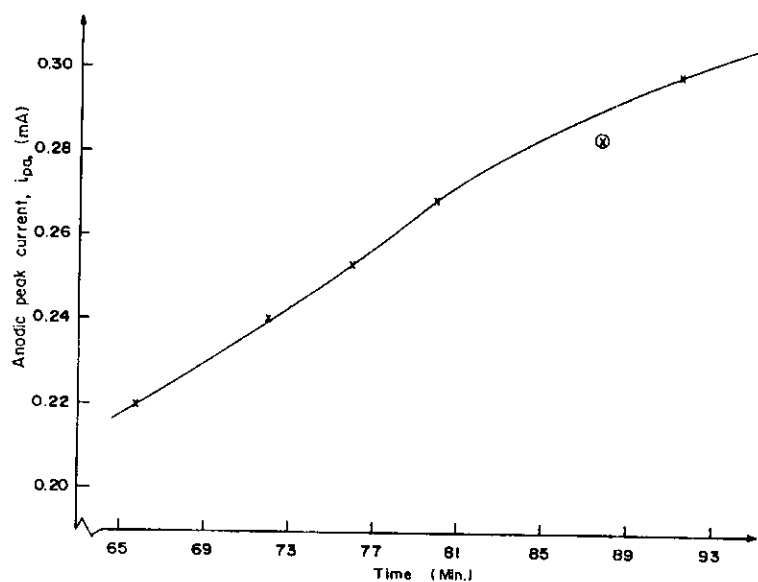


Fig. 4.50: Plot of anodic peak current versus time for  $Ad_3$  in 2M  $H_2SO_4$  on a bentonite modified electrode. Potential range -0.2V to 1.0V.

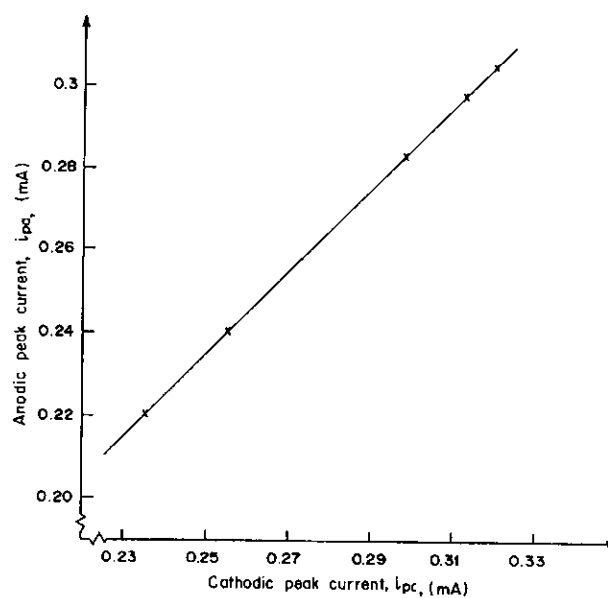


Fig. 4.51: Plot of anodic peak current versus cathodic peak current for  $Ad_3$  in 2M  $H_2SO_4$  electrodeposited on a bentonite modified electrode.

Scan rate dependence studies revealed that the anodic peak current varies linearly with the square root of scan rate (see fig. 4.52). Further analysis was done to establish the pH effect on redox potential of  $Ad_3$  redox peak. Plot anodic peak potential versus pH

yielded a slope of approximately 66.7mV/pH (fig. 4.53) suggesting a one proton, one electron process.

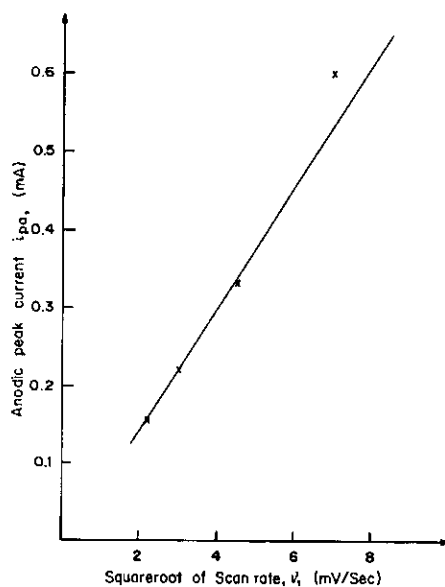


Fig. 4.52: Scan rate dependence studies; Plot of  $i_{pa}$  versus square root of scan rate for  $Ad_3$  in 2M  $H_2SO_4$ .

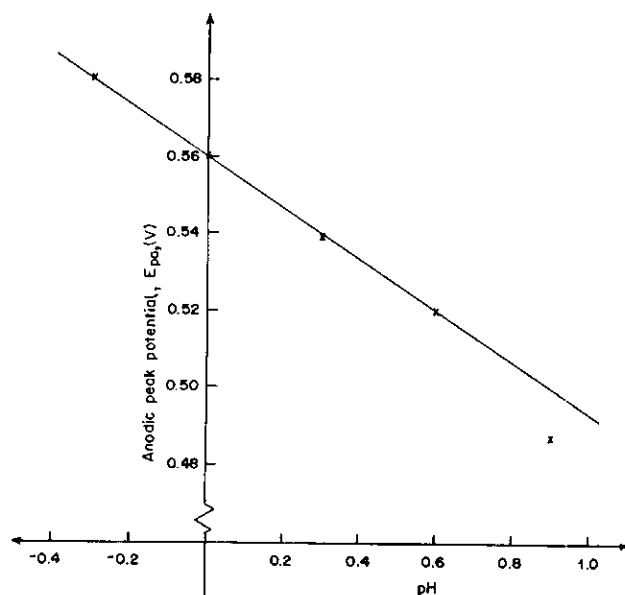


Fig. 4.53: pH dependence studies; Plot of  $E_{pa}$  versus pH for  $Ad_3$  in 2M  $H_2SO_4$  on bentonite modified electrode.

Fresh samples of  $Ad_3$  in  $H_2SO_4$  were prepared and two control experiments set up to study permeation of redox species into the host matrix. In one case the bentonite-modified electrode was cycled in the electrolyte media for a certain period and the rate of

electrodeposition monitored. In the second case the bentonite-modified electrode was just dipped into the electrolyte media and allowed to sit for the same amount of time as the first case except in this second case, the electrode was not subjected to potential cycling. This latter electrode was then subjected to potential cycling and the rate of electrodeposition monitored. The two rates of electrodeposition were found to differ with the first case being  $3.26 \times 10^{-3}$  mA/min and the second case  $1.25 \times 10^{-2}$  mA/min. The oxidation /reduction potential of the second case occurred at 0.447V/0.37V indicating a 33mV shift to the left on the oxidation peak.

It is noteworthy that though the electrodeposition was higher in the second case its redox efficiency was lower i.e. 100% *vis a viz.* 82.9%. This brings out an important point in that pre-concentrating the host matrix with the electrolyte does not enhance the redox efficiency of the process. It was observed that when both electrodes were subjected to pH studies (after electrodeposition of the plant material) the change in oxidation peak potential versus pH was different in both cases with case one being 66mV/pH and case two 89mV/pH. This observation is a veil pointer to the different proton/electron transfer dynamics in both systems.

Similar electrochemical experiments as mentioned in case 1 and 2 were repeated for known chemical standards occurring in the plant material components. In this analysis the rate of electrodeposition, redox efficiency and shift in pH with respect to oxidation potential were obtained for riboflavin, thiamine and ascorbic acid. The values obtained are shown in the tables below.

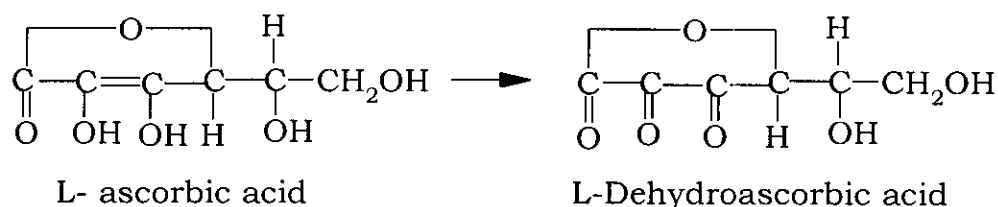
Table 4.13: Responses of riboflavin, thiamine and ascorbic acid on CME subjected to electrochemistry from the beginning (Case 1)

Standard	Rate of electrodeposition $di_{pa}/dt$ (mA/min)	Redox efficiency %	$dE/pH$ (mV/pH)
Riboflavin (Vit. B <sub>2</sub> )	$2.16 \times 10^{-2}$	96.6	60.5
Thiamine (Vit. B <sub>1</sub> )	$1.97 \times 10^{-2}$	95.2	61.1
Ascorbic Acid (Vit. C)	$2.5 \times 10^{-2}$	94.4	104

Table 4.14: Response of Riboflavin, thiamine and ascorbic acid on CME initially dipped into the electrolyte before being subjected to potential cycling (Case 2).

Standard	Rate of electrodeposition $di_{pa}/dt$ (mA/min)	Redox efficiency (%)	$dE/pH$ (mV/pH)
Riboflavin	$3.89. \times 10^{-2}$	93.5	72
Thiamine	$3.47 \times 10^{-2}$	96.3	
Ascorbic acid	$3.3 \times 10^{-2}$	100	

In general the behaviour in both case studies resembles what was observed with the plant material. However, it is noteworthy that in the case of ascorbic acid when analysis is done using modified electrode we now observe a well-defined reduction peak unlike the case of bare carbon (discussed elsewhere in this thesis). This is probably due to the fact that ascorbic acid is physically adsorbed on the bentonite host matrix. This facilitates the oxidation/reduction of ascorbic acid from ascorbic acid to dehydroascorbic forms (see schematic diagram below).



The redox process would involve two protons, a fact that is corroborated by the 104mV/pH shift observed for this system. It also important to mention that the aspect of physical adsorption of ascorbic on true host matrix is confirmed from the scan rate dependence studies which yield a linear plot of anodic peak current versus scan rate (see fig. 4. 54). This contradicts the linear plot obtained in the case of  $i_{pa}$  versus square root of scan rate.

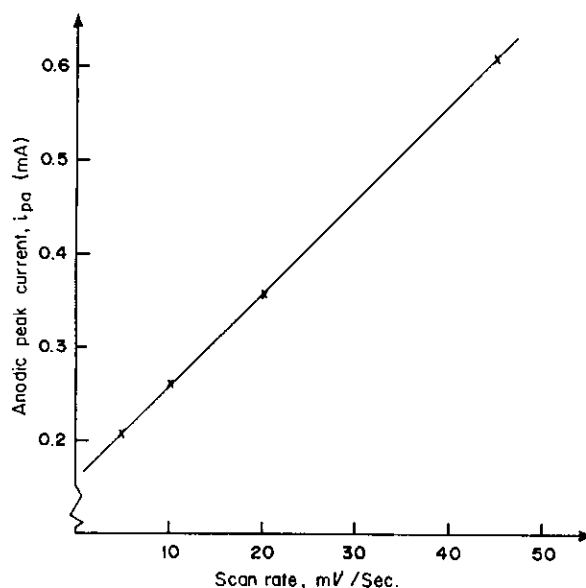


Fig. 4.54: Plot of anodic peak current versus scan rate for ascorbic acid adsorbed onto bentonite-modified electrode.

This is confirmed even further by the cyclic voltammetric response for the two case studies of ascorbic acid (see fig. 4.55 and 4.56) where we observed the typical adsorption shoulder which characterized such process, a phenomena already observed by other researchers [91].

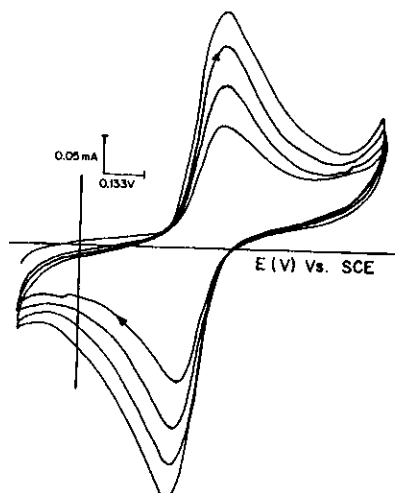


Fig. 4.55: CV response for a bentonite modified electrode cycled from -0.2V to 1.0V in solution containing 0.1M ascorbic acid in 1M  $\text{H}_2\text{SO}_4$  (Case 1).

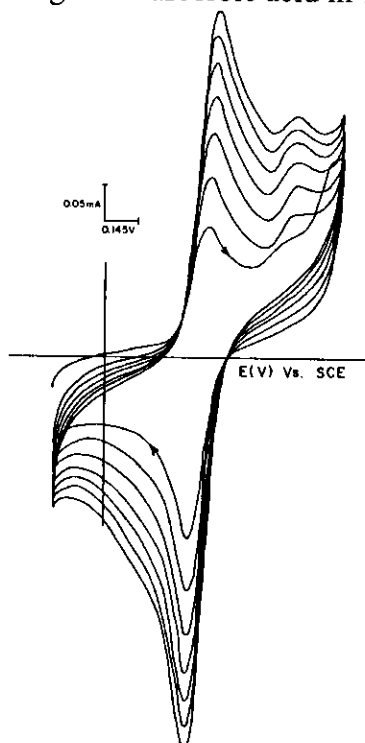


Fig. 4.56: CV response when a bentonite modified electrode allowed to sit for two hours (no potential cycling) in a solution of 0.01M ascorbic acid in 1M  $\text{H}_2\text{SO}_4$  before being cycled in within the potential -0.2V to 1.0V in the same solution at a scan rate of 20mV/sec (Case 2).

Further experiments with  $\text{Ad}_3$  plant material were carried out by dissolving 0.1g of  $\text{Ad}_3$  in 1M HCl so as to establish whether there was any significant difference in the different anions. The clay-modified electrode was cycled from -0.2V to 0.98V at a scan

rate of 20mV/sec. The oxidation/reduction potentials were observed at 0.461V/0.374V (see fig. 4.57) while the rate of deposition was  $9.28 \times 10^{-3}$  with the redox efficiency approaching 100%.

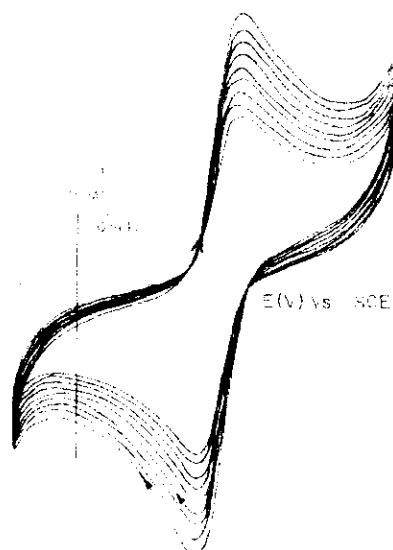


Fig. 4.57: CV response when bentonite modified electrode is cycled from -0.2V to 0.98V in a solution containing  $\text{Ad}_3$  in 2M HCl. Scan rate 20mV/sec.

The key difference in the two electrolyte media (i.e. HCl and  $\text{H}_2\text{SO}_4$ ) is the rate of electrodeposition whereby, the HCl deposition rate is approximately three times that observed in  $\text{H}_2\text{SO}_4$  (i.e.  $3.26 \times 10^{-3}$  mA/min). This is not surprising as already indicated earlier that the  $\text{Cl}^-$  ions have a smaller ionic radii than  $\text{SO}_4^{2-} / \text{HSO}_4^-$  ions and so the rate of permeation into the bentonite matrix should be much higher in the case of  $\text{Cl}^-$  ions. We expect this situation to be so despite the hydration factor.

Experiments to study the effect of permeation in the case of HCl electrolyte media were repeated as in Case 2, in the  $\text{H}_2\text{SO}_4$  electrolyte media referred to, in the above paragraphs. A freshly prepared bentonite electrode was allowed to sit in the electrolyte media without subjecting it to the potential cycling from -0.2V to 0.98V at a scan rate of 20mV/sec. The resultant cyclic voltammetric response gave oxidation/reduction peaks at

a potential of 0.432V/0.331V. The rate of electrodeposition was found to be  $2.05 \times 10^{-2}$  mA/min (approximately double the  $\text{H}_2\text{SO}_4$  case, i.e.  $1.25 \times 10^{-2}$  MA/min) and the redox efficiency was 71.4%. This is generally similar to the results obtained inn the case of  $\text{H}_2\text{SO}_4$ .

### **(c) $\text{Ad}_3$ – Adsorbed bentonite modified electrodes**

Adsorption studies were obtained for  $\text{Ad}_3$  in HCl and  $\text{H}_2\text{SO}_4$  electrolyte media.  $\text{Ad}_3$  plant material was allowed to dissolve in various concentrations of HCl and  $\text{H}_2\text{SO}_4$  i.e. 1M, 1.3M, 2M and 4M. A certain amount of electrode modification material, bentonite, (5g) was then put into each solution and stirred and left to equilibrate, for 15 hours. These samples were then air dried in the oven at  $80^\circ\text{C}$  for another 15 hours.

The dried plant material/bentonite was then used in derivatization of the working electrode surface. These electrodes were subjected to electrochemistry by cycling the potential from  $-0.2\text{V}$  to  $1.0\text{V}$  (for HCl samples) and  $1.2\text{V}$  (for  $\text{H}_2\text{SO}_4$  samples) at a scan rate of  $20\text{mV/sec}$ . The electrolyte media did not contain any plant material other than the acid. In general, the cyclic voltammetric response for each class of acid appears similar.

The tables below show the variation of oxidation/reduction potentials, electrodeposition rate and the redox efficiency as a function of the concentration of the acid in the solution. From tables it is apparent that the variation in oxidation potentials are more significant in the case of HCl while in the case of  $\text{H}_2\text{SO}_4$  they seem inconsistent. The electrodeposition rates do not appear to have any pattern in either of the acids but they are generally higher in the sulphuric acid case.



Table 4.15: Variation of oxd/red potential, electrodeposition rate and redox efficiency of  $Ad_3$  in different concentrations adsorbed onto bentonite (HCl media).

Concentration of solution (M)	Oxidation/reduction potential, E (V)	Electrodeposition rates, $di_{pa}/dt$ (mA/min)	Redox efficiency (%)
1	0.501/0.413	$1.88 \times 10^{-2}$	89.7
1.3	0.479/0.391	$2.5 \times 10^{-2}$	96.2
2	0.472/0.398	$3.0 \times 10^{-2}$	92.7
4	0.455/0.361	$1.8 \times 10^{-2}$	86.7

Table 4.16: Variation of oxd/red potential, Electrodeposition rate and redox efficiency of  $Ad_3$  in varying concentrations adsorbed onto bentonite ( $H_2SO_4$  media).

Concentration of solution (M)	Oxd/red potential E,(V)	Electrodeposiotion rates, $di_{pa}/dt$ (mA/min)	Redox efficiency (%)
1	0.662/0.74	$4.0 \times 10^{-2}$	95.8
1.3	0.523/0.273	$1.7 \times 10^{-1}$	94.7
2	0.611/0.147	$9.4 \times 10^{-2}$	83.3
4	0.667/0.037	$1.6 \times 10^{-1}$	50.7

The redox efficiencies in the case of  $H_2SO_4$  decrease with increasing concentration. It is worth mentioning that the adsorption data on sulphuric acid should be treated cautiously since the bentonite material allowed to stay in sulphuric acid/plant material solution proved difficult to use in derivatization of the working electrode and had to be mixed in a 1:1 ratio with fresh untreated bentonite sample. This kind of arrangement clearly will not give accurate preconcentration values for the plant material which can be used in

comparative studies with HCl and also brings to question the homogeneity of the redox active plant component of the host matrix.

However it was observed that the peak current varied linearly with scan rates in both acids suggesting a surface attached species as opposed to diffusion controlled process characterized by the earlier experiments that were done using ordinary bentonite for modification (see figures 4.58 and 4.59).

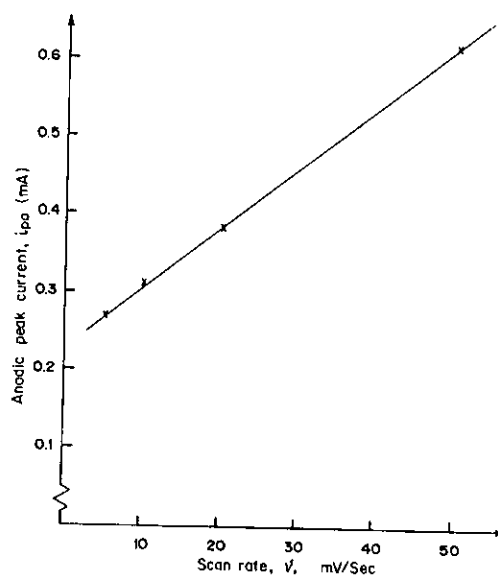


Fig. 4.58: Scan rate dependence studies; Plot of anodic peak current versus scan rate for  $Ad_3$  (in 4M HCl)- adsorbed onto bentonite electrode cycled in 1M HCl.

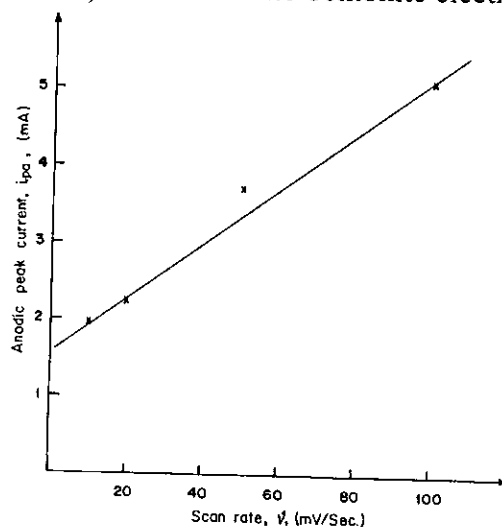


Fig. 4.59: Plot of anodic peak current versus scan rate for  $Ad_3$  in 2M  $H_2SO_4$  when studied on ordinary bentonite.

Further experiments done using  $\text{Ad}_3$  in  $2\text{M H}_2\text{SO}_4$  but this time the electrode was modified using pillared clay. The pillared clay modified electrode had to be cycled from  $-0.4\text{V}$  to  $1.4\text{V}$  at  $20\text{mV/sec}$  for about 72 hours (not continuously) in order to obtain a significant voltammetric response (see fig. 4.60).

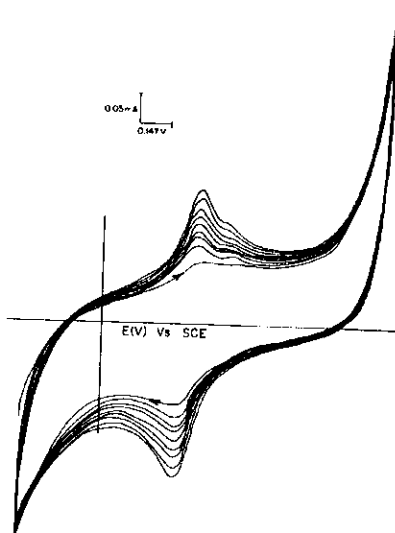


Fig. 4.60: CV response when heat pillared clay-modified electrode is cycled from  $-0.4\text{V}$  to  $1.4\text{V}$  in a solution containing  $\text{Ad}_3$  in  $2\text{M H}_2\text{SO}_4$ . Scan rate  $20\text{mV/sec}$ .

The oxidation /reduction potentials were observed at  $0.450\text{V}/0.369\text{V}$ . The long duration of this process is not surprising given the effect of pillaring on the bentonite. The electrodeposition rate was found to be  $3.75 \times 10^{-3} \text{ mA/min}$  (initial slope) see fig. 4.61.

The redox efficiency was computed to be  $74.1\%$ , a value much lower when compared with the un-pillared case. This is not surprising given the restrictions imposed on the bentonite matrix by pillaring. The scan rate dependence studies yielded a linear plot for anodic peak current versus scan rate as seen in fig. 4.62.

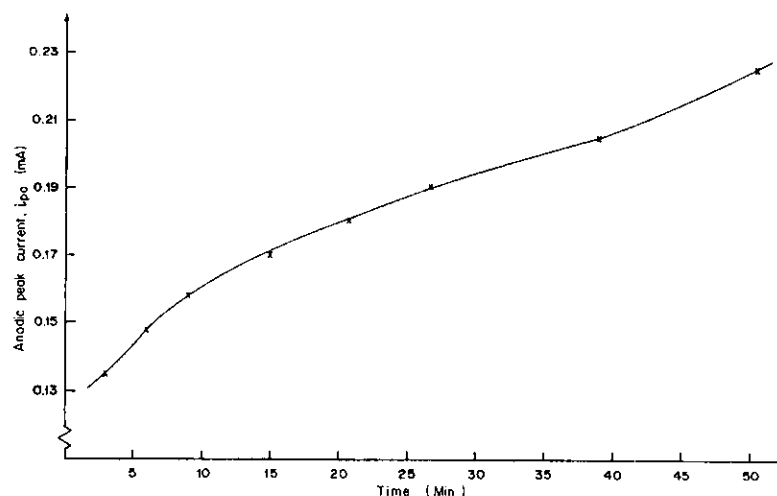


Fig. 4.61: Plot of anodic peak current versus time for  $Ad_3$  on pillared clay modified electrode.

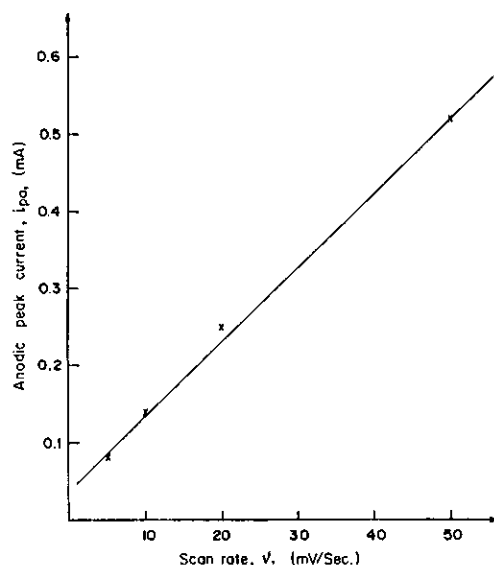


Fig. 4.62: Plot of anodic peak current versus scan rate  $Ad_3$  on pillared clay modified electrode.

#### 4.2.4 *Adansonia digitata* SEED, $Ad_4$

The analysis of *Adansonia digitata* seed was initially given a two pronged approach. In the first case the outer hard seed kernel was not interfered with, referred to as  $Ad_4$  (i) and the second case the seed was crushed to expose the soft nutty inside portion to the acid solutions directly, referred to as  $Ad_4$  (ii). Unlike the previous sections

of Ad<sub>1</sub>, Ad<sub>2</sub> and Ad<sub>3</sub>, where the mass of the samples used was approximately 0.1g, in the case of the Ad<sub>4</sub> all the experiments were done using, whole seeds. Given that the masses of the seeds are not uniform, the masses used in various experiments vary slightly.

#### 4.2.4.1 Analyses using bare carbon

Different masses of seed i.e. 0.5466 g of Ad<sub>4</sub> (i) and 0.5118 g of Ad<sub>4</sub> (ii), were allowed to dissolve in 1M H<sub>2</sub>SO<sub>4</sub> while 0.4922 g of Ad<sub>4</sub> (i) and 0.4562 g of Ad<sub>4</sub> (ii) were dissolved in 2M H<sub>2</sub>SO<sub>4</sub>. The potential of the working electrode was cycled from -0.4V to 1.4V at a scan rate of 20mV/sec. The cyclic voltammetric responses in both cases yielded oxidation/reduction potentials at 0.488V/0.327V and 0.482V/0.347V for the 1M case and 0.475V/0.372V and 0.52V/0.53V for the 2M case for Ad<sub>4</sub> (i) and Ad<sub>4</sub> (ii) respectively. See fig. 4.63 (a) & (b).

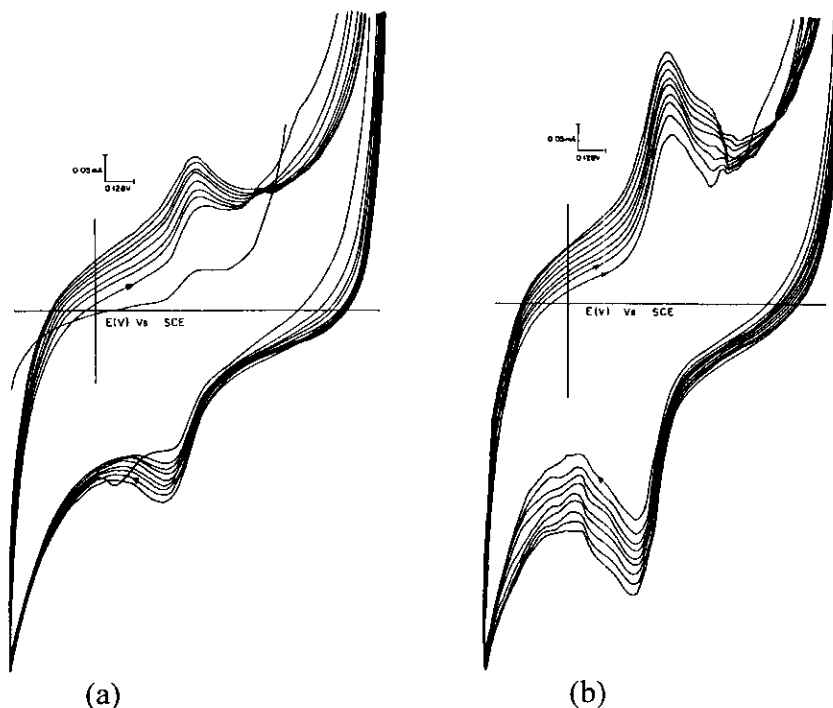


Fig. 4.63: CV response when bare carbon working electrode is cycled from -0.4V to 1.4V in a solution containing (a) uncrossed seed and (b) crushed seed in 2M H<sub>2</sub>SO<sub>4</sub> at a scan rate of 20mV /sec.

The redox potentials are basically the same, at most differing by approximately 50mV, which implies that the redox moiety in both seed components may or may not be the same. The electrodeposition rates computed from the initial slope yielded values of  $3.33 \times 10^{-3}$  mA/min for the Ad<sub>4</sub> (i) and  $4.38 \times 10^{-3}$  mA/min for Ad<sub>4</sub> (ii) in the case of 2M H<sub>2</sub>SO<sub>4</sub>. In all the studies the rates of electrodeposition of the plant material was found to be higher in the case 2M H<sub>2</sub>SO<sub>4</sub> for a particular seed components than in the 1M H<sub>2</sub>SO<sub>4</sub> and rate of electrodeposition is higher for Ad<sub>4</sub> (ii) than for Ad<sub>4</sub> (i). These differences can be attributed probably to the concentration of the redox active species being higher in the crushed seed.

When pH dependence studies were done on the crushed seed, the resultant plot of oxidation peak potential versus pH yielded a slope of approximately 58mV/pH suggesting a one proton, one electron process. The uncrushed seed on the hand yielded a slope of approximately 21mV/pH. The scan rate dependence studies for both cases gave a linear plot for the anodic current versus square root of scan rate suggesting diffusion controlled processes, (see fig 4.64). The redox efficiency for the process was over 85% irrespective of the acid concentration in the electrolyte media.

Fresh analysis using crushed Ad<sub>4</sub> (0.4155g) and a fresh electrode, were repeated with HCl as the supporting electrolyte. On cycling the potential of the working from -0.4V to 0.98V at 50mV/sec the CV response obtained for the crushed Ad<sub>4</sub> in 1M HCl showed well defined oxidation/reduction peaks occurring at 0.55V/0.301V (see fig. 4.65).

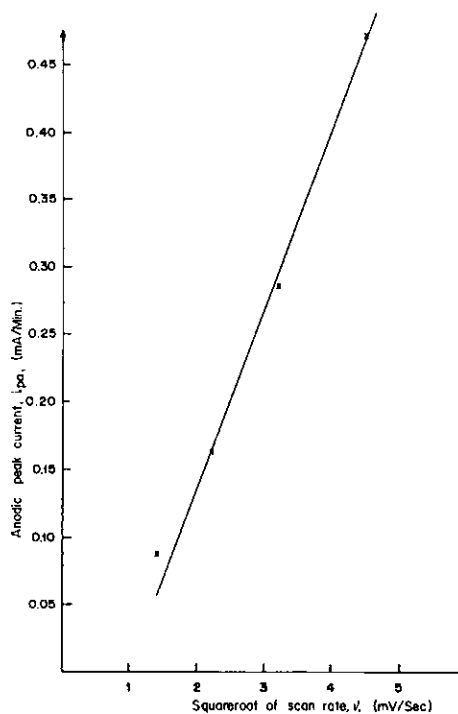


Fig. 4.64: Plot of anodic peak current versus square root of scan rate for crushed  $Ad_4$  in 2M  $H_2SO_4$ .

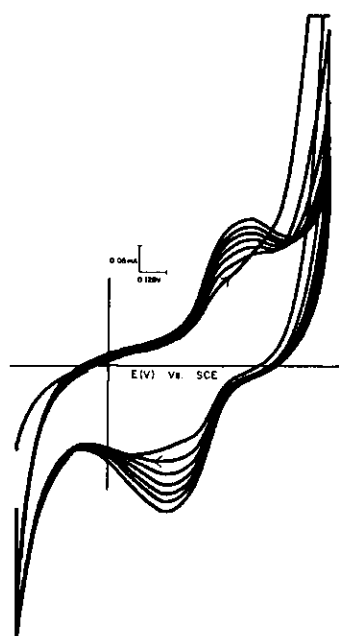


Fig. 4.65: Cyclic voltammetric response when bare carbon working electrode was cycled within the potential range -0.4V to 0.98V in a solution containing crushed  $Ad_4$  in 1M  $HCl$ . Scan rate 20mV/sec.

The rate of electrodeposition on plotting anodic peak current versus time yielded a discontinuous curve, the rates for the first and second phase being  $5.71 \times 10^{-3}$  mA/min and  $5.6 \times 10^{-3}$  mA/min respectively. The redox efficiencies were 53.3% and 91.2% for the first and second phase respectively. This discontinuity in the rate of electrodeposition can be attributed to autocatalysis, such a phenomena has been observed especially in the case of conducting polymers - see fig. 4.66 (a) and (b).

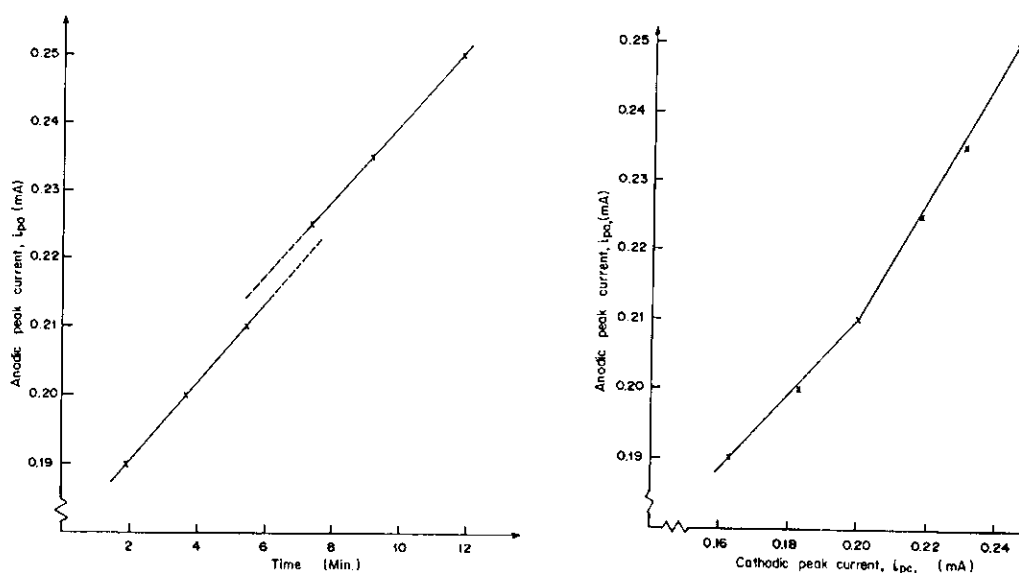


Fig. 4.66: Plot of anodic peak current versus (a) time and (b) cathodic peak current for crushed seed in 1M HCl studied using bare carbon

#### 4.2.4.2 Identification of $Ad_4$ from FTIR spectrum

As already mentioned in chapter 1,  $Ad_4$  is known to contain carbohydrates, proteins, fatty acids and vitamins  $B_1$ ,  $B_2$  and C. One interesting observation is that the oxidation/ reduction peak potentials for the crushed seed in both HCl and  $H_2SO_4$  electrolytes match exactly with those of ascorbic acid in the two electrolyte media. This implies that the seed contains vitamin C. On the other hand, results for the uncrushed seed kernel appear to have a lot of similarity with those obtained in the case of  $Ad_2$ . From



these results it is apparent that the redox active moieties in the crushed seed and the uncrushed seed are different. Some of the functional groups identified from the FTIR spectrum of the crushed seed, fig. 4.67, include

3700 – 3000cm<sup>-1</sup> - OH, NH (amines, amides)

1600 – 1700 cm<sup>-1</sup> - CONH<sub>2</sub>

Other groups which are obviously present in the Ad<sub>4</sub> include C-H groups, CH<sub>2</sub>=CH<sub>2</sub> i.e. part of the carbon chain. The FTIR spectrum of the seed is shown below.

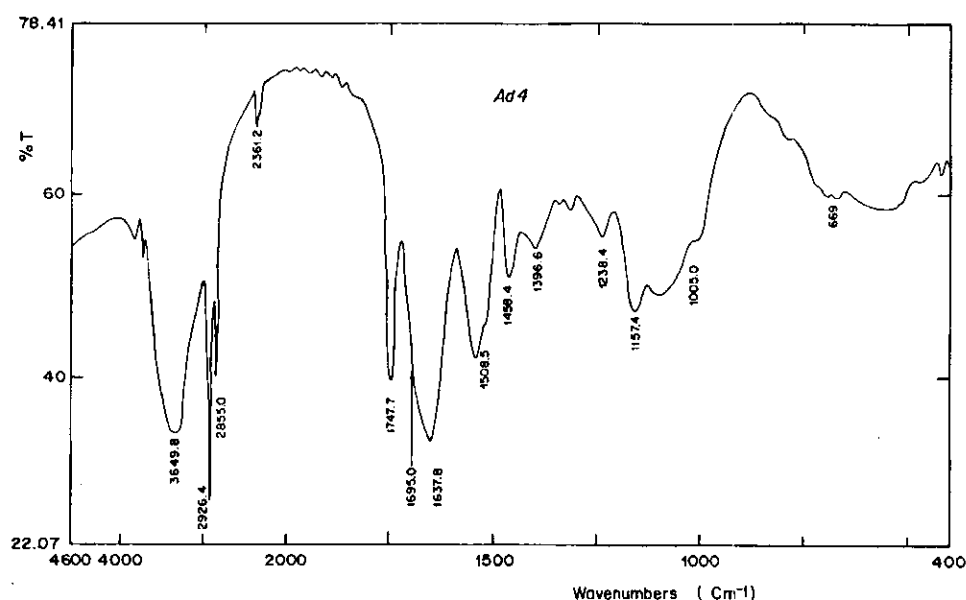


Fig. 4.67: FTIR spectrum for Ad<sub>4</sub>

#### 4.2.4.3 Effect of solvent on Ad<sub>4</sub> Redox Chemistry

Analyses were repeated for crushed Ad<sub>4</sub> in a solution consisting of water/acetonitrile mixture in the ratio 1:1. Sulphuric acid was used as the supporting electrolyte and the potential of the working electrode cycled from -0.4V to 0.7V at 20mV/sec. The cyclic voltammetric response (see fig. 4.68) yielded oxidation/reduction peak potentials at 0.55V/0.275V.

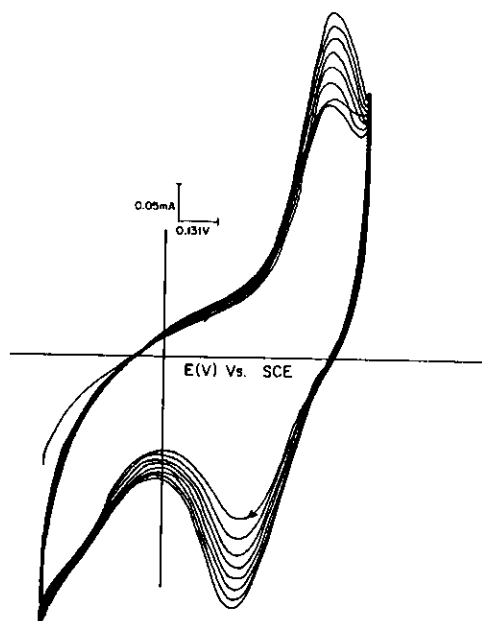
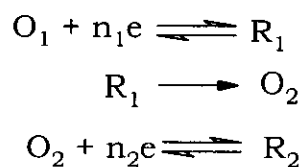


Fig. 4.68: CV response of the bare carbon-working electrode cycled from -0.4V to 0.7V in a solution containing  $\text{Ad}_4$  in  $\text{CH}_3\text{CN}/\text{H}_2\text{O}$  mixture. Scan rate, 20mV/sec.

Comparing this with the case of  $\text{Ad}_4$  in 1M  $\text{H}_2\text{SO}_4$  (no acetonitrile) where oxidation/reduction potentials were 0.48V/0.35V, it is apparent that the oxidation potential is shifted 70mV in the positive direction. This is not surprising and can be attributed to the proton deficiency.

The initial slope values of electrodeposition rate curve was found to be  $1.33 \times 10^{-2}$  mA/min as compared to  $3.4 \times 10^{-3}$  mA/min in the absence of acetonitrile. These differences in the rate can be attributed to enhanced solubility of the  $\text{Ad}_4$  in the non-polar solvent. The redox efficiency of the process in the presence of acetonitrile was 77.4% as compared to 86.3% in the absence of acetonitrile. This implies that the incremental increase in the oxidative peak does not correspond to the incremental increase in the reduction peak. This could imply that in the case of the non-aqueous media some of the oxidation products probably undergo a chemical reaction i.e. suggesting an ECE mechanism.



#### ECE mechanism

The scan rate dependence studies yielded a linear plot for anodic peak current versus square root of scan rate suggesting a diffusion limited process. From the pH dependence studies it was observed that there was no change in the oxidation potential in the pH range 0.3 to 0.9 while in the case of the lower pH the peak potentials shifted negative i.e. approximately 36mV/pH. This is not the case in the absence of acetonitrile whereby the anodic peak potential shifts positively as we lower the pH. Too much emphasis should not be laid on the contra-direction shifts but rather the importance of the protonation/ deprotonation equilibrium in the foregoing study (see fig. 4.69).

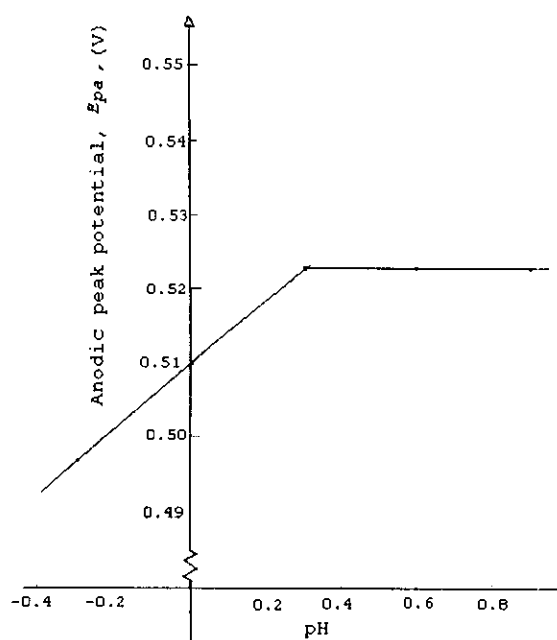


Fig. 4.69: Plot of  $E_{pa}$  versus pH for  $\text{Ad}_4$  in  $\text{CH}_3\text{CN}/\text{H}_2\text{O}$  mixture

#### 4.2.4.4 Analysis of $\text{Ad}_4$ on Modified Electrodes

##### (a) Polyaniline Modified Electrodes

The working electrode was modified using polyaniline a conducting polymer. This was achieved by cycling the potential of the working electrode in a solution containing 1M  $\text{H}_2\text{SO}_4$  and 0.1M aniline at a scan rate of 20mV/sec from -0.2V to 0.75V. The polyaniline derivatized electrode was then used to study  $\text{Ad}_4$  in 2M  $\text{H}_2\text{SO}_4$  with the potential being cycled from -0.2V to 0.65V at scan rate of 20mV/sec. The positive potential limit was reduced from 0.75V to 0.65V to cushion the polyaniline modified electrode from electrodegradation as polyaniline is known to degrade in solutions that do not contain the monomer when in cycled far positive. The derivatized electrodes of analysis were of different thickness classified as thin and thick films – a parameter established from the anodic peak current since the latter is directly proportional to film thickness. The resultant CV responses are shown in figures 4.70 and 4.71.

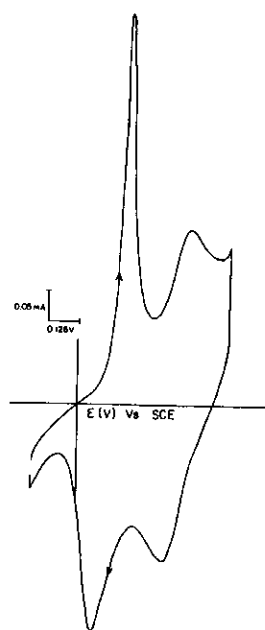


Fig. 4.70: CV response when a polyaniline (thin film) modified electrode was cycled from -0.2V to 0.65V in a solution containing  $\text{Ad}_4$  in 2M  $\text{H}_2\text{SO}_4$ . Scan rate, 20mV/sec.

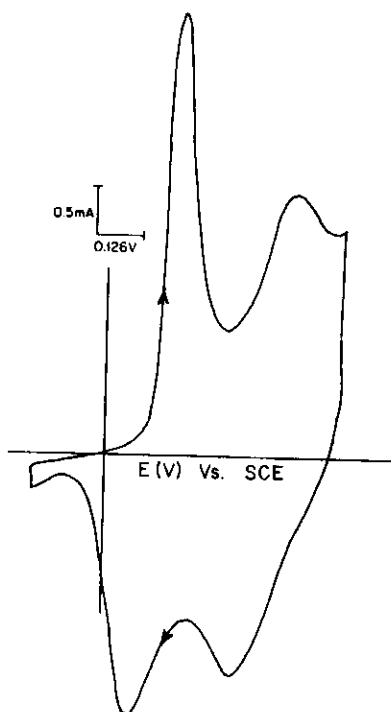


Fig. 4.71: CV response for polyaniline (thick film) modified electrode was cycled from -0.2V to 0.65V in a solution containing  $\text{Ad}_4$  in 2M  $\text{H}_2\text{SO}_4$ . Scan rate, 20mV/sec.

The cyclic voltammetric responses had well defined oxidation /reduction peaks with potentials occurring at 0.494V/0.377V for the thin film (0.0134  $\mu\text{m}$ ) and 0.507V/0.36V for the thick film (0.0497  $\mu\text{m}$ ) in the case of uncrushed seed,  $\text{Ad}_4$  (i). The crushed seed,  $\text{Ad}_4$  (ii), had oxidation/reduction potentials occurring 0.484V/0.365V for thin film (0.011 $\mu\text{m}$ ) and 0.488V/0.379V for thick (0.0564  $\mu\text{m}$ ).

Comparing these results with the oxidation /reduction peaks potentials of the seed on bare carbon which occurred at 0.475V/0.37V and 0.52V/0.353V for  $\text{Ad}_4$  (i) and  $\text{Ad}_4$  (ii) respectively, we observe that the presence of polyaniline on the working electrode surface lowers the oxidation potential of the  $\text{Ad}_4$  (ii) moiety. This can be attributed to electrocatalytic property of polyaniline, a phenomena which has been observed in  $\text{Ad}_1$  and  $\text{Ad}_3$  components of the seed discussed elsewhere in this thesis.  $\text{Ad}_4$  (i) on the other

hand, appears to be shifted positively, which is interestingly similar to what was observed in  $\text{Ad}_2$  case.

The shifts in the oxidation potential on polyaniline derivatized electrode were found to depend on the thickness of the polymer, which in turn is proportional to the number of electroactive sites. The thin film cases yielded lower oxidation potential than the thick films, i.e. differences of 4 to 20 mV. This can be attributed to the changes in the morphology of the polyaniline a fact that has already been observed from Quartz crystal Microbalance (QCM) studies [54] and the number of redox active sites.

Scan rate dependence studies yielded liner plots for anodic peak current versus scan rate implying that the polyaniline modified electrode was surface attached. This was not the case with the unmodified electrode where we obtained linear plot of  $i_{pa}$  versus square root of scan rate suggesting diffusion limited process (see fig. 4.72).

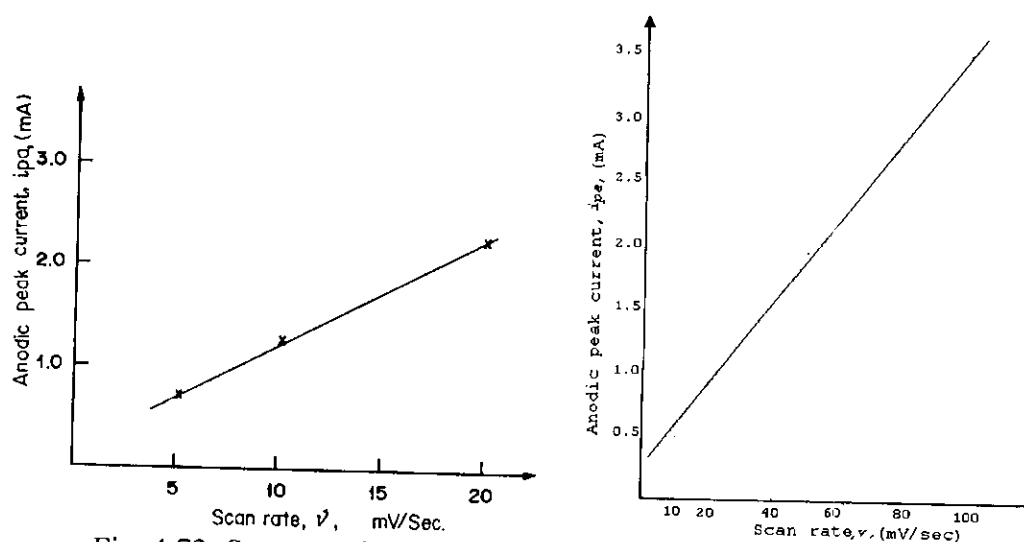


Fig. 4.72: Scan rate dependence studies; Plots of  $i_{pa}$  versus scan rates (5 - 20 mV/sec and 10 - 100 mV/sec) for PAN modified electrode in a solution containing  $\text{Ad}_4$  in 2M  $\text{H}_2\text{SO}_4$ .

The same experiments were repeated using polyaniline film generated in 1M HCl. This was then cycled for -0.2V to 0.65V in a solution containing plant material in 2M

HCl at a scan rate of 20mV/sec. The oxidation/reduction potentials for Ad<sub>4</sub> (i) occurred at 0.464V/0.385V for the thin film (0.0142  $\mu\text{m}$ ) and 0.484V/0.385V for thick film (0.0615 $\mu\text{m}$ ) while for Ad<sub>4</sub> (ii) they occurred at 0.438V/0.414V for the thin film (0.0167  $\mu\text{m}$ ) and 0.52V/0.366V for the thick film (0.063  $\mu\text{m}$ ). In all the cases the oxidation potential in the thick film was found to be much higher as compared to the thin film.

This behaviour just as was discussed in the case of sulphuric acid can be attributed to the polyaniline electrocatalytic effects/changes in the film morphology and probably the effects of the anion, which maintains electroneutrality in the film. However, the potentials obtained here were much lower than the case of bare carbon (0.55V/0.301V). The scan dependence studies just as in the case of H<sub>2</sub>SO<sub>4</sub> yielded linear plots for  $i_{pa}$  versus scan rate suggesting surface attached species.

#### **(b) Bentonite Modified Electrodes**

The carbon graphite working electrode was modified as already described in the experimental section using bentonite. The electrode potential was cycled from -0.2V to 1.0V in a solution containing 0.4252 g of crushed seed in 2M H<sub>2</sub>SO<sub>4</sub> at a scan rate of 20mV/sec. The resultant cyclic voltammetric response yielded oxidation/reduction peak potentials at 0.46V/0.36V (see fig. 4.73). The electrodeposition rate was found to be  $1.92 \times 10^{-2}$  mA/min (see fig. 4.74) while the redox efficiency was computed to be approximately 100%.

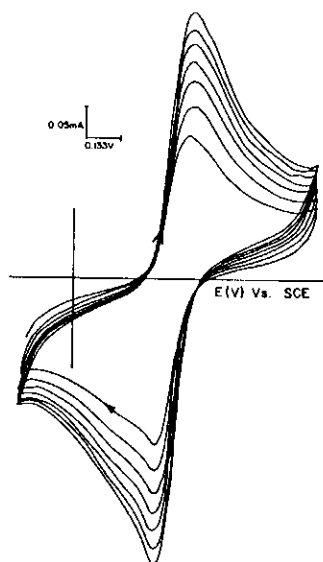


Fig. 4.73: CV response for a bentonite modified electrode cycled from -0.2V to 1.0V in a solution containing crushed  $\text{Ad}_4$  in 2M  $\text{H}_2\text{SO}_4$ . Scan rate, 20mV/sec.

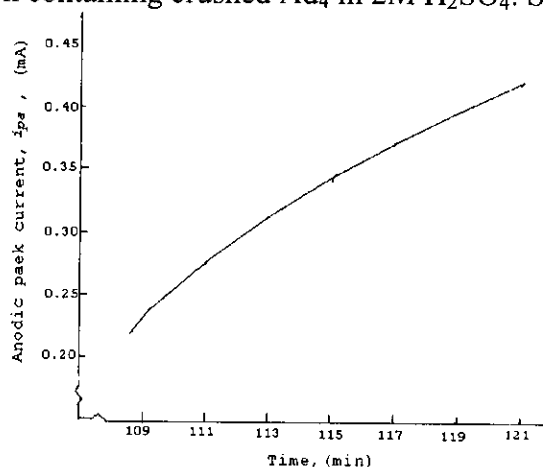


Fig. 4.74: Plot of anodic peak current versus time for crushed  $\text{Ad}_4$  in 2M  $\text{H}_2\text{SO}_4$  studied on a bentonite modified electrode.

The scan rate dependence studies yielded linear plots for anodic peak current versus square root of scan rate suggesting a diffusion limited process (see fig. 4.75). The pH dependence studies carried out in solution containing 0.125M, 0.25M, 0.5M, 1.0M and 2M  $\text{H}_2\text{SO}_4$  led to the oxidation peaks shifting in the positive direction i.e. 77 mV/pH suggesting one proton, one electron process.

In general the oxidation potential in bentonite is lower than the case of carbon graphite or polyaniline derivatized electrode by 60mV and 20mV respectively. This once



again can be attributed to electrocatalytic effect of bentonite resulting from the redox activities of the metal cations intercalated in the bentonite matrix.

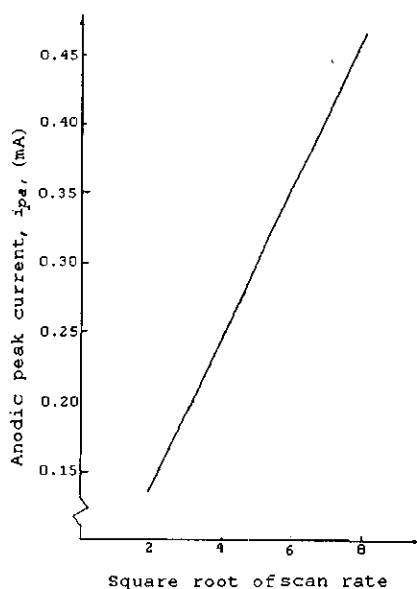


Fig. 4.75: Plot of  $i_{pa}$  versus square root of scan rate for  $Ad_4$  in 2M  $H_2SO_4$  studied on a bentonite modified electrode.

Fresh experiments were conducted to establish the effect of adsorption of  $Ad_4$  on bentonite electrode. This was done by allowing the bentonite electrode to sit in a solution containing 0.426 g of crushed  $Ad_4$  in 2M  $H_2SO_4$  for 2 hours without any cycling of the potential. The electrode was then air dried for approximately 12 hours and then subjected to potential cycling from  $-0.2V$  to  $1.0V$  at a scan rate of  $20mV/sec$ . The cyclic voltammetric response is shown in fig. 4.76 and the oxidation/reduction potentials are occurring at  $0.45V/0.37V$ .

There was an irreversible oxidation peak at  $0.785V$ ; a peak, which we propose, is associated with adsorption of the  $Ad_4$  on the bentonite matrix. This observation had been observed in the case of adsorption of ascorbic acid standard on a bentonite electrode (see fig. 4.56). The peak indicating presence of ascorbic acid in the seed confirms the findings

of other researchers [10] that the seed of *A. digitata* contains significant amounts of ascorbic acid.

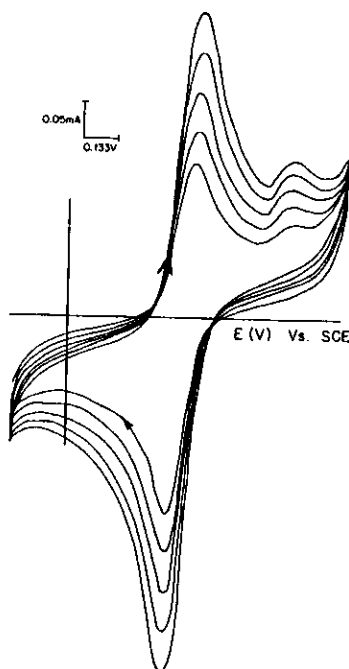
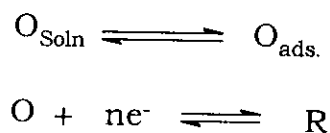


Fig. 4.76: CV response for bentonite modified electrode initially dipped into the solution of  $\text{Ad}_4$  in 2M  $\text{H}_2\text{SO}_4$  for sometime (with no potential cycling), air-dried and then cycled within the potential -0.2V to 1.0V at 20mV /sec in the same solution.

The voltammetric pattern obtained is an indicator of a strong product adsorption. The oxidation/reduction peak at 0.45V/0.37V corresponds to the reaction of solution species whilst the peak at 0.79V corresponds to the reaction of the adsorbed species. Since both the adsorbed and solution species are electroactive, the redox process can be represented as follows [97]:



The fact that the potential of the peak associated with the adsorption is approximately 340mV more positive than the corresponding solution peak suggests that

the adsorbed product is stabilised and reacts less readily with respect to the electrode reaction. Such a strong product adsorption has been observed in the reduction of proton on a platinum electrode even though in this case the peaks were reversible. The duality obtained from the scan rate dependence studies can be apportioned with the linear variation with scan rate being due to adsorption and that with square root of scan rate being attributed to the solution species. The significant separation i.e. 340mV between the solution and adsorption peaks is a pointer to the relative strength of the adsorption [97].

However although Ad<sub>3</sub> is also known to contain ascorbic the adsorption peak was not very conspicuous as in the case of Ad<sub>4</sub> which could be explained by the fact that in the latter the seed kernel preserved the ascorbic acid. In the case of Ad<sub>3</sub>, which was kept at room temperature in the course of the study its possible that the ascorbic acid could have decomposed in some way since its known to be adversely affected by moisture during storage.

Further electrochemical analysis with regard to the foregoing electrode revealed redox efficiency of the first oxidation peak (i.e. at 0.45V/0.37V) was 97.1% (see fig. 4.77) which is less efficient compared to the case where Ad<sub>4</sub> was not allowed to adsorb on the electrode prior to the electrochemical analysis. This as already discussed is related to the entropy effects associated with adsorption process.

The scan rate dependence studies yielded a linear plot for anodic peak current versus square root of scan rate suggesting a diffusion limited process. The electrodeposition rate for the first peak occurring at 0.45V was  $2.7 \times 10^{-2}$  mA/min while for peak at 0.785V was  $1.21 \times 10^{-2}$  mA/min (see fig. 4.78).

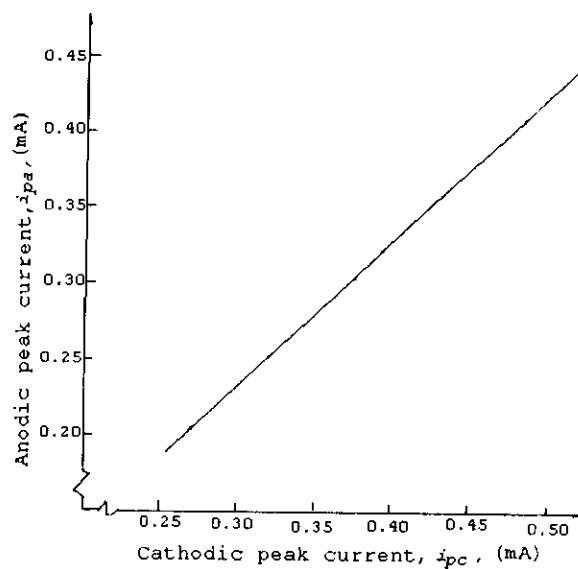


Fig. 4.77: Plot of  $i_{pa}$  versus  $i_{pc}$  for bentonite modified electrode initially dipped into a solution of crushed  $Ad_4$  before subjecting it to potential cycling.

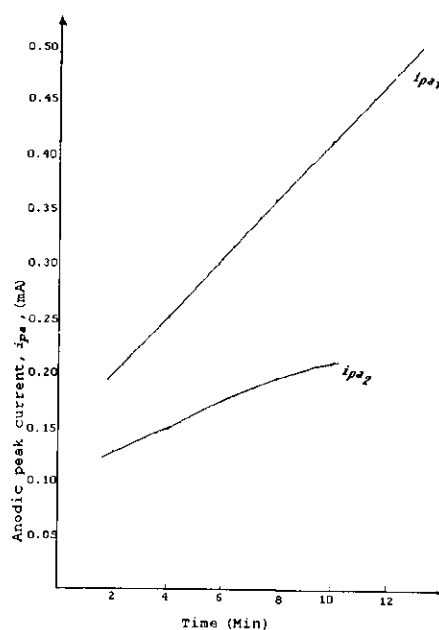


Fig. 4.78: Plot of  $i_{pa}$  versus time for the solution and adsorbed peaks in crushed  $Ad_4$

When similar experiments were repeated in HCl (i.e. the bentonite-modified electrode was cycled in a solution containing  $Ad_4$  in 2M HCl) we obtained a voltammetric response with the oxidation/reduction potentials occurring at 0.483V/0.389V which is

approximately 20mV more positive than the case of  $\text{H}_2\text{SO}_4$ . The voltammogram remains the same in terms of reversibility of the redox peaks (see fig. 4.79).

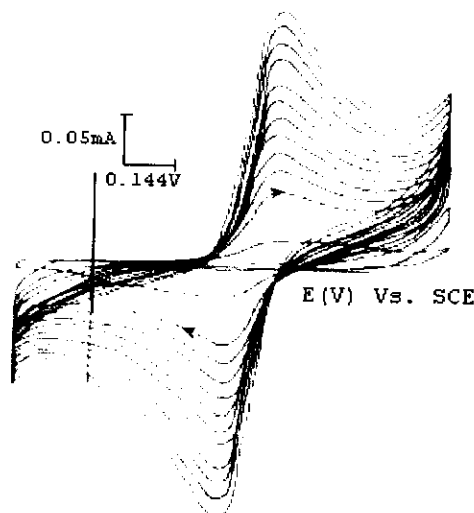


Fig. 4.79: CV response when a bentonite modified electrode was cycled from -0.2V to 0.98V in a solution containing  $\text{Ad}_4$  in 2M  $\text{HCl}$ . Scan rate 20mV/sec.

The redox efficiency of the process as obtained from the slope of the plot of anodic versus cathodic peak current yielded a value of 96.2%. This redox process is less efficient as compared to the case of  $\text{H}_2\text{SO}_4$  (100%). This inherent difference can be due to the anion effect and/or the high concentration of protons in the sulphuric acid media assuming complete ionization to the  $\text{SO}_4^{2-}$  ions. These factors would affect the solvent population in the bentonite matrix, which would in turn affect the redox properties of the redox active moieties in the plant materials. The scan rate dependence studies yielded a linear plot for anodic peak current versus square root of scan rate suggesting a diffusion limited process (see fig. 4.80).

The same experiments were repeated in solutions of different pH (i.e. 0.903, 0.602, 0.301, 0, and -0.301) and no significant shifts in the peaks were observed for the oxidation and reduction peak unlike in the case of sulphuric acid. This suggests that the

anion probably affects the protonation/deprotonation equilibrium in the redox active moiety in the plant material.

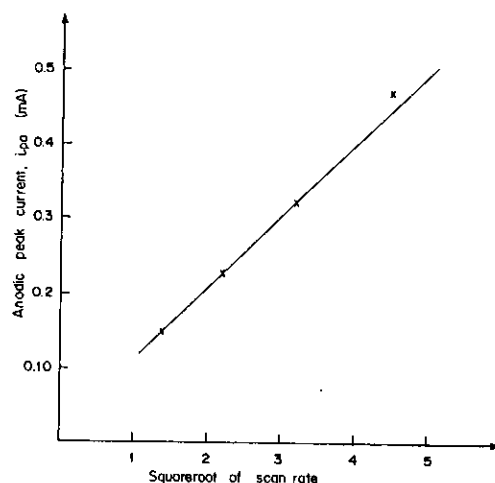


Fig. 4.80: Scan rate dependence studies; Plot of  $i_{pa}$  versus square root of scan rate for crushed  $Ad_4$  in 2M HCl.

### (c) $Ad_4$ -adsorbed Bentonite modified Electrodes

$Ad_4$  was adsorbed on the bentonite matrix by dissolving varying amounts of the crushed seed in different concentrations of HCl i.e. 0.4315g/ 1M HCl, 0.4785g/ 1.3M HCl, 0.455g/ 2M HCl, and 0.3343 g/ 4MHCl. To each of these mixtures, 5g of bentonite were added and allowed to sit there for 15 hours. This was then filtered and air-dried in an oven at 80° C for another 15 hours. The dry mixture was crushed into fine powder and used to modify the working electrode surface as already discussed in chapter 3.

The  $Ad_4$ -adsorbed bentonite modified electrodes were subjected to electrochemical analysis in 1M HCl solution by cycling the potential from -0.2V to 1.0V at 20 mV/sec. The cyclic voltammetric responses obtained in all the cases (see fig. 4.81 for the case of 0.3343g/ 4MHCl) yielded a quasi-reversible redox peaks with oxidation/reduction potentials as shown in Table 4.17.

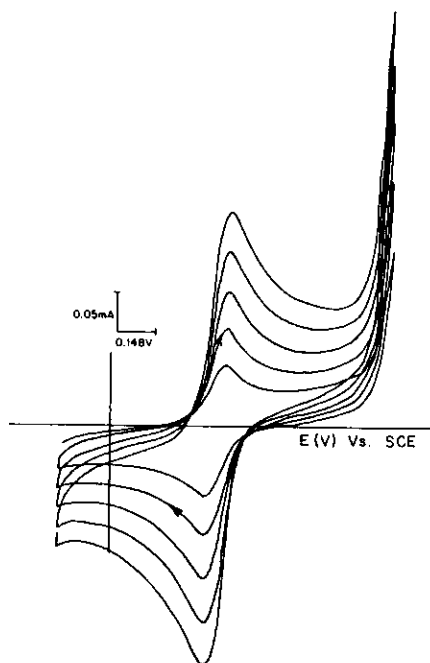


Fig. 4.81: CV response when the potential of the  $\text{Ad}_4$ -adsorbed bentonite modified electrode was cycled in a 1M HCl solution within the potential range -0.2V to 1.0V. Scan rate 20mV/sec.

Table 4.17: Mixtures of  $\text{Ad}_4/\text{HCl}$  that were adsorbed onto the bentonite used in electrode modification and their corresponding oxidation/reduction potentials, electrodeposition rates and redox efficiencies.

Mixture	Oxd/red potential E, (V)	Rate of electrodeposition $di_{pa}/dt$ (mA/min)	Redox efficiency (%)
0.4315g/1M HCl	0.51/0.386	$7.5 \times 10^{-3}$	100
0.4785g/1.3M HCl	0.499/0.411	$1.35 \times 10^{-2}$	90.3
0.455g/2M HCl	0.465/0.391	$1.08 \times 10^{-2}$	93.1
0.3343g/4M HCl	0.450/0.391	$2.32 \times 10^{-2}$	90.9

From the table it is apparent that the oxidation potentials decrease with increase in acid concentration used in the adsorption. This phenomenon is not surprising as it has also been observed with  $\text{Ad}_2$  and  $\text{Ad}_3$  and we attribute it to entropic effects resulting from the surface adsorption. This is further corroborated from scan rate dependence studies see

fig. 4.82) which yields a linear plot for the case of anodic peak current versus scan rate confirming the presence attached species.

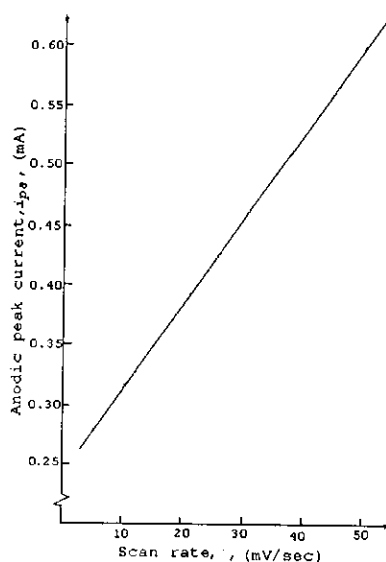


Fig. 4.82: Plot of anodic peak current versus scan rate for  $Ad_4$ -adsorbed bentonite modified electrode.

The redox efficiency is substantially high in all the cases. The results suggest an increase in the rate of electrodeposition as pH of the solution decreases. It is also important to mention that the variation in the masses of  $Ad_4$  will also affect the electrodeposition rates as it affects the amount of  $Ad_4$  adsorbed since adsorption in most cases is an extensive property. Relative to 0.4315g amount of  $Ad_4$  in 1M case the percentage differences are 11% (1.3M), 5.4% (2M) and 23% (4M).

A comparison of electrodeposition rates, oxidation potential and redox efficiency for the various electrode systems studied thus far revealed that, for the case of 1M HCl the adsorbed  $Ad_4$  has a lower oxidation potential but a higher redox rate and redox efficiency values than the bare carbon case. Similarly on comparison of the adsorbed  $Ad_4$  in 2M HCl case to that of ordinary bentonite the oxidation potential and electrodeposition rate of the former are higher and the redox efficiency is lower. In the case of polyaniline



modified electrode the only comparison possible was the redox potentials whereby the oxidation potential is significantly much lower in the thin film modified electrode than that of adsorbed  $Ad_4$ . It was difficult to compute the electrodeposition rate in the case of polyaniline due to the fact that electrodeposition of  $Ad_4$  occurs at high positive potential, which will lead to electrodegradation of polyaniline film in the absence of aniline monomer. The actual comparison values are shown in 4.18 below.

Table 4.18: Comparison of oxidation potentials, electrodeposition rates and redox efficiency for various electrode systems used on  $Ad_4$  with HCl as the supporting electrolyte.

Electrode system	Electrolyte media	Oxidation potential, E (V)	Electrodeposition rate, $di_{pa}/dt$ (mA/min)	Redox efficiency (%)
(a) Bare carbon	0.415g/ 1MHCl	0.55	$5.6 \times 10^{-3}$	91.2
(b) Adsorbed $Ad_4$ -bentonite-modified	0.4315g/ 1M HCl	0.51	$7.5 \times 10^{-3}$	100
(a) Ordinary bentonite	0.452g/ 2M HCl	0.483	$4.29 \times 10^{-3}$	96.2
(b) Adsorbed $Ad_4$ -bentonite-modified	0.455g/ 2M HCl	0.499	$1.08 \times 10^{-3}$	93.1
(a) PAN modified	0.457g/ 2MHCl	0.438		
(b) Adsorbed $Ad_4$ -bentonite modified	0.455g/ 2MHCl	0.499		

The adsorption experiments were repeated for the sulphuric acid media with the varying combination of masses of crushed seed and acid concentration as previously done in the

HCl case. For modification of the electrode surface the  $\text{Ad}_4$ -adsorbed bentonite had to be mixed with ordinary bentonite in the ratio of 1:1 to facilitate its adhesion on the working electrode. This implies that the actual masses of the  $\text{Ad}_4$  were therefore reduced on mixing the  $\text{Ad}_4$ -adsorbed bentonite with the ordinary bentonite. This material was then used in electrode modification and an example of the voltammetric response is shown in figure 4.83 ( $\text{Ad}_4/1\text{M H}_2\text{SO}_4$  case). The CV response clearly displays a large  $\Delta E_p$  (0.76V), which is an indication of poor reversibility in the redox system in the case of  $\text{H}_2\text{SO}_4$ .

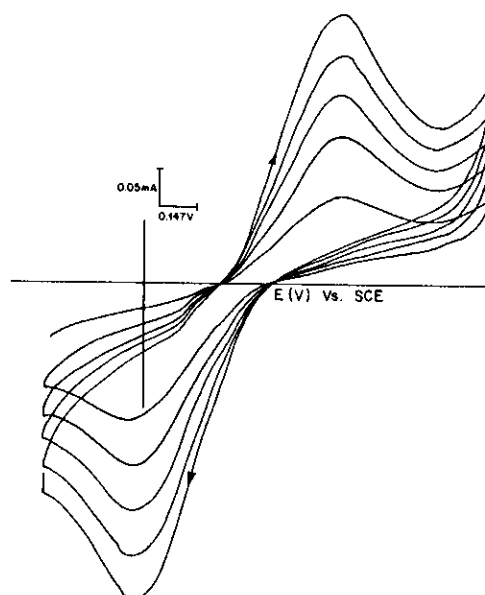


Fig. 4.83: CV response obtained when  $\text{Ad}_4/\text{H}_2\text{SO}_4$ -adsorbed bentonite modified electrode is cycled from -0.4V to 1.4V in a 1M  $\text{H}_2\text{SO}_4$  solution. Scan rate 20mV/sec.

The oxidation potentials, electrodeposition rates and redox efficiency for four  $\text{Ad}_4/\text{H}_2\text{SO}_4$  mixtures are displayed in table 4.19. The results shown clearly indicate inconsistency in the oxidation potentials and the redox efficiency, with 1.3M case having the highest oxidation potential and the lowest redox efficiency. However, in general the oxidation potentials are much higher in the  $\text{H}_2\text{SO}_4$  system as compared to HCl case.

Similarly electrodeposition rates are much higher and they seem to increase with decreasing pH.

Table 4.19: Oxidation potentials, electrodeposition rates and redox efficiencies for different  $\text{Ad}_4/\text{H}_2\text{SO}_4$  mixtures that were adsorbed onto bentonite for modification of the working electrode surface.

$\text{Ad}_4 / \text{H}_2\text{SO}_4$ mixture	Oxidation potential, E(V)	Electrodeposition rates, $di_{pa}/dt$ (mA/min)	Redox efficiency (%)
0.591g $\text{Ad}_4$ / 1M $\text{H}_2\text{SO}_4$	0.781	$1.82 \times 10^{-2}$	90
0.52g $\text{Ad}_4$ / 1.3M $\text{H}_2\text{SO}_4$	0.855	$2.29 \times 10^{-2}$	64.3
0.464g $\text{Ad}_4$ / 2M $\text{H}_2\text{SO}_4$	0.708	$3.86 \times 10^{-2}$	80.8
0.4048g $\text{Ad}_4$ / 4M $\text{H}_2\text{SO}_4$	0.796	$4.42 \times 10^{-1}$	89.6

The scan rate dependence studies yielded linear plots for anodic peak current versus scan rate, confirming the redox active species is surface attached (see fig. 4.84).

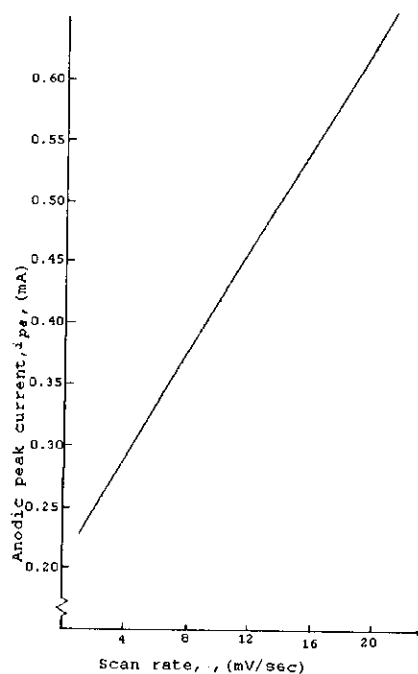


Fig. 4.84: Scan rate dependence studies; Plot of  $i_{pa}$  versus scan rate for  $\text{Ad}_4/\text{H}_2\text{SO}_4$  adsorbed bentonite modified electrode.

#### 4.3.0 Use of Electrochemical Signal to Confirm the Presence of Flavonoids and Terpenes in parts of *A. digitata* Fruit

Since previous researchers have identified that the roots of *A. digitata* contain triterpenes, flavonoids, steroids and lipids and the leaves contain triterpenes coumarins and steroids [23, 24], we decided to carry out investigations to establish whether we could attribute any of the peaks to presence of diterpenes, alkaloids and/or flavonoids. The foregoing chemical compounds, which had been extracted using standard organic procedures and identified using  $C^{13}$  and Proton NMR in the natural products laboratory, were dissolved in 2M  $H_2SO_4$ . The various solutions were then subjected to electrochemical study by cycling the potential of the bare carbon working electrode within the range -0.4V to 1.4V at scan rates of 50 or 20 mV/ sec. The resultant cyclic voltammograms are shown in figures 4.85 - 4.87.

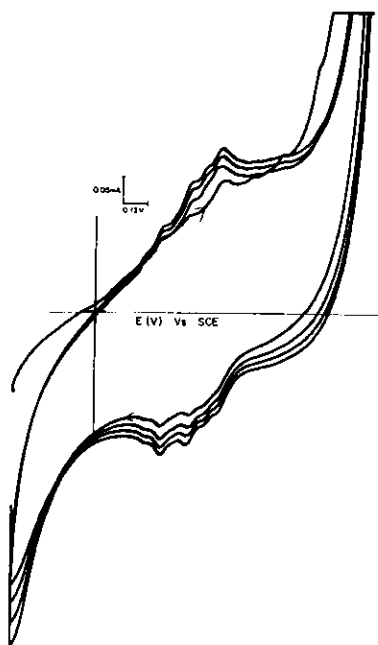


Fig. 4.85: CV response of bare carbon working electrode when cycled within the potential range -0.4V to 1.35V in a solution containing 0.05g of alkaloid extract in 2M  $H_2SO_4$  at a scan rate of 20mV/ sec.

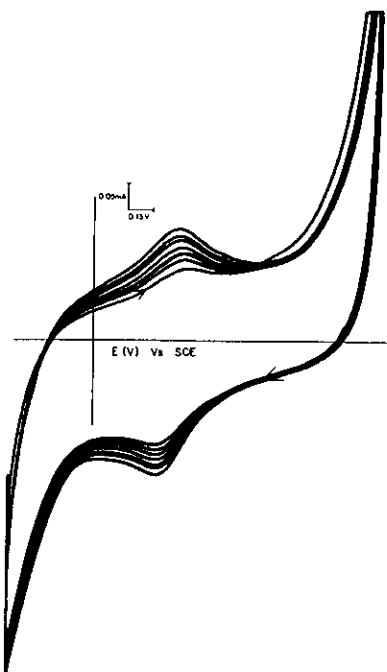


Fig. 4.86: CV response of bare carbon working electrode when cycled within the potential range -0.4V to 1.4V in a solution containing 0.05g of Flavonoid extract in 2M  $\text{H}_2\text{SO}_4$  at a scan rate of 50mV/ sec.

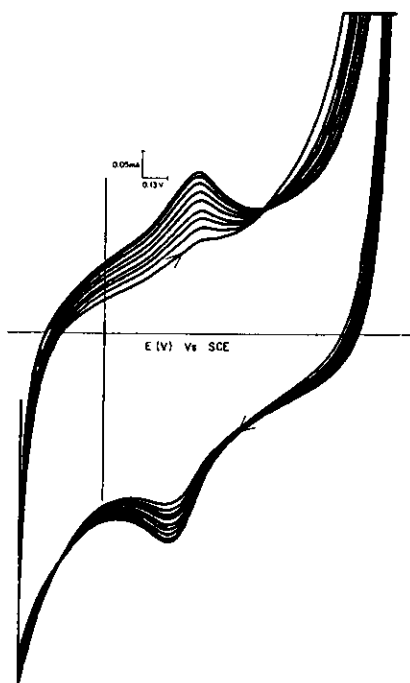


Fig. 4.87: CV response of bare carbon working electrode when cycled within the potential range -0.4V to 1.4V in a solution containing 0.05g of diterpene extract in 2M  $\text{H}_2\text{SO}_4$  at a scan rate of 50mV/ sec.

It is apparent that the voltammograms differ significantly. The latter voltammograms are poorly defined suggesting slow electron transfer kinetics. The oxidation peak potentials are very broad and occur at 0.449V/0.325V for flavonoids and 0.454V/0.337V for diterpenes. The voltammogram for alkaloids shows three oxidative peaks occurring at 0.325V, 0.467V and 0.610V and the reduction potential are almost coinciding i.e.  $\Delta E_p$  is very minimal.

The redox peaks obtained in the case of diterpenes and flavonoids closely match those obtained in Ad<sub>2</sub> and also uncrushed seed, Ad<sub>4</sub> (i) that showed oxidation/reduction peak potentials at 0.449V/0.379V and 0.475V/0.372V respectively, when studied on bare carbon as mentioned elsewhere in the thesis. The Ad<sub>4</sub> (i) gives results that differ from the crushed seed because in the former it's the seed kernel that is most probably subjected electrochemical tests since a very tough seed kernel covers *A. digitata* seed. The results obtained in this work indicate the presence of flavonoids and the diterpenes in the woody part of the fruit. The redox active moieties in triterpenes and diterpenes are similar which explains why the oxidation/reduction potentials are indicating presence of the terpenes. However further work still needs to be done to differentiate between the two classes of terpenes. The electrodeposition rates for diterpenes and flavonoids were found to be  $5.38 \times 10^{-3}$  mA/min and  $2.62 \times 10^{-3}$  mA/min while the redox efficiencies were 58.7% and 83.3% respectively. The cyclic voltammogram of the alkloids is distinctly different and it obvious there is no resemblance in our plant material which could imply that there are no alkaloids in the woody parts of the fruit.

The oxidation/ reduction potentials for bare carbon working electrode for all the four components of *Adansonia digitata* fruit and the chemical standards worked on this work are summarized in the table 4.20 below.

Table 4.20: Summary of the oxidation/ reduction potentials of the four components of *A. digitata* fruit and the standards in the bare carbon working electrode system.

Component	Oxidation/reduction potentials, E (V)	
	In H <sub>2</sub> SO <sub>4</sub> media (2M in the case of plant material)	In HCl media (1M)
Ad <sub>1</sub>	0.501V/0.340V	0.474V/0.416V
Ad <sub>2</sub>	0.449V/0.379V	0.473V/0.415V
Ad <sub>3</sub>	0.546V/0.279V	0.477V/0.361V
Ad <sub>4</sub> (crushed)	0.520V/0.353V	0.55V/0.301V
Chlorophyll	0.494V/0.382V	0.501V/0.419V
Ascorbic acid	0.520V-0.560V (no reduction peak)	0.550V(no reduction peak)
Thiamin	0.488V/0.364V	0.483V/0.381V
Riboflavin	-0.026V/-0.051V; 0.501V/0.34V and 1.027V	-0.013V/-0.05V and 0.495V/0.384V

The cyclic voltammograms in the bare carbon working electrode were observed to be quasi reversible with  $\Delta E_p$  being 161mV, 64mV, 267mV and 167mV in the case of H<sub>2</sub>SO<sub>4</sub> and 58mV, 58mV, 116mV and 249mV in the case of HCl for Ad<sub>1</sub>, Ad<sub>2</sub>, Ad<sub>3</sub> and Ad<sub>4</sub> respectively.

When we consider the experiments where H<sub>2</sub>SO<sub>4</sub> was the supporting electrolyte we observe that in the polyaniline modified electrode the oxidation potential shifted

negative by approximately 13.2mV for Ad<sub>1</sub>, 65mV for Ad<sub>3</sub> and 36mV for Ad<sub>4</sub> as compared to the bare carbon case. In the case of Ad<sub>2</sub> the shift was not significant since on bare carbon the oxidation peak was observed to be in range 0.449-0.482V (due to positive shifts on continued cycling) and on PME the range of oxidation peak was 0.452-0.459V when both were cycled for about twenty-two minutes. In the CME case the oxidation potential of the plant material was shifted negatively by approximately 51mV, 3mV, 76mV and 60mV for Ad<sub>1</sub>, Ad<sub>2</sub>, Ad<sub>3</sub> and Ad<sub>4</sub> respectively.

### CONCLUSION

From the results obtained it is apparent that electrochemical analysis of raw plant materials yield results, which can be used as confirmatory test for the presence of different chemical substances, found in the material. The results on bare carbon working electrode show that the potentials of the standard chlorophyll match with those of Ad<sub>1</sub>, which is also known to contain chlorophyll. Ad<sub>3</sub> and Ad<sub>4</sub> on the other hand have potentials that match closely with those of ascorbic acid. This is the vitamin that is present in these two parts of the fruit in much higher quantities. It is worth mentioning that the presence of ascorbic acid in Ad<sub>4</sub> (the seed) was much more pronounced than in Ad<sub>3</sub>. This is probably attributed to the stability of ascorbic acid resulting from its preservation in the seed kernel. The presence of the other vitamins is not as clear as that of ascorbic acid and chlorophyll, although there was a peak observed in Ad<sub>3</sub> the presence of NaCl which could be a pointer to the presence of riboflavin. The electrochemical signals in the woody part of the fruit i.e. the seed kernel and woody covering indicate the presence of flavonoids and terpenes.

The results obtained from the surface modified electrode analysis i.e. PME and CME clearly indicate that surface modified electrodes can be used in electrochemical study



of raw plant materials and that the redox potentials for plant materials is affected by the host matrix resulting in the observed lowering of the redox potential.

The observation that the electrochemical signal attributed to ascorbic acid in the *A. digitata* seed is significant (i.e. large peak current and well defined peaks) on the bentonite modified electrode, despite the fact that it is estimated that the concentration of the ascorbic in the seed is not more than 250mg /100g, points to the preconcentration effect and/ or electrocatalytic role of the bentonite host matrix. The product adsorption, fingerprints ascorbic acid detection on bentonite modified electrode. This means that bentonite modified electrodes can be used in quality control monitoring in fruits that are known to contain ascorbic acid. However this is an area that still needs further investigation.

The results presented indicate that electrochemical techniques have a potential in natural products analyses and is less involving as compared to the standard organic chemistry procedures.

## REFERENCES

1. Herbal, R (1963) *Families of flowering plants of Southern Africa* University of Kentucky Press
2. Wickens, G. E. (1982) The Baobab; Africa's Upside Down tree *Tree Kew Bulletin* **37**, (2) 173-209
3. Maheshwari, J. K. (1971) The Baobab tree; Disjunctive, Distribution and Conservation *Biological conservation* **4**(1) 57-60
4. Mabberley, D. J. (1987) *The plant book* Cambridge University Press
5. Hutchsons, J. (1959) *The families of flowering plants –Dicotyledons Vol. 1*, 2<sup>nd</sup>Ed. Oxford University Press.
6. Beentjie, H. J. (1994) *Kenya Trees, Shrubs and Lianas* National Museums of Kenya
7. Owen, J. (1974) A contribution to the ecology of the African Baobab *Savannah* **3**(1) 1-12
8. Muok, B., Owour, B., Dawson, I., and Were, J. (1998) The potential of Indigenous fruit trees- Results of a survey in Kitui District Kenya (*Unpublished Report*)
9. Gilbert, A. (1989) Baobab: *Adansonia digitata* Indigenous trees Series KENGO
10. Owen, M. (1999) The baobab fruit and Oil – Desk study Safire Zimbabwe
11. Sidibé, M., Scheuring, J. F., Koné, M., Schierle, J. and Frigg, M (1998) A (and C) for Africa: The baobab tree as a source of Vitamins *Agroforestry Today* **10** (4) 7-10
12. Anon. (1989) Trees – a solution for drought, *African Farming* Sept./Oct. pg. 2
13. Leakey, R. R. B. (1999) Potential for novel food products from agroforestry trees: a review. *Food Chemistry* **66** (1) 1-14
14. Kokwaro, J. O. (1976) *Medicinal plants for East Africa* Literature Bureau
15. Adensanya, S. A., Idowu, T. B. and Elujoba, A. A. (1980) Antisickling activity of *Adansonia digitata*. *Plant. Med.* **54** (4) 374
16. Wickens, G. E. (1979) Taxonomic aspects African economic Botany-Proceedings of IX plenary meeting of AETFAT Las Palmas de Gran Canana 18-23 March 1978. Ed. by Kunkel, G.
17. Sibidé, M. Scheuring, J. F., Temberly, D., Sibidé, M. M., Hofman, P. and Frigg, M. (1996) Baobab – Home-grown vitamin C for Africa. *Agroforestry Today* **8** (2) 13-15

18. Becker, B. (1983) The contributions of wild plants to human nutrition in Ferlo (Northern Senegal) *Agroforestry Systems* **1** 257-267
19. Eromosele, I. C., Eromosele, C. O. and Kuzhkuzha, D. M. (1991) Evaluation of mineral elements and ascorbic acid contents in fruits of some wild plants *Plants for human Nutrition* **41** 151-154
20. Saka, J. D. K. and Msonthi, J. D. (1994) Nutritional value of edible fruits of indigenous wild trees in Malawi *Forest Ecology and Management* **64** 245-248
21. Saka, J. D. K. (1995) The nutritional value of edible indigenous fruits; present research status and future directions – in Improvement of indigenous fruit trees of the miombo woodlands of Southern Africa Eds. Maghembe, J. A., Ntupanyama, Y. and Chirwa, P. W. ICRAF
22. Maundu, P. M., Ngugi, G.W. and Kabuye, C.H. S. (1999) *Traditional Food Plants of Kenya*. Kenya Resource Center for indigenous knowledge. National Museums of Kenya
23. Msonthi, J. D. and Magombo, D. (1983) Medicinal Herbs in Malawi and their uses *Hamdard* **26** (2) 94
24. Ramesh, D., Dennis, T. J. and Shingara, M. S. (1992) Constituents of *Adansonia digitata* root bark. *Fitoterapia* **63** (3) 278
25. Sawyer, D. T. and Roberts Jr., J. L. (1974) *Experimental Electrochemistry for chemists* John Wiley and Sons Inc. NY
26. Reiger, P. H. (1987) *Electrochemistry* Prentice-Hall Inc. N. J.
27. Bard, A. J. and Faulkner, L. R. (1980) *Electrochemical methods- Fundamental and applications*. John Wiley and Sons NY
28. Murray, R. W. (1984) Chemically modified electrodes (ed. by Bard, A. J.) in *Electoanal. Chem.* **13** Marcel Dekker Inc. NY 191
29. Lane, R. F. and Hubbard, A. T. (1973) Electrochemistry of chemisorbed molecules I Reactions connected to electrodes through olefinic substituents. *J. Phy. Chem.* **77** 1401
30. Lane, R. F. and Hubbard, A. T. (1973) Electrochemistry of chemisorbed molecules II The influence of charged chemisorbed molecules on the electrode reaction of Platinum complexes. *J. Phys. Chem.* **77** 1411
31. Arnold, B. B. and Murphy, G. W. (1961) Studies on the electrochemistry of carbon and chemically modified carbon surfaces *J. Phys. Chem.* **65** 135

32. Brown, A. P., Koval, C. and Anson, F. C. (1976) Illustrative electrochemical behaviour of reactants irreversibly adsorbed on graphite surfaces *J. Electroanal. Chem.* **72**, 379-87
33. Brown, A. P. and Anson, F. C. (1977) *Anal. Chem.* **49**, 1589
34. Watkins, B. F., Miller, L. L., Kariv, E. and Behling, J. R. (1975) Chiral Electrode. *J. Am. Chem. Soc.* **97** 3549-50
35. Murray, R. W., Wier, L. and Moses, P. R. (1975) Chemically modified tin oxide electrode. *Anal. Chem.* **47**, 1882-7
36. Moses, P. R. and Murray, R. W. (1976) Chemically modified electrodes. 3. SnO<sub>2</sub> and TiO<sub>2</sub> electrodes bearing electroactive reagent.
37. Utereker, D. F., Lennox, J. C., Wier, L., M., Moses P. R. and Murray, R. W. (1977) Chemically modified electrodes. Evidence of formation of monolayers bonded on organosilanes. *J. Electroanal. Chem.* **81**, 309-318
38. Finklea, F. O. and Murray, R. W. (1979) Chemically modified electrodes. Effects of salinization on titanium oxide electrodes. *J. Phys. Chem.* **83**, 353-8
39. Wrington, M. S. Palazzotto, M. C., Bocarsly, A. B., Bolts, J. M., Fischer, A. B. and Nadjio, L. (1978) Preparation of chemically derivatized platinum and gold electrode surfaces. Synthesis, characterisation and surface attachment of trichlorosilane and 1,1'-Bis(tiethoxySilyl)Ferrocene *J. Am. Chem. Soc.* **100**, 7264
40. Wrington, M. S. and Bolts, J. M. (1978) Chemically derivatized n-type semi-conducting germanium photoelectrodes. Persistent attachment and photoelectrochemical activity of ferrocene derivatives. *J. Am. Chem. Soc.* **100**, 5257
41. Diaz, A. F., Uetzler, U. and Kay, E. (1977) Inelastic electron tunnelling spectroscopy of a chemically modified electrode. *J. Am. Chem. Soc.* **99**, 6780
42. Lenhard, J. R. and Murray, R. W. (1978) Chemically modified electrodes-Monolayers/Multilayer coverage, decay, kinetics, solvent and interaction effects for ferrocenes covalently linked to platinum electrode. *J. Am. Chem. Soc.* **100**, 7870
43. White, H. S. and Murray, R. W. (1979) Fluorescence and x-ray photoelectron spectroscopy surface analyses of metal oxide electrodes chemically modified with Dansylated alkylamine
44. Abruna, H. Meyer, T. J. and Murray, R. W. (1979) *Inorg. Chem.* **11**, 3233
45. Koval, C. A. and Anson, F. C. (1978) Electrochemistry of the Ruthenium (3<sup>+</sup>, 2<sup>+</sup>) couple attached to graphite.
46. Lin, A. W. C., Yen, P. and Kuwana, T. (1977) *J. Electroanal. Chem.* **84**, 41

47. Yacynch, A. M. and Kuwana, T (1978) Cyanuric chloride as a general linking agent for modified electrode attachment of redox groups to pyrolytic graphite. *Anal. Chem.* **50**, 640
48. Lennox, J. C. and Murray, R. W. (1978) Chemically modified electrode 10. Electron spectroscopy for chemical analyses and alternating current voltammetry of glassy carbon – bound tetra (amino phenyl) porphyrins. *J. Am. Chem. Soc.* **100**, 3710
49. Murray, R. W. (1980) Chemically modified electrodes *Acc. Chem. Res.* **13**, 135
50. Elliot, C. M. and Murray, R. W. (1976) Chemically modified carbon electrodes *Anal. Chem.* **48**, 1247
51. Mazur, S., Matusinovic, T. and Cammann (1977) Organic reactions of oxide free carbon surface and electroactive derivatives. *J. Am. Chem. Soc.* **99**, 3888
52. Oyama, N., Brown, A. P. and Anson, F. C. (1978) Introduction of amine groups on graphite electrode surfaces and their use in attachment of ruthenium (II) to the electrode surface. *J. Electroanal. Chem.* **87**, 435
53. Miller, L. I. and Van de Mark (1978) Electrode surface modification via polymer adsorption. *J. Am. Chem. Soc.* **100**, 639
54. Orata, D. O. and Buttry, D. A. (1987) Determination of ion population and solvent content as a function of redox state and pH in polyaniline *J. Am. Chem. Soc.* **109**, 3574
55. Oyama, N. and Anson F. C. (1979) Facile attachment of transition metal complexes to graphite electrodes coated with polymer ligands observation and control of metal-ligand-coordination among reactants confined to electrode surface. *J. Am. Chem. Soc.* **101**, 739
56. Kerr, J. B., Miller, L. L. and Van De Mark, M. R. (1980) Apoly-p-nitrostyrene on platinum electrode polymer charging kinetics and electrocatalysis of organic dihalide reductions. *J. Am. Chem. Soc.* **102**, 3383.
57. Merz, A. and Bard, A. J. (1978) A stable surface modified Platinum Electrode prepared by coating with electroactive polymer *J. Am. Chem. Soc.* **100**, 3222.
58. Itaya, K. and Bard, A. J. (1978) Chemically modified polymer electrodes –Synthetic approach employing poly (methylacryl chloride) anchors. *Anal. Chem.* **50**, 1487.
59. Orata, D. O. and Osoro, F. N. (1992) stabilisation of polyaniline films in the presence of *p*-aminophenol. *Bull. Chem. Soc. Ethiop.* **6**(1) 27
60. Paul, E. W., Ricco, A. J. and Wrington, M. S. (1985) Resistance of polyaniline film as a function of electrochemical potential and the fabrication of polyaniline based microelectrode devices. *J. Phy. Chem.* **89**, 1441.

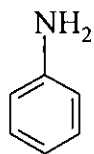
61. Orata, D. O. and Osoro, F. N. (1983) Electrochemical degradation of a metallated polyaniline. *Reactive Polymers* **20**, 81
62. Helfferich, F. (1962) *Ion exchange* Mc Graw Hill Series in Advanced Chemistry
63. Jenny, H. (1932) Studies on the mechanism of ionic exchange in colloidal aluminium silicates. *J. Phy. Chem.* **36**, 2217
64. Marshal, C. E. (1949) *The colloid chemistry of the silicate materials* Academic Press NY
65. Barrier, R. M. (1948) Synthesis of a zeolitic mineral with chabazite-like sorptive properties. *J. Am.. Chem. Soc.* 127
66. Reed, T. B. and Breek, D. W. (1956) Crystalline zeolites II Crystal structure of synthetic zeolites type A. *J. Am, Chem.. Soc.* **78**, 5972
67. Ullman's Encyclopeadia of industrial chemistry (1986)j 5<sup>th</sup> Edition Vol. A7, 109
68. Theng, B. K. G. (1974)*The chemistry of clay organic reactions* Hilger London
69. Grim, R. E. (1953) *Clay mineralogy* Mc Graw hill book company Inc. NY
70. Van Olphan, H. (9177) *An introduction t o clay colloid chemistry* 2nd Edn. Wiley NJ
71. Forsind, E. (1953) The clay water system II Water adsorption and cationic exchange in montmorillonite. *Act. Polytech.* **115**
72. Rudzinski, W. E. and Bard, A. J.(1886) Clay modified electrodes Part VI Aluminium and Silicon modified electrodes. *J. Electroanal. Chem.* **199**, 323
73. Pulfrey, W. Timau and Athi river clays *Unpublished report* Mines and Geology Dept. Kenya
74. Heinze, J. and Merz, A. (1990) *Topics in current chemistry* Springer Verlag Berlin
75. Ege, D., Ghosh, P. K., White, J. R., Egey, J. F. and Bard, A. J. (1985) *J. Am. Chem. Soc.* **107**,5644
76. Bard, A. J. and Itaya, K. (1985) Clay modified electrode 5. Preparation and electrochemical characterization of pillared clay modified membranes, *J. Phy. Chem.* **89**, 5565
77. MacDiarmid, A. G. and Estemad, S. and Heeger, A. J. (1982) Polyacetylene, (CH)<sub>x</sub>. The prototype conducting polymer. *Ann. Rev. Phys. Chem.* **33** 443
78. Orata, D. and Matheka, A. (1994) Suppression of polyaniline electrochemical degradation in salt solutions. *Bull. Chem. Soc. Ethiop.* **8**(1) 21

79. Orata, D. O. and Kariuki, B. (1996) Charge-state trapping at a conducting polymer-redox ion-exchanger interface – a bilayer electrode *React. and Funct. Poly.* **28**, 287
80. Orata, D. O. and David, S. K. (2000) A comparative study of the electrochemical/electrodegradation of polyaniline from aniline loaded in a clay-mineral/polyaniline composite matrix to that of the bulk solution. *React. and Funct. Poly.* **43**, 133
81. Underwood, A. L. and Burnet, R. W. (1973) Electrochemistry of biological compounds (Ed. by Bard, A. J.) in *Electroanal. Chem.* **6**, Marcel Dekker Inc. NY.
82. Smith, D. L. and Elvin, P. J. (1962) Electrochemical reduction of pyrimidine, cytosine and related compound; Polarography and macroscale electrolyses. *J. Am. Chem. Soc.* **84**, 2741
83. Adam, R. N. (1969) Electrochemistry at solid electrodes – Monographs in electroanalytical chemistry and electrochemistry (ed., by Bard, A. J.) Marcel Dekker NY.
84. Orata, D. O. and Segor, F. (1999) Bentonite (clay montmorillonite) as a template for electrosynthesis of thyroxine. *Catalyses Letters* **58** 157
85. Orata, D. O. and Segor, F. (1993) Oxidation of ascorbic acid on a polyaniline modified electrode. *Bull. Chem. Soc. Ethiop.* **7**, (1) 53
86. Barrow, G. M. (1966) *Physical Chemistry* Mc Graw Hill book company
87. Shoemaker, D. P., Gerland, C. W., Jeffery, I. S. and Nibler, J. W. (1981) *Experiments for Physical chemistry* 4th Ed. Mc Graw Inc.
88. Daniel, H. (1991) *Quantitative chemical Analysis* 3<sup>rd</sup> Edition. W. H. Freeman & Co. NY.
89. Willard, H. H., Meritt, Jr. L. L., Dean, J. A. and Settle, Jr. F. A. (1988) *Instrumental methods of analysis* 7<sup>th</sup> Ed. Wadworth Publication company CA
90. Skoog, D. A., West, D. M. and Holler, E. J. (1992) *Fundamentals of analytical chemistry* 6<sup>th</sup> Ed.: Skoog, D. A. (19-- ) *Principles of Instrumental analysis* 3<sup>rd</sup> Ed. Saunders NY.
91. South Hampton Group (1985) *Instrumental methods in electrochemistry* Ellis Horwad Publishers Chichester
92. Shimadzu Fourier Transform Infrared spectrophotometer FTIR-8000 Series Instruction manual
93. Espen, P. V., Jansen, K. and Swenter, F. Axil X-ray analysis Software users manual
94. Kump, P. Quantitative analysis of environmental samples 1993 IAEA

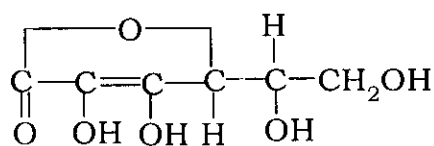
95. Morrison, R. T. and Boyd, R.N. (1987) *Organic chemistry* 5<sup>th</sup> Edition. Allyn and Bacon, Inc. Boston
96. Lacroix, J. C. and Diaz, A. F., (1988) *J. Elctrochem. Soc.* **135**, 1457.
97. Wopschall, R. H. and Shain, I (1967) *Anal. Chem.* **39** 1514



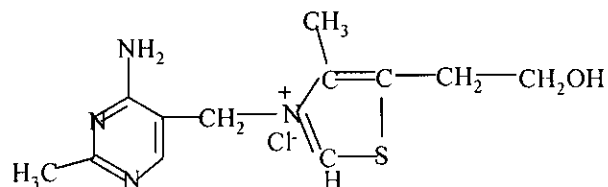
## APPENDIX



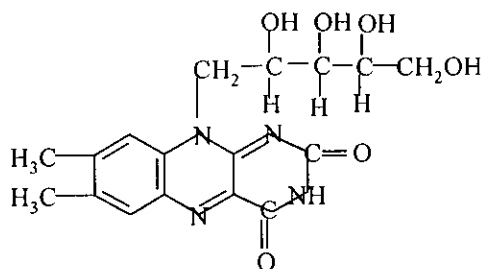
Aniline



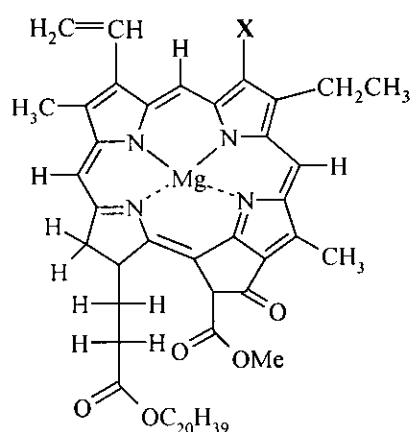
L - Ascorbic acid



Vitamin B<sub>1</sub> - Thiamin



Vitamin B<sub>2</sub> - Riboflavin



Structure of Chlorophylls;  
Chlorophyll a, X = -CH<sub>3</sub>; Chlorophyll b, X = -CHO